Universitat de Lleida

Análisis multiescalar de efectos del cambio global en ecosistemas forestales

Pere Joan Gelabert Vadillo

http://hdl.handle.net/10803/687496

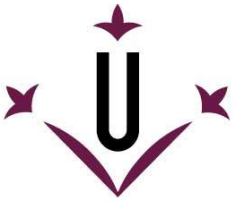

Universitat de Lleida

TESI DOCTORAL

Análisis multiescalar de efectos del cambio global en ecosistemas forestales

Pere Joan Gelabert Vadillo

Memòria presentada per optar al grau de Doctor per la Universitat de Lleida

Prog. de Doctorat en Gestió Forestal i del Medi Natural

Director/a

Marcos Rodrigues Mimbrero
Cristina Vega García

Tutor/a

Cristina Vega García

2022

Agraïments

Malgrat estar al principi del document, aquest apartat especial és l'últim a escriure's, sent de summa importància ja que ha de reflectir el tancament d'una etapa. En tota etapa viscuda és necessari agrair a tot aquell que hagi contribuït directament o indirectament en el desenvolupament d'aquesta. Per això, a les primeres persones que vull expressar la meva major gratitud és als meus directors, Marcos i Cristina. Vosaltres m'heu donat la total llibertat per a desenvolupar les línies de recerca en les quals em podia sentir més còmode, amb una vigilància constant permetent així el bon desenvolupament i el exitós final de la present Tesi Doctoral.

A Marcos agrair-li encaridament que, pesi no estar de manera presencial, sempre l'he trobat a l'altre costat de les plataformes de videoconferència per a resoldre dubtes tècnics en qüestió de minuts. Reconèixer i expressar gratitud ja que han estat moltes les hores invertides en la meva formació com a investigador, cosa que ha propiciat a convertir-te en el meu guia i referent cientificotècnic.

Cristina, agrair-te l'oportunitat que em vas brindar en aconseguir finançament perquè pogués desenvolupar-me com a investigador, pel dia a dia, per les revisions exhaustives i tot l'ensenyament transversal en la part més operativa de la ciència amb la inclusió i implicació directa en projectes de recerca. Voldria dedicar-te un esment especial ja que en els teus moments personals més difícils has seguit amb la mateixa energia, implicació i il · lusió per treure aquesta Tesi endavant. De tota manera, a tots dos, eternament agraït.

D'altra banda, Aitor, soc conscient de l'okupació i invasió del teu espai vital en el despatx. No obstant això, el bon rotllo, els acudits dolents i l'estima personal et converteixen en el company que tot mundà volgués

tenir davant. Sé que t'agradaria estar sol, però per a això cal estar acreditat a Catedràtic o ocupar algun càrrec de sacrificada gestió, així que espero i desitjo que aviat hagi d'abandonar aquest espai pel primer motiu. A Lluís reconèixer-li que m'encanta el pique personalla seva competitivitat -algun dia encertaràs amb l'esquerra- i els punyals que ens clavemhumor, arrencant-me els riures i amenitzant l'ambient diàriament. Sortint d'aquestes línies d'humor, no vull acabar el paràgraf sense agrair-vos també totes les aportacions científiques i suports en diversos capítols d'aquesta Tesi.

En la literatura es poden trobar decàlegs de bones pràctiques de convivència en laboratoris i equips de treball. No obstant això, en el nostre laboratori no en seguim cap ja que no ens fa falta. Vull manifestar la meva gran gratitud a totes les persones que han deixat i deixen empremta al laboratori. Bontou, Iris, Fermín, Mara, Lucía, Gil, Jordi, Vicente, Miguel Ángel, Judith i Anna, per la companyia, suport, amistat i els bons moments amb llargs dinars i cafès.

En el suport econòmic he d'agrair en primera instància a la Universitat de Lleida pel finançament del meu contracte pre-doctoral sota el *programa d'ajudes a la recerca Ajuts UdL, Jade Plus i Fundació Bancària La Caixa* [Acord 79/2018 del Consell de Govern de la Universitat de Lleida]. Al projecte *IMAGINE* [CGL2016-80400-R] i la seva IP Teresa Sebastià per servirme de marc per a desenvolupar aquesta tesi. També a Cristina que amb la seva lluita incansable per obtenir fons m'ha permès ampliar aquesta etapa durant un any més. Finalment agrair al *Instituto Universitario de Investigación en Ciencias Ambientales de Aragón* (IUCA), a Teresa Lamelas, Antonio Montealegre i Darío Domingo per finançar amb una beca d'iniciació a la recerca la meva primera endinsada en el món científic. A més de plantejar i desenvolupar un capítol d'aquesta tesi.

A la família agrair-li tots els esforços i suports que m'han permès arribar fins aquí i poder fer aquest somni realitat. Per a finalitzar, vull dedicar l'últim agraïment a la persona que m'ha acompanyat emocionalment en aquest viatge. Mapi gràcies per donar-me suport, guiar-me i aguantar-me

des de la distància. Part d'aquest èxit també és teu i espero poder celebrar el teu pròximament.

Índice

Resum

El sistema Terra experimenta canvis d'escala global, accelerats des de la segona meitat del segle XX. Les principals alteracions lligades a aquests canvis són produïdes per canvis en el model i estructura socioeconòmica, que condueixen a un escalfament global i a canvis en les localitzacions de les activitats productives i assentaments humans. Els boscos són ecosistemes dinàmics el principal motor dels quals de canvi són les pertorbacions. El canvi global està alterant els règims naturals d'algunes d'elles, afectant la seva freqüència, distribució espacial i intensitat i, en últim terme, afectant àmplia varietat de serveis ecosistèmics derivats. Per a poder mitigar els possibles impactes negatius en la provisió d'aquests serveis és essencial conèixer en profunditat l'estructura i funcionament de les nostres comunitats forestals.

Les tecnologies de la informació geogràfica brinden múltiples oportunitats per a aprofundir en el coneixement sobre el medi natural. Aquesta tesi suposa una contribució original en l'àmbit forestal. En ella s'investiga i utilitza una àmplia varietat de fonts i tècniques d'anàlisis d'informació, amb un marcat caràcter espacial, que permeten comprendre l'estructura i el funcionament dels boscos. En ella s'aborden diverses anàlisis relacionades amb l'impacte de pertorbacions, la dinàmica forestal i els possibles efectes del canvi global:

Capítol 4. LandTrendr smoothed spectral profiles enhance woody encroachment monitoring

A Europa l'agricultura ha experimentat un procés de concentració i intensificació cap a espais on existeixen més facilitats per a la producció i, per tant, un major rendiment. Des de mitjan S. XX s'ha observat un gradual abandonament d'espais rurals, especialment notable en ambients de muntanya. Aquest tipus de comunitats forestals són de vital importància en termes ambientals ja que són enclavaments amb una alta biodiversitat

que, a més, han evolucionat de la mà de l'ésser humà en una sort de paisatges culturals. El recent i abrupte abandó d'activitats humanes en aquests ambients pot tenir conseqüències perjudicials tant a curt com llarg termini. Per exemple, l'acumulació de biomassa forestal es tradueix en una major càrrega de combustible i un paisatge més homogeni, presentant nous reptes crucials per a la gestió forestal sostenible o la mitigació del risc i incendi forestal.

En el segon capítol s'implementa una metodologia per a caracteritzar l'evolució espaitemporal de l'ocupació per boscos sobre els espais agraris abandonats a partir de sèries temporals d'imatges multiespectrals (Landsat 5-7-8 als Pirineus espanyols. Els Pirineus són segon sistema muntanyenc més alt de la Península Ibèrica (entre 500 i 3400 m.s.n.m.) amb una extensió de 19.000 km^2. Els espais oberts Aquests espai són espais productius que s'abandonen a causa de noves dinàmiques socioeconòmiques. Treballar les sèries temporals sense preprocessar pot incorporar sorolls i no permetre una captura adequada de la resposta. En aquest capítol es demostra la utilitat dels algorismes de segmentació espai temporal (i.e. Landtrendr) per a caracteritzar i capturar la dinàmica espaitemporal del fenomen de l'avanç del bosc sobre cultius i pastures abandonades. La metodologia plantejada permet quantificar l'expansió del bosc sobre àrees obertes i cultius antics resultant una taxa de recobriment forestal de 6000 ha/any en els últims 10 anys. A més, també permet analitzar la dinàmica temporal, existint unes taxes majors de recobriment en la dècada dels 80's i una estabilització de la taxa a partir de l'any 1992.

Capítol 5. Spatially explicit modeling of the probability of land abandonment in the Spanish Pyrenees

El coneixement obtingut sobre l'avanç de les comunitats forestals en zones agrícoles i pastures abandonades permet aprofundir en la identificació dels factors que es relacionen amb aquest abandó. En aquest capítol s'investiga la influència dels factors socioeconòmics, topogràfics, climàtics i ecològics amb l'objectiu d'estimar la susceptibilitat a l'abandó en el futur des

d'una perspectiva espacialment explicita. En línies generals, les majors taxes d'abandó es van donar en els assentaments rurals i als pobles de les valls del fons, on el turisme i les activitats recreatives han proliferat al llarg dels anys. És més pronunciat en aquells pobles als quals els uneix una connexió ràpida i còmoda entre les principals àrees metropolitanes (per exemple, Barcelona i Saragossa), cosa que també fomenta l'activitat turística i la creació de nous assentaments.

Capítol 6. On the relationship between tree height, elevation and climate in European mountain ranges

En aquest capítol es planteja l'anàlisi dels efectes del canvi climàtic sobre les comunitats forestals. Per a això s'analitzen les noves dades Global Ecosystem Dynamics Investigation que ens permeten caracteritzar l'estructura dels boscos a escala global. L'anàlisi s'ha centrat en les principals cadenes muntanyenques a Europa: Pirineus, Alps, Carpats i Caucas. L'estudi es planteja sobre la hipòtesi de l'existència d'una relació entre l'altura màxima de l'arbratge i la influència climàtica. En aquesta relació s'observa un decreixement abrupte de l'altura de l'arbratge a partir d'un cert llindar d'altitud en totes les cadenes muntanyenques analitzades. Aquest llindar ve definit pel límit superior de les condicions òptimes de creixement de la vegetació. En un context d'escalfament global aquest òptim de creixement es desplaçarà cap a cotes més elevades alterant la dinàmica del bosc i podent propiciar la desaparició d'espècies d'alt valor localitzades en el pis alpí.

Capítol 7. Forest structural diversity characterization in Mediterranean landscapes affected by fires using Airborne Laser Scanning data

En aquest últim capítol, en primer lloc, s'avaluen els efectes del foc en l'estructura forestal mitjançant tecnologia LiDAR, avaluant la petjada estructural en diverses etapes de recuperació post-foc. Tecnologies com el LiDAR aerotransportat ens permeten caracteritzar aquests canvis i registrar aquelles àrees que han sofert una pertorbació i els seus nivells de severitat. Els índexs de diversitat i d'equitat altures han permès sintetitzar i caracteritzar la recuperació post incendio. Els resultats mostren que, en els incendis

més recents, al voltant del 70% dels retorns del làser procedien dels estrats d'herba i arbustos, la qual cosa va produir valors baixos dels índexs de diversitat i d'equitat. Per contra, les zones cremades fa més de 20 anys presentaven valors dels índexs de diversitat i d'equitat més elevats a causa del creixement dels estrats arbustius i arboris. Mitjançant test de comparació de mitjanes (Kruskall-Wallis), s'ha observat que després d'un incendi i durant els c.a. 35 anys posteriors es mantenen diferències estructurals recognoscibles en relació amb la situació prèvia a l'incendi.

Resumen

El sistema Tierra experimenta cambios de escala global, acelerados desde la segunda mitad del siglo XX. Las principales alteraciones ligadas a estos cambios son producidas por cambios en el modelo y estructura socioeconómica, que conducen a un calentamiento global y a cambios en las localizaciones de las actividades productivas y asentamientos humanos. Los bosques son ecosistemas dinámicos cuyo principal motor de cambio son las perturbaciones. El cambio global está alterando los regímenes naturales de algunas de ellas, afectando a su frecuencia, distribución espacial e intensidad y, en último término, afectando a amplia variedad de servicios ecosistémicos derivados. Para poder mitigar los posibles impactos negativos en la provisión de estos servicios es esencial conocer en profundidad la estructura y funcionamiento de nuestras comunidades forestales.

Las tecnologías de la información geográfica brindan múltiples oportunidades para profundizar en el conocimiento sobre el medio natural. Esta tesis supone una contribución original en el ámbito forestal. En ella se investiga y utiliza una amplia variedad de fuentes y técnicas de análisis de información, con un marcado carácter espacial, que permiten comprender la estructura y el funcionamiento de los bosques. En ella se abordan diversos análisis relacionados con el impacto de perturbaciones, la dinámica forestal y los posibles efectos del cambio global:

Capítulo 4. LandTrendr smoothed spectral profiles enhance woody encroachment monitoring

En Europa la agricultura ha experimentado un proceso de concentración e intensificación hacia espacios donde existen más facilidades para la producción y, por tanto, un mayor rendimiento. Desde mediados del S. XX se ha observado un paulatino abandono de espacios rurales, especialmente notable en ambientes de montaña. Este tipo de comunidades forestales son

de vital importancia en términos ambientales ya que son enclaves con una alta biodiversidad que, además, han evolucionado de la mano del ser humano en una suerte de paisajes culturales. El reciente y abrupto abandono de actividades humanas en estos ambientes puede tener consecuencias perjudiciales tanto a corto como largo plazo. Por ejemplo, la acumulación de biomasa forestal se traduce en una mayor carga de combustible y un paisaje más homogéneo, presentando nuevos retos cruciales para la gestión forestal sostenible o la mitigación del riesgo e incendio forestal.

En el segundo capítulo se implementa una metodología para caracterizar la evolución espacio-temporal de la ocupación por bosques sobre los espacios agrarios abandonados a partir de series temporales de imágenes multiespectrales (Landsat 5-7-8) en los Pirineos españoles. Los Pirineos son segundo sistema montañoso más alto de la Península Ibérica (entre 500 y 3400 m.s.n.m.) con una extensión de 19.000 km^2. Los espacios abiertos son espacios productivos que se abandonan debido a nuevas dinámicas socioeconómicas. Trabajar las series temporales sin preprocesar puede incorporar ruidos y no permitir una captura adecuada de la respuesta. En este capítulo se demuestra la utilidad de los algoritmos de segmentación espacio-temporal (i.e. Landtrendr) para caracterizar y capturar la dinámica espacio-temporal del fenómeno del avance del bosque sobre cultivos y pastos abandonados. La metodología planteada permite cuantificar la expansión del bosque sobre áreas abiertas y cultivos antiguos resultando una tasa de recubrimiento forestal de 6000 ha/año en los últimos 10 años. Además, también permite analizar la dinámica temporal, existiendo unas tasas mayores de recubrimiento en la década de los 80's y una estabilización de la tasa a partir del año 1992.

Capítulo 5. Spatially explicit modeling of the probability of land abandonment in the Spanish Pyrenees

El conocimiento obtenido sobre el avance de las comunidades forestales en zonas agrícolas y pastos abandonados permite profundizar en la identificación de los factores que se relacionan con este abandono. En este capítulo se investiga la influencia de los factores socioeconómicos, topográficos,

climáticos y ecológicos con el objetivo de estimar la susceptibilidad al abandono en el futuro desde una perspectiva espacialmente explicita. En líneas generales, las mayores tasas de abandono se dieron en los asentamientos rurales y en los pueblos de los valles del fondo, donde el turismo y las actividades recreativas han proliferado a lo largo de los años. Es más pronunciado en aquellos pueblos a los que les une una conexión rápida y cómoda entre las principales áreas metropolitanas (por ejemplo, Barcelona y Zaragoza), cosa que también fomenta la actividad turística y la creación de nuevos asentamientos.

Capítulo 6. On the relationship between tree height, elevation and climate in European mountain ranges

En este capítulo se plantea el análisis de los efectos del cambio climático sobre las comunidades forestales. Para ello se analizan los nuevos datos *Global Ecosystem Dynamics Investigation* que nos permiten caracterizar la estructura de los bosques a escala global. El análisis se ha centrado en las principales cadenas montañosas en Europa: Pirineos, Alpes, Cárpatos y Cáucaso. El estudio se plantea sobre la hipótesis de la existencia de una relación entre la altura máxima del arbolado y la influencia climática. En esta relación se observa un decrecimiento abrupto de la altura del arbolado a partir de cierto umbral de altitud en todas las cadenas montañosas analizadas. Este umbral viene definido por el límite superior de las condiciones óptimas de crecimiento de la vegetación. En un contexto de calentamiento global este óptimo de crecimiento se desplazará hacia cotas más elevadas alterando la dinámica del bosque y pudiendo propiciar la desaparición de especies de alto valor localizadas en el piso alpino.

Capítulo 7. Forest structural diversity characterization in Mediterranean landscapes affected by fires using Airborne Laser Scanning data

En este último capítulo, en primer lugar, se evalúan los efectos del fuego en la estructura forestal mediante tecnología LiDAR, evaluando la huella estructural en diversas etapas de recuperación post-fuego. Tecnolo-

gías como el LiDAR aerotransportado nos permiten caracterizar estos cambios y registrar aquellas áreas que han sufrido una perturbación y sus niveles de severidad. Los índices de diversidad y de equidad alturas han permitido sintetizar y caracterizar la recuperación post incendio. Los resultados muestran que, en los incendios más recientes, alrededor del 70% de los retornos del láser procedían de los estratos de hierba y arbustos, lo que produjo valores bajos de los índices de diversidad y de equidad. Por el contrario, las zonas quemadas hace más de 20 años presentaban valores de los índices de diversidad y de equidad más elevados debido al crecimiento de los estratos arbustivos y arbóreos. Mediante test de comparación de medias (Kruskall-Wallis), se ha observado que después de un incendio y durante los c.a. 35 años posteriores se mantienen diferencias estructurales reconocibles en relación con la situación previa al incendio.

Abstract

The Earth system is undergoing changes on a global scale, which have accelerated since the second half of the 20th century. The main alterations linked to these changes are produced by changes in the socioeconomic model and structure, leading to global warming and changes in the locations of productive activities and human settlements. Forests are dynamic ecosystems whose main drivers of change are disturbances. Global change is altering the natural regimes of some of these disturbances, affecting their frequency, spatial distribution and intensity and, ultimately, affecting a wide variety of derived ecosystem services. In order to mitigate potential negative impacts on the provision of these services, it is essential to have a deep understanding of the structure and functioning of our forest communities.

Geographic information technologies provide multiple opportunities to expand the knowledge of the natural environment. This thesis is an original contribution in the forestry field. It investigates and uses a wide variety of sources and techniques of information analysis, with a marked spatial character, that allow us to understand the structure and functioning of forests. It addresses various analyses related to the impact of disturbances, forest dynamics and the possible effects of global change:

Chapter 4. LandTrendr smoothed spectral profiles enhance woody encroachment monitoring.

In Europe, agriculture has undergone a process of concentration and intensification towards areas where there are more production facilities and, therefore, higher yields. Since the middle of the 20th century, a gradual abandonment of rural areas has been observed, especially in mountain environments. These types of forest communities are of vital importance in environmental terms as they are enclaves with a high biodiversity that have

also evolved hand in hand with humans into a kind of cultural landscape. The recent and abrupt abandonment of human activities in these environments can have detrimental consequences in both the short and long term. For example, the accumulation of forest biomass results in a higher fuel load and a more homogeneous landscape, presenting crucial new challenges for sustainable forest management or wildfire risk mitigation.

The second chapter implements a methodology to characterize the spatio-temporal evolution of forest occupation over abandoned agricultural spaces from time series of multispectral images (Landsat 5-7-8) the Spanish Pyrenees. The Pyrenees are the highest mountain system of the Iberian Peninsula (between 500 and 3400 m.a.s.l.) with an extension of 19,000 km^2. The open spaces are productive spaces that are abandoned due to new socio-economic dynamics. Working the time series without preprocessing may incorporate noise and not allow an adequate capture of the response. This chapter demonstrates the usefulness of spatiotemporal segmentation algorithms (i.e. Landtrendr) to characterize and capture the spatiotemporal dynamics of the phenomenon of forest encroachment on abandoned crops and pastures. The proposed methodology allows quantifying the expansion of the forest over open areas and old crops resulting in a forest cover rate of 6000 ha/year in the last 10 years. In addition, it also allows analyzing the temporal dynamics, with higher cover rates in the 80's and a stabilization of the rate from 1992 onwards.

Chapter 5. Spatially explicit modeling of the probability of land abandonment in the Spanish Pyrenees

The knowledge obtained on the advance of forest communities in agricultural areas and abandoned pastures allows us to further identify the factors related to this abandonment. This chapter investigates the influence of socioeconomic, topographic, climatic and ecological factors in order to estimate the susceptibility to abandonment in the future from a spatially explicit perspective. Generally speaking, the highest rates of abandonment occurred in rural settlements and in villages in the bottom valleys, where tourism and recreational activities have proliferated over the years. It is

more pronounced in those villages that are linked by a fast and convenient connection between the main metropolitan areas (e.g., Barcelona and Zaragoza), which also encourages tourist activity and the creation of new settlements.

Chapter 6. On the relationship between tree height, elevation and climate in European mountain ranges

This chapter analyses the effects of climate change on forest communities. For this purpose, we analyze the new Global Ecosystem Dynamics Investigation data that allow us to characterize the structure of forests at a global scale. The analysis is focused on the main mountain ranges in Europe: Pyrenees, Alps, Carpathians and Caucasus. The study is based on the hypothesis of the existence of a relationship between maximum tree height and climatic influence. This relationship shows an abrupt decrease in tree height above a certain altitude threshold in all the mountain ranges analyzed. This threshold is defined by the upper limit of optimal vegetation growth conditions. In a context of global warming, this growth optimum will shift towards higher altitudes, altering the dynamics of the forest and potentially leading to the disappearance of high-value species located on the alpine belt.

Chapter 7. Forest structural diversity characterization in Mediterranean landscapes affected by fires using Airborne Laser Scanning data

In this last chapter, first, the effects of fire on forest structure are evaluated using LiDAR technology, assessing the structural footprint at various stages of post-fire recovery. Technologies such as airborne LiDAR allow us to characterize these changes and record those areas that have suffered a disturbance and their severity levels. Diversity and equity height indices have allowed us to synthesize and characterize post-fire recovery. The results show that, in the most recent fires, about 70% of the laser returns came from the grass and shrub strata, which produced low values of diversity and equity height indices. In contrast, areas burned more than 20 years ago had higher diversity and equity height indices values due to the growth

of shrub and tree strata. By using the Kruskall-Wallis test, it was observed that after a fire and during the subsequent 35 years, recognizable structural differences were maintained in relation to the pre-fire situation.

Capítulo 1

Introducción

1. Introducción

1.1. La concepción del espacio natural: del paisaje a los servicios ecosistémicos.

Los bosques son conjuntos de ecosistemas complejos formados principalmente por comunidades arbóreas, acompañadas o no de estratos arbustivos y/o herbáceos (sotobosque). Estos espacios son de suma importancia para el desarrollo y subsistencia de la vida en la Tierra. Los bosques han colonizado una amplia variedad de ambientes (Trumbore *et al.* 2015, Albrich *et al.* 2020), entre los que destacan seis tipologías principales. El bosque tropical, localizado en latitudes cercanas al ecuador, cuenta con los mayores niveles de desarrollo de la vegetación y biodiversidad del planeta, favorecidos por condiciones de temperatura y precipitación generalizadamente altas durante todo el año. Entre los trópicos y las latitudes medias predominan los bosques subtropicales. Se trata de formaciones con un alto desarrollo de la vegetación, aunque menor que en los bosques tropicales debido a diferencias estacionales en pluviometría y donde también se registran temperaturas más moderadas. Estas dos regiones bioclimáticas albergan 55% de los bosques mundiales (FAO 2020a), y almacenan cerca del 45% del carbono a nivel mundial (Saatchi *et al.* 2011). No obstante, al ser las regiones más productivas del mundo, es donde actualmente existe un mayor nivel de presión antrópica y extracción de recursos, ya sea en forma de aprovechamientos de madera o de intensificación agrícola.

En latitudes medias se encuentran los bosques templados y los mediterráneos. Los primeros destacan por su mezcla de especies coníferas y frondosas caducifolias, con diferencias marcadas en temperatura durante las diferentes estaciones y una precipitación homogéneamente repartida durante todo el año. En cambio, los bosques mediterráneos son bosques que se caracterizan principalmente por su adaptación a la sequía estival (especies xerófilas y esclerófilas) y a los incendios forestales (especies pirófitas, estrategias de regeneración como la serotinia o el rebrote, y adaptaciones fisiológicas como cortezas más gruesas) (Le Houerou 1974). Además de ser

susceptibles a la alteración por perturbaciones, estos son considerados bosques seminaturales debido a la intervención humana con prácticas pastorales y agrícolas, elemento cultural que ha modificado las especies dominantes y las coberturas arbóreas y arbustivas hasta la mitad del S.xx (Aurelle *et al.* 2022).

En las latitudes polares dominan los bosques boreales (o Taiga), formados por pastos, tundra y coníferas adaptadas a largos periodos nivales, que conforman masas con mayor desarrollo de la biomasa bajo tierra, siendo la ecorregión con mayor capacidad de almacenamiento de carbono bajo el suelo. Finalmente, los bosques de montaña son ecosistemas donde alternan especies de coníferas y caducifolias con distintos niveles de adaptación a la temperaturas y abundancia hídrica. La composición y estructura de estos bosques varía a lo largo del gradiente altitudinal, hasta llegar al límite climático donde las condiciones de temperatura no permiten el desarrollo de la vegetación (Paulsen and Körner 2014), siendo, en definitiva, muy sensibles a las variaciones climáticas. Además, como en los entornos mediterráneos, son espacios donde las labores pastorales y agrícolas se han abandonado, principalmente por la dificultad de intensificación y mecanización, dando lugar a la creación de espacios de recreo y ocio relacionados con la naturaleza (Price *et al.* 2011, Schirpke *et al.* 2019). Efecto que produce una colonización de los espacios productivos por bosques primarios.

La percepción y uso de los bosques por parte del ser humano ha variado a lo largo de la historia; partiendo de su consideración como una fuente de recursos, pasando por su valoración y protección en función de sus cualidades paisajísticas –nacimiento de las figuras de protección "*Parques*" – hasta su posterior consideración como elemento crucial para el desarrollo sostenible incluyendo la provisión –y necesaria conservación– de numerosos servicios ecosistémicos (Martínez de Pisón 2000, Price *et al.* 2011, Bravo *et al.* 2017) (Fig. 1.1). Desde la transición de sociedad recolectora a sociedad agrícola sedentaria -el mayor cambio acontecido en la historia de la humanidad- hasta finales del S.xix, la naturaleza y el bosque se conciben como un recurso energético (madera, leña) y alimentario (caza, frutos, plantas comestibles), siendo un medio a aprovechar (Ramos-Gorostiza 2007). Con la aparición de las primeras figuras y formas de protección de los montes en

la segunda mitad del S.xix y principios del S.xx (Catálogo de Montes de Utilidad Pública (1862), Parque Nacional de Yellowstone (1872), Parque Nacional de Ordesa y Monte Perdido (1918)) y 1960 (expansión de Parques Nacionales), empiezan a tomarse en consideración los valores paisajísticos y espirituales del medio natural (Martínez de Pisón 2000, Santamarina-Campos 2019). En este periodo comienza a vislumbrarse el inicio de un cambio en la percepción del bosque y de la naturaleza donde estos adquieren una nueva dimensión complementaria a la anterior, en la que se valoran además como un espacio de recreo y disfrute. En la segunda mitad del S.xx, tras la recuperación socioeconómica de la 2ª Guerra Mundial, en Europa y Estados Unidos surgen los primeros movimientos ideológicos bajo el paradigma de la biología de la conservación. Estos movimientos abogan por la implicación institucional y política en la conservación biológica de especies y ecosistemas (Chazdon *et al.* 2016). De éstos nace el concepto de *ecosistema forestal*, que hace referencia a *la "interacción como unidad funcional de plantas, animales y microorganismos entre si y el medio abiótico"* (Conference on Biological Diversity, 2006). Por tanto, a su valoración como recurso energético, alimentario y estético-recreativo, se suma la demanda de su conservación en espacios y paisajes de alto valor ecológico y ambiental (Ojeda-Rivera 1999, Santamarina-Campos 2019).

Las Conferencias de Ginebra (1990) y de Río (1992) inician un nuevo cambio de paradigma donde se pone de relieve la función de mitigación del cambio de climático que desempeñan los bosques y la necesidad de crear redes internacionales de protección. En el Protocolo de Kyoto (UNFCCC 1997) se hace ya referencia expresa a la importancia de las formaciones forestales en el balance de carbono y su potencial regulador del clima. En la entonces Comunidad Económica Europea (CEE) se adoptan los principios de la "*Declaración de Río*" sobre el Medio Ambiente y el Desarrollo sostenible recogidos en la Directiva 92/43/CEE – más conocida como la "Directiva Hábitats" – que inició la creación de una red de conservación y desarrollo sostenible a nivel europeo, la Red Natura 2000. Actualmente, la concepción de la conservación de la naturaleza desde la creación de la Plataforma Intergubernamental sobre Diversidad Biológica y Servicios de los Ecosistemas (IPBES) en 2012, se asienta sobre la combinación de la conservación biológica, el desarrollo sostenible y la preservación de los servicios

ecosistémicos (Daily 1997, Bravo *et al.* 2017). Se aboga por la cooperación internacional para alcanzar una gestión sostenible de los bosques y frenar la degradación ambiental de estos ecosistemas (IPCC 2019). Por tanto, desde un enfoque contemporáneo, en el último informe técnico de clima y territorio (IPCC 2019) se fomenta la implementación de prácticas de gestión forestal sostenible - como el fomento de masas jóvenes los cuales registran mayores tasas de crecimiento – para incrementar el efecto sumidero de los bosques a nivel global.

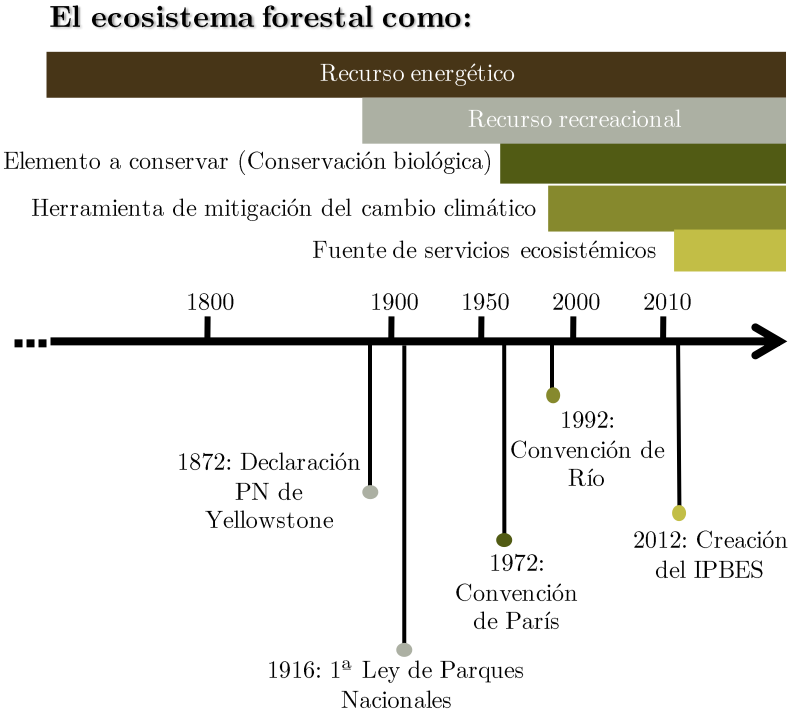

Figura 1.1*: Evolución temporal de la concepción del ecosistema forestal y efemérides asociadas. Elaboración propia.*

1.2. Bosques y cambio global

En la actualidad se reconoce que los ecosistemas forestales del mundo proporcionan servicios y bienes esenciales para la sociedad humana, inter-

viniendo en la regulación y provisión de aguas dulces, suministrando madera y biocombustibles, nutrientes, contribuyendo a la purificación del aire y el secuestro de carbono, entre otros beneficios (Jenkins and Schaap 2018, Albrich *et al.* 2020). Los bosques mediterráneos destacan también por su larga interrelación con las sociedades humanas, en regiones europeas. Además, presentan estrategias adaptativas de recuperación frente a perturbaciones y, a su vez, elevada biodiversidad. Sin embargo, son los bosques de montaña los que proveen de estos servicios a la mitad de la población mundial (Price *et al.* 2011). Siendo estos altamente sensibles a las variaciones climáticas en la región mediterránea, además han sido sometidos a una presión humana intensa hasta la segunda mitad del pasado siglo, lo que conforma un ecosistema mediterráneo de montaña altamente cambiante de especial interés.

El cambio global y sus alteraciones en el sistema Tierra, derivadas de los cambios socioeconómicos acontecidos desde la "*Gran Aceleración*" iniciada en la segunda mitad del siglo XX, amenazan la provisión de estos servicios (Steffen *et al.* 2015). Desde ese momento la población mundial aumenta a un ritmo promedio anual de 81 millones de personas, con un crecimiento del 226% desde 1950 hasta la actualidad (World Bank 2022). El incremento continuo de la población conlleva el aumento paralelo de la actividad industrial y agrícola para satisfacer las crecientes necesidades humanas, desencadenado transformaciones en el territorio e impactos en el medio ambiente, los océanos y la atmósfera. Las emisiones de gases de efecto invernadero (GEI) asociadas a la mayor producción energética y su consumo también se han incrementado drásticamente. Según reporta la Organización Meteorológica Mundial (WMO 2021a) la concentración de CO_2 ha aumentado en un 149%, la de metano (CH_4) un 262%, y un 123% la de óxido de nitrógeno (N_2O) desde la era preindustrial (1750). Las emisiones de GEI ligados al despegue industrial han contribuido a un aumento de la temperatura media global de 1,11ºC (WMO 2021b). Por otra parte, la mayor demanda de alimentos ha incrementado la producción agrícola en un 50% desde principios de siglo XXI (FAO 2020b). Esta mayor capacidad de producción requiere de más superficie de tierras en explotación y con mayor productividad y rentabilidad (FAO 2020b). En las zonas más productivas del planeta existe un proceso masivo de deforestación por el que se han

transformado hasta la fecha 50 millones de hectáreas de bosque en nuevas zonas de cultivo durante los últimos 5 años (FAO, 2020b). Por otro lado, la menor rentabilidad económica y la menor capacidad agronómica de las tierras ligadas a la agricultura tradicional provocan el abandono de las actividades de labranza en zonas de montaña o de difícil mecanización (Alcantara *et al.* 2012, García-Ruiz *et al.* 2015, Lasanta *et al.* 2017) y, por consiguiente, un rápido aumento de masa boscosa joven (Pueyo and Beguería 2007, Rey Benayas *et al.* 2007, Vidal-Macua *et al.* 2018), especialmente notable en Europa. En estas zonas se han llegado a reforestar 25 millones de hectáreas (FAO 2020a). Resulta así un balance global negativo de 25 millones de hectáreas perdidas de bosque a nivel mundial, aunque con manifiestas diferencias espaciales, y con diferentes impactos.

1.3. La dinámica forestal y el régimen de perturbaciones

Los bosques son ecosistemas dinámicos siendo las perturbaciones – entendidas como eventos recurrentes que suponen la alteración drástica de un ecosistema – su principal motor de cambio (Turner 2010). El cambio global está afectando los regímenes de algunas de ellas, alterando su frecuencia, distribución espacial e intensidad y, en último término, amenazando la provisión de servicios ecosistémicos derivados (Daily 1997, Bravo *et al.* 2017, Jenkins and Schaap 2018). En ausencia de influencia antrópica, la dinámica forestal viene marcada por la alteración de un ecosistema por parte de una perturbación. Dependiendo de la severidad y el clima posterior a una perturbación, variará la capacidad de recuperación hacia un ecosistema de características similares o hacia otro diferente (McDowell *et al.* 2020) (Fig. 1.2). Además, dicha capacidad de recuperación está influenciada por el aumento en la frecuencia (y en ocasiones magnitud) de las perturbaciones como efecto directo del cambio global, dificultando el retorno a la madurez reproductiva de las especies existentes, limitando así la recuperación hacia el ecosistema maduro (Peñuelas and Sardans 2021).

Los incendios forestales son la principal perturbación que afecta a los bosques en la Europa Mediterránea. La actividad antrópica (que altera los

patrones de ignición y el mosaico de combustibles), el clima (que condiciona el peligro meteorológico y la humedad del combustible), así como la propia estructura y composición de las comunidades forestales (adaptaciones y resistencia al fuego) modulan su frecuencia, tamaño, intensidad y estacionalidad (Rodrigues *et al.* 2016, Costafreda-Aumedes *et al.* 2017, Turco *et al.* 2018, Aquilué *et al.* 2020, Nolan *et al.* 2020, Rodrigues, Trigo, *et al.* 2020, Kim *et al.* 2021), factores que a su vez están siendo alterados por el cambio global. Estas alteraciones tienen el potencial para modificar los regímenes de incendio hacia situaciones de mayor peligrosidad y riesgo en el futuro (Dupuy *et al.* 2020, Cochrane and Bowman 2021). La ocurrencia de incendios forestales fuera de sus regímenes naturales o culturales tiene efectos negativos en la mortalidad de la vegetación, la erosión del suelo, la cantidad de materia orgánica en el suelo, o la propia capacidad de recuperación de las comunidades forestales, especialmente aquellas menos adaptadas al fuego (Shakesby 2011, Costa *et al.* 2017, Moreira *et al.* 2020). Más aún, eventos extremos de incendio forestal pueden alterar irreversiblemente los hábitats de flora y fauna, la producción de madera, el uso recreativo de las zonas afectadas, los servicios ecosistémicos en general, y afectar a las vidas y propiedades de las personas, pudiendo influir en la salud de la población por sobreexposición al humo incluso a media-larga distancia (Fernandes 2013, Balde and Vega-García 2019).

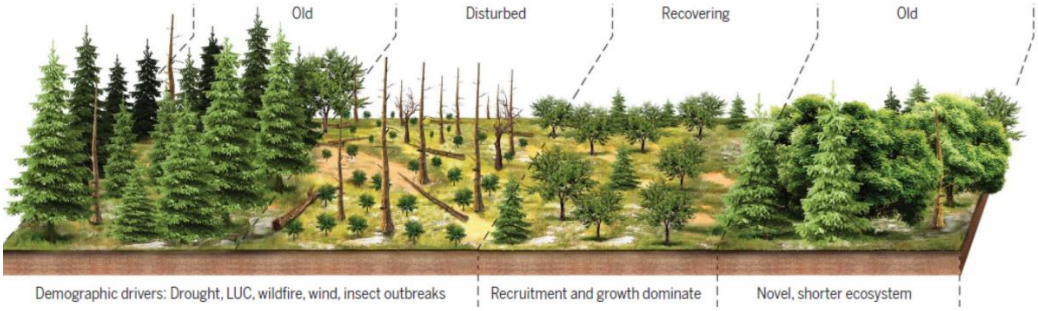

Figura 1.2: *Diagrama conceptual de los componentes de la dinámica forestal. Con permiso de (McDowell et al., 2020).*

Son múltiples las alteraciones ligadas al cambio global y climático que pueden conducir a situaciones más adversas para los bosques en el futuro.

La temperatura es el principal limitante para el desarrollo fisiológico de las especies del estrato arbolado a escala global (Körner and Paulsen 2004). Las bajas temperaturas registradas en los pisos alpinos condicionan el crecimiento de especies arbóreas y propician la existencia de especies únicas adaptadas a estos ambientes (Paulsen and Körner 2014). Los ambientes alpinos son ricos en biodiversidad, albergando una serie de especies adaptadas a las condiciones de alta montaña (Greenwood and Jump 2014). Un aumento de la temperatura condicionaría la supervivencia de esas especies y el desplazamiento de especies desde el piso subalpino al alpino (Greenwood and Jump 2014, Elsen *et al.* 2020). Ligado al calentamiento global se espera un aumento en la intensidad, duración y frecuencia de las sequias en las próximas décadas, ya especialmente severa en el ámbito mediterráneo (Cook *et al.* 2018, Lionello and Scarascia 2018). En estas condiciones se espera no solo un aumento del peligro de incendio (Bedia *et al.* 2014), sino también una reducción en la producción primaria neta (PPN) de las comunidades forestales. Ante una eventual reducción extrema de la PPN es posible que aumente la susceptibilidad a plagas y/o enfermedades (Camarero *et al.* 2015, Sangüesa-Barreda *et al.* 2015, Gely *et al.* 2020). Por otra parte, las plántulas germinadas tras la ocurrencia de un incendio podrían no sobrevivir a episodios de sequía extrema en el intervalo de tiempo inmediatamente posterior a un incendio, condicionando la composición y estructura del futuro bosque. Dado el aumento de la temperatura global, se espera una mayor actividad energética en la atmosfera incrementándose así la intensidad y frecuencia de turbonadas o tormentas de viento que pueden causar altas tasas de mortalidad, reducir la densidad de arbolado y modificar la estructura del bosque (Dale *et al.* 2001, González-Alemán *et al.* 2019). Las posibles interacciones entre perturbaciones (por ejemplo, los derribos por viento o mortalidad por plagas, aumentando la carga combustible) pueden acarrear una pérdida de masa forestal que conllevará una reducción de los servicios ecosistémicos prestados actualmente por los bosques, por ello las estrategias de gestión deben ir encaminadas a paliar la pérdida de estos servicios (Seidl *et al.* 2011, Vilà-Cabrera *et al.* 2018).

1.4. Información geográfica y técnicas de observación del territorio

1.4.1. La teledetección aplicada al ámbito forestal

Para garantizar la conservación de los bosques y su provisión de servicios ecosistémicos forestales frente a la amenaza del cambio global es de vital importancia disponer de información sobre el estado y dinámica de las comunidades forestales. Las tecnologías y ciencias de información geográfica (GIScience and Remote Sensing), entendidas como el conjunto de técnicas que permiten almacenar, procesar y analizar información espacial procedentes de diferentes fuentes (fotointerpretación, teledetección, levantamientos topográficos…) son de gran utilidad para analizar fenómenos de naturaleza espacial y temporal. Los avances vinculados a los sistemas de información geográfica y al tratamiento y análisis de datos espaciales, la disponibilidad y acceso a fuentes de información interoperables, o el desarrollo de nuevos sensores de observación de la tierra proporcionan nuevas y renovadas formas de analizar y entender nuestro planeta y, en concreto, el medio ambiente y las comunidades naturales (Goodchild 2010, Shafique *et al.* 2022).

Una de las disciplinas relacionadas con la información espacial que ha experimentado un progreso más notable durante las últimas décadas es la teledetección. En un sentido amplio la teledetección (o *remote sensing*) se define como el conjunto de técnicas para adquirir información sobre la superficie terrestre mediante dispositivos y sensores remotos, es decir, a través de medios que no entran en contacto directo con el territorio. La teledetección cuenta a día de hoy con una larga tradición y trayectoria en el análisis del medio natural de forma sistemática y continua en el espacio y el tiempo (Cavender-Bares *et al.* 2022). El amplio y variado abanico de instrumentos y datos disponibles en el campo de la teledetección permite abordar el estudio y seguimiento de los espacios forestales desde diversas perspectivas (Lechner *et al.* 2020) (Fig. 1.3). Los sensores son los instrumentos que, a bordo de plataformas o vehículos, captan la información. Existen dos tipologías: los sensores pasivos, los cuales recogen la energía solar reflejada por

la superficie terrestre, mientras que los sensores activos emiten y recogen su propio haz de energía.

Los programas de observación de la Tierra instrumentados mediante sensores pasivos espectrales son los más ampliamente utilizados y accesibles (Zhu *et al.* 2019). En el caso del programa Landsat, su resolución espacial y espectral, sumados a su longevidad, convierten en un producto particularmente apto para realizar análisis diacrónicos de los cambios antropogénicos y naturales acontecidos desde la escala local hasta la global (Roy *et al.* 2014, Masek *et al.* 2020). Los datos derivados de los sensores pasivos permiten aplicaciones forestales como la cartografía de las áreas boscosas (Alcantara *et al.* 2012, Kowalski *et al.* 2020), los cambios de uso del suelo (Wulder *et al.* 2018) o el análisis de severidad de las diferentes perturbaciones (Fernandez-Manso *et al.* 2016, Lizundia-Loiola *et al.* 2020), entre otros. Hoy en día también se apuesta por una mayor resolución temporal de toda la superficie terrestre, a costa de reducir la resolución espacial (e.g.: MODIS, Sentinel 3). Con este tipo de observación se obtienen aplicaciones forestales como por ejemplo el avance de un gran incendio (Wooster *et al.* 2012, Xu *et al.* 2022), la detección de anomalías térmicas en la superficie de la tierra (Libonati *et al.* 2015, Wang *et al.* 2022) o la identificación del tipo de bosque (Alcantara *et al.* 2012, Coops *et al.* 2022). Otra tipología instrumental dentro de los sensores ópticos son los sensores hiperespectrales, muy similares a los anteriores, con el elemento diferenciador de constar de una muy alta resolución espectral (Kumar *et al.* 2020). Este tipo de datos, si bien en auge, no es tan comúnmente utilizado debido al coste de adquisición de éstas imágenes y la escasez de datos de libre acceso. No obstante, ofrecen otras posibilidades de análisis en ambientes forestales como el análisis de las propiedades del suelo (Mzid *et al.* 2022), la cantidad de humedad (Castaldi *et al.* 2015, Yang *et al.* 2022), aplicaciones en sanidad vegetal (Torres *et al.* 2021) y la detección de especies (Vangi *et al.* 2021) y, por consiguientes, estimaciones de diversidad florística.

Por otra parte, los sensores activos son aquellos que registran su propia energía previamente emitida. De esta tecnología destacan los programas de observación radar de apertura sintética (SAR) (Wegmuller and Werner 1995) y Light Detection and Ranging (LiDAR) (Vosselman and Maas

2010). Los sensores LiDAR operar a bordo de plataformas aerotransportadas, circunstancia que no facilita obtener una captura periódica y sistemática como las que ofrecen plataformas satelitales. En el caso de España, , se dispone de un Plan Nacional de Ortofotografía Aérea (PNOA) que pone a disposición pública una doble cobertura LiDAR de todo el territorio a una resolución de 0.5 – 14 puntos/m^2, permitiendo así análisis topográficos – plan concebido para ello – y aplicaciones forestales (Gómez *et al.* 2019). Estos planes, al tener un alto coste económico, solo están disponibles en un número reducido de países[1]. Dada la alta demanda para el desarrollo de aplicaciones forestales, y el incremento constante de las capacidades de almacenamiento, servicio y procesado, las diferentes administraciones han acordado aumentar las densidades de puntos en la futura 3^a cobertura. Por otro lado, en las últimas décadas han proliferado las plataformas satelitales con ins-trumental radar de apertura sintética (SAR) -e.g. Sentinel 1, PALSAR-. La gran mayoría de datos SAR de acceso abierto son capturados en la longitud de onda C, siendo una banda poco idónea para caracterizar la estructura forestal (Schlund and Davidson 2018). En los próximos años, con la puesta en órbita de NISAR por parte de la NASA (banda L - 2024) y BIOMASS por parte de la ESA (banda P – Ago 2023), se abrirán abanicos de posibilida-des de análisis en los análisis de la estructura forestal a diversas escalas. En los últimos años hay experiencias con sensores láser a bordo de plataformas espaciales (e.g. ICEsat y GEDI). La principal ventaja de la tecnología activa frente a la pasiva es la posibilidad de capturar de la estructura vertical del territorio y, por tanto, del bosque (Wulder *et al.* 2012, Listopad *et al.* 2015), permitiendo así el análisis y estimación de parámetros forestales estructurales (Domingo *et al.* 2018, Potapov *et al.* 2021) o estimaciones de biomasa asociada (Sinha *et al.* 2015, Duncanson *et al.* 2020).

1.4.2. Cartografía de la ocupación del suelo e inventarios forestales

Actualmente, instituciones gubernamentales y científicas ponen en abierto una cantidad ingente de datos relativos a la descripción del medio

[1] Países con Plan Nacional de cobertura LiDAR aerotransportado: Canadá, Dinamarca, Eslovenia, España, Estados Unidos, Estonia, Finlandia, Inglaterra, Letonia, Nueva Zelanda, Países Bajos, Polonia y Suecia.

natural y el territorio. Toda esta información auxiliar puede ayudar a comprender y analizar de forma más eficiente las relaciones existentes en la naturaleza. Las bases de datos espaciales más comunes en estudios ambientales son las cartografías de uso del suelo. Existen espacializaciones desde la escala global (Buchhorn et al., 2020), Europea (e.g.: Corine Land Cover – CLC), nacional (e.g.: *Sistema de Información sobre Ocupación del Suelo de España - SIOSE*) o regional (e.g.: *Mapa d'usos i cobertes del sòl de Catalunya*). En el ámbito forestal, estas bases de datos son interesantes desde el punto de vista diacrónico dado que ofrecen información relativa a los cambios sustanciales en la extensión de diferentes ecosistemas. El abanico de aplicaciones varía desde el medioambiente y la salud, como herramienta de soporte para caracterizar ambientes verdes y azules urbanos y la prevalencia de Leucemia en edades tempranas (Ojeda-Sánchez 2022), hasta las referidas a problemas ambientales –e.g. para determinar que parámetros paisajísticos en olivares favorecen las poblaciones de abejas (Pascual 2022). Otras bases de datos de ámbito nacional como los mapas topográficos sirven como base para geoposicionar elementos de interés e introducirlo en modelos para predecir, por ejemplo, la probabilidad de contención de un incendio (Rodrigues, Alcasena, *et al.* 2020). Por otro lado, disponemos de cartografía y bases que guían directamente el conocimiento y caracterización de la vegetación forestal: los Mapas Forestales e Inventarios Forestales. Estas fuentes de datos son las únicas que proporcionan las especies y ocupaciones de las mismas a nivel nacional, lo que abre un abanico de análisis para la modelización forestal (Blanco *et al.* 2020). En cambio, si se pretende caracterizar el impacto de la sociedad sobre algún fenómeno o alteración natural, bases de datos provenientes de censos, campañas estadísticas pueden proveer información georeferenciada de gran utilidad para comprender y modelar las interacciones sociedad-naturaleza.

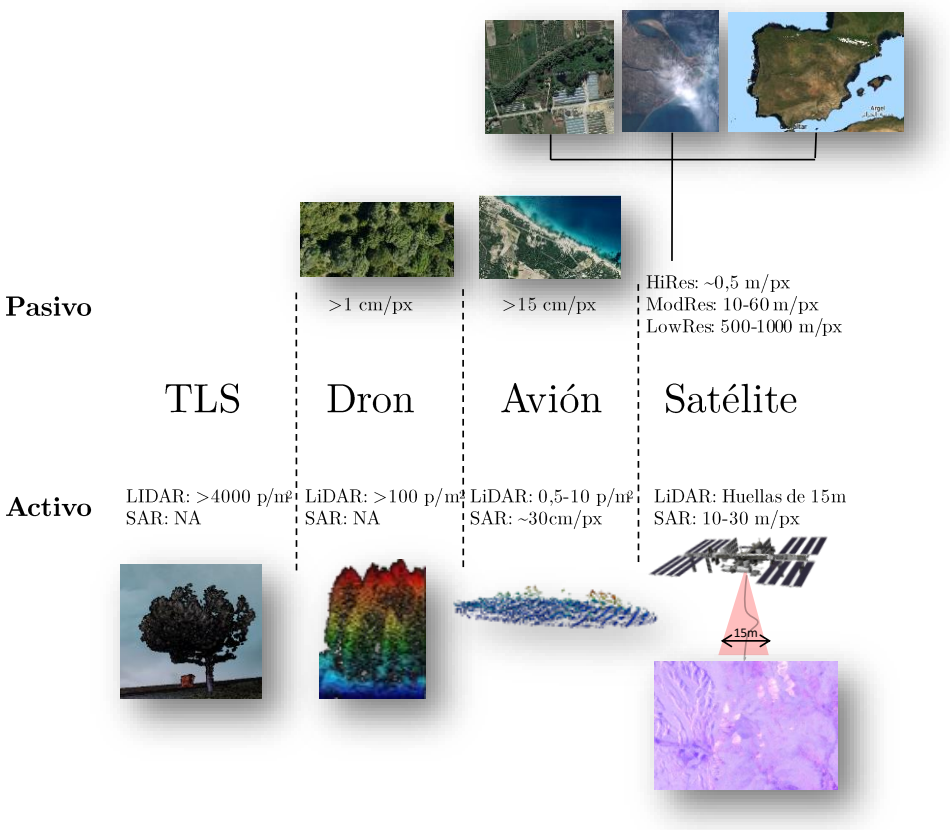

Figura 1.3: *Principales fuentes de datos provenientes de sensores remotos. Elaboración propia.*

1.4.3. Cartografía para la caracterización ambiental

Por otro lado, la caracterización de variables ambientales, como clima, suelo, topografía, tiende a realizarse utilizando productos espacializados a escala global. Un ejemplo es la caracterización climática global pasada (1970-2000) y los escenarios futuros del *Intergovernmental Panel on Climate Change* (IPCC) de Worldclim (Fick and Hijmans 2017). También destaca la espacialización fisicoquímica de suelos a escala global en la BBDD Soilgrids (Poggio *et al.* 2021). Relacionado con el clima destaca el monitoreo de la sequía con el índice *Standardised Precipitation-Evapotranspiration*

*Index (*SPEI) calculado y espacializado a escala global (Vicente-Serrano *et al.* 2010) y los reanálisis del tiempo de las ultimas 4 décadas (Copernicus Climate Change Service 2022).

1.4.4. Escala de los procesos ambientales

Los fenómenos naturales y las alteraciones del medio forestal se producen a diversas escalas espacio-temporales. A modo de generalización, existe una relación directa entre la escala espacial y temporal, entendiéndose que los fenómenos dados a escala de parcela o de comunidad forestal suelen darse en un espacio de tiempo más corto, e.g. defoliaciones. En contraposición, los que suceden a una escala regional o global tienden a producirse de forma más lenta e.g. dinámica general del bosque. Respecto a las perturbaciones, dado que la perturbación se da en un lapso de tiempo reducido, la escala espacial varía según el proceso perturbador. En cambio, el análisis de la recuperación post perturbación se da a la misma escala espacial en la que actúa la perturbación y a una escala temporal muy amplia, dependiente de un conjunto de variables condicionantes de la recuperación. A la hora de trabajar con teledetección en ambientes forestales debe buscarse la fuente de datos que nos ofrezca la escala espacio-temporal necesaria. Los sensores que operan a alta resolución espacial, e.g. drones, satélites de muy alta resolución, son capaces de capturar elementos individuales como los árboles. Además, si estos tienen la copa poco densa pueden dar paso a la captura en imagen de las ramas y el suelo existente bajo la copa conllevando a posibles ruidos generados por la diferencia de reflectividad del suelo y la vegetación y las sombras producidas por las ramas. Por otro lado, bajas resoluciones pueden producir un efecto de suavizado en la respuesta de un fenómeno debido a la diversidad de coberturas o intensidades del fenómeno existentes en un mismo pixel. En definitiva, es recomendable utilizar aquellas fuentes que mejor se adapten a la dinámica espacio-temporal del fenómeno analizado.

1.4.5. Tratamiento de los datos

Los datos espaciales masivos, con el apoyo de los datos auxiliarles, requieren de un tratamiento específico para poder extraer relaciones y conclusiones sobre los fenómenos acontecidos en el sistema natural (Kwenda *et al.* 2022). La naturaleza de los datos y sus grandes tamaños muestrales requieren de la utilización de otras técnicas de análisis más robustas que la estadística tradicional (Arab *et al.* 2022).. En este caso, las técnicas de *machine learning* abren nuevas oportunidades de análisis debido a su flexibilidad y robustez. De forma genérica, los algoritmos de ML presentan mayor flexibilidad ya que no están sujetos a distribuciones predefinidas y pueden capturar fenómenos de comportamiento no lineal, difíciles de analizar con estadística convencional (Rodrigues and de la Riva 2014). Además, "aprenden" el comportamiento subyacente de un sistema a partir de un conjunto de datos, por procedimientos iterativos que los convierten en métodos robustos (Vapnik 1998). A todo esto, se le suma la versatilidad de algunos algoritmos al permitir el modelado de regresión y clasificación (Cortes and Vapnik 1995, Breiman 2001, Liaw and Wiener 2002). Por otro lado, el incremento de las capacidades computacionales, y el nacimiento de nuevas herramientas para el tratamiento de datos también han contribuido al alcance y diseño de nuevas aplicaciones con gran volumen de datos. Destaca la plataforma Google Earth Engine, basada en la nube, que pone a disposición terabytes de datos junto con la capacidad de computación de Google (Gorelick *et al.* 2017) convirtiéndola en una de las herramientas más potentes. Por otro lado, R, junto con Python, es uno de los lenguajes de programación con mayor acogida entre los científicos de datos. Sus principales ventajas son su gratuidad, seguido de la versatilidad y personalización de los análisis estadísticos y visualizaciones. La popularidad de R, entre otros motivos, viene marcada por la revolución de internet, donde usuarios de todo el mundo comparten sus desarrollos y rutinas en forma de paquetes. En el año 2003, punto de inflexión al alza en la popularidad de R, existían

300 paquetes publicados (Tippmann 2015), en la actualidad casi se alcanzan los 19.000 (R Core Team 2022), siguiendo una tendencia exponencial, lo que pone de manifiesto la relevancia y uso extendido de este lenguaje.

Capítulo 2

Justificación de la tesis y objetivos

2. Justificación de la tesis y objetivos

El objetivo central de la presente Tesis es el análisis multiescalar de las alteraciones y perturbaciones que, ligadas al cambio global, alteran el establecimiento, la dinámica y/o la estructura forestal a partir de información obtenida mediante sensores remotos. La tesis aborda el análisis de diversos procesos que se asocian estrechamente con la persistencia y funcionamiento de los sistemas forestales: los incendios forestales, el abandono de tierras de cultivo y el cambio climático. Estos procesos operan a muy diferentes escalas, tanto espaciales como temporales, lo que requiere la utilización tanto de técnicas como de fuentes de información adecuadas. El enfoque seguido es clara y deliberadamente espacial, con el objetivo último no tan solo de comprender cómo operan dichos procesos, sino de evaluar el alcance y magnitud de los efectos que de ellos se derivan. Para ello se plantea dar respuesta a los siguientes objetivos generales (OG1-OG5) a partir de las siguientes hipótesis de partida, (i) capacidad de los sensores activos para caracterizar la estructura forestal; (ii) potencial de los sensores ópticos para analizar dinámicas y cambios en los usos del suelo; (iii) disponibilidad de plataformas y técnicas para el tratamiento de datos masivos.

OG1 – Conocer la dinámica espacio-temporal de la sucesión secundaria a causa del abandono agrícola en áreas montañosas mediterráneas.

OG2 – Analizar qué factores son los principales responsables del reciente abandono agrícola.

OG3 – Caracterizar mediante el uso de sensores activos los factores limitantes que condicionan el desarrollo del arbolado en zonas de montaña.

OG4 - Predecir la expansión de los bosques de montaña bajo los efectos del calentamiento global.

OG5 – Identificación de la ocurrencia y efectos de perturbaciones pasadas sobre masas forestales utilizando sensores activos.

Objetivos específicos

La respuesta a las anteriores preguntas se aborda desde la consecución de los siguientes objetivos:

i. Caracterizar la dinámica espacio-temporal del abandono agrícola en áreas de montaña mediterráneas (OG1-OG2).

ii. Comparar metodologias para la caracterización temporal del abandono agrícola utilizando algoritmos de segmentación temporal (OG1).

iii. Representar la distribución espacial de la probabilidad de abandono de tierras (OG1-OG2).

iv. Conocer la importancia relativa y el efecto marginal de los factores que condicionan la probabilidad de abandono (OG2).

v. Caracterizar la altura de la vegetación a escalas locales y globales (OG3-OG4-OG5).

vi. Análizar de la diversidad estructural en bosques mediterráneos (OG1-OG5).

vii. Estimar la recuperación de la estructura forestal post incendio.

viii. Evaluar la existencia de un patrón segmentado en la relación entre la altura del arbolado y la elevación en los principales bosques de montaña europeos (OG3).

ix. Identificar las variables climáticas que limitan el desarrollo de la vegetación en las principales cadenas montañosas europeas (OG3-OG4).

Publicaciones

Esta Tesis Doctoral està conformada por tres artículos científicos publicados en revistas indexadas de alto impacto y un articulo en preparación.

A continuación, se presentan los datos bibliométicos de las diferentes publicaciones:

Autores	**Título**	**Año**	**Revista**	**Factor de impacto**	**Cuartil**
Gelabert, P.J., Montealegre, A.L., Lamelas, M.T., Domingo, D.	Forest structural diversity characterization in Mediterranean landscapes affected by fires using Airborne Laser Scanning data	2020	*GIScience & Remote Sensing*	6.23	Q1
https://doi.org/10.1080/15481603.2020.1738060					
Gelabert, P.J., Rodrigues, M., de la Riva, J., Ameztegui, A., Sebastià, M.T., Vega-Garcia, C.	LandTrendr smoothed spectral profiles enhance woody encroachment monitoring.	2021	Remote Sensing of Environment	10.16	Q1
https://doi.org/10.1016/j.rse.2021.112521					
Gelabert, P.J., Rodrigues, M., Vidal-Macua, J.J., Ameztegui, A., Vega-Garcia, C.	Spatial explicit modeling of the probability of land abandonment in the Spanish Pyrenees	2022	Landscape and Urban Planning	6.14	Q1
https://doi.org/10.1016/j.landurbplan.2022.104487					
Gelabert, P.J., Rodrigues, M., Coll, L., Vega-Garcia, C., Ameztegui, A.	On the relationship between tree height, elevation and climate in European mountain ranges	n.d.	-	-	-
En preparación. Será enviado a Nature Ecology & Evolution					

Tabla 2.1: *Correspondencia entre los objetivos planteados y las publicaciones relacionadas.*

Objetivos	Publicación
i. Caracterización espacio-temporal del abandono agrícola (OG1-OG2).	Gelabert, P.J., Rodrigues, M., de la Riva, J., Ameztegui, A., Sebastià, M.T., Vega-Garcia, C., 2021. LandTrendr smoothed spectral profiles enhance woody encroachment monitoring. *Remote Sensing of Environment 262, 112521.* https://doi.org/10.1016/j.rse.2021.112521 Gelabert, P.J., Rodrigues, M., Vidal-Macua, J.J., Ameztegui, A., Vega-Garcia, C. (2022) Spatial explicit modeling of the probability of land abandonment in the Spanish Pyrenees. *Landscape and Urban Planning.* https://doi.org/10.1016/j.landurbplan.2022.104487
ii. Comparación de metodológica de la caracterización temporal del abandono agrícola utilizando algoritmos de segmentación temporal y la serie temporal sin ajustar (OG1).	Gelabert, P.J., Rodrigues, M., de la Riva, J., Ameztegui, A., Sebastià, M.T., Vega-Garcia, C., 2021. LandTrendr smoothed spectral profiles enhance woody encroachment monitoring. *Remote Sensing of Environment 262, 112521.* https://doi.org/10.1016/j.rse.2021.112521
iii. Representación de la distribución espacial de la probabilidad de abandono de tierras (OG1-OG2).	Gelabert, P.J., Rodrigues, M., de la Riva, J., Ameztegui, A., Sebastià, M.T., Vega-Garcia, C., 2021. LandTrendr smoothed spectral profiles enhance woody encroachment monitoring. *Remote Sensing of Environment 262, 112521.* https://doi.org/10.1016/j.rse.2021.112521 Gelabert, P.J., Rodrigues, M., Vidal-Macua, J.J., Ameztegui, A., Vega-Garcia, C. (2022) Spatial explicit modeling of the probability of land abandonment in the Spanish Pyrenees. *Landscape and Urban Planning.* https://doi.org/10.1016/j.landurbplan.2022.104487
iv. Conocer la importancia relativa y el efecto marginal de los	Gelabert, P.J., Rodrigues, M., Vidal-Macua, J.J., Ameztegui, A., Vega-Garcia, C. (2022) Spatial explicit modeling of

factores que condicionan la probabilidad de abandono (OG2).	the probability of land abandonment in the Spanish Pyrenees. *Landscape and Urban Planning.* https://doi.org/10.1016/j.landurbplan.2022.104487
v. Caracterización de la altura de la vegetación a escalas locales y globales (OG3-OG4-OG5).	Gelabert, P.J., Montealegre, A.L., Lamelas, M.T., Domingo, D., 2020. Forest structural diversity characterization in Mediterranean landscapes affected by fires using Airborne Laser Scanning data. *GIScience & Remote Sensing.* https://doi.org/10.1080/15481603.2020.1738060 Gelabert, P.J., Rodrigues, M., Coll, L., Vega-Garcia, C., Amezteguí, A. (n.d.) On the relationship between tree height, elevation and climate in European mountain ranges. *In prep.*
vi. Análisis de la diversidad estructural forestal (OG1-OG5)	Gelabert, P.J., Montealegre, A.L., Lamelas, M.T., Domingo, D., 2020. Forest structural diversity characterization in Mediterranean landscapes affected by fires using Airborne Laser Scanning data. *GIScience & Remote Sensing.* https://doi.org/10.1080/15481603.2020.1738060 Gelabert, P.J., Rodrigues, M., Coll, L., Vega-Garcia, C., Amezteguí, A. (n.d.) On the relationship between tree height, elevation and climate in European mountain ranges. *In prep.*
vii. Recuperación de la estructura forestal post incendio	Gelabert, P.J., Montealegre, A.L., Lamelas, M.T., Domingo, D., 2020. Forest structural diversity characterization in Mediterranean landscapes affected by fires using Airborne Laser Scanning data. *GIScience & Remote Sensing.* https://doi.org/10.1080/15481603.2020.1738060
viii. Evaluación de la existencia un patrón segmentado en la relación entre la altura del arbolado y la elevación en los principales bosques de montaña europeos (OG3).	Gelabert, P.J., Rodrigues, M., Coll, L., Vega-Garcia, C., Amezteguí, A. (n.d.) On the relationship between tree height, elevation and climate in European mountain ranges. *In prep.*

ix. Identificación de variables climáticas que limitan el desarrollo de la vegetación en las principales cadenas montañosas europeas (OG3-OG4).	Gelabert, P.J., Rodrigues, M., Coll, L., Vega-Garcia, C., Ameztegui, A. (n.d.) On the relationship between tree height, elevation and climate in European mountain ranges. *In prep*

Capítulo 3

Materiales y métodos

3. Materiales y métodos

3.1. Ámbito de aplicación

Esta Tesis se investigan dos ambientes de interés altamente vulnerables a los efectos del cambio climático: el bosque mediterráneo y los bosques de montaña. El bosque mediterráneo se caracteriza por su adaptación a la sequía estival dado que está dominado por especies xerófilas y esclerófilas. Por otro lado, los incendios en la cuenca mediterránea son una perturbación recurrente (Rodrigues, Jiménez-Ruano, *et al.* 2020) y la vegetación está adaptada con estrategias de respuesta al fuego como la pirofilia –aquellas plantas que su reproducción viene estimulada por el fuego- (Le Houerou 1974, Nolan *et al.* 2021). A pesar de estas adaptaciones, es esperable una alteración hacia regímenes de incendio relacionados con mayor peligro de incendio bajo los escenarios de cambio climático, limitando así la disponibilidad de semilla y, por ende, la capacidad de regeneración de las zonas perturbadas (Pausas and Keeley 2014). Además, en zonas de montaña, es ampliamente conocido que el desarrollo de la vegetación responde a factores hídricos y térmicos (Paulsen and Körner 2014). Dadas las proyecciones de cambio climático, es esperable un aumento de la temperatura dando lugar así un desplazamiento cota arriba de las condiciones climáticas actuales en las zonas de montaña. Este desplazamiento puede comportar cambios en la productividad, sugiriéndose aumentos en las cotas más elevadas y una reducción en las cotas más bajas (Albrich *et al.* 2020). Dadas estas posibles alteraciones en sendos ambientes, resulta de alto interés el análisis y monitorización de la adaptación de estos ecosistemas al cambio climático. Finalmente, son destacables las nuevas oportunidades de seguimiento de los fenómenos naturales con las nuevas tecnologías (Gómez *et al.* 2019). No obstante, es necesario considerar un compromiso entre la escala a la que opera el fenómeno natural y a la que registra el sensor elegido (Lechner *et al.* 2020). En el presente caso se ha optado por seleccionar la mejor tecnología disponible que permitiera caracterización espacio-temporal del fenómeno analizado. A continuación, se detallan los diferentes recursos utilizados.

3.2. Fuentes de información utilizadas

3.2.1. Teledetección y técnicas de observación del territorio

Las imágenes procedentes de sensores ópticos a bordo de plataformas satelitales nos permiten un seguimiento sistemático de la superficie terrestre. Estos sensores registran la cobertura terrestre a diferentes longitudes de onda permitiendo así adaptar los análisis a la respuesta espectral de las diferentes coberturas de interés (Wulder *et al.* 2018). Concretamente, Landsat es el programa de observación de la tierra más longevo, permitiendo así analizar los cambios en la cubierta terrestre desde la década del año 1972 hasta la actualidad. Sumado a la longevidad, destaca por la resolución espacial – de 30 m- y espectral -visible, infrarrojo cercano e infrarrojo de onda corta-, propiedades que convierten a esta fuente de datos en un recurso apto para monitorizar y analizar la evolución de los bosques (Roy *et al.* 2014, Masek *et al.* 2020). Como ejemplos a nivel internacional destaca el uso de estos datos dentro del marco de la detección de perturbaciones (Kennedy *et al.* 2010, Hermosilla *et al.* 2018, Peñuelas and Sardans 2021), el inventario nacional de la captura carbono en Australia (Lehmann *et al.* 2013) o la monitorización de la deforestación en bosques tropicales (Smith *et al.* 2019). Por otro lado, en ambientes mediterráneos ha sido ampliamente utilizado para caracterizar los efectos de los incendios forestales, desde estimaciones y calibraciones de modelos de severidad (Fernández-García *et al.* 2018, 2019), caracterización de recuperación post incendio (Fernandez-Manso *et al.* 2016, Viana-Soto *et al.* 2017) o la evaluación de la dinámica de la biomasa (Gómez *et al.* 2019). Por lo referido a tratamiento y preparación de datos destinados al análisis de ambientes forestales, el tratamiento individual de las bandas espectrales ha demostrado no tener el potencial que pueden llegar a tener las transformaciones e índices espectrales que combinan varias regiones espectrales. En este sentido, los ejes *tasseled cap* (Crist and Cicone 1984), transformación espectral diseñada para derivar indicadores espectrales resumidos en los tres ejes de brillo, verdor y humedad, han resultado de alta utilidad para el análisis fenológico o para la

caracterización estructural de masas boscosas. Para poder analizar la evolución del bosque en espacios abiertos (OG1), se ha optado por el uso de un conjunto de imágenes Landsat TM, ETM+ y OLI entre 1984 y 2019, ubicadas entre los *paths* 197-200 y las *rows* 30 y 31. Se obtuvieron las imágenes ya transformadas en valores de reflectividad en superficie y con las correcciones atmosféricas, geométricas y radiométricas aplicadas por el equipo científico de la misión. Concretamente se adquirieron 642 imágenes repartidas de la siguiente manera: primavera (marzo-mayo, 213 imágenes), verano (junio-agosto, 216) y otoño (septiembre-noviembre, 213). Al trabajar con diferentes sensores, el primer paso consistió en homogeneizar los valores espectrales de toda la serie temporal, para ello se harmonizan para que los datos del sensor OLI fueran comparables con los datos de los sensores TM/ETM+; las imágenes se transformaron utilizando los coeficientes derivados de las relaciones lineales encontradas en Roy et al., (2016). A continuación, agregamos los valores temporales a través del cálculo del medoide anual – valor que alberga la mínima disimilaridad media con resto de valores - a nivel de píxel sobre cada periodo estacional.

Por otro lado, los sensores activos, a diferencia de los pasivos, emiten su propio haz energético y penetran el dosel de la vegetación, posibilitando el análisis de la estructura forestal mediante la información tridimensional adquirida. En el caso concreto de los sensores LiDAR-ALS (*Laser Detection and Ranging - Airborne Laser Scanner*) de puntos discretos son sensores de uso ampliamente extendido en la ciencia forestal. Particularmente existen aplicaciones para la estimación de biomasa (Domingo *et al.* 2018, 2019), de variables estructurales propias de los inventarios forestales (Wulder *et al.* 2012, Coops *et al.* 2022) y modelos de combustibles (Domingo *et al.* 2020). El principal limitante de esta tecnología es su alto coste de adquisición y la falta de bases de datos públicas en gran parte del mundo. A pesar de ello, en España existen varias coberturas públicas y accesibles bajo el *Plan Nacional de Ortofotografía Aérea (PNOA).* Las coberturas LiDAR-ALS del PNOA primeramente fueron concebidas con el objetivo de generar cartografía topográfica de referencia de alta precisión. No obstante, la comunidad científica ha sabido poner en valor estos datos y darles una nueva aplicación en la ciencia forestal (Gómez *et al.* 2019). Tanto que las nuevas

coberturas, acompañadas del avance tecnológico, dispondrán de mayor densidad permitiendo análisis más detallados de la estructura forestal. En relación con lo anterior, para poder caracterizar la estructura forestal postincendio (OG5) se utilizaron los datos *Light Detection and Ranging* (LiDAR) del *Plan Nacional de Ortofotografía Aérea* (PNOA), concretamente los datos de la segunda cobertura servidos por el *Instituto Geográfico de Aragón* (IGEAR). Concretamente, los datos son generados por el sensor Leica ALS80, el cual opera en la región del infrarrojo próximo (1.064 µm). Una vez depurado el producto obtenido, las densidades de la nube de puntos varían entre 1.1 y 2.0 puntos/m^2, con una precisión vertical de ±10 cm y una horizontal inferior a 30 cm.

En cambio, si se pretende trabajar a una escala regional o global (OG3 y OG4) el LiDAR aerotransportado de onda discreta no es la fuente de datos idónea dada su densidad de observaciones y su costoso tratamiento computacional. No obstante, recientes iniciativas como la de *Global Ecosystem Dynamics Investigation* (GEDI -Dubayah, Blair, *et al.* 2020) que proveen de datos capturados por un sensor láser de onda continua, siguiendo el patrón orbital de la estación espacial internacional, operan a la resolución adecuada para este tipo de análisis. El sensor GEDI está instrumentado con 3 láseres, uno de los cuales se divide en dos haces de cobertura, mientras que los otros dos permanecen a plena potencia. Cada uno de estos 4 haces se trasloca cada dos disparos, lo que permite producir 8 transeptos de datos separadas 600 m entre sí. En todos los casos, los centros de las huellas están separados por 60 m en la dirección de la órbita (Fig. 3.1) con una geolocalización muy precisa, mostrando precisiones muy altas, errores inferiores a 8 m en horizontal y de 10 cm en vertical (Dubayah, Blair, *et al.* 2020). Finalmente, comentar que la metodología diseñada por el equipo científico de la misión para calcular la altura del arbolado se basa en la resta entre el retorno más alto (primer retorno) y la elevación, interpretada como la moda del valor más bajo en la onda recibida (Fig. 3.2) (Dubayah, Hofton, *et al.* 2020).

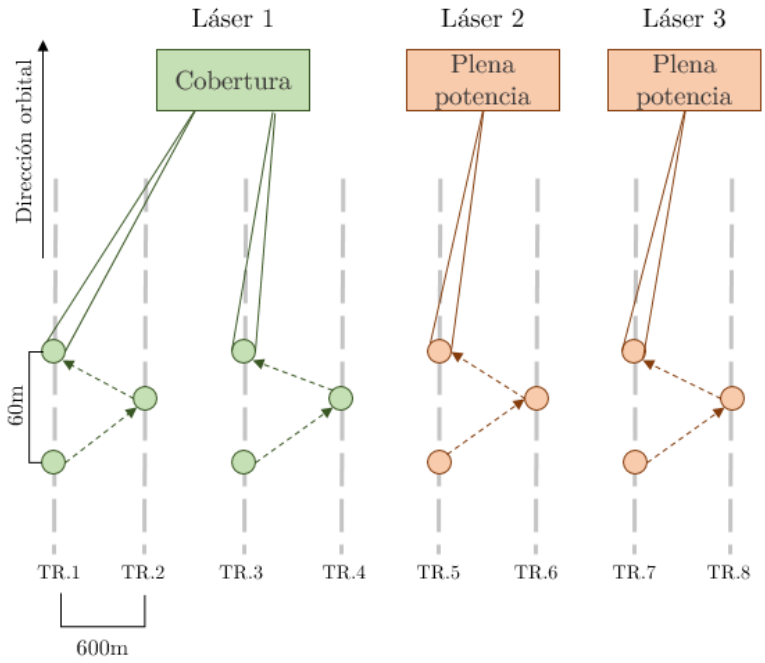

Figura 3.1: *Patrón de escaneo de GEDI. Elaboración propia.*

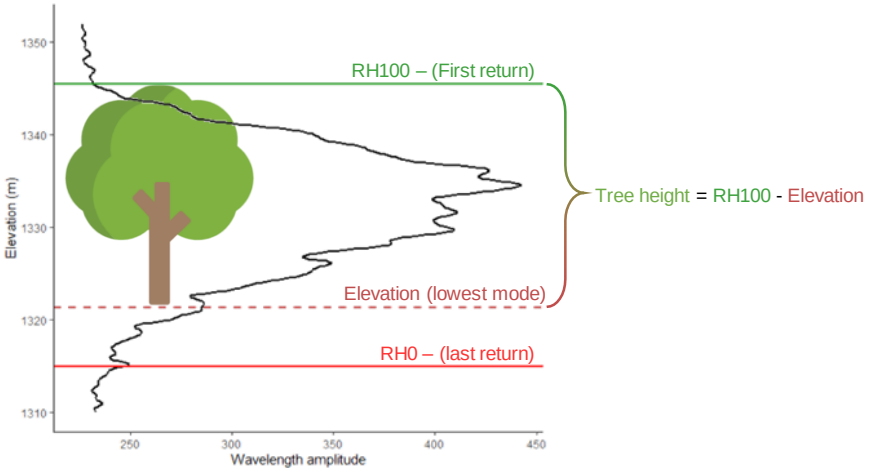

Figura 3.2: *Onda recibida de GEDI y métricas para derivar la altura del arbolado. Elaboración propia.*

3.2.2. Cartografía de ocupación del suelo y ortofotos

Las bases de datos y cartografías temáticas referidas a usos del suelo son uno de los productos cartográficos básicos con un uso extendido en diferentes disciplinas. La evolución de los usos del suelo es crucial para entender procesos socioeconómicos y ambientales subyacentes que se reflejan en la dinámica y cambio de los mismos (Wulder *et al.* 2018). Existen diversidad de productos elaborados a distintas escalas, desde la global (GlobCover) a la de país o región (SIOSE o Mapa de Cobertes del Sòl de Catalunya). Por otro lado, las ortofotografías, son imágenes de alta resolución, capturadas desde avioneta, que sirven de apoyo para la generación de las cartografías de usos del suelo más detalladas y para interpretar fenómenos que operen a una escala mayor y no sean capturados en la cartografía, como por ejemplo el avance del bosque (OG1). En el marco de esta tesis se utilizó el SIOSE 2014 como cartografía base para guiar la fotointerpretación y, posteriormente, generar información de referencia para calibrar un modelo de clasificación supervisada con el fin de predecir avances anuales de cobertura boscosa sobre pastos y cultivos en los Pirineos. La fotointerpretación fue realizada con las series de imágenes detalladas a continuación (Tabla 3.1):

Tabla 3.1: *Resumen de ortofotografías utilizadas.*

Ámbito	**Institución**	**Programa**	**Escala**	**Resolución**	**Año de captura**
España	IGN	PNOA	1:15.000	0,25 m	2017-2018
España	IGN	OLISAT	1:30.000	0,50 m	1997 & 1999
España	IGN	SIGPAC	1:40.000	0,50 m	1997, 2002 & 2003
Cataluña	ICGC	-	1:5.000	0,50 m	1988
Navarra	IDENA	-	1:5.000	0,50 m	1982

Finalmente, los mapas topográficos son cartografías usadas como referencia para georreferenciar e identificar elementos singulares que sean de interés para caracterizar fenómenos socioeconómicos. En caso de esta tesis, la Base Topográfica Nacional 1:25000 (BTN25) ha sido de gran utilidad para el posicionamiento de las infraestructuras turísticas, los núcleos urbanos y carreteras como variables explicativas del proceso de abandono rural en el Pirineo (OG2).

3.2.3. Datos para la caracterización territorial y ambiental

En la última década, numerosos productos para la caracterización ambiental han sido puestos a disposición pública. Por lo general, son productos que registran fenómenos ambientales a escala global, como por ejemplo WorldClim 2.0 (Fick and Hijmans 2017), Soilgrids (Poggio *et al.* 2021), ERA5 (Copernicus Climate Change Service 2022), mapa global de la altura del arbolado (Potapov *et al.* 2021). La sequía es una perturbación que supone grandes perjuicios para la agricultura la economía y el medio ambiente (Marengo *et al.* 2022). Desde un punto de vista agrícola, resulta una variable importante a la hora de analizar el peso de las variables bioclimáticas ante el abandono de tierras (Lasanta *et al.* 2017). En este sentido, el *Standardized Precipitation Evapotranspiration Index* (SPEI) es un índice que brinda información relativa al balance hídrico a diferentes escalas temporales y una resolución espacial de 1 grado decimal a escala global (Vicente-Serrano *et al.* 2010). Además, las propiedades fisicoquímicas del suelo también pueden influir en la productividad agrícola y favorecer el abandono en aquellas tierras menos productivas, para ello se recurrió a la base de datos de SoilGrids que es una cartografía global de la distribución espacial de las propiedades del suelo a una resolución espacial de 250 m (Poggio *et al.* 2021). Concretamente, se utilizó la densidad aparente del suelo como aproximación de la porosidad del suelo, parámetro físico del suelo limitante en cultivos (Koulouri and Giourga 2007).

El clima es uno de los principales moduladores de las diferentes dinámicas acontecidas en los bosques. La colección de datos meteorológicos para elaborar resúmenes climáticos resulta compleja, ya sea por la poca disponi-

bilidad de estaciones meteorológicas en según qué zonas (e.g. zonas de montaña (Gonzalez-Hidalgo *et al.* 2020) o por las diferencias tecnológicas y protocolarias en la captura y recolección de los datos entre diferentes países del mundo. Para evitar los motivos anteriormente expuestos, y por la alta resolución espacial (~1 km^2) WorldClim 2.0 se convierte en una fuente de datos idónea para analizar relaciones climáticas a escala global o regional (Fick and Hijmans 2017). Además de ofrecer un conjunto de datos con la serie histórica, cuenta con las proyecciones de cambio climático bajo diferentes trayectorias predichas por diferentes modelos recogidos en el último informe del IPCC (IPCC 2022). Cabe destacar que en el nuevo informe del IPCC se han modificado los escenarios de concentraciones de gases GEI por trayectorias socioeconómicas compartidas (SSP - *Shared Socioeconomic Pathways*), es decir, escenarios que consideran los posibles cambios socioeconómicos a escala global hasta el 2100. A continuación, se presenta una tabla resumen (Tabla 3.2) con los diferentes escenarios, los diferentes supuestos de políticas ambientales, forzamiento radiativo – definido como la diferencia entre la insolación absorbida por la Tierra y la energía irradiada de vuelta al espacio – y el rango de incremento de temperaturas esperado.

Tabla 3.2: *Descripción de los diferentes Shared Socioeconomic Pathways contemplados en el 6º Informe del IPCC (IPCC 2022).*

Escenario	**Descripción**	**Forzamiento radiativo (W/m^2)**	**Δ Temperatura (ºC)**
SSP1-1.9	Escenario de muy bajas emisiones de GEI con políticas de sostenibilidad desarrolladas a escala global. Con el objetivo de alcanzar cero emisiones de CO_2 en 2050	1,9	1-1,8
SSP1-2.6	Escenario de bajas emisiones de GEI con políticas de sostenibilidad desarrolladas a escala global. Con el objetivo	2,6	1,3-2,4

	de alcanzar cero emisiones de CO_2 en 2075		
SSP2-4.5	Escenario con un volumen de emisiones de GEI intermedio. Donde exista una rivalidad entre estados lo que propiciaría una lucha por recursos y una baja prioridad a nivel internacional por los problemas ambientales.	4,5	2,1-3,5
SSP3-7.0	Escenario con un alto volumen de emisiones de GEI donde se incrementan las desigualdades socioeconómicas entre diferentes partes del mundo y las políticas ambientales se reducen al ámbito local de las zonas con mayor riqueza.	7,0	2,8-4,6
SSP5-8.5	Escenario con un alto volumen de emisiones de GEI donde se triplicarían las emisiones de cara al 2075. Donde habría un gran desarrollo económico ligado a la explotación y dependencia masiva de combustibles fósiles.	8,5	3,3-5,7

3.3. Métodos

Los lenguajes de programación han supuesto un punto de inflexión en el tratamiento de datos, siendo en la actualidad uno de los lenguajes más utilizados en los campos de *machine leaning,* biomedicina, tratamiento de datos e bioinformática (Davidson *et al.* 2019). R fue diseñado a principios de los años 90 como una implementación en software libre del lenguaje estadístico S. El hecho de ser un software libre, y la existencia de una fuerte comunidad desarrolladora y de mantenimiento ha propiciado un incremento de su popularidad a lo largo del tiempo. En el año 2003 se da un punto de inflexión en la popularidad de R donde se pasó de 300 paquetes publicados por diferentes desarrolladores (Tippmann 2015) hasta los 19.000 que existen

actualmente siguiendo una tendencia exponencial (R Core Team 2022). La existencia de este lenguaje ha permitido el desarrollo de análisis a escalas regionales en amplios intervalos de tiempo. Particularmente, en la presente Tesis se ha utilizado como herramienta de tratamiento y procesado de datos.

3.3.1. Machine learning

En todos los capítulos se han utilizado diversas técnicas de modelado para poder analizar las relaciones existentes. Se han usado técnicas estadísticas convencionales y, a medida que se trabajaba un mayor volumen de datos, con técnicas de *machine learning* (ML). Los algoritmos de ML no están sujetos a distribuciones predefinidas y "aprenden" el comportamiento subyacente de un sistema a partir de un conjunto de datos. Por tanto, la versatilidad y robustez postula estas técnicas como idóneas para trabajar con grandes bases de datos de información espacial (Kotsiantis *et al.* 2006, Arab *et al.* 2022).

El algoritmo de ML más sencillo utilizado es el de K-vecinos más próximos (k-NN) (Fix and Hodges 1951). k-NN es una técnica no paramétrica de aprendizaje supervisado: en procesos de clasificación se asigna una categoría a un elemento en base a la categoría mayoritaria de los k elementos más cercanos. La Fig 3.3 representa un ejemplo en el cual se pretende clasificar el color. En el primer caso, donde se eligen los 3 vecinos más próximos (k=3) el color asignado resultaría el *verde*. Mientras que, en el caso de k=5 el color asignado seria *naranja* (Fig. 3.3). Las principales limitaciones de este algoritmo hacen referencia al tamaño muestral y al dimensional. Al ser un algoritmo basado en distancia, el incrementar el número de observaciones y dimensiones puede suponer un cálculo más lento y un peor ajuste.

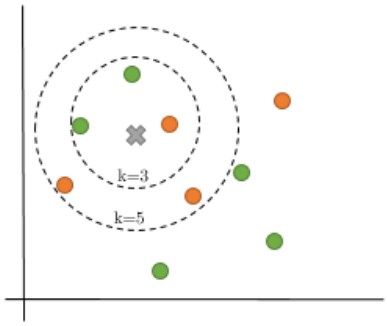

Figura 3.3: *Funcionamiento teórico de k-NN. Elaboración propia.*

Por otra parte, *Random Forest* (RF) es un modelo de ensamblaje de árboles de decisión (Breiman 2001). Los árboles de decisión son métodos muy sensibles a la estructura de los datos y pequeñas alteraciones en ellos pueden producir resultados muy diferentes. Para revertir ese efecto, RF usa la técnica de bagging (*Bootstrap + aggregating*) que consigue la generación de diversos modelos – árboles de decisión- a partir de submuestras aleatorias de los datos de entrenamiento, lo que disminuye la varianza y evita un sobreajuste. Finalmente, predice los valores en cada uno de los árboles, asignando el valor mayoritario o moda en el caso de la clasificación y en los casos de regresión el valor promedio de todas las predicciones. En cuanto a rasgos metodológicos generales, en RF cada nodo se divide por medio del umbral de máxima división de los datos en la mejor variable. Este valor se estima a partir de métricas como la impureza de gini, la ganancia de información o la entropía.

Operacionalmente, RF necesita ser parametrizado. El paquete *Caret* de R (Kuhn, 2008) nos permite optimizar el mejor ajuste de los siguientes parámetros. *"mtry"* numero de variables seleccionadas aleatoriamente en

cada iteración, y el número mínimo de observaciones en cada nodo. A continuación, se presenta una figura resumen del funcionamiento del algoritmo como clasificador (Fig. 3.4).

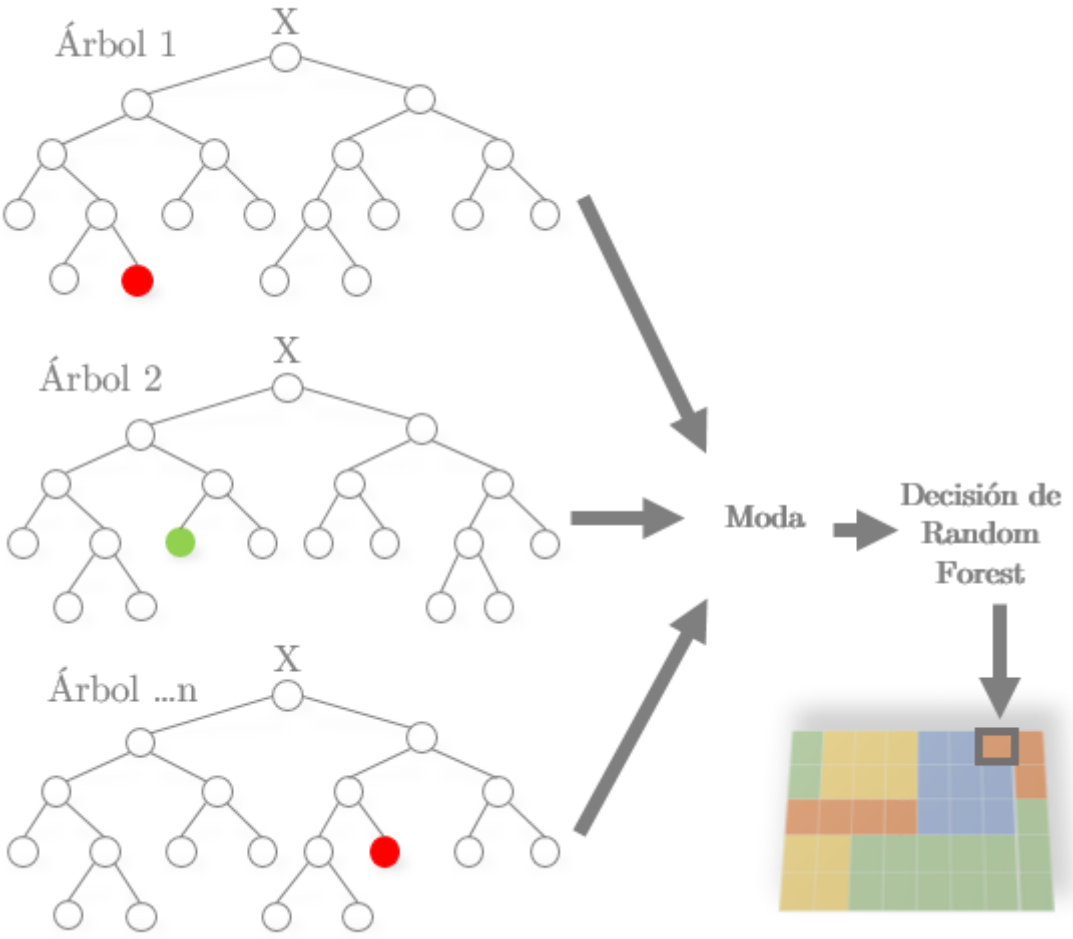

Figura 3.4: *Ejemplo ilustrativo del funcionamiento de un modelo de clasificación Random Forest. Elaboración propia.*

Support Vector Machines (SVM) (Cortes and Vapnik 1995) es un método de aprendizaje supervisado optimizado para analizar datos y reconocer patrones. Al igual que RF, SVM, puede ser utilizado para resolver problemas de regresión y de clasificación. El funcionamiento de SVM se basa en encontrar el hiperplano máximo de separación entre clases. Para ello, se plantean los hiperplanos negativo y positivo definidos por los vectores de soporte, que son aquellas observaciones que interceptan el hiperplano. Finalmente, en el espacio central existente entre los hiperplanos previamente definidos se define el *hiperplano de separación optima*, que nos permite asignar la categoría correspondiente a cada observación (Fig. 3.5). Un modelo de SVM, como otras técnicas de ML, requiere de parametrización. Primero debe establecerse la función del kernel (lienar, polinomial, sigma o radial), además del parámetro cost que hace referencia al coeficiente de penalización (error permitido), y el parámetro gamma que se define como el radio del área de influencia de los vectores de soporte.

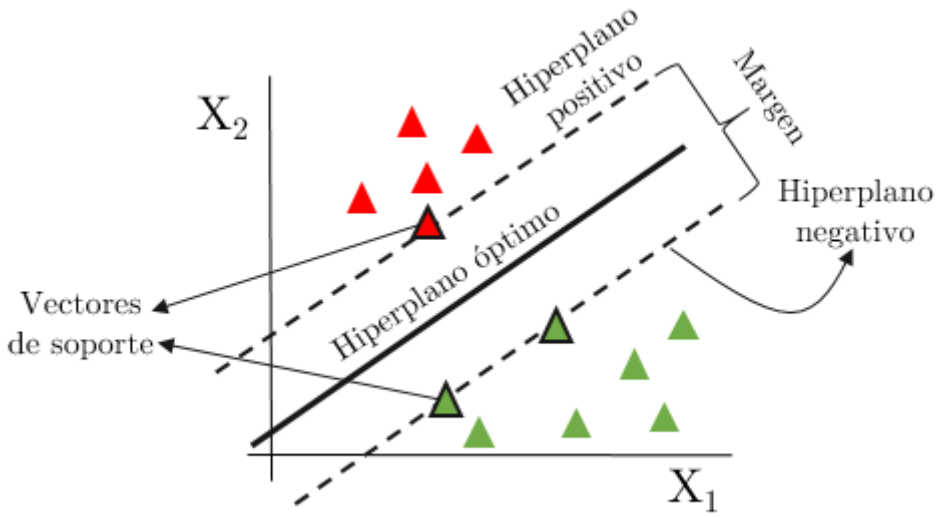

Figura 3.5: *Fundamento teórico de algoritmo support vector machine con kernel lineal. Elaboración propia.*

3.3.2. Estadística convencional

Finalmente, en el último capítulo se ha optado por el uso de técnicas de modelado convencionales. Al observar una respuesta no lineal de la relación entre la altura del arbolado y la cota, se ha procedido a usar modelos lineales segmentados y modelos gaussianos. Los primeros están definidos por modelos lineales "segmentos" y los puntos de corte que definen los segmentos (Eq. 3.1 - definición de un modelo de dos segmentos). Por otro lado, conocida la forma descrita por la relación de variables, también se utilizó el modelo gaussiano que describe la curva formada por la campana de Gauss (Eq. 3.2).

$$\log(y) = \begin{cases} \alpha_1 + \beta_1 \cdot x \; \forall x \; \leq \Psi \\ \alpha_2 + \beta_2 \cdot x \; \forall x \; > \Psi \end{cases} \# \tag{3.1}$$

Dónde α1 and α2 son las intercepciones, β1 y β2 son las pendientes de las relaciones por encima y debajo del punto de corte, mientras que ψ es el punto de corte.

$$\mathrm{y} = exp\left[-\frac{1}{2}\left(\frac{x-a}{b}\right)\right]^2 \tag{3.2}$$

Donde a y b son parámetros estimados por el modelo.

3.3.3. Otras plataformas y algoritmos

Hoy en día existen múltiples productos de teledetección en acceso abierto, todo ello sumado a un uso de computación y almacenaje en la nube sin precedentes supone una revolución en el tratamiento de datos de teledetección satelital. Esta nueva era de la teledetección en la nube está siendo

liderada por la plataforma *Google Earth Engine* dado que ofrece un amplio catálogo de información y una potente plataforma de procesamiento en nube, agilizando así los procedimientos y análisis espaciales a escalas globales y en rangos temporales amplios (Gorelick et al., 2017). Tras la apertura del archivo Landsat al uso del público general en 2008 se inician los análisis de series temporales (Roy *et al.* 2014), que en la actualidad se han vuelto más comunes desde la aparición de las plataformas de procesado en nube (Pasquarella *et al.* 2022). Dado el interés de la comunidad científico-técnica en análisis de series temporales desde diversas instituciones científicas se diseñan los algoritmos de segmentación espacio-temporal (i.e. CCDC, LandTrendr). En esta tesis se ha utilizado LandTrendr (LT - Kennedy et al., 2010) (OG1), un algoritmo diseñado para la detección y aislamiento de cambios mediante la segmentación temporal de las trayectorias espectrales. En líneas generales, el algoritmo calcula el medioide que agrega los valores espectrales de cada rango temporal seleccionado por año (e.g. los meses de junio, julio y agosto de cada año). Sobre esos valores agregados, las trayectorias de las series temporales originales se simplificaron de forma iterativa identificando los vértices clave del cambio. Una vez identificados los vértices potenciales, se eliminan uno a uno, de manera recursiva, hasta encontrar el modelo segmentado que ofrezca un mejor ajuste. El algoritmo, como datos de salida, ofrece las imágenes con los valores ajustados con el modelo segmentado, y una ristra de métricas del segmento de interés, como los valores inicial y final del segmento; la magnitud; el año de detección de inicio del segmento o la duración del mismo (Fig. 3.6).

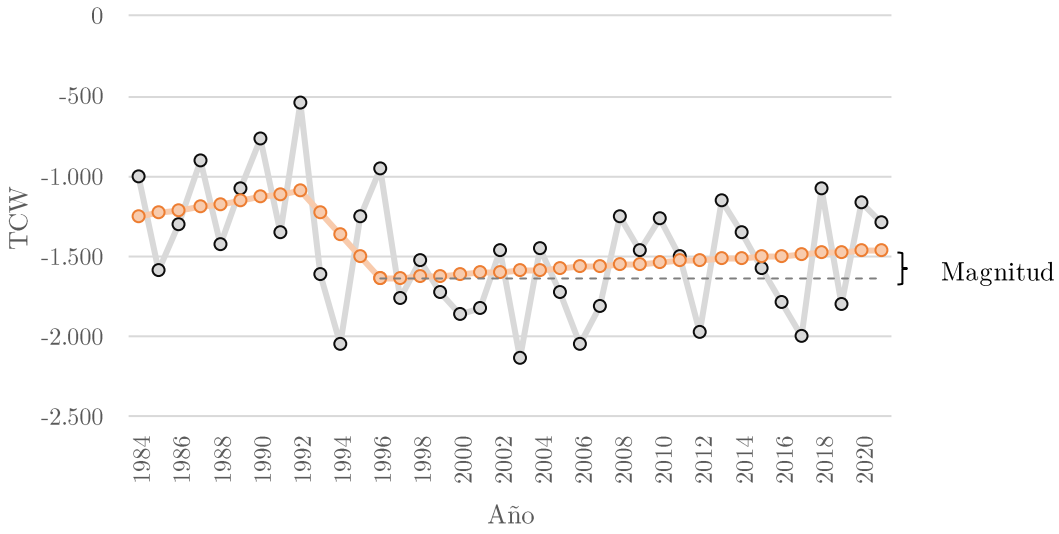

Figura 3.6: *Ejemplo segmentación temporal con LT. En el que se representa la magnitud como la diferencia entre el valor inicial y final del segmento de interés. Elaboración propia.*

3.3.4. Índices de diversidad aplicados al análisis de recuperación de la estructura forestal post incendio

Los conjuntos de datos públicos de LiDAR aéreo han brindado nuevas oportunidades para el análisis de la estructura forestal. En el caso particular de esta tesis, se pretende caracterizar la estructura post incendio e intentar discernir si existen diferencias significativas en estructura entre diferentes masas e intervalos de tiempo de recuperación. Para poder analizar la estructura, esta debía transformarse en un valor numérico continuo que posibilite los análisis cuantitativos. Es por ello que se recurrió a la adaptación de los índices de *diversidad de Shannon* (Eq. 3.3) y el de *uniformidad de Pielou* (Eq. 3.4) a los datos LiDAR, diseñada por Listopad et al., (2015), para resumir las diferentes estructuras forestales a nivel de pixel. La adaptación de los índices sigue la siguiente formulación:

$$LHDI = -\sum[(p_h) \times ln(p_h)] \tag{3.3}$$

$$LHEI = \frac{LHDI}{ln(p_h)} \tag{3.4}$$

Donde p es la proporción de retornos en el intervalo h (definidos cada 0,15;0,3 y 0,5 m).

3.4. Análisis espacial

El análisis espacial puede ser definido como el análisis cuantitativo de las relaciones espaciales ente diferentes fenómenos, siendo de suma relevancia la posición, distancia y superficie de los mismos (Olaya 2020). Por tanto, los análisis espaciales han sido fundamentales para la generación de nuevas variables y para el análisis del comportamiento de las mismas. Dentro de los principales grupos de técnicas de análisis espacial – superposición, distancia, y distribución – se han utilizado distancias euclidianas, densidad de observaciones y combinaciones de información por superposición.

Las distancias euclidianas u ordinarias, definidas como la longitud del segmento recto que separa dos puntos, nos ha servido para transformar variables discretas (e.g. localización pistas de esquí) en variables continuas (ráster con valores representando la distancia más corta entre el centro del píxel y el elemento de interés). En cambio, si se pretende transformar una variable discreta numérica (e.g.: superficie parcelaria) en una continua debe recurrirse a la densidad kernel definida como una función de densidad para crear una magnitud de unidades por área. Este procedimiento devuelve un conjunto de datos continuo, en formato ráster, donde se agregan los valores de todas las superficies de kernel en el centroide de cada celda. Además, puede ser ponderado por el valor de una variable obteniendo así un valor relativo a las unidades de medida de la misma. Finalmente, los análisis espaciales de superposición han servido para realizar consultas espaciales, y

así poder ubicar información bajo unos criterios definidos, y los de intersección para poder vincular las diferentes informaciones en un único conjunto de datos.

A modo de resumen (Fig. 3.7), se han utilizado informaciones procedentes de sensores ópticos, concretamente Landsat 5-7-8; de sensores activos como GEDI y la segunda cobertura del LiDAR-PNOA. Por otro lado, informaciones explicativas se han derivado de BBDD globales como WorldClim, GridSoils o SPEI, y de cartografías específicas como SIOSE o el Mapa topográfico 1:25.000.

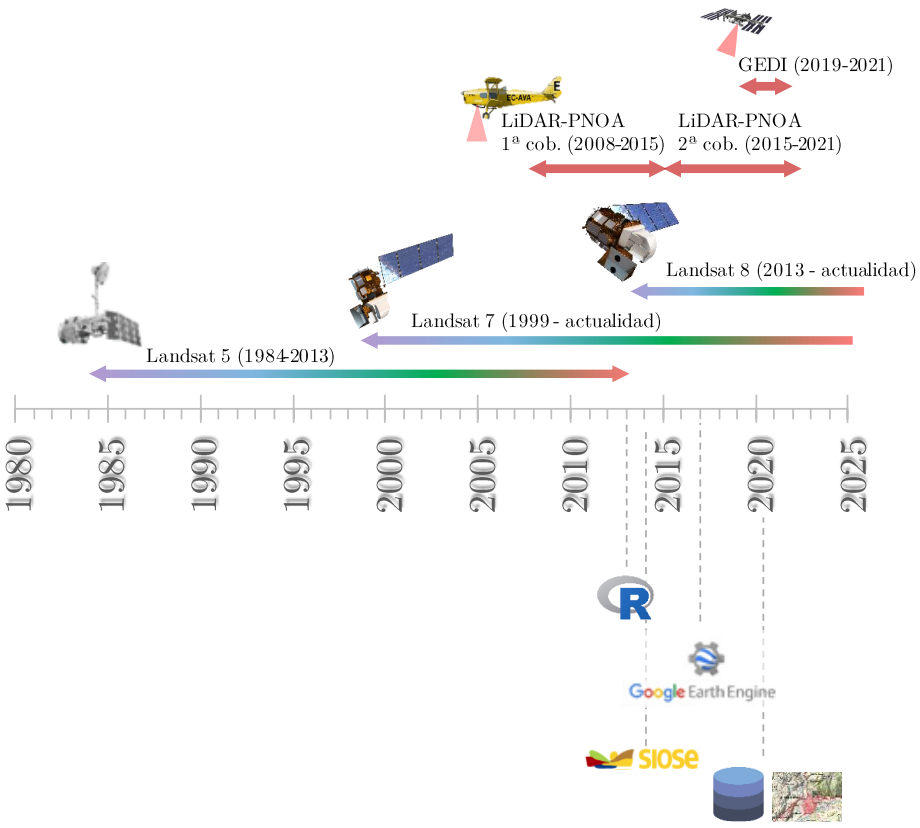

Figura 3.7: *Relación de materiales utilizados para desarrollar los diferentes objetivos. Elaboración propia.*

Capítulo 4

LandTrendr smoothed spectral profiles enhance woody encroachment monitoring

4. LandTrendr smoothed spectral profiles enhance woody encroachment monitoring

Cita: Gelabert, P. J., Rodrigues, M., de la Riva, J., Ameztegui, A., Sebastià, M. T., & Vega-García, C. (2021). LandTrendr smoothed spectral profiles enhance woody encroachment monitoring. Remote Sensing of Environment, 262, 112521. https://doi.org/10.1016/j.rse.2021.112521

Abstract

Secondary succession (SS) is one of the main consequences of the abandonment of agricultural and forestry practices in rural areas, causing -among other processes- woody encroachment on former pastures and croplands. In this study we model and monitor the spatial evolution of SS over semi-natural grassland communities in the mountain range of the Pyrenees in Spain, during the last 36 years (1984-2019). Independent variables for 'annual-based' and 'period-based' modeling were drawn from a suite of Surface Reflectance Landsat images, LandTrendr (LT)-algorithm-adjusted images and LT outputs. Support vector machine (SVM) classifiers were trained and tested using all possible variable combinations of all the aforementioned datasets. The best modeling strategy involved yearly time series of LT-adjusted Tasseled Cap Brightness (TCB) and Wetness (TCW) axes as predictors, attaining a F1-score of 0.85, a Matthew Correlation Coefficient (MCC) of 0.67 and an AUC 0.83. Woodlands encroached above 480,000 ha of grasslands and crops during the study period. A model using LT outputs for the whole period also denoted good performance (F1-score=0.85, MCC=0.75) and estimated a similar area of woodland expan-

sion (~509,000 ha), but this 'period' approach was unable to provide temporal information on the year or the encroachment dynamics. Our results suggest an overall proportion of 66% for the Pyrenees being affected by SS, with higher intensity in the west-central part, decreasing towards the eastern end.

Keywords: *Landsat, LandTrendr, Land abandonment, SVM.*

4.1. Introduction

Global change promotes swift environmental responses through sharp socio-economic and environmental dynamics (Lahsen et al. 2010), leading to land cover transformations such as those triggered by land abandonment.

Grassland communities are among the most extended biomes around the world (Latham et al. 2014, Ali et al. 2016), and are an important food provider for humans through livestock grazing. Livestock transform forages not suitable for human consumption into food such as milk and meat (O'Mara 2012), accounting for up to 27% of the global meat supply in 2018 (FAO 2018). Natural grasslands such as savannah or steppes cover vast areas in Asia, Africa, America and Australia, whereas managed and semi-natural grasslands are predominant in Europe and North America (Foley et al. 2005, O'Mara 2012).

In Europe, semi-natural grasslands extend over large areas in the Central and Eastern plains, the British islands and the Mediterranean basin (Foley et al. 2005). In all European countries, the abandonment of traditional agricultural practices (e.g., free-ranging livestock, and sheep- or cattle-grazed rainfed crops) since the 1950's has led to the pervasive loss of semi-natural grasslands, colonized by shrub and tree communities in an ecological process known as secondary succession (SS). Land abandonment and SS have particularly affected mountain areas (Lasanta et al. 2017), and have both positive and negative side effects (Ustaoglu and Collier 2018).

The most widely recognized positive impact is carbon sequestration (Navarro and Pereira 2012), though some recent studies suggest the expansion of shrubland-type communities may reduce the overall carbon pool at the ecosystem level (Sørensen et al. 2018). Well-managed grasslands also act as CO2 sinks, with considerable potential for soil organic carbon storage (0.01 to 0.3 Gt C yr-1; (Lal 2004). On the negative side, biodiversity usually decline after woody encroachment (Van Auken 2009), as do water availability and river flow. Potential undesired effects, including biodiversity loss, damage to ecosystem services, fuel built-up, or land degradation, are often a consequence of the withdrawal of human stewardship that has kept these cultural landscapes open. In fire-prone ecosystems, the SS process increases wildfire hazard due to fuel accumulation (Lasanta et al. 2018, Pausas and Bond 2020).

Monitoring the evolution of SS contributes to a better understanding of its drivers and ecological implications, while being a helpful source of information for environmental assessment, decision-making and planning. Remote Sensing (RS) is both a powerful tool and a valuable resource to assess land cover dynamics at multiple scales. Satellite imagery has been extensively used to monitor land cover change (Turner et al. 1994), particularly SS following land abandonment. Without being exhaustive, we found examples in eastern Europe (Kuemmerle et al. 2008a, 2009, Baumann et al. 2011), or the entire European continent (Alcantara et al. 2012, Estel et al. 2015).

Though threatened by SS after land abandonment, sub-alpine grasslands in the central and eastern Pyrenees are one of the larger hotspots of managed grasslands in the world (Ali et al. 2016). In the Pyrenees, experiences on SS monitoring are scarce to date (Gartzia et al. 2014, Vidal-Macua et al. 2017) and mostly limited to the local scale (valley or watershed). Several studies in the Spanish Pyrenees have assessed SS based on visual photointerpretation (Poyatos et al. 2003a, Mottet et al. 2006, Améztegui et al. 2010, Cervera et al. 2019) or temporal trends of spectral indices (Vicente-Serrano et al. 2006, Lasanta and Vicente-Serrano 2007). In the French Pyrenees, (Vacquie et al. 2015) analyzed future land use changes at regional

level under different scenarios. Nonetheless, to date there is no comprehensive analysis of the spatial and temporal evolution of SS over the highly diverse and valuable managed grasslands covering the entire range of the Spanish Pyrenees.

In this study, we developed and exemplified a methodological procedure to assess and monitor the dynamic of SS. To do so, we leveraged the LandTrendr algorithm (Kennedy et al. 2010), an innovative technique specifically designed to detect land cover changes. According to (Kennedy et al. 2010) there are two broad types of change detection procedures using RS. One focuses on identifying deviations on the spectral signal (e.g. Vegetation Change Tracker (VCT) (Huang et al. 2010) and Continuous Change Detection and Classification (CCDC) (Zhu and Woodcock 2014); the second approach isolates changes in time-series by fitting smoothing algorithms to simplify chronosequences into representative temporal trajectories. LT, which falls within the later approach, uses a set of spectral-temporal segmentation algorithms optimized for Landsat imagery, allowing the detection of changes in the Earth's surface (Kennedy et al. 2010). LT computes trajectory-based spectral data series, omitting or at least significantly reducing the noise in the spectral signal (Kennedy et al. 2010). Former applications of LT have addressed forest changes and disturbance detection (Kennedy et al. 2010, 2012, Senf et al. 2015, Cohen et al. 2018) or general land cover change (Franklin et al. 2015), but SS of grassland ecosystems after abandonment remains unexplored. SS develops over decades, with the additional technical challenge posed in our study by the topographic and socioeconomic complex mountain environment of the Pyrenees. In this work, we applied LT to the complete series of Landsat images (1984 - 2019) using the Google Earth Engine platform. We combined RS imagery with highly detailed (1:25,000) land cover maps and aerial ortophotography by means of machine learning algorithms to (i) compare the performance of raw spectral indices, LT trajectories and LT outputs in monitoring grassland losses at regional and local scales and, (ii) develop a reliable procedure to detect and map SS over 36 years (1984-2019).

4.2. Study area

The study region covers the Spanish side of the Pyrenees mountain range (Fig. 4.1). The Pyrenees extend over a 400 km range over the Iberian Peninsula isthmus between Spain and France. It is the second highest mountain system in the Iberian Peninsula (500 to 3400 m.a.s.l.). The climate is high mountain microclimate with oceanic influence at the western part, with rainfall accumulation varying across an altitudinal gradient and ranging from 700 to 2500 mm/yr, and mean annual temperatures from 4 to 8 ºC (Cuadrat *et al.,* 2007). Crops and grasslands cover approximately 10% of the Pyrenees (SIOSE, 2014), with environmental conditions favoring a wide spectrum of vegetation species and communities, arranged in elevation belts. Herbaceous crops are cultivated in lowlands, sometimes combined with woody crops in the southern part. Above 1600 m.a.s.l. the temperature conditions do not allow cereal growing, being predominant natural and managed grasslands/pastures (García Ruiz and Lasanta, 2018) combined mainly with mountain pine (*Pinus uncinata Ramond*) forests. In forested montane belt areas (600 - 1600 m.a.s.l.) beech (*Fagus sylvatica L.*) and fir (*Albies alba Mill.*) predominate in shaded aspects.

During the last decades, the agrarian economic sector was progressively replaced by tourism activities transforming economy, landscape and demographic trends (Lasanta et al., 2013). This reduction is evidenced by the reduction of livestock units between 1999 and 2009, with a decrease of 77,000 units (-12%) (INE, 2009, 1999). Specifically, there was a drastic reduction of goat and sheep cattle, and a slight increase of cows and horses, being the last one a special case of breed for recreational purposes.

4.3. Methods

The identification of areas that experienced SS was based on the combination of land cover information and RS imagery. We developed two modeling approaches, one based on the temporal ('annual-based') progression of land cover types characterizing SS (grasslands and woodlands) and a second that distinguished areas historically affected by SS from those with persistent grassland communities ('period-based'). The first approach leveraged time series of spectral imagery while the second relied on complex spectral indices of magnitude and direction of change in the spectral response. Remote sensing imagery and spectral indices were accessed and built using the Google Earth Engine platform (GEE; Gorelick et al. 2017) and the LT algorithm (Kennedy et al., 2018, 2010). Statistical analyses and models were conducted using the R software (R Core Team, 2020).

Figure 4.1: *Study area. Hillshade is used as background.*

4.3.1. Response variables

4.3.1.1. Grassland versus woody communities

Land cover types involved in SS, i.e., all grasslands types and woody vegetation communities, were retrieved from the Spanish Land Cover Information System (SIOSE). The SIOSE dataset provided highly accurate (1:25,000 scale) land cover information for recent years (2005, 2009, 2011 and 2014), but not for the whole study period (1984-2019). We used the latest version of SIOSE (2014) to retrieve the most up-to-date spatial distribution of croplands and grasslands (categories 212 [Herbaceous crops], 290 [Pastures] and 300 [Grasslands]), shrublands (320) and forested areas (311 [Hardwood], 312 [Deciduous], 313 [Evergreen] and 316 [Coniferous]). Water layers (514 [Reservoir], 511 [Rivers], 512 [Lagoons], 513 [Lakes] and 411 [Swamps]), bare ground (354 [Quaternary lava washes], 352 [Rocky outcrop]) and urban areas (111 [Urban continuous], 112 [Urban discontinuous] and 113 [Other urban areas]) were excluded from further analyses. This information was used to model the temporal evolution of SS as described in section C4 - 3.3.1.

4.3.1.2. Evidence of SS

In order to obtain 'ground truth' information to discriminate encroached sites from persistent grassland communities over the whole study period, we carried out a photointerpretation of the available historical series of aerial orthophotography in Spain, longer than the SIOSE dataset. The main goal was identifying areas that transitioned anytime in 1984-2019 from 'grassland or cropland' into 'woodland' (either scrublands, trees or both) to serve as test sample for the evaluation of model performance. We built a complementary modeling procedure upon this information by train-

ing and testing binary models for the whole period based on historical evidence of SS opposed to locations with persistent grasslands (see section C4 - 3.3.2).

From the collection of orthophotographs, we were able to identify a set of 477 locations including 250 sites not experiencing SS and 227 locations affected by SS. We visually analyzed and digitized sites in the series of orthophotographs provided by the Spanish Geographic Institute (IGN) from the National Plan of Aerial Orthophotography (PNOA 2019), the OLISAT project (1997/1998) and the SIGPAC (1997/2003). Digital orthophotographs were supplied via the Spatial Data Infrastructure of Navarra (IDENA), Catalonia (ICGC) and the Spanish Geographical Institute (IGN). Tab. 4.1 provides information on these sources of aerial orthophotography. The selection of sampling sites was based on a systematic approach guided by a 5x5 km grid covering the entire study area. Each grid point was visually inspected to determine whether it experienced SS any time during the period of analysis.

Table 4.1: *Description of aerial orthophotography datasets used in this study.*

	Server	**Project/Program**	**Scale**	**Resolution**	**Year**
Spain	IGN	PNOA	1:15,000	0.25 m	2017-2018
Spain	IGN	OLISAT	1:30,000	0.50 m	1997 & 1999
Spain	IGN	SIGPAC	1:40,000	0.50 m	1997, 2002 & 2003
Catalonia	ICGC	-	1:5,000	0.50 m	1988
Navarra	IDENA	-	1:5,000	0.50 m	1982

4.3.2. Spectral response of the land cover

Models to identify SS were trained from land cover based data and the spectral signal of the land cover. A set of Landsat TM, ETM+ and OLI surface reflectance images (SR images) for spring (March-May, 213 images), summer (June-August, 216) and autumn (September-November, 213) were used in our analyses. We retrieved and processed images via the GEE environment (Gorelick et al. 2017) Tier 1 surface reflectance collection in the period 1984 to 2019, covering the region between paths 197 to 200 and rows 30 and 31. First, we homogenized OLI data to be comparable with TM/ETM+ sensors data, images were transformed as suggested by Roy et al. (2016). Then, we calculated the band value annual medoid at pixel level on a seasonal basis.

4.3.2.1. Image pre-processing and preparation

The Tasseled Cap transformation (TC; Crist and Cicone 1984) was applied to synthetize the original set of 6 spectral bands into a smaller subset of covariates. TC is an orthogonal transformation of spectral data based on the 'physical-sense' of the 3 resulting axes: brightness (TCB), greenness (TCG) and wetness (TCW). Time series of the 3 components transformation (further referred to as TC Raw) were obtained applying the weighting scheme (Table S-4.1 – supplementary material) proposed by Crist (1985). As aforementioned, the spectral information from TM and ETM+ images were homogenized using the procedure described by Roy et al. (2016). The procedure allows applying the same weights to images from either TM, ETM+ or OLI sensors.

The Tasseled Cap Angle (TCA) was also calculated as the angle formed by the TCG and TCB axes (Eq. 1). It works as a proxy of the vegetation

plane (Crist and Cicone, 1984), i.e., the proportion of vegetation to non-vegetation (Gómez et al., 2011).

$$TCA = \arctan\left(\frac{TCG}{TCB}\right) \quad (1)$$

4.3.2.2. LT processing

TC time series were submitted to the LT algorithm. LT consists of a series of spectral-temporal segmentation algorithms to isolate changes in time series. Generally speaking, the trajectories in the original time series were iteratively simplified by identifying the key vertexes of change. Potential vertexes were identified and linked using flexible fitting rules, and then different segments in the updated trajectory were removed and remodeled to ultimately pick the best model (Kennedy et al., 2010). We used the GEE's version of LT as implemented by Kennedy et al. (2018). Processing data with GEE significantly reduced computational time consumption while ensuring the replicability of the procedure elsewhere (Gorelick et al., 2017). The LT algorithm was applied to get fitted-to-vertex time series for every pixel and TC component (further referred to as LTTC). Furthermore, we also retrieved LT's change detection outputs (change magnitude, pre-change value and change duration) for each TC input (LT outputs). Change magnitude relates to the highest difference between two vertexes. Pre-change refers to the initial or starting value in a trajectory. Change duration denotes the slowest change in a given trajectory (usually gain in TCA, TCG, TCW and decline in TCB). We obtained it sorting by the slowest gain and the slowest loss for each TC. After that, in a subsequent process, we selected the magnitude of change and merge loss and gain outputs filtering overlaps by the slowest change.

4.3.3. Classification models

In order to identify areas experiencing SS, we applied the Support Vector Machine (SVM) classification algorithm. Among the machine learning algorithms, SVM has been reported to better discriminate into binary categories (Rodrigues and de la Riva, 2014) being frequently used to model agricultural abandonment (Alcantara et al., 2012; Kuemmerle et al., 2008). SVM has been specifically designed to analyze and recognize patterns. It is based on the constructing of a set of hyperplanes in a high-dimensional space searching for the maximum separability between classes (Cortes and Vapnik, 1995; Vapnik, 1998, 1995). SVM parameters must be optimized, selecting the combination of hyperparameters that achieved the highest classification accuracy (see sections C4 - 3.3.1 and C4 - 3.3.2). We used a Radial Basis Function (RBF) kernel, the most commonly applied strategy in land cover classification due to its good performance (Noi and Kappas, 2018). Cost and gamma parameters were tuned exploring all values ranging from 1–700 and 0.001–1, respectively. Model optimization was conducted using a 10-fold cross validation as implemented in the "caret" package (Kuhn, 2008). In addition, we used the "raster" package (Hijmans, 2019) to generate spatial predictions and outputs.

4.3.3.1. Modeling the annual progression of SS

This approach aimed at monitoring the temporal evolution of SS year by year, thus enabling to ascertain both when and where SS took place. The method was developed in two stages. First, we calibrated 'grassland' vs 'woodland' classification models from TC axes on a single year (2014); and then we predicted the spatial distribution of 'grassland' vs 'woodland' in the entire time series (1984-2019). To do so, we built a response variable consisting on a binary 'grassland' vs 'woodland' categorical variable, created from SIOSE 2014 (see section C4 - 3.1.1). To ensure consistency with

the land cover dataset used to construct the response variable, models were trained using imagery in 2014. Models were built using a training sample of 2,878 locations, accounting for 75% of the SIOSE 2014 sample, (1,039 pastures and grasslands; 1,839 areas with tree and/or shrublands). A total of 56 models were calibrated, resulting from the combination of 3 seasons (spring, summer and fall), 9 possible permutations of TC outputs, avoiding overlapping of TCA with TCB and TCG, and exploring both TC Raw values and LTTCs trajectories. The comparison between using raw values or fitted trajectories was a particular goal of this classification approach.

The second stage of this approach addressed the performance assessment, characterization and mapping of locations experiencing SS. We aimed at determining when SS did occur based on the predicted evolution of 'grassland' and 'woodland'. We inspected the 54 annual time series of classified images, labeling as affected by SS those pixels initially categorized as 'grassland' that were later predicted to be 'woodland'. To account for potential uncertainty due to variability or noise in the spectral signal, we examined the temporal consistency in the classification. That is, for those pixels tagged as affected by SS we estimated a persistence index (PI). The PI was calculated as the ratio between the times (years) 'woodland' was predicted and the number of remaining images (Eq. 2) after the first prediction of SS. From a theoretical standpoint, PI values ranged from 0 to 1; a PI value of 0 indicated no chance of SS while 1 indicated certain occurrence of SS. Values between 0 to 1 informed on the chance of SS, i.e., the consistency with which 'woodland' was subsequently predicted after the first detection. The PI may be understood as a fuzzy classification approach in which each pixel was assigned a likelihood value; the higher the PI, the more likely SS actually happened.

$$PI = \frac{\sum_{y_{ss}}^{y_f} p_{y_{ss}}}{\sum_{y_{ss}}^{y_f} p} \quad (2)$$

where PI is the persistence index; y_{ss} is the first year when SS is predicted; y_f is the last year of the time series; $p_{y_{ss}}$ is a pixel being predicted as affected by SS.

Determining which pixels must be ultimately labeled as affected by SS depended on the PI value. In order to obtain the most reliable SS classification and inform about the sensitivity to the PI threshold (i.e., the value of PI above which we label a given pixel as SS) we conducted a validation and model selection procedure based on the calculation of F1-score (F1) (Chinchor, 1992) in the classification (including commission and omission errors), Mathew Correlation Coefficient (MCC) (Matthews, 1975) and the Area Under the Receiver Operating Characteristic Curve (AUC). Performance indexes were calculated from data described in section C4 - 3.1.2 (Orthophotography-derived dataset, not used for model building), explored along the continuum of all possible thresholds in the range 0-1. The optimal threshold was obtained using the best separability point from AUC (Specificity equal to Sensitivity).

Given the temporal nature of the procedure, PI values were influenced by the time of detection, involving different sample sizes depending on the year were SS was first predicted. For example, the PI of a pixel where SS started in 2000 would be calculated upon 15 records of yearly classification data whereas in a pixel detected in 2017, PI would be calculated with just the 2 remaining years of information. To evidence this potential issue we reported the year when SS was predicted, labelled as 'year of change'. This procedure resulted in two raster layers, one layer gathering the spatial distribution of the PI and a second layer including the year of SS occurrence.

4.3.3.2. Modeling the 'period-based' progression of SS

The 'period-based' classification approach leveraged LT outputs (see section 4.3.2.2) to identify locations affected by SS at any stage during the period 1984-2019. Contrary to the former classification system, this procedure focused on obtaining a 'static' classification of SS, rather than its temporal evolution. Again, a SVM model was trained and tested. The response variable was created from the aerial orthophotography dataset (see section C4 - 3.1.2). We used 80% of the data (198 non-affected locations and 175 areas affected by SS) to train the SVM model and the remaining 20% of the locations to test the model (52 non-affected by SS and 42 experiencing SS). Instead of temporal series of TC components, we calibrated the model from LT outputs calculated in TCB, TCG, TCW and TCA. Again, we explored several combinations of predictors, reporting their performance according to percent accuracy and Cohen's Kappa.

4.4. Results

4.4.1. Spatial distribution of SS

TC Raw and LTTC models performed well in monitoring SS. Out of the 54 possible combinations of variables, several models achieved a satisfactory classification accuracy (Table S-4.2, supplementary material). The most successful combination was obtained with LTTC fitted components in spring, requiring only TCW and TCB as predictors (tied if only TCB used). Overall, models calibrated from LTTC chronosequences outperformed their TC Raw counterparts, though by a slim margin. Note that the best combination of variables in TC Raw coincides with that of LTTC but in summertime. Likewise, spring and summer models tended to work best, with fall models attaining 3% less accuracy on average.

The monitoring of areas affected by SS using the temporal approach was conducted using an optimal PI of 0, as suggested by the sensitivity analysis (Fig. 4.2B). The LTTC and TC raw models were rather insensitive to changes in the PI, though its performance slightly dropped as the PI increased in TC raw. The classification accuracy of the best TC raw model was lower than its LTTC counterpart at any PI threshold. Noticeably, the omission error escalated drastically as the PI threshold increased in the TC raw model (Fig. 4.2A).

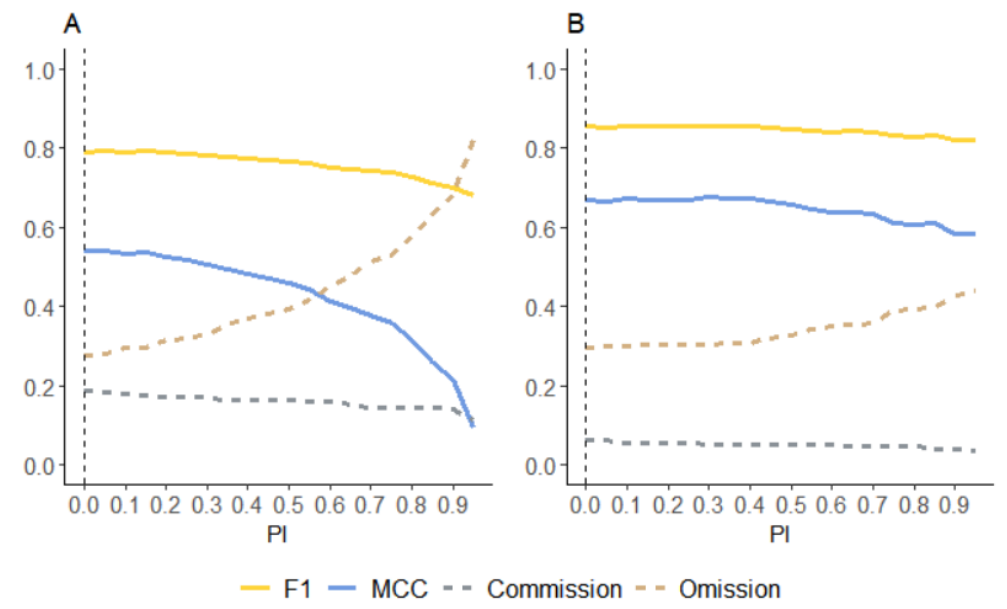

Figure 4.2: *Sensitivity analysis of 'annual-based' modeling strategies to the PI threshold. The vertical dashed line represents the lower limit of the best PI threshold. A: TC raw model and B: LTTC model.*

The comparison of the models' performance in identifying SS evidenced the LTTC approach as the best strategy (Tab. 4.2). LTTC attained a predictive F1-score of 0.85, a MCC of 0.67 and an AUC of 0.83, estimating an affected extension of 479,703 ha, representing an encroachment of 66% of former grasslands (herbaceous crops and grasslands) by woody species.

Commission and omission errors stood at 0.06 and 0.29, respectively. The classification accuracy of LTTC was notably higher than TC Raw's (F1 = 0.79, MCC = 0.54 and AUC = 0.75) predicting an affected area of 508,840 ha (≈70% of analyzed area). Likewise, LTTC outperformed the LT output approach (F1=0.71 and MCC = 0.61), with an encroached area of 533,043 ha representing 74% of the grasslands in the study area. None of the 14 models from LT outputs combinations (see Table S-4.3 - supplementary materials) achieved a higher accuracy than the best LTTC. Nonetheless, as in LTTC models, the strongest spectral predictors were the TCB and TCW components. Tab. 4.2 summarizes the performances of the three modeling approaches on the validation dataset (ground truth obtained by orthophotography).

Table 4.2: *Confusion matrix and performance assessment of the proposed modeling approaches. F1; MCC; C: commission error; O: omission error; SS area: predicted surface of SS.*

	LTTC			**TC Raw**			**LT Outputs**		
	Non-SS	***SS***	***Total***	***Non-SS***	***SS***	***Total***	***Non-SS***	***SS***	***Total***
Non-SS	230	15	245	200	46	246	41	8	49
SS	64	153	217	60	157	217	10	33	43
Total	294	168		260	203		51	41	
	F1=0.85 C = 0.06 MCC=0.67 O = 0.29			F1=0.79 C = 0.28 MCC=0.54 O = 0.19			F1=0.81 C = 0.16 MCC=0.61 O = 0.23		
	SS area: 479,703 ha			SS area: 508,840 ha			SS area: 533,043ha		

From a spatial standpoint, the LTTC approach seemed to capture best the spatial and temporal coverage of the SS phenomena (Fig. 4.3 to 4.5). As observed in Fig. 4.3B, SS took place earlier in the southwestern end, advancing progressively from valleys to the top of the mountain range. Even though it gave no information on SS temporal progression, the pattern obtained with LT outputs resembled that from LTTC (Fig. 4.3A). TC Raw

models seemed to overestimate the spatial extent of SS while not revealing clear temporal patterns.

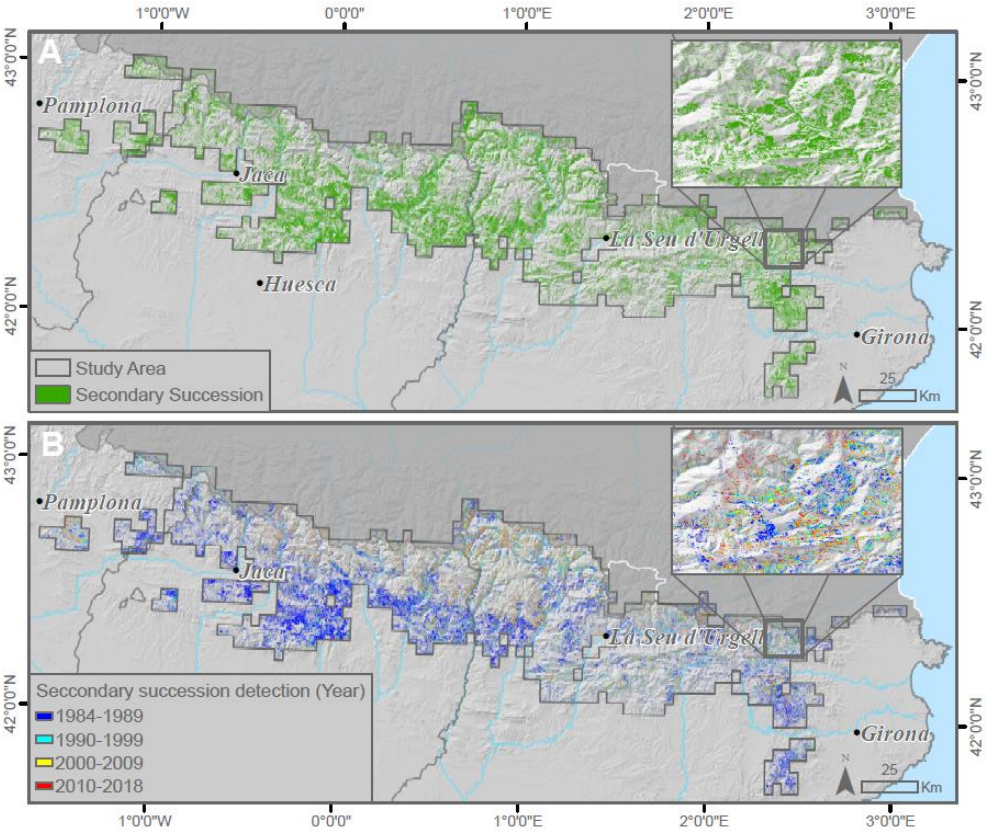

Figure 4.3: *a) Areas affected by SS using LTTC fitted images; b) Areas affected by SS per year using LTTC fitted images. Hillshade is used as background.*

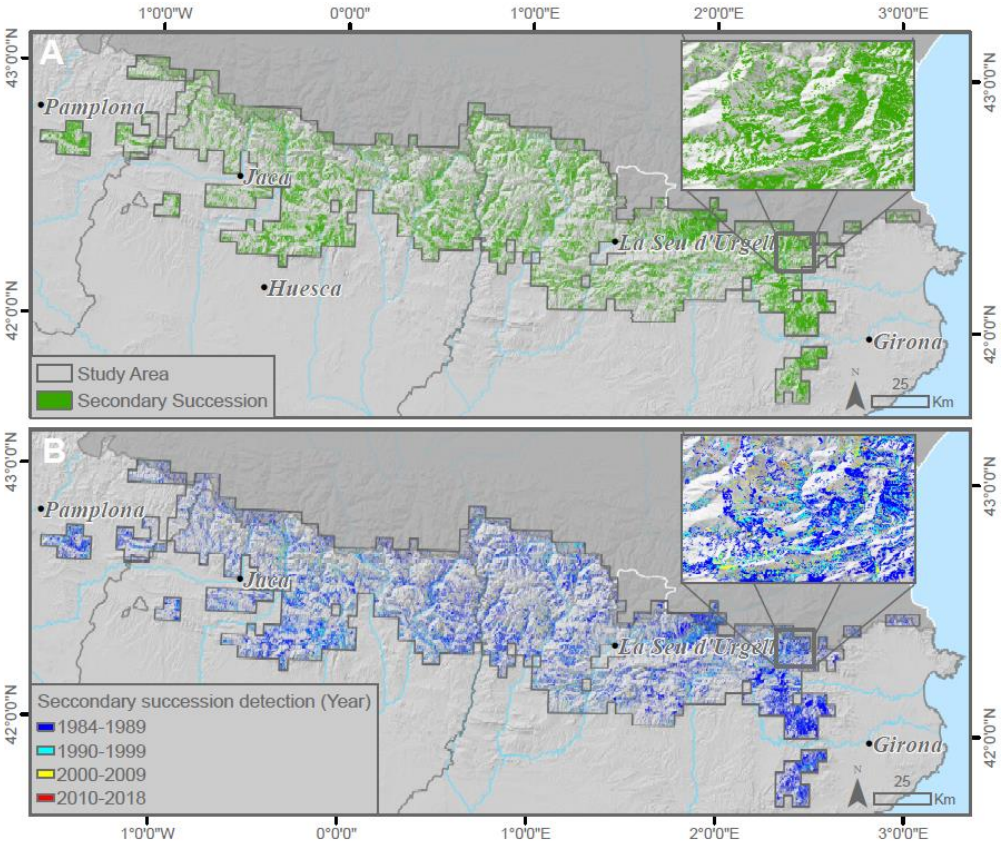

Figure 4.4: *a) Areas affected by SS using TC raw images; b) Areas affected by SS per year using TC raw images. Hillshade is used as background.*

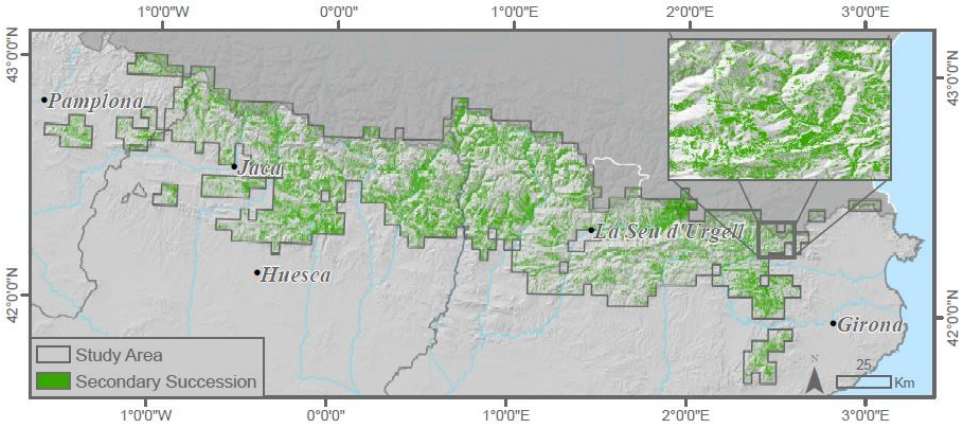

Figure 4.5: *Areas affected by SS using LT output images. Hillshade is used as background.*

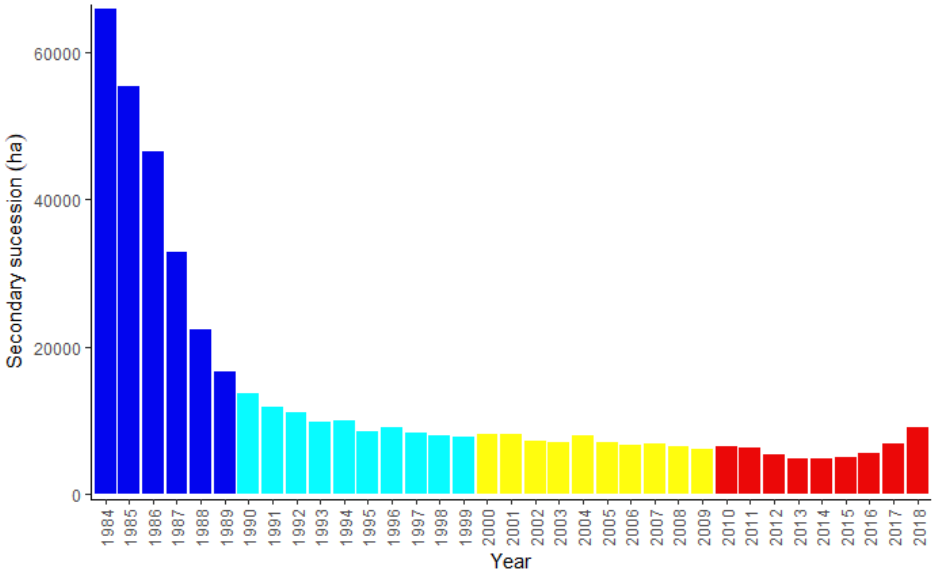

Figure 4.6: *Temporal evolution of SS. Colors represents the different decades.*

4.4.2. Temporal evolution of SS

The analysis of the temporal distribution of SS, extracted from the LTTC cartographical output (Fig. 4.3B), along the period 1984-2019 revealed a non-stationary profile in the temporal dynamics: encroachment rates were not steady. The major progression was observed during the 80's decade, decreasing sharply until 1990, and remaining stationary afterward. During the 80's the average annual surface experiencing SS was of approximately 39,000 ha/yr, declining from over 60,000 ha between 1984 and 1985 to less than 10,000 hectares in 1990. Since 1990 the average affected area stayed at 7,200 ha/yr, descending to 6,000 ha/yr over the 20th century (Fig. 4.6).

4.5. Discussion

We successfully evaluated a wide array of RS inputs and analysis techniques to identify the best methodology to monitor and assess the occurrence and extent of SS after rural abandonment in mountainous areas, an environmental process with high potential impacts on ecosystem services like biodiversity, fire hazard or carbon balances. The proposed procedure was exemplified in the Spanish Pyrenees, assessing the occurrence of SS over a period of 36 years using the complete series of available Landsat imagery.

LT-based models (LTTC and LT outputs) attained an outstanding performance (Fig. 4.3 and 4.5) compared to those calibrated from raw spectral information (TC Raw), either in terms of overall accuracy or commission and omission errors (Tab. 4.2). Using LT fitted spectral information significantly reduced noise from differences in illumination conditions, phenological changes, atmospheric conditions, or geometric registration (Kennedy et al., 2010). Despite the fact that both LTTC and LT outputs models

showed very good accuracy in detecting spatial patterns of SS (Fig. 4.3 and 4.5), the highest accuracy was obtained using LTTC (Tab. 4.2). LT-based methods predicted 464,626 (64% of former grasslands) and 533.043 ha (77%) experiencing SS in the period 1984-2019, using LTTC and LC Outputs, respectively. TC Raw models seemed to overestimate the surface affected by SS (commission error = 0.34). According to prior local experiences, 70-80% of the lands were abandoned in Central Pyrenees (both Spanish and French sides). In the Eastern Pyrenees, 36% of the cultivated land were abandoned between 1993 and 2005 (Badia et al., 2014). The reported rates of land abandonment in the Eastern Pyrenees were quite dissimilar, ranging between 96% in Alta Garrotxa (Vila Subirós et al., 2009) and 25% in Cal Rodó (Poyatos et al., 2003).

The most accurate strategy involved LTTC fitted images using the TCB and TCW components. Both TCB and TCW are known to be suitable indicators to discriminate wooded from non-wooded land covers (Frazier et al., 2015). Dense forest communities and, to a lesser extent shrublands, are broadly characterized by higher TCW (increased ability to retain moisture due to shadowing on the understory) and lower TCB values (reduced albedo by lambertian shading due to the rougher texture of the surface) when compared to open stands (Healey et al., 2005). The performance of models including TCG was usually poor, but TCG is considered a weak driver of structural differences (grass, shrub or tree) between forest communities (Frazier et al., 2015; Pickell et al., 2016). Above a threshold of certain biomass density or leaf area, greenness-related indexes do not capture significant differences between vegetation communities (Pickell et al., 2016; Tanase et al., 2011). Models incorporating the combination of TCG and TCB via TCA did not offer better results either. The TCA is an indirect measure of the proportion of vegetation in the pixel; the higher the TCA, the higher vegetation cover (Gómez et al., 2012). Since it largely refers to

vegetation cover, it holds low discriminant power to discern grassland from other vegetation covers.

When modeling the annual progression of SS, the temporal pattern obtained with LTTC was clearly different from TC Raw's. Setting aside the reported over commission of TC Raw models, their prediction of the year when SS started, i.e, the first detection of the transition from 'grasslands' to 'woody communities', was noticeably biased towards the beginning of the analysis period. Validation results confirmed the unreliable nature of the TC Raw's temporal distribution, in favor of the LTTC approach (AUCs of 0.83 and 0.75 respectively). Nonetheless, the temporal pattern obtained from LTTC also indicated higher SS rates during the first years, decreasing until the early 90s. The observed evolution afterwards points towards the stabilization of the progression of SS.

The temporal pattern described agrees with the literature in the topic. According to Lasanta and Vicente-Serrano (2007), the biggest changes associated to SS in the Pyrenees occurred between the 60s and 80s. Since 1990 there was a decreasing trend in forest expansion over grasslands and abandoned croplands (Vicente Serrano et al., 2003). Since the 19th to the mid-20th century, steep-sloped lands in mountain areas were cultivated (García-Ruiz et al., 2015). During the 1960 decade the Spanish Government funded many hydraulic infrastructures to promote agriculture in arid regions (Alonso-Sarría et al., 2016), leading to the decline in competitiveness of agricultural lands in mountain regions, the abandonment of croplands (van Leeuwen et al., 2019), and the decrease in population (moving mostly to cities in a pervasive rural exodus). During the rural exodus, due to reduced productivity, unsuitability for mechanization and poor accessibility, north-facing sites were abandoned first (Ameztegui et al., 2010). After those, lands under steep slopes were progressively abandoned (García-Ruiz et al., 2015; Lasanta and Vicente-Serrano, 2007; Vicente Serrano et al.,

2003). Nowadays agriculture in the Pyrenees remains mostly in the bottom of the mountain valleys (Lasanta et al., 2013). The promotion of recreational and touristic activities coupled to the low economic competitiveness of agriculture further favored land abandonment (van Leeuwen et al., 2019). This is also evidenced by the observed reduction in the number of goat and sheep cattle (INE, 2009, 1999) and the increase in horse livestock, often used in recreational activities (Hjalager, 1996). In fact, these trends pose an additional challenge since goats are not forage selectors and therefore the greater presence of cows and horses selective grazing mainly consume the best forage (Sebastià et al., 2008). Despite the strong agreement with findings in the literature, a certain bias towards the first years might exist in our timing of SS. The PI helps in controlling potential temporal inconsistences, stabilizing the response of shrub encroachment over the whole time series, especially in middle-late temporal stages. However, several factors such as smoothing side-effects LT predictors or the fact that we set the moment of change to the first year when SS was predicted, favors detection of SS at earlier stages.

The process of land abandonment followed by SS occurred with different intensities across the study region. Forest expansion produced by land abandonment had strong ecological consequences, both again positive and negative. In any case, the 64% reduction in managed grasslands and crops in the Spanish Pyrenees over the last 36 years implied a drastic decline in biodiversity and other ecosystem services linked to these valuable and fragile cultural landscapes.

4.6. Conclusions

The computational power and image collection of the Google Earth Engine platform joined to the implementation of the time-series harmonization algorithm LT allowed to estimate encroachment locations and timing

in the Spanish Pyrenees for the last 36 years. Our results demonstrate the feasibility of the Landsat Tasseled Cap transformation time series, harmonized with LT (LTTC), to monitor annual SS in abandoned mountainous environments, using TCB and TCW in a SVM classification model. In general, non-harmonized time series offer worse performances and overestimate woodland expansion. Models using the LT outputs are also promising, but they do not offer temporal information on changes within the period of analysis.

4.7. Acknowledgements

This work was supported by project IMAGINE [CGL2016-80400-R] funded by the Spanish Science Foundation (FECYT) and by the research grant program Ajuts UdL, Jade Plus i Fundació Bancària La Caixa [Agreement 79/2018 of the Governing Council of the University of Lleida].

4.8. References

Alcantara, C., Kuemmerle, T., Prishchepov, A. V., and Radeloff, V.C., 2012. Mapping abandoned agriculture with multi-temporal MODIS satellite data. Remote Sensing of Environment, 124, 334–347.

Ali, I., Cawkwell, F., Dwyer, E., Barrett, B., and Green, S., 2016. Satellite remote sensing of grasslands: From observation to management. Journal of Plant Ecology, 9 (6), 649–671.

Alonso-Sarría, F., Martínez-Hernández, C., Romero-Díaz, A., Cánovas-García, F., and Gomariz-Castillo, F., 2016. Main Environmental Features Leading to Recent Land Abandonment in Murcia Region (Southeast Spain). Land Degradation and Development, 27 (3), 654–670.

Améztegui, A., Brotons, L., and Coll, L., 2010. Land-use changes as major drivers of mountain pine (Pinus uncinata Ram.) expansion in the Pyrenees. Global Ecology and Biogeography, 19 (5), 632–641.

Van Auken, O.W., 2009. Causes and consequences of woody plant encroachment into western North American grasslands. Journal of Environmental Management.

Badia, A., Pèlachs, A., Vera, A., Tulla, A.F., and Soriano, J.J., 2014. Land use and land cover change and the effects on vulnerability to forest fire of counties in the mountains of Catalonia: from managing the land to managing a threat. Pirineos, 169.

Baumann, M., Kuemmerle, T., Elbakidze, M., Ozdogan, M., Radeloff, V.C., Keuler, N.S., Prishchepov, A. V., Kruhlov, I., and Hostert, P., 2011. Patterns and drivers of post-socialist farmland abandonment in Western Ukraine. Land Use Policy.

Cervera, T., Pino, J., Marull, J., Padró, R., and Tello, E., 2019. Understanding the long-term dynamics of forest transition: From deforestation to afforestation in a Mediterranean landscape (Catalonia, 1868–2005). Land Use Policy, 80, 318–331.

Chinchor, N., 1992. MUC-4 Evaluation Metrics. In: Proceedings of the 4th Conference on Message Understanding. USA: Association for Computational Linguistics, 22–29.

Cohen, W.B., Yang, Z., Healey, S.P., Kennedy, R., and Gorelick, N., 2018. A LandTrendr multispectral ensemble for forest disturbance detection. Remote Sensing of Environment.

Cortes, C. and Vapnik, V., 1995. Support-Vector Networks. Machine Learning.

Crist, E.P., 1985. A TM Tasseled Cap equivalent transformation for reflectance factor data. Remote Sensing of Environment.

Crist, E.P. and Cicone, R.C., 1984. A Physically-Based Transformation of Thematic Mapper Data—The TM Tasseled Cap. IEEE Transactions on Geoscience and Remote Sensing.

Cuadrat, J.M., Saz, M.A., and Vicente-Serrano, S.M., 2007. Atlas climático de Aragón. Gobierno de Aragón.

Estel, S., Kuemmerle, T., Alcántara, C., Levers, C., Prishchepov, A., and Hostert, P., 2015. Mapping farmland abandonment and recultivation across Europe using MODIS NDVI time series. Remote Sensing of Environment, 163, 312–325.

FAO, 2018. FAOSTAT statistical database. Crops, National Production.

Foley, J.A., DeFries, R., Asner, G.P., Barford, C., Bonan, G., Carpenter, S.R., Chapin, F.S., Coe, M.T., Daily, G.C., Gibbs, H.K., Helkowski, J.H., Holloway, T., Howard, E.A., Kucharik, C.J., Monfreda, C., Patz, J.A., Prentice, I.C., Ramankutty, N., and Snyder, P.K., 2005. Global consequences of land use. Science, 309 (5734), 570–574.

Franklin, S.E., Ahmed, O.S., Wulder, M.A., White, J.C., Hermosilla, T., and Coops, N.C., 2015. Large Area Mapping of Annual Land Cover Dynamics Using Multitemporal Change Detection and Classification of Landsat Time Series Data. Canadian Journal of Remote Sensing, 41 (4), 293–314.

Frazier, R.J., Coops, N.C., and Wulder, M.A., 2015. Boreal Shield forest disturbance and recovery trends using Landsat time series. Remote Sensing of Environment, 170, 317–327.

García Ruiz, J.M. and Lasanta, T., 2018. El Pirineo Aragonés como paisaje cultural. Pirineos.

García-Ruiz, J.M., López-Moreno, J.I., Lasanta, T., Vicente-Serrano, S.M., González-Sampériz, P., Valero-Garcés, B.L., Sanjuán, Y., Beguería, S., Nadal-Romero, E., Lana-Renault, N., and Gómez-Villar, A., 2015. Los efectos geoecológicos del cambio global en el pirineo central español: Una revisión a distintas escalas espaciales y temporales. Pirineos, 170.

Gartzia, M., Alados, C.L., and Pérez-Cabello, F., 2014. Assessment of the effects of biophysical and anthropogenic factors on woody plant encroachment in dense and sparse mountain grasslands based on remote sensing data. Progress in Physical Geography, 38 (2), 201–217.

Gómez, C., White, J.C., and Wulder, M.A., 2011. Characterizing the state and processes of change in a dynamic forest environment using hierarchical spatio-temporal segmentation. Remote Sensing of Environment.

Gómez, C., Wulder, M.A., White, J.C., Montes, F., and Delgado, J.A., 2012. Characterizing 25 years of change in the area, distribution, and carbon stock of Mediterranean pines in Central Spain. International Journal of Remote Sensing, 33 (17), 5546–5573.

Gorelick, N., Hancher, M., Dixon, M., Ilyushchenko, S., Thau, D., and Moore, R., 2017. Google Earth Engine: Planetary-scale geospatial analysis for everyone. Remote Sensing of Environment.

Healey, S.P., Cohen, W.B., Zhiqiang, Y., and Krankina, O.N., 2005. Comparison of Tasseled Cap-based Landsat data structures for use in forest disturbance detection. Remote Sensing of Environment, 97 (3), 301–310.

Hijmans, R.J., 2019. raster: Geographic Data Analysis and Modeling.

Hjalager, A.-M., 1996. Agricultural diversification into tourism. Tourism Management.

Huang, C., Goward, S.N., Masek, J.G., Thomas, N., Zhu, Z., and Vogelmann, J.E., 2010. An automated approach for reconstructing recent forest disturbance history using dense Landsat time series stacks. Remote Sensing of Environment.

INE, 1999. Censo Agrario.

INE, 2009. Censo Agrario.

Vidal-Macua, J., Ninyerola, M., Zabala, A., Domingo-Marimon, C., and Pons, X., 2017. Factors affecting forest dynamics in the Iberian Peninsula from 1987 to 2012. The role of topography and drought. Forest Ecology and Management, 406 (June), 290–306.

Kennedy, R., Yang, Z., and Cohen, W.B., 2010. Detecting trends in forest disturbance and recovery using yearly Landsat time series: 1. LandTrendr - Temporal segmentation algorithms. Remote Sensing of Environment.

Kennedy, R., Yang, Z., Cohen, W.B., Pfaff, E., Braaten, J., and Nelson, P., 2012. Spatial and temporal patterns of forest disturbance and regrowth within the area of the Northwest Forest Plan. Remote Sensing of Environment.

Kennedy, R., Yang, Z., Gorelick, N., Braaten, J., Cavalcante, L., Cohen, W.B., and Healey, S., 2018. Implementation of the LandTrendr algorithm on Google Earth Engine. Remote Sensing.

Kuemmerle, T., Chaskovskyy, O., Knorn, J., Radeloff, V.C., Kruhlov, I., Keeton, W.S., and Hostert, P., 2009. Forest cover change and illegal logging in the Ukrainian Carpathians in the transition period from 1988 to 2007. Remote Sensing of Environment, 113 (6), 1194–1207.

Kuemmerle, T., Hostert, P., Radeloff, V.C., Van Der Linden, S., Perzanowski, K., and Kruhlov, I., 2008a. Cross-border comparison of post-socialist farmland abandonment in the Carpathians. Ecosystems, 11 (4), 614–628.

Kuemmerle, T., Hostert, P., Radeloff, V.C., Van Der Linden, S., Perzanowski, K., and Kruhlov, I., 2008b. Cross-border comparison of post-socialist farmland abandonment in the Carpathians. Ecosystems, 11 (4), 614–628.

Kuhn, M., 2008. Building predictive models in R using the caret package. Journal of statistical software, 28 (5), 1–26.

Lahsen, M., Sanchez-Rodriguez, R., Lankao, P.R., Dube, P., Leemans, R., Gaffney, O., Mirza, M., Pinho, P.,

Osman-Elasha, B., and Smith, M.S., 2010. Impacts, adaptation and vulnerability to global environmental change: Challenges and pathways for an action-oriented research agenda for middle-income and low-income countries. Current Opinion in Environmental Sustainability.

Lal, R., 2004. Soil carbon sequestration impacts on global climate change and food security. Science.

Lasanta, T., Arnáez, J., Pascual, N., Ruiz-Flaño, P., Errea, M.P., and Lana-Renault, N., 2017. Space–time process and drivers of land abandonment in Europe. Catena, 149, 810–823.

Lasanta, T., Beltran, O., and Vaccaro, I., 2013. Socioeconomic and territorial impact of the ski industry in the spanish pyrenees: Mountain development and leisure induced urbanization. Pirineos, 168 (168), 103–128.

Lasanta, T., Khorchani, M., Pérez-Cabello, F., Errea, P., Sáenz-Blanco, R., and Nadal-Romero, E., 2018. Clearing shrubland and extensive livestock farming: Active prevention to control wildfires in the Mediterranean mountains. Journal of Environmental Management, 227 (September), 256–266.

Lasanta, T. and Vicente-Serrano, S.M., 2007. Cambios en la cubierta vegetal en el pirineo aragonés en los últimos 50 años. Pirineos, (162), 125–154.

Latham, J., Cumani, R., Rosati, I., and Bloise, M., 2014. FAO Global Land Cover SHARE. Database Beta-Release Verion 1.0.

van Leeuwen, C.C.E., Cammeraat, E.L.H., de Vente, J., and Boix-Fayos, C., 2019. The evolution of soil conservation policies targeting land abandonment and soil erosion in Spain: A review. Land Use Policy, 83 (February), 174–186.

Matthews, B.W., 1975. Comparison of the predicted and observed secondary structure of T4 phage lysozyme. Biochimica et Biophysica Acta (BBA) - Protein Structure, 405 (2), 442–451.

Mottet, A., Ladet, S., Coqué, N., and Gibon, A., 2006. Agricultural land-use change and its drivers in mountain landscapes: A case study in the Pyrenees. Agriculture, Ecosystems and Environment.

Navarro, L.M. and Pereira, H.M., 2012. Rewilding Abandoned Landscapes in Europe. Ecosystems.

Noi, P.T. and Kappas, M., 2018. Comparison of random forest, k-nearest neighbor, and support vector machine classifiers for land cover classification using sentinel-2 imagery. Sensors, 18(1).

O'Mara, F.P., 2012. The role of grasslands in food security and climate change. Annals of Botany, 110 (6), 1263–1270.

Pausas, J.G. and Bond, W.J., 2020. Alternative Biome States in Terrestrial Ecosystems. Trends in Plant Science, 1–14.

Pickell, P.D., Hermosilla, T., Frazier, R.J., Coops, N.C., and Wulder, M.A., 2016. Forest recovery trends derived from Landsat time series for North American boreal forests. International Journal of Remote Sensing, 37 (1), 138–149.

Poyatos, R., Latron, J., and Llorens, P., 2003a. Land Use and Land Cover Change After Agricultural Abandonment. Mountain Research and Development, 23 (4), 362–368.

Poyatos, R., Latron, J., and Llorens, P., 2003b. Land Use and Land Cover Change After Agricultural Abandonment. Mountain Research and Development, 23 (4), 362–368.

R Core Team, 2017. R: A Language and Environment for Statistical Computing.

Rodrigues, M. and de la Riva, J., 2014. An insight into machine-learning algorithms to model human-caused wildfire occurrence. Environmental Modelling & Software, 57, 192–201.

Roy, D.P., Kovalskyy, V., Zhang, H.K., Vermote, E.F., Yan, L., Kumar, S.S., and Egorov, A., 2016. Characterization of Landsat-7 to Landsat-8 reflective wavelength and normalized difference vegetation index continuity. Remote Sensing of Environment, 185, 57–70.

Sebastià, M.T., De Bello, F., Puig, L., and Taull, M., 2008. Grazing as a factor structuring grasslands in the Pyrenees. Applied Vegetation Science.

Senf, C., Pflugmacher, D., Wulder, M.A., and Hostert, P., 2015. Characterizing spectral-temporal patterns of defoliator and bark beetle disturbances using Landsat time series. Remote Sensing of Environment.

Sørensen, M.V., Strimbeck, R., Nystuen, K.O., Kapas, R.E., Enquist, B.J., and Graae, B.J., 2018. Draining the Pool? Carbon Storage and Fluxes in Three Alpine Plant Communities. Ecosystems.

Tanase, M.A., de las Heras, J., Santoro, M., Pérez-Cabello, F., and Kasischke, E., 2011. Sensitivity of SAR data to post-fire forest regrowth in Mediterranean and boreal forests. Remote Sensing of Environment, 115 (8), 2075–2085.

Turner, B.L.I.I., Meyer, W.B., and Skole, D.L., 1994. Global land-use/land-cover change: Towards an integrated study. Ambio, 23 (1), 91–95.

Ustaoglu, E. and Collier, M.J., 2018. Farmland abandonment in Europe: An overview of drivers, consequences, and assessment of the sustainability implications. Environmental Reviews, 26 (4), 396–416.

Vacquie, L., Houet, T., Sohl, T., Reker, R., and Sayler, K., 2015. Modelling Regional Land Change Scenarios to Assess Land Abandonment and Reforestation Dynamics in th he Pyrenees (France). Jounal of Mountains Science, 12 (2), 905–920.

Vapnik, V., 1995. The Nature of Statistical Learning Theory. The Nature of Statistical Learning Theory.

Vapnik, V., 1998. Statistical Learning Theory. New York: Wiley.

Vicente Serrano, S.M., Lasanta, T., and Romo, A., 2003. Diferencias espaciales en la evolución del NDVI en la cuenca alta del Aragón : efectos de los caminos en el uso del suelo. Cuadernos de Investigación Geográfica, 29 (0), 51.

Vicente-Serrano, S.M., Beguería, S., and Lasanta, T., 2006. Diversidad espacial de la actividad vegetal en campos abandonados del pirineo central español: Anílisis de los procesos de sucesión mediante imágenes landsat (1984-2001). Pirineos, (161), 59–84.

Vila Subirós, J., Ribas Palom, A., Varga Linde, P., and Llausàs Pascual, A., 2009. Medio siglo de cambios paisajísticos en la montaña mediterránea. Percepción y valoración social del paisaje en la alta Garrotxa (Girona). Pirineos, 164.

Zhu, Z. and Woodcock, C.E., 2014. Continuous change detection and classification of land cover using all available Landsat data. Remote Sensing of Environment.

Capítulo 5

Spatially explicit modeling of the probability of land abandonment in the Spanish Pyrenees

5. Spatially explicit modeling of the probability of land abandonment in the Spanish Pyrenees

Cita: Gelabert, P.J., Rodrigues, M., Vidal-Macua, J.J., Ameztegui, A., Sebastià, M.T., Vega-Garcia, C. (2022) Spatial explicit modeling of the probability of land abandonment in the Spanish Pyrenees. Landscape and Urban Planning. 104487, https://doi.org/doi.org/10.1016/j.landurbplan.2022.104487

Abstract

Many mountain regions in Europe have experienced massive migrations towards metropolitan areas, with far-reaching implications for societies and the environment, especially croplands and grasslands. In this work, we tailored a geospatial framework to envisage the probability of land abandonment in the Spanish Pyrenees at moderate spatial resolution. We predicted the likelihood of land abandonment combining machine learning algorithms, geospatial data and historical observations of land abandonment in the period 1980 to 2019. The model attained a high predictive performance (AUC = 0.85) at a moderate resolution (30 m), providing insights into the spatial behavior of the potential for both abandonment and its main driving forces. The highest rates of abandonment were found in rural settlements and towns in bottom valleys where tourism and recreational activities have proliferated over the years. Fast and comfortable connections between the main metropolitan areas (e.g. Barcelona and Zaragoza) and the mountain regions foster touristic activity and lead to the creation of new settlements. Ecotourism and mountain sports promote land abandonment as evidenced by the high probability predicted over the Central Pyrenees (from Pallars Jussà to Alto Gállego counties). Our results provide spatially explicit probability and uncertainty outputs, providing insights into site-specific abandonment potential and the influence of its drivers. These results can

substantially assist land planners in decision-making, enabling assessments at local scale.

Keywords: *Land abandonment, tourism, modeling, Random Forest, high mountain.*

5.1. Introduction

Land abandonment is globally pervasive, though it occurs preferably in developed countries (Beilin *et al.*, 2014). Industrialization and the resulting "rural exodus" that took place during the 20th century fostered changes in land use, promoting the abandonment of low-income agricultural lands (Pereira *et al.*, 2010; Stoate *et al.*, 2009) in what has been, to date, the largest land cover and use transformation over Europe (Estel *et al.*, 2015; Lasanta *et al.*, 2017; Terres *et al.*, 2015). Vast areas of natural and semi-natural pastures in mountain systems in Europe were particularly prone to land abandonment (Gartzia *et al.*, 2014; Gellrich and Zimmermann, 2007; Lasanta *et al.*, 2017; MacDonald *et al.*, 2000). These grassland-type communities are in fact cultural landscapes resulting from long-term human intervention (Dieterich and Van Der Straaten, 2004), maintained over centuries by extensive livestock grazing. They hold intrinsic natural and aesthetic features (Prados, 2008) and provide valued recreational, environmental and cultural services and goods (Serra *et al.*, 2014). In the particular case of the Pyrenees massif, there is strong evidence of landscape and environmental degradation after land abandonment, including soil degradation, increased fire risk and reduction of river flows (Ameztegui *et al.*, 2010, 2021; Cervera *et al.*, 2019; Lasanta *et al.*, 2017; Lasanta and Vicente-Serrano, 2007; Mottet *et al.*, 2006; Nadal-Romero *et al.*, 2011; Perpiña *et al.*, 2020; Poyatos *et al.*, 2003; Vacquie *et al.*, 2015; Vidal-Macua *et al.*, 2018).

Land abandonment fosters multiple impacts at different spatial and temporal scales. Woody encroachment, the advance of forest lands over former pastures and croplands, is perhaps the preeminent consequence in

the Pyrenees (Gartzia et al., 2014) and is the main driver behind the upward displacements of the treeline. The treeline since the 1950's has moved upwards approximately 40 m.a.s.l. from 2,111 m.a.s.a.l. (Ameztegui *et al.*, 2016). The colonization by woody communities is often linked to ecological degradation and loss of biodiversity, both in terms of species richness and functional diversity (Jongman, 2002). Landscape features such as connectivity, patch size and patch diversity are also altered by land abandonment, triggering an important cultural heritage loss and diminishing its aesthetic properties (Ameztegui *et al.*, 2021; Schirpke *et al.*, 2019). Moreover, forest progression boosts wildfire hazard (increasing fire intensity and spread potential) by enabling fuel accumulation and intruding in the traditional mosaic of vegetation patches intermingling with croplands that was once a distinctive trait of the Mediterranean mountains (Pais *et al.*, 2020). Soil erosion is boosted in lands where vegetation does not re-colonize abandoned plots; under extreme rainfall events, this process may accelerate soil degradation, losing organic matter content in the top-soil horizons (García-Ruiz and Lana-Renault, 2011).

Several endogenous (site-specific features) and exogenous drivers (socioeconomic and political context) are behind the abandonment of agricultural lands in the European mountainous areas (Lasanta *et al.*, 2017; Terres *et al.*, 2015). The low economic revenue of traditional agriculture due to poor mechanization potential, linked to the lack of subsidies for rainfed crops, promoted the consolidation of irrigated lands away from mountains (Nainggolan *et al.*, 2012; van Leeuwen *et al.*, 2019). The low income obtained by the primary sector triggered cascading effects like the rise of tourism and the subsequent development of second residential housing (Serra *et al.*, 2014). This process was more noticeable in the vicinity of National Parks or Natural Protected areas (NPAs), giving rise to the term "*Naturbanization*" (Prados, 2008) which refers to the urbanization of rural and natural areas as second homes for leisure activities in the environment (hiking or winter sports, among others).

To date, there is extensive knowledge of the processes and factors favoring land abandonment, as evidenced by the numerous studies cited so

far. Nonetheless, the process itself holds an intrinsic spatial nature, being often difficult to foresee it with the necessary spatial accuracy to adopt suitable measures to prevent or reverse its impacts. The existing research focused heavily on unravelling the role of the drivers (Corbelle-Rico *et al.*, 2012; Garbarino *et al.*, 2020; Vidal-Macua *et al.*, 2018), but previous analyses providing a spatial representation of the phenomenon are scarce (Morán-Ordóñez *et al.*, 2011); especially those conducted at a resolution sufficient to enable decision-making. The implementation of management initiatives to prevent and restore abandonment effects often takes place at the very local level (e.g., concentration of land ownership) but couples necessarily to region-wide initiatives (e.g., subsidize plans), thus requiring a spatial accuracy that enables assessments at multiple scales.

In this research, we analyzed the relationships of the factors from a regional perspective, obtaining a relative importance of each factor on the probability of land abandonment. Therefore, the greater or lesser presence of each factor can be associated with differences in the intensity of the phenomenon at the local level. Based on the existing literature that analyzes the drivers of land abandonment in other mountain regions in Europe, or in smaller areas of the Pyrenees, we hypothesized that socioeconomic drivers would be the main responsible of recent land abandonment. Moreover, touristic development is often negatively associated with traditional farming and livestock breeding, so we expected those variables related to tourism would be particularly important. Lastly, given that socioeconomic processes are not totally independent from topography and relief, variables such as elevation and aspect are also likely to play an important role in land abandonment. The method was calibrated and validated in the Pyrenees, one of the major remaining hot spots of natural and semi-natural grasslands in Europe (Ali *et al.*, 2016). Our results can guide managers and decision-makers to explore and design preventive measures related to economic diversification and rural depopulation reduction, in order to preserve these valuable microenvironments and the cultural landscapes they are immersed in.

5.2. Materials and methods

5.2.1. Study area

The Pyrenees are a mountain range located northeast of the Iberian Peninsula, a natural border between Spain and France. Climate is characterized by an altitudinal gradient (elevation ranges from 600 m to 3000 m), fostering increasing rainfall and decreasing temperatures as elevation is gained. The average annual precipitation stands around 1500 mm, equally distributed throughout the year, though it is slightly lower during the summer. Temperature in winter is cold (0-5 ºC), mild during the summer season (10-12 ºC). However, temperature peaks at W-E ends of the mountain range due to the sea influence and the lower elevations.

The elevation gradient governs land cover distribution and types, but the current treeline position (2,200-2,400 m.a.s.l.) and structure, the subalpine and montane pastures, and the predominance of a few tree species arise from historical landscape transformations (Ninot *et al.*, 2007). The **basal** belt (600-900 m.a.s.l.) is dominated by sclerophyllous forests of *Quercus ilex* mixed with serial xerophilous garigues and shrubs (*Rosmarinus, Cistus*). The **submontane** belt (with upper limit at 1100-1300 m.a.s.l.) holds Submediterranean forests of marcescent oaks (*Q. pubescens, Q. faginea*) and pines (*Pinus nigra* or *P. sylvestris*). The **montane** belt (reaching 1,600 m.a.s.l.) is dominated by *Fagus sylvatica and Abies alba* in the humid sites, and by *Pinus sylvestris* in the Eastern, more Mediterranean regions. Above 1600 m.a.s.l., the main tree species is *Pinus uncinata,* which constitutes the treeline in most of the massif. The treeline position lies at 2,200-2,400 m.a.s.l., well below its climatic potential due to centuries of intense human activity, and the **subalpine** belt holds natural and managed grasslands/pastures (García Ruiz and Lasanta, 2018) produced by the "alpinization" of the *Pinus uncinata* forests. The **alpine** belt (up to 2,800 m.a.s.l.) is dominated by short grassland communities (e.g., *Oxytropido-Elynetum* pastures*, Hieracio-Festucetum supinae*, *Leontodonto-Caricetum curvulae, Festuca eskia, Festuca gautieri* grasslands), noteworthy in specific habitats for their species richness or the presence of endemic plants.

Forestry and agriculture shaped the region into cultural landscape mosaics, especially in the 600-1,600 m.a.s.l. altitudinal range. Historically, the primary sector was the economic "engine" of the Pyrenees, with cereal growing (wheat, vetch, barley, or oats) and livestock farming as main activities. Nowadays, herbaceous crops (swath meadow) devoted to forage production have replaced the cereal crops, and agriculture is being either abandoned or replaced by tertiary activities (tourism) linked to mountain sports (ski, hiking, etc.), promoting camping accommodations and second residences (Lasanta *et al.*, 2007, 2013).

The study was framed in the Spanish Pyrenees side, encompassing the potential forest region as outlined by Rivas-Martinez (1987). We selected open areas (pastures, grasslands and croplands) that due to its bioclimatic conditions are suitable to hold forests, in the range between 600-2,400 m.a.s.l. (Fig. 5.1).

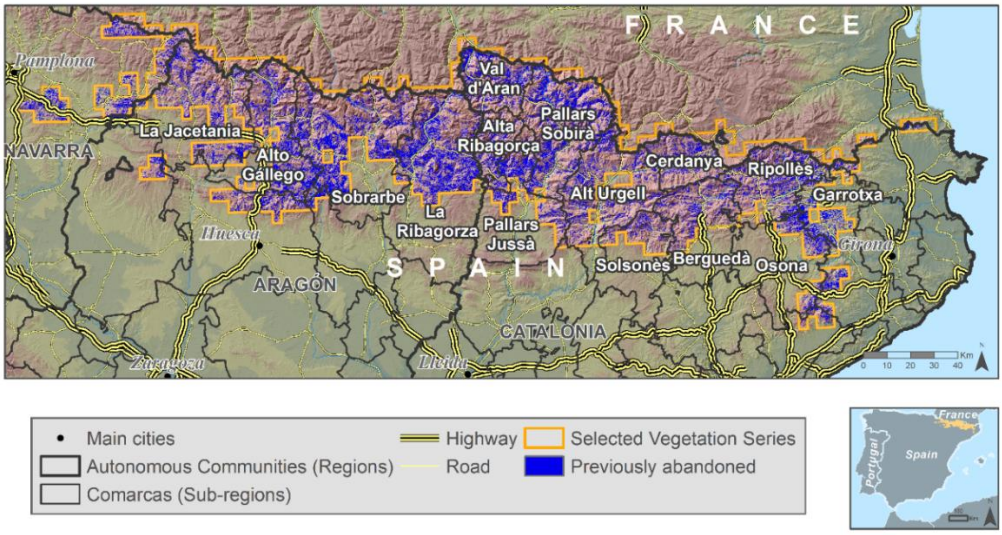

Figure 5.1: *Location of the study area and boundaries of the analysis. Previously abandoned areas (Gelabert et al., 2021) were highlighted in blue.*

5.2.2. Methods

5.2.2.1. Response variable

Predicting the probability of land abandonment required a binary response variable observing the occurrence (1) or the absence (0) of past abandonment. Candidate locations comprised either abandoned locations that were formerly dominated by grasslands or crops now forested with a coverage greater than 50% in areas bigger than 1ha (coded as 1) or non-abandoned grassland communities or crops that persisted over time also in areas bigger than 1ha (coded as 0). The site selection was carried out by visual inspection of an ortophotographic series, using a regular 5x5km grid to stratify the sampling process. We collected all detectable sites under the aforementioned considerations and a balanced sample in number of abandoned plots. Candidate sites were subsequently converted into single point locations. In non-abandoned locations we used the centroid of the plot polygon. In abandoned plots the point was placed in the region with higher evidence of vegetation succession (Please see an example in Supplementary fig. S-5.1). We were able to identify a set of 477 "ground truth" locations composed of 250 non-abandoned sites (0) and 227 abandoned (1) at some point in the period 1982-2018. These samples have an average nearest neighbor distance of 2.85km. We used all the available ortophotographies served by the Spanish Geographic Institute (IGN) from the PNOA (2019), OLISAT (1997/1998), and SIGPAC (1997/2003) programs (see Table 5.1 for further information).

5.2.2.2. Explanatory variables

The literature recognizes three main types of drivers of land abandonment: **ecological constraints**, such as topography or edaphology and climate, **socioeconomic drivers**, e.g. demographic variations, accessibility to markets and policies, and **land mismanagement**, e.g. overexploitation, floods or water contamination (García-Ruiz and Lana-Renault, 2011; Lasanta *et al.*, 2017; Rey Benayas, 2007; Rey Benayas *et al.*, 2007; Terres *et al.*, 2015; Ustaoglu and Collier, 2018). Land abandonment is triggered

by the combination of these three types of drivers, being often prevalent the socioeconomic factors (Sluiter and de Jong, 2007).

Table 5.1: *Description of the ortophotographies used to construct the response variable.*

Extent	Server	Project/Program	Scale	Resolution	Year
Spain	IGN	PNOA	1:15,000	0.25 m	2017-2019
Spain	IGN	OLISAT	1:30,000	0.50 m	1997 & 1999
Spain	IGN	SIGPAC	1:40,000	0.50 m	1997, 2002 & 2003
Catalonia	ICGC	-	1:5,000	0.50 m	1988
Navarra	IDENA	-	1:5,000	0.50 m	1982

The explanatory covariates of land abandonment were selected based on an extensive literature review (e.g. MacDonald *et al.* 2000; Mottet *et al.* 2006; Zaragozí *et al.* 2012; Terres *et al.* 2015; Lasanta *et al.* 2017; Vidal-Macua *et al.* 2018; Schirpke *et al.* 2019) and we favored those available at detailed spatial resolution. Spatial proxies for each driver type were created at a 30 m resolution, as a trade-off solution between processing time and capturing the spatial variability with sufficient accuracy. To pair response locations and predictors, we overlay the candidate locations to each raster layer corresponding, extracting the value of the underlying pixel.

Topography and relief

The shape and arrangement of the relief influence the chance of abandonment mostly in relation to land productivity. In short, the more productive the land the less prone to abandonment (Gellrich and Zimmermann, 2007). The bottom of mountain valleys is usually more productive since mechanization is feasible. Slope and aspect also affect productivity, which tends to be higher in sunny and moderate slopes areas opposed to shady and steep areas (Vidal-Macua *et al.*, 2018). We used a digital elevation

model (DEM) at 25 m of resolution, obtained from the Spanish Geographical Institute (MDT25; IGN 2015) and resampled to 30 m using bilinear interpolation, to retrieve elevation (in m.a.s.l.) and standard relief features such as slope angle (in degrees), aspect, and curvature metrics by means of the topographic position index (TPI; Weiss 2001).

Climate-related drivers

The potential influence of climate conditions on abandonment was explored through the temporal evolution of drought spells over the region (Arnaez *et al.*, 2011). We used the Standardized Precipitation Evapotranspiration Index (SPEI) as calculated in the Global Drought Monitor database (Vicente-Serrano *et al.*, 2010). SPEI was calibrated using ERA-5 reanalysis data from 1961 to 2019 (from the Copernicus Climate Change Service, C3S) and spatialized at a ~100km^2 resolution. SPEI is a drought-related index that synthesizes the water balance anomaly accounting for both precipitation and temperature (the latter being involved in the calculation of the potential evapotranspiration). SPEI ranges from -3 to 3, with moist conditions occurring when SPEI is above 0.84 and dry spells below -0.84 (Vicente-Serrano *et al.*, 2010). SPEI can be calculated at different temporal scales (from 1 up to 48 months). In this work, we retrieved the 12-month anomaly for December (SPEI12) on a yearly basis. We then calculated the Sen's slope of the SPEI12 (Sen, 1968), a trend detection procedure that summarizes the direction (increase or decline), magnitude (slope absolute value) and significance of a trend in a time series of data.

Ecological related drivers

Ecological constraints reduce competitiveness for farmers (Arnaez *et al.*, 2011). Soil characteristics are key in crop productivity. Therefore, the first fields to be abandoned are those with poor soil quality, shallow and stony soils (Gellrich and Zimmermann, 2007). We indirectly estimated soil porosity by using soil bulk density (cg/cm^3) in the first 15 cm from SoilGrids 2.0 – 250 m (Poggio *et al.*, 2021).

Socioeconomic and human-related drivers

The process of land abandonment relates heavily to the potential for agricultural revenue and impact of recreational activities (Lasanta *et al.*, 2017; Schirpke *et al.*, 2019). Overall, the former acts as an anchor for agriculture and grasslands whereas the latter promotes abandonment.

Tourism is the main driving force of socioeconomic change and land transformation in the Pyrenees (Schirpke *et al.*, 2019; Serra *et al.*, 2014). Despite a wider tourism opportunity spectrum in recent years, ski, hiking, camping and resorts remain the predominant recreational activities (Lasanta *et al.*, 2013, 2007). The spatial footprint of tourism was rated in terms of distance to stable tourism-related facilities, ski resorts and camping sites, as concentration points for visitors that engage in varied recreational activities (e.g., hiking). We obtained the spatial location of ski and camping sites from the 1:25.000 scale National Topographic Database (BTN25, IGN 2018). Then, we calculated the Euclidean distance (in meters) to the closest site.

Population dynamics are a key indicator of socioeconomic evolution (Collantes and Pinilla, 2004; Marín-Yaseli and Lasanta, 2003); loss of population due to either migration or aging is linked to economic decline (MacDonald *et al.*, 2000). In turn, this promotes the abandonment of traditional agricultural activities and lands (Lasanta *et al.*, 2017; Vidal-Macua *et al.*, 2018). We retrieved yearly population density (inhabitats/km^2) records at municipality level in the period 1986 to 2019 from the municipal population registries ("*Padrón*") accessed through the Spanish Statistics Institute (INE). Again, we characterized population trends by synthesizing the change in the annual number of inhabitants using the Sen's Slope (Sen, 1968).

Plot structure also contribute to understand land abandonment (Renwick *et al.*, 2013). To an extent, the size of agricultural plots relates to the productivity (Lasanta *et al.*, 2017). Larger plots tend to attain higher productivity rates by allowing mechanization and monoculture, and they

often belong to agricultural holdings with a single proprietor. Conversely, small plots are often arranged in complex mosaics, being the mechanization effort less profitable. We used plot size as a proxy for land structure and agricultural economic profitability. We calculated kernel density of polygon size (km^2) at 30 m spatial resolution, for each individual agricultural plot from the cadastral vector information (DGC, 2020).

Accessibility plays a crucial role in economic development (MacDonald *et al.*, 2000; Terres *et al.*, 2015). Proximity to population settlements or the road network facilitates the access to touristic infrastructures (Cervera *et al.*, 2019; Lasanta *et al.*, 2007), boosting the withdrawal of traditional activities and favoring the growth of the touristic and tertiary activities (Serra *et al.*, 2014). We calculated the Euclidean distance (in meters) to roads from a set of vector layers outlining the road network (roads, paths, and forest tracks) all of them accessible by car, representing the full road network obtained from the 1:25.000 scale National Topographic Database (BTN 25,IGN 2018); Euclidean distance to villages was also obtained from the same source (BTN 25, IGN 2018).

5.2.2.3. Modeling land abandonment

We modeled the spatial distribution of land abandonment probability by means of presence-absence binomial classification models. We used Random Forest (RF), a popular non-parametric and stochastic tree-based algorithm (Breiman, 2001; Liaw and Wiener, 2002). This algorithm is sensible to correlation between variables, but in our case there were no high pairwise correlations between variables (Supplementary Fig. S-5.5). RF was calibrated, validated and tested using the *caret* R's package (Kuhn, 2008).

Model training and calibration

RF models require hyper-parameters tuning like the number of predictors to be used at each split on any given "tree" (*mtry*), the number of trees (*ntrees)* or the minimum number of observations at the end nodes (*min node size*). The split rule followed the Gini index and we used AUC as

model validation metric. These parameters were optimized during the calibration stage using a 10-fold repeated cross-validation with 5 replications. To account for potential sensitivity to the locations that conform the response variable (see section 2.4) and prevent overfitting, we implemented an additional k-fold cross-validation (k=3) to split the original sample into 3 training (66%) and test (33%) datasets. This procedure led to a set of 30 models that were later aggregated into a single final prediction. Each model produced an individual raster map corresponding to model predicted probabilities. The predictions were averaged as the median value of the 30 raster maps, and as a measure of uncertainty and reproducibility, the coefficient of variation was provided. Additionally, we tested for spatial autocorrelation in prediction residuals using the Moran's I index (Moran, 1950), to warrant the spatial coherence of the results.

We tested this previous calibration as a null model to account for spatial autocorrelation. We computed a semivariogram using the model residuals (Supplementary Fig. S-5.3 and S-5.4); the stabilization of semivariance (Range) was around 8km. To control this effect in the model, we created a train subsample with a set minimum distance of 10km. Additionally, to control for spatial bias in our phenomena we added coordinates X and Y to the model as explanatory variables.

Model testing and performance

Model performance was evaluated via the previous 3-fold (section 2.4.1) cross-validation procedure. At each step, we used test samples to estimate the predictive performance of the RF models. We calculated the area under the curve (AUC) (Hanley and McNeil, 1982) of the receiver operating characteristic (ROC), a threshold-independent measure of the goodness-of-fit of any classifier. AUC measures the relationship between the false-positive (sensitivity) and true-positive (specificity) rates. It ranges from 0.5 to 1 representing random outcome and perfect prediction, respectively. According to Zhou *et al.* (2011) AUC values greater than 0.7 are sufficiently accurate to trust predictions (Mandrekar, 2010).

Variable performance

Machine learning algorithms tend to "hide" information on how they reach predictions, largely due to the complexity of the algorithm itself. To deliver insights into the role of the involved covariates, we retrieved their relative importance for each model. We used the node impurity, which defines the optimal condition to split tree branches during the training process. Averaging the impurities of each predictor provides a measure of its importance to the forest and, thus, the prediction.

Moreover, we addressed the graphical representation of the explanatory sense of covariates using partial dependence plots (PDP; Friedman 2001). PDPs are a graphical way to represent the marginal effect one variable has on the machine learning model prediction. We built 2-dimensional PDPs using a LOESS function (Locally Weighted Scatterplot Smoothing), showing the marginal response of the model (y-axis) along the range of values of a given predictor (x-axis). PDPs were built using the *pdp* (Greenwell, 2017) and *ggplot2* (Wickham, 2016) packages.

5.3. Results

5.3.1. Spatial pattern of predicted land abandonment probability

The spatial distribution of abandonment probability portrayed clear differences between the eastern and western ends of the Pyrenees (Fig. 5.2). Abandonment was more likely in the east (Ripollès, Garrotxa, Osona and Selva counties), with many areas over the 0.8 probability threshold. This region has excellent road connectivity with the Metropolitan area of Barcelona, which has contributed to the spread of second homes and investment properties. Probability rates were consistently intermediate-high up to the central Pyrenees, roughly on the border between Aragon and Catalonia. The western half (extending from *Pallars Sobirà to La Jacetania*) was characterized by a mosaic of hot and cold probability spots. Very low probability values (below 0.3) were observed inside and around protected

areas intermingling with higher probability (above 0.3) in locations specialized in rural tourism or skiing. Despite the presence of cold spots, values between 0.4-0.6 were predominant, with peaks above 0.6 in *Sobrarbe*, *Alto Gállego* and *Val d'Aran*. The uncertainty levels were consistently low throughout the study area, aside from some minor clusters of high variability in mountain summits and most protected areas in the central Pyrenees (Fig. 5.2B). A close-up view in Fig. 5.3 allows to best discern the effect of topography, accessibility, and proximity to touristic activities. Higher probability values were located in valley bottoms, close to cities and camping resorts. The probability of abandonment decreased with the altitudinal gradient. Furthermore, the inset view of the *Benasque* valley demonstrates the suitability of the model to address large-scale areas (1:100,000), identifying sharp transitions that enable the spatial characterization of the abandonment phenomenon.

5.3.2. Predictive performance of the RF models

The predictive performance of the models was satisfactory, with all RF models yielding a consistently high AUC ranging from 0.64 to 0.83 (mean AUC = 0.74, Fig. 5.4A). We observed a clear gap (Kruskal-Wallis test significant; $p<0.05$) at 0.5 probability (Fig. 5.4B) that separates the predicted probability between abandoned and non-abandoned locations. The density plots corroborated the high contrast between categories (Fig. 5.4B). In non-abandoned locations, we found a frequency peak close to 0.3, after which the curve flattens. In abandoned locations probability peaked near 0.65, decreasing fast into low density values below the 0.5 threshold. Taken together, all diagnostics support the satisfactory performance of the models, thus endorsing our findings.

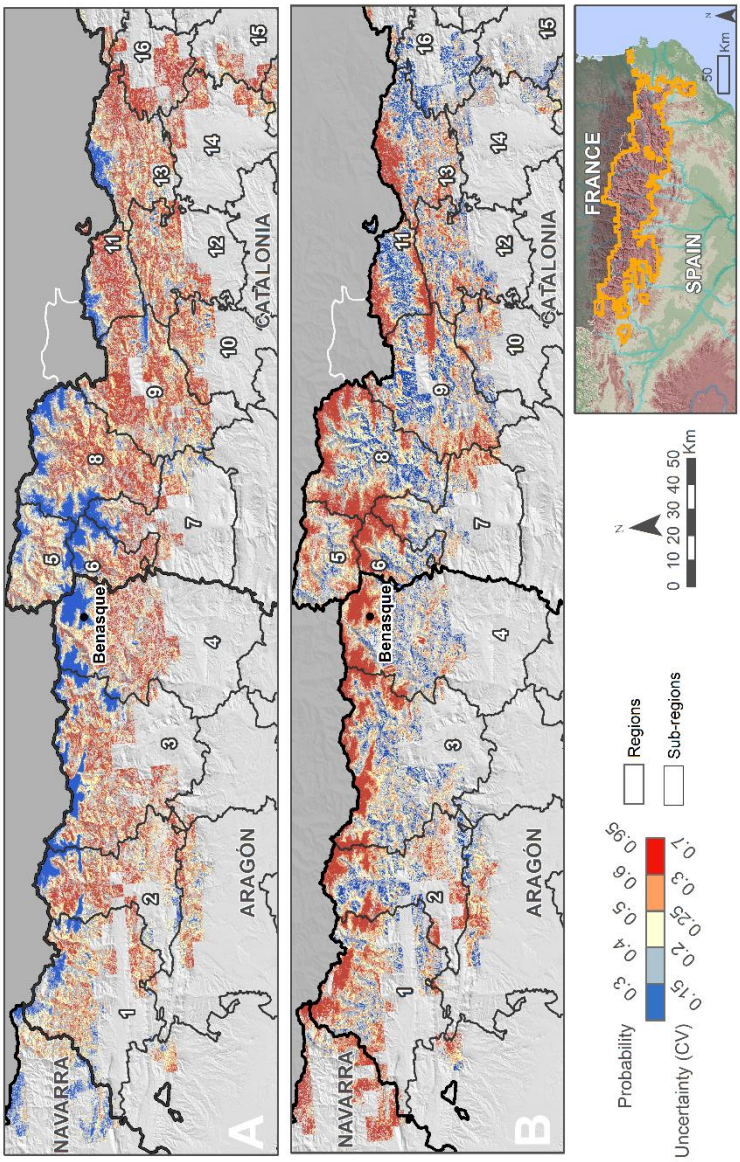

Figure 5.2: *Spatial distribution of land abandonment probability and uncertainty in the prediction. a) Probability of land abandonment and b) Uncertainty measured using the coefficient of variation of each of the 30 predictions. A shaded relief surface is used as backdrop. Previously abandoned areas (Gelabert et al., 2021) were masked in gray. Sub-regions labels: 1. La Jacetania, 2. Alto Gállego, 3. Sobrarbe, 4. La Ribagorza, 5. Val d'Aran, 6.*

Alta Ribagorça, 7. Pallars Jussà, 8. Pallars Sobirà, 9. Alt Urgell, 10. Solsonès, 11. La Cerdanya, 12. Berguedà, 13. Ripollès, 14. Osona, 15. Garrotxa, 16. Selva.

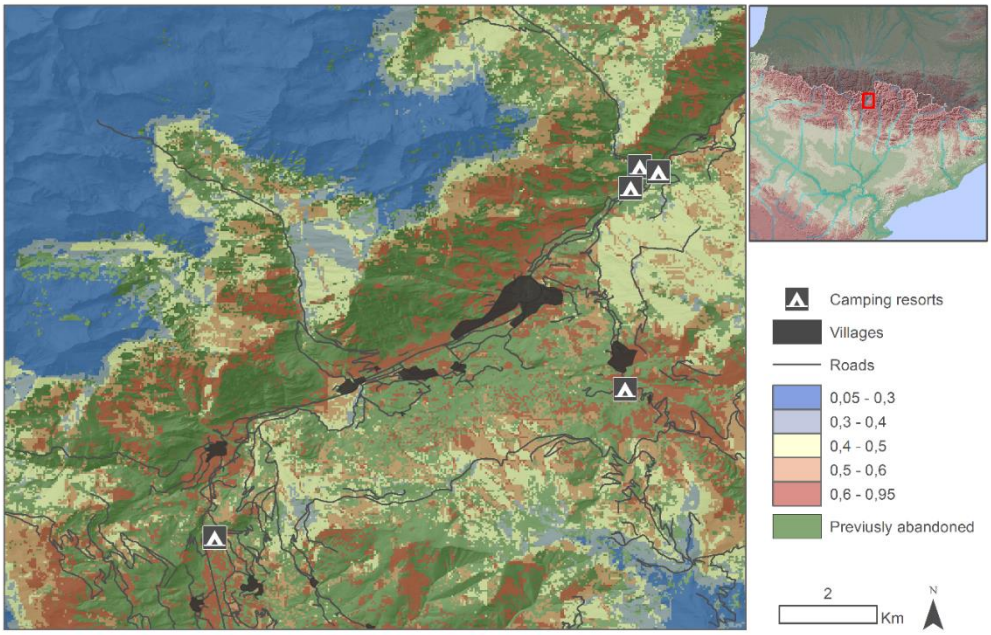

Figure 5.3: *Close-up view (1:100,000) of the Benasque valley. A shaded relief surface is used as backdrop.*

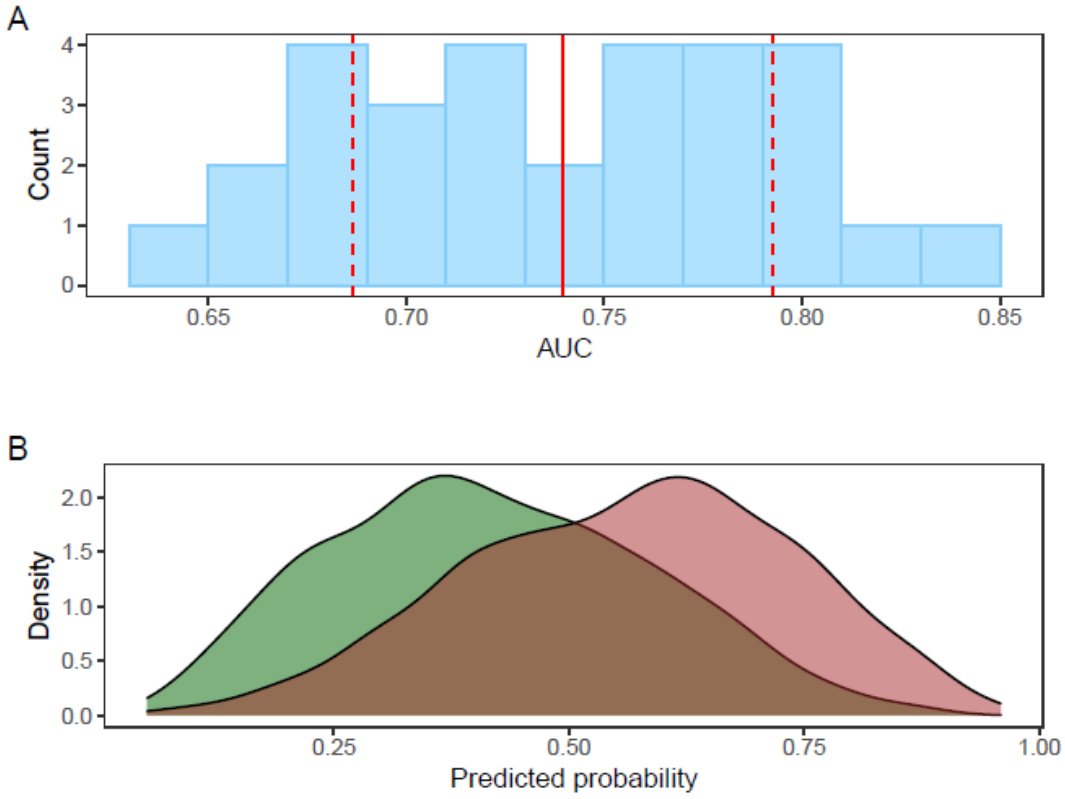

Figure 5.4: *A) Frequency values of AUC using RF. The solid line represents the mean AUC and dashed line ±1 standard deviation. B) and density histograms of predicted probability classified as abandoned (red) non abandoned (green).*

5.3.3. The role and performance of abandonment drivers

Fig. 5.5 ranks model covariates according to their relative importance in the predictions. Overall, distance to villages was the most influential factor, but soil bulk density and elevation also had a strong influence on land abandonment. Distance to camping sites and roads were the main socioeconomic drivers, and exerted a considerable influence in the probability of land abandonment, especially when compared with the remaining topographic variables, which were consistently found as the least important.

In a mid-tier position, we found aspect, followed closely by density population dynamics and agricultural plot size. Coordinates, slope and TPI were next in importance, and more influential than the remaining factors (SPEI, and distance to ski resorts).

Additionally, we analyzed the marginal effect in the predicted probability of abandonment of each covariate (Fig. 5.6). From this information, we extracted the characteristic traits of locations prone to land abandonment. The more likely locations were those (i) near to villages, (ii) in dense soils, (iii) in intermediate/high elevations (iii) with good accessibility (iv) but near to camping sites, (v) in south/east aspects (vi), where population density is increasing, (vii) preferably in large-size plots (viii) in steep slopes or (ix) bottom valleys and also (x) in zones with higher productivity (in bioclimatic terms).

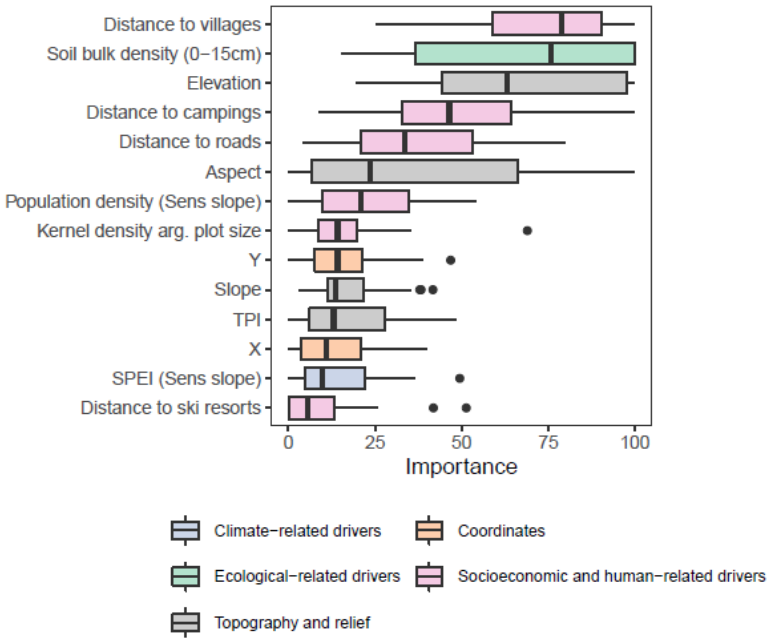

Figure 5.5: *Box-plots with variable performance in terms of node impurity. Boxes represent the distribution of increment in MSE across models. The boxes indicate the 1st/3rd quartiles,*

the whiskers indicate 10th/90th percentiles, the black line within the box is the median, and the dots indicate values below the 10th percentile or above the 90th percentile.

5.4. Discussion

Land abandonment locations in the Iberian Pyrenees in 1982-2018 shared common characteristics that allowed to identify future areas likely to be affected by this environmental impact (Lasanta *et al.*, 2017; Rey Benayas, 2007).

Previous work on the abandonment process and the role played by its drivers is relatively abundant in the literature. From a methodological standpoint, our analysis aligns with the work by Vidal-Macua *et al.* (2018) in the Pyrenees, Garbarino *et al.* (2020) in the Alps and Apennines, or Morán-Ordóñez *et al.* (2011) in *the Cantabrian mountains* (northwest Spain), relying on statistical or machine learning algorithms to model the probability of land abandonment from a set of driving factors. Our modeling results stand equal or above these works in terms of performance and in agreement with the overall behavior of the drivers.

One critical difference with previous studies laid in our use of continuous variables (as opposed to discrete in a spatial sense), allowing for mapping. The use of variables aggregated using administrative units provided explanatory insights to these authors, but precluded the detailed mapping of model outcomes (Thieken *et al.*, 2006; Zandbergen and Ignizio, 2010). Excepting the study by Morán-Ordóñez *et al.* (2011), their focus was usually in the performance of the model or the explanatory significance of the drivers, but neither the spatial nature of the phenomena nor the spatial footprint of abandonment potential was fully addressed.

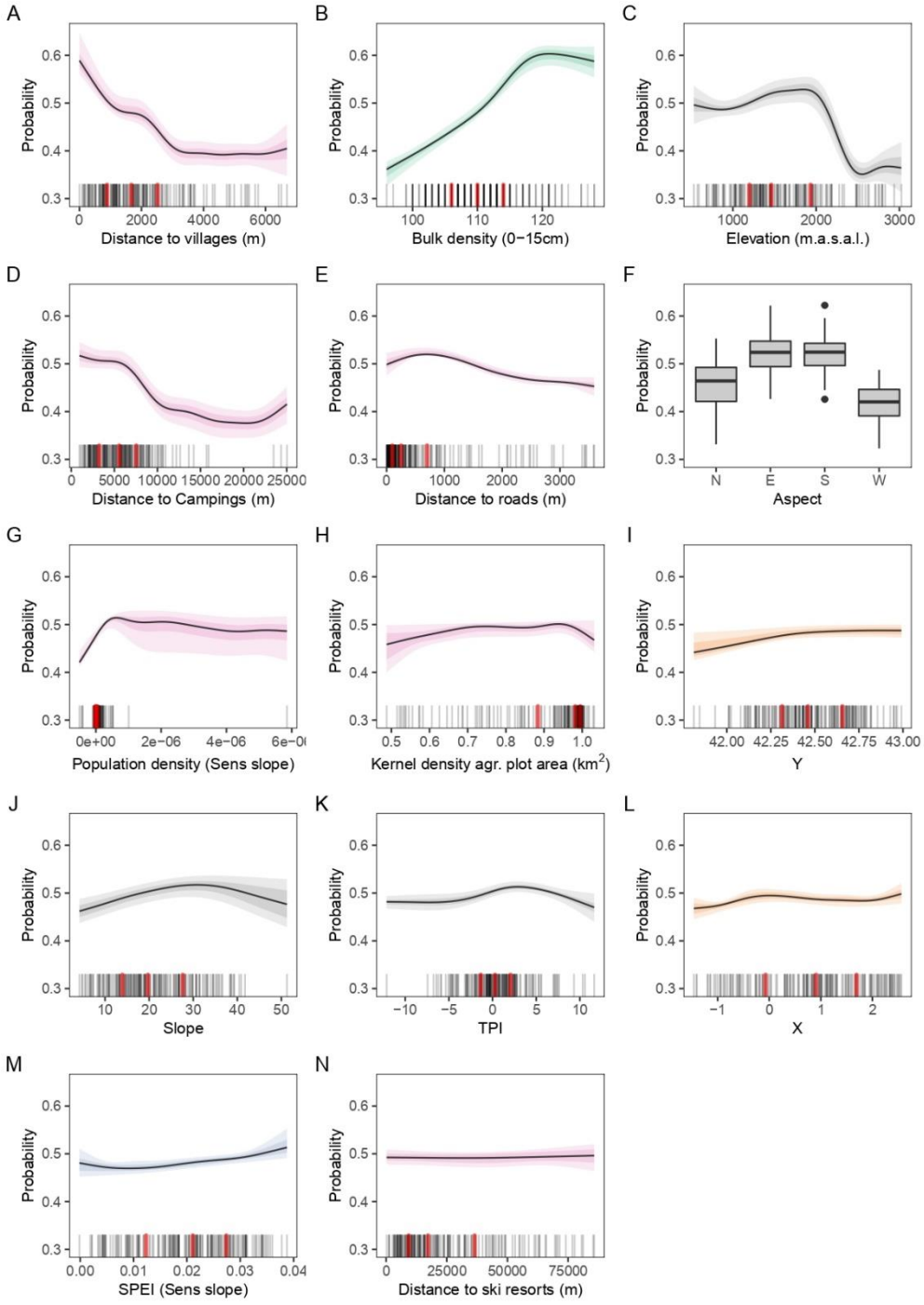
A
Probability
Distance to villages (m)
B
Bulk density (0−15cm)
C
Elevation (m.a.s.a.l.)
D
Distance to Campings (m)
E
Distance to roads (m)
F
N
E
S
W
Aspect
G
Population density (Sens slope)
H
Kernel density agr. plot area (km2)
I
Y
J
Slope
K
TPI
L
X
M
SPEI (Sens slope)
N
Distance to ski resorts (m)

Figure 5.6: *Partial dependence plots of (A) distance to ski resorts, (B) distance to camping resorts, (C) distance to villages, (D) distance to roads, (E) Sen's slope statistic for population variation, (F) Plot structure, (G) Aspect, (H) Slope, (I) TPI, and (J) Elevation, and (K) Sen's slope statistic for SPEI variation. The x-axis represents the value of the covariate, and the y-axis represents the associated predicted probability. The solid line represents the averaged dependence whereas dark and light shaded areas represent 1st to 3rd quartile range and minimum and maximum range, respectively. Color represents driver domains: grey, physiography; pink, socioeconomic; and blue climate; green, ecological; orange, coordinates. The density of presence events is represented by vertical black lines above the x-axes, and overlaid red ticks depict the quartiles.*

As Morán-Ordóñez *et al.* (2011), we do supply spatial predictions. In fact, our outcomes in the Pyrenees complement and support their discoveries in *Cantabrian mountains*. We found that land abandonment in the Pyrenees not only was driven by similar factors but also depicted a similar spatial pattern. This suggests the existence of homogeneous causal relations for land abandonment in the northern Iberian Peninsula.

In the specific case of the Spanish Pyrenees, abandonment started in the early 2oth century (García-Ruiz *et al.*, 2015) as a consequence of the industrialization process. During the second half of the century, the rural migrations towards main industrial cities and land abandonment reached their peak. Nowadays, the abandonment in the Pyrenees continues, though at a slower pace. The process is now linked to the raise of tertiary activities, mainly tourism and second residences in mountain regions (Prados, 2008; Serra *et al.*, 2014). Tourism is thus the main element promoting socioeconomic change in the Pyrenees in recent decades (Lasanta and Vicente-Serrano, 2007). Primary activities, such as agriculture and livestock farming, have been abandoned in favor of activities linked to tourist facilities, or at least complemented with part-time dedication to tertiary activities aimed to provide an outflow of agricultural products with greater added value (Cánoves *et al.*, 2004; Petrou *et al.*, 2007; Vidal-Macua *et al.*, 2018). In addition, side effects from the Common Agricultural Policy (Cazcarro *et al.*, 2015) and other subsidies funded by the European Union such as the LEADER program – aimed at stabilizing and promoting repopulation – and INTERREG – designated to fund transnational initiatives – ended up in

investments that favored the development of tertiary activities (Lasanta and Marín-Yaseli, 2007).

While in agreement with these drivers and causal relations, we found strong regional and local differences in the potential for land abandonment within the Pyrenees. The observed spatial pattern responds to site-specific combinations of certain drivers operating at different levels. The higher land abandonment potential occurs in the eastern end of the massif, in the sub-regions of *Osona, Garrotxa, Ripollès, Cerdanya* and the north of *Berguedà,* all of them belonging to Catalonia (Badía *et al.*, 2004; Vilà-Cabrera *et al.*, 2017). We believe this cluster responds to the growth of second residential housing encouraged by good accessibility (Fig. 5.6 A and E). Their relative position to the main road network (*C-17* and *C-16* speedways) connecting with the metropolitan area of Barcelona (the largest in the region) has favored the sprawl of leisure housing and other forms of accommodation, such as campings and hotels (Fig. 5.6D). In Aragon, a similar pattern is observed along the corridors around the *A- 23, A-21* and *N-350, N-240* roads, all of them linking with Zaragoza. A different role is played by type of road, with high abandonment rates in locations connected to main roads (Vidal-Macua *et al.*, 2018), but low around secondary and local roads (Fig. 5.6E). The presence of skiing and winter sports exerted a contrasting influence associated to local conditions. Lasanta *et al.* (2013) noted that ski resorts in Aragon are close to villages whereas in Catalonia they locate farther away. Accordingly, the predicted probability of abandonment near ski facilities is higher in Aragon than in Catalonia, suggesting that the ski resorts do not foster abandonment by themselves (Fig. 5.6 N) but rather for their complementary recreational offer to villages and towns. The behavior of population dynamics further evidenced that regions experiencing increased number of inhabitants were more prone to abandonment and vice versa. In other words, regions with greater tourism tradition – L*a Jacetania, Alto Gállego, Sobrarbe, Pallars Sobirà and Val d'Aran* – grew due to opportunities derived from the touristic activity abandoning primary activities (Fig. 5.6G) (García-Ruiz *et al.*, 2015). In this line, LEADER and other programs fund actions in the tourism sector (rural tourism modalities and ecotourism) to anchor population (Lasanta and Marín-Yaseli, 2007). Our

findings support that the growth in population and accessibility by road related to the development of tourist resorts increases the probability of land abandonment (Cervera *et al.*, 2019; Lange *et al.*, 2013). Likewise, the increasing number of inhabitants –and housing- is often associated to new job opportunities in the service sector (Ameztegui *et al.*, 2010; Gellrich and Zimmermann, 2007; Lasanta *et al.*, 2017, 2013, 2007; MacDonald *et al.*, 2000).

Topographical features operate on a local level. The complex reliefs of mountainous areas for mechanization, coupled with the low mobility of an aged population, demote economic competitiveness (Corbelle-Rico *et al.*, 2012; García-Ruiz and Lana-Renault, 2011; Lasanta *et al.*, 2017; MacDonald *et al.*, 2000; Terres *et al.*, 2015). The chance of abandonment increases as we gain elevation reaching the maximum around 2000 m (Ameztegui *et al.*, 2010). Also, abandonment seems to be more likely on south and east facing steep slopes which attain higher productivity potential (Fig. 5.6Fand J) and in bottom valleys (Fig. 5.6 K). In Pyrenees agricultural plots are relatively large, around 1km^2 between 1st and 3rd percentile (0.9 and 1.1 km^2). In agreement with Renwick *et al.* (2013), we found smaller plots more prone to abandonment than medium-size one. Nonetheless, large plots, even though not abundant, were also linked to increased chance of abandonment (Fig. 5.6H); probably the higher abandonment incidence in small plots is be due to their location in valley bottoms.

Finally, results from SPEI Sen's slope analysis surprisingly concluded that the abandonment is currently taking place in areas where productivity is higher (in bioclimatic terms), suggesting a greater influence of socioeconomic factors in land dynamics (Fig. 5.6M). Gehrig-Fasel, Guisan, and Zimmermann (2007) and Ameztegui *et al.* (2010) found that in the Pyrenees forest advance responds to land abandonment rather than climate. It may happen that climate change is warming mountain regions, rendering climate relationships more difficult to assess (López-Moreno *et al.*, 2008). Soil properties also attain high importance in land abandonment probability. Fig 6B shows that in areas where abandonment has occurred the soil bulk density is higher than in cultivated areas (Koulouri and Giourga, 2007).

Overall, we found land abandonment favors areas with an accumulation of activities, infrastructure and population related to the tourism sector. In particular, easy access to high-capacity road infrastructures, far from contributing to the fixation of rural population in the territory, favors the sprawl of touristic resorts and leisure housing eventually leading to land abandonment. Relying economically only on tourism has proven risky, whereas diversification promotes resilient economies. The recovery of traditional agricultural practices, or reinvented ones based in the introduction of new bio-economy ventures, and their integration with recreational activities and new tourism modalities is thus necessary to avert the abandonment process and to prevent ecological and cultural degradation. Rural economic development is very sensitive to economic crises and extraordinary events such as the COVID-19 outbreak (Gössling *et al.*, 2020). Consequently, both socioeconomic diversification and control of land abandonment in our mountain landscapes are crucial. Predicting and mapping the abandonment hot spots in the Spanish Pyrenees provides a much-needed basis for implementation of land management alternatives.

5.5. Conclusions

The identification of strategic locations where land abandonment will be more likely in the future is critical to design effective policies to prevent and reverse the process and its associated impacts. In this work, we present an approach based on highly accurate geospatial information to map the probability of land abandonment. Our results provide spatially explicit probability and uncertainty outputs, providing insights into site-specific abandonment potential and the influence of its drivers.

Our modeling approach captures both linear and nonlinear relationships between abandonment probability and its driving forces. We found that land abandonment in the Spanish Pyrenees is more likely to occur in areas, near to villages, with high touristic activity, with good road connectivity, and in plots with dense soil bulk density. Targeting hot spots for control of land abandonment allows restoring valuable ecosystem services

generated by Pyrenean cultural landscapes as well as generating more resilient economies. Our outputs allow planners to make decisions at multiple scales, from local land management plans to region-wide policy programs.

5.6 Acknowledgements

This work was supported by project IMAGINE [CGL2016-80400-R] funded by the Spanish Science Foundation (FECYT) and under the research grant program Ajuts UdL, Jade Plus i Fundació Bancària La Caixa [Agreement 79/2018 of the Governing Council of the University of Lleida].

5.7. References

Ali, I., Cawkwell, F., Dwyer, E., Barrett, B., and Green, S., 2016. Satellite remote sensing of grasslands: From observation to management. *Journal of Plant Ecology*, 9 (6), 649–671.

Ameztegui, A., Brotons, L., and Coll, L., 2010. Land-use changes as major drivers of mountain pine (Pinus uncinata Ram.) expansion in the Pyrenees. *Global Ecology and Biogeography*, 19 (5), 632–641.

Ameztegui, A., Coll, L., Brotons, L., and Ninot, J.M., 2016. Land-use legacies rather than climate change are driving the recent upward shift of the mountain tree line in the Pyrenees. *Global Ecology and Biogeography*, 25 (3), 263–273.

Ameztegui, A., Morán-Ordóñez, A., Márquez, A., Blázquez-Casado, Á., Pla, M., Villero, D., García, M.B., Errea, M.P., and Coll, L., 2021. Forest expansion in mountain protected areas: Trends and consequences for the landscape. *Landscape and Urban Planning*, 216, 104240.

Arnaez, J., Lasanta, T., Errea, M.P., and Ortigosa, L., 2011. Land abandonment, landscape evolution, and soil erosion in a Spanish Mediterranean mountain region: The case of Camero Viejo. *Land Degradation & Development*, 22 (6), 537–550.

Badía, A., Pèlachs, A., Vera, A., Tulla, A.F., and Soriano, J.M., 2004. Cambios en los usos y cubiertas del suelo y los efectos

en la vulnerabilidad en las comarcas de montaña de Cataluña. Del rol del fuego como herramienta de gestión a los incendios como amenaza. *Pirineos*, 169.

Beilin, R., Lindborg, R., Stenseke, M., Pereira, H.M., Llausàs, A., Slätmo, E., Cerqueira, Y., Navarro, L., Rodrigues, P., Reichelt, N., Munro, N., and Queiroz, C., 2014. Analysing how drivers of agricultural land abandonment affect biodiversity and cultural landscapes using case studies from Scandinavia, Iberia and Oceania. *Land Use Policy*, 36, 60–72.

Breiman, L., 2001. Random forests. *Machine Learning*, 45, 5–32.

Cánoves, G., Villarino, M., Priestley, G.K., and Blanco, A., 2004. Rural tourism in Spain: an analysis of recent evolution. *Geoforum*, 35 (6), 755–769.

Cazcarro, I., Duarte, R., Martín-Retortillo, M., Pinilla, V., and Serrano, A., 2015. Water scarcity and agricultural growth in Spain: from curse to blessing? *In: Natural Resources and Economic Growth*.

Cervera, T., Pino, J., Marull, J., Padró, R., and Tello, E., 2019. Understanding the long-term dynamics of forest transition: From deforestation to afforestation in a Mediterranean landscape (Catalonia, 1868–2005). *Land Use Policy*.

Collantes, F. and Pinilla, V., 2004. Extreme Depopulation in the Spanish Rural Mountain Areas: A Case Study of Aragon in the Nineteenth and Twentieth Centuries. *Rural History*, 15 (2), 149–166.

Corbelle-Rico, E., Crecente-Maseda, R., and Santé-Riveira, I., 2012. Multi-scale assessment and spatial modelling of agricultural land abandonment in a European peripheral region: Galicia (Spain), 1956–2004. *Land Use Policy*, 29 (3), 493–501.

DGC, 2020. Cadastral data. *Instituto Nacional de Estadística*.

Dieterich, M. and Van Der Straaten, J., 2004. *Cultural Landscapes and Land Use*. Springer.

Estel, S., Kuemmerle, T., Alcántara, C., Levers, C., Prishchepov, A., and Hostert, P., 2015. Mapping farmland abandonment and recultivation across Europe using MODIS NDVI time series. *Remote Sensing of Environment*, 163, 312–325.

Friedman, J.H., 2001. Greedy function approximation: A gradient boosting machine. *The annals of statistics*, 29 (5), 44.

Garbarino, M., Morresi, D., Urbinati, C., Malandra, F., Motta, R., Sibona, E.M., Vitali, A., and Weisberg, P.J., 2020. Contrasting land use legacy effects on forest landscape dynamics in the Italian Alps and the Apennines. *Landscape Ecology*.

García Ruiz, J.M. and Lasanta, T., 2018. *El Pirineo Aragonés como paisaje cultural*. Pirineos.

García-Ruiz, J.M. and Lana-Renault, N., 2011. Hydrological and erosive consequences of farmland abandonment in Europe, with special reference to the Mediterranean region - A review. *Agriculture, Ecosystems and Environment*, 140 (3–4), 317–338.

García-Ruiz, J.M., López-Moreno, J.I., Lasanta, T., Vicente-Serrano, S.M., González-Sampériz, P., Valero-Garcés, B.L., Sanjuán, Y., Beguería, S., Nadal-Romero, E., Lana-Renault, N., and Gómez-Villar, A., 2015. Los efectos geoecológicos del cambio global en el pirineo central español: Una revisión a distintas escalas espaciales y temporales. *Pirineos*, 170.

Gartzia, M., Alados, C.L., and Pérez-Cabello, F., 2014. Assessment of the effects of biophysical and anthropogenic factors on woody plant encroachment in dense and sparse mountain grasslands based on remote sensing data. *Progress in Physical Geography: Earth and Environment*, 38 (2), 201–217.

Gehrig-Fasel, J., Guisan, A., and Zimmermann, N.E., 2007. Tree line shifts in the Swiss Alps: Climate change or land abandonment? *Journal of Vegetation Science*, 18 (4), 571–582.

Gelabert, P., Rodrigues, M., de la Riva, J., Ameztegui, A., Sebastià, M.T., and Vega-Garcia, C., 2021. LandTrendr smoothed spectral profiles enhance woody encroachment monitoring. *Remote Sensing of Environment*, 262, 112521.

Gellrich, M. and Zimmermann, N.E., 2007. Investigating the regional-scale pattern of agricultural land abandonment in the Swiss mountains: A spatial statistical modelling approach. *Landscape and Urban Planning*, 79 (1), 65–76.

Gössling, S., Scott, D., and Hall, C.M., 2020. Pandemics, tourism and global change: a rapid assessment of COVID-19. *Journal of Sustainable Tourism*, 0 (0), 1–20.

Greenwell, B.M., 2017. pdp: An R Package for Constructing Partial Dependence Plots. *The R Journal*, 9 (1), 421–436.

Hanley, J.A. and McNeil, B.J., 1982. The meaning and use of the area under a receiver operating characteristic (ROC) curve. *Radiology*.

IGN, 2015. MDT25. *Instituto Geográfico Nacional. Gobierno de España.*

IGN, 2018. Mapas vectoriales y bases cartográficas y topográficas a escala 1:25,000 para explotación y consulta mediante sistemas de información geográfica. *Instituto Geográfico Nacional. Gobierno de España.*

Jongman, R.H.G., 2002. Homogenisation and fragmentation of the European landscape: ecological consequences and solutions. *Landscape and Urban Planning*, 58 (2), 211–221.

Koulouri, M. and Giourga, Chr., 2007. Land abandonment and slope gradient as key factors of soil erosion in Mediterranean terraced lands. *CATENA*, 69 (3), 274–281.

Kuhn, M., 2008. Building predictive models in R using the caret package. *Journal of statistical software*, 28 (5), 1–26.

Lange, A., Piorr, A., Siebert, R., and Zasada, I., 2013. Spatial differentiation of farm diversification: How rural attractiveness and vicinity to cities determine farm households' response to the CAP. *Land Use Policy*, 31, 136–144.

Lasanta, T., Arnáez, J., Pascual, N., Ruiz-Flaño, P., Errea, M.P., and Lana-Renault, N., 2017. Space–time process and drivers of land abandonment in Europe. *Catena*, 149, 810–823.

Lasanta, T., Beltran, O., and Vaccaro, I., 2013. Socioeconomic and territorial impact of the ski industry in the spanish pyrenees: Mountain development and leisure induced urbanization. *Pirineos*, 168 (168), 103–128.

Lasanta, T., Laguna, M., and Vicente-Serrano, S.M., 2007. Do tourism-based ski resorts contribute to the homogeneous development of the Mediterranean mountains? A case study

in the Central Spanish Pyrenees. *Tourism Management*, 28 (5), 1326–1339.

Lasanta, T. and Marín-Yaseli, M.L., 2007. Effects of European Common Agricultural Policy and Regional Policy on the Socioeconomic Development of the Central Pyrenees, Spain. *Mountain Research and Development*, 27 (2), 130–137.

Lasanta, T. and Vicente-Serrano, S.M., 2007. Cambios en la cubierta vegetal en el pirineo aragonés en los últimos 50 años. *Pirineos*, (162), 125–154.

van Leeuwen, C.C.E., Cammeraat, E.L.H., de Vente, J., and Boix-Fayos, C., 2019. The evolution of soil conservation policies targeting land abandonment and soil erosion in Spain: A review. *Land Use Policy*, 83 (February), 174–186.

Liaw, A. and Wiener, M., 2002. Classification and regression by randomForest. *R news*, 2 (3), 18–22.

López-Moreno, J.I., Goyette, S., and Beniston, M., 2008. Climate change prediction over complex areas: spatial variability of uncertainties and predictions over the Pyrenees from a set of regional climate models. *International Journal of Climatology*, 28 (11), 1535–1550.

MacDonald, D., Crabtree, J.R., Wiesinger, G., Dax, T., Stamou, N., Fleury, P., Gutierrez Lazpita, J., and Gibon, A., 2000. Agricultural abandonment in mountain areas of Europe: Environmental consequences and policy response. *Journal of Environmental Management*, 59 (1), 47–69.

Mandrekar, J.N., 2010. Receiver Operating Characteristic Curve in Diagnostic Test Assessment. *Journal of Thoracic Oncology*, 5 (9), 1315–1316.

Marín-Yaseli, M.L. and Lasanta, T., 2003. Competing for Meadows. *Mountain Research and Development*, 23 (2), 169–176.

Moran, P.A.P., 1950. Notes on continuous stochastic phenomena. *Biometrika*, 37, 17–23.

Morán-Ordóñez, A., Suárez-Seoane, S., Calvo, L., and de Luis, E., 2011. Using predictive models as a spatially explicit support tool for managing cultural landscapes. *Applied Geography*, 31 (2), 839–848.

Mottet, A., Ladet, S., Coqué, N., and Gibon, A., 2006. Agricultural land-use change and its drivers in mountain landscapes: A

case study in the Pyrenees. *Agriculture, Ecosystems and Environment*.

Nadal-Romero, E., Lasanta, T., Regüés, D., Lana-Renault, N., and Cerdà, A., 2011. Hydrological response and sediment production under different land cover in abandoned farmland fields in a mediterranean mountain environment. *Boletin de la Asociacion de Geografos Espanoles*, (55).

Nainggolan, D., de Vente, J., Boix-Fayos, C., Termansen, M., Hubacek, K., and Reed, M.S., 2012. Afforestation, agricultural abandonment and intensification: Competing trajectories in semi-arid Mediterranean agro-ecosystems. *Agriculture, Ecosystems & Environment*, 159, 90–104.

Ninot, J.M., Carrillo, E., Font, X., Carreras, J., Ferré, A., Masalles, R.M., Soriano, I., and Vigo, J., 2007. Altitude zonation in the Pyrenees. A geobotanic interpretation. *Phytocoenologia*, 37 (3–4), 371–398.

Pais, S., Aquilué, N., Campos, J., Sil, Â., Marcos, B., Martínez-Freiría, F., Domínguez, J., Brotons, L., Honrado, J.P., and Regos, A., 2020. Mountain farmland protection and fire-smart management jointly reduce fire hazard and enhance biodiversity and carbon sequestration. *Ecosystem Services*, 44, 101143.

Pereira, H.M., Leadley, P.W., Proença, V., Alkemade, R., Scharlemann, J.P.W., Fernandez-Manjarrés, J.F., Araújo, M.B., Balvanera, P., Biggs, R., Cheung, W.W.L., Chini, L., Cooper, H.D., Gilman, E.L., Guénette, S., Hurtt, G.C., Huntington, H.P., Mace, G.M., Oberdorff, T., Revenga, C., Rodrigues, P., Scholes, R.J., Sumaila, U.R., and Walpole, M., 2010. Scenarios for Global Biodiversity in the 21st Century. *Science*, 330 (6010), 1496–1501.

Perpiña, C., Coll, E., Lavalle, C., and Martínez, J.C., 2020. An Assessment and Spatial Modelling of Agricultural Land Abandonment in Spain (2015–2030). *Sustainability*, 12 (2), 560.

Petrou, A., Pantziou, E.F., Dimara, E., and Skuras, D., 2007. Resources and Activities Complementarities: the Role of Business Networks in the Provision of Integrated Rural Tourism. *Tourism Geographies*, 9 (4), 421–440.

Poggio, L., de Sousa, L.M., Batjes, N.H., Heuvelink, G.B.M., Kempen, B., Ribeiro, E., and Rossiter, D., 2021. SoilGrids 2.0: producing soil information for the globe with quantified spatial uncertainty. *SOIL*, 7 (1), 217–240.

Poyatos, R., Latron, J., and Llorens, P., 2003. Land use and land cover change after agricultural abandonment: The case of a Mediterranean Mountain area (Catalan Pre-Pyrenees). *Mountain Research and Development*.

Prados, M.J., 2008. Naturbanization: New identities and processes for rural-natural areas [online]. *Naturbanization*. Available from: https://www.taylorfrancis.com/ [Accessed 10 Jun 2020].

Renwick, A., Jansson, T., Verburg, P.H., Revoredo-Giha, C., Britz, W., Gocht, A., and McCracken, D., 2013. Policy reform and agricultural land abandonment in the EU. *Land Use Policy*, 30 (1), 446–457.

Rey Benayas, J., 2007. Abandonment of agricultural land: an overview of drivers and consequences. *CAB Reviews: Perspectives in Agriculture, Veterinary Science, Nutrition and Natural Resources*, 2 (057).

Rey Benayas, J.M., Martins, A., Nicolau, J.M., and Schulz, J.J., 2007. Abandonment of agricultural land: an overview of drivers and consequences. *CAB Reviews: Perspectives in Agriculture, Veterinary Science, Nutrition and Natural Resources*, 2 (057).

Rivas-Martinez, S., 1987. *Memoria del mapa de series de vegetación de España*. Madrid: ICONA. Ministerio de Agricultura, Pesca y Alimentación.

Schirpke, U., Altzinger, A., Leitinger, G., and Tasser, E., 2019. Change from agricultural to touristic use: Effects on the aesthetic value of landscapes over the last 150 years. *Landscape and Urban Planning*, 187, 23–35.

Sen, P.K., 1968. Estimates of the Regression Coefficient Based on Kendall's Tau. *Journal of the American Statistical Association*, 63 (324).

Serra, P., Vera, A., Tulla, A.F., and Salvati, L., 2014. Beyond urban–rural dichotomy: Exploring socioeconomic and land-use processes of change in Spain (1991–2011). *Applied Geography*, 55, 71–81.

Sluiter, R. and de Jong, S.M., 2007. Spatial patterns of Mediterranean land abandonment and related land cover transitions. *Landscape Ecology*, 22 (4), 559–576.

Stoate, C., Báldi, A., Beja, P., Boatman, N.D., Herzon, I., van Doorn, A., de Snoo, G.R., Rakosy, L., and Ramwell, C., 2009. Ecological impacts of early 21st century agricultural change in Europe – A review. *Journal of Environmental Management*, 91 (1), 22–46.

Terres, J.-M., Scacchiafichi, L.N., Wania, A., Ambar, M., Anguiano, E., Buckwell, A., Coppola, A., Gocht, A., Källström, H.N., Pointereau, P., Strijker, D., Visek, L., Vranken, L., and Zobena, A., 2015. Farmland abandonment in Europe: Identification of drivers and indicators, and development of a composite indicator of risk. *Land Use Policy*, 49, 20–34.

Thieken, A.H., Müller, M., Kleist, L., Seifert, I., Borst, D., and Werner, U., 2006. Regionalisation of asset values for risk analyses. *Natural Hazards and Earth System Sciences*, 6 (2), 167–178.

Ustaoglu, E. and Collier, M.J., 2018. Farmland abandonment in Europe: An overview of drivers, consequences, and assessment of the sustainability implications. *Environmental Reviews*, 26 (4), 396–416.

Vacquie, L., Houet, T., Sohl, T., Reker, R., and Sayler, K., 2015. Modelling Regional Land Change Scenarios to Assess Land Abandonment and Reforestation Dynamics in th he Pyrenees (France). *Jounal of Mountains Science*, 12 (2), 905–920.

Vicente-Serrano, S.M., Beguería, S., and López-Moreno, J.I., 2010. A Multiscalar Drought Index Sensitive to Global Warming: The Standardized Precipitation Evapotranspiration Index. *Journal of Climate*, 23 (7), 1696–1718.

Vidal-Macua, J.J., Ninyerola, M., Zabala, A., Domingo-Marimon, C., Gonzalez-Guerrero, O., and Pons, X., 2018. Environmental and socioeconomic factors of abandonment of rainfed and irrigated crops in northeast Spain. *Applied Geography*, 90 (September 2017), 155–174.

Vilà-Cabrera, A., Espelta, J.M., Vayreda, J., and Pino, J.,

2017. "New Forests" from the Twentieth Century are a Relevant Contribution for C Storage in the Iberian Peninsula. *Ecosystems*, 20 (1), 130–143.

Weiss, A.D., 2001. Topographic Position and Landforms Analysis. *In*: *ESRI International User Conference,*. San Diego: ESRI.

Wickham, H., 2016. *ggplot2: Elegant Graphics for Data Analysis*. Springer-Verlag New York.

Zandbergen, P.A. and Ignizio, D.A., 2010. Comparison of Dasymetric Mapping Techniques for Small-Area Population Estimates. *Cartography and Geographic Information Science*, 37 (3), 199–214.

Zaragozí, B., Rabasa, A., Rodríguez-Sala, J.J., Navarro, J.T., Belda, A., and Ramón, A., 2012. Modelling farmland abandonment: A study combining GIS and data mining techniques. *Agriculture, Ecosystems & Environment*, 155, 124–132.

Zhou, X.H., Obuchowski, N.A., and McClish, D.K., 2011. *Statistical Methods in Diagnostic Medicine*. Statistical Methods in Diagnostic Medicine.

Capítulo 6

On the relationship between tree height, elevation and climate in European mountain ranges

6. On the relationship between tree height, elevation and climate in European mountain ranges

Cita: Gelabert, P.J., Rodrigues, M., Coll, L., Vega-Garcia, C., Ameztegui, A. (n.d.) On the relationship between tree height, elevation and climate in European mountain ranges. *In prep.*

6.1. Introduction

Mountain forests account for 23% of the forested lands worldwide and sustain about half of the world's population (Price *et al.* 2011). They provide a wide array of goods and services such as freshwater, timber, biofuel, shelter from animals, nutrient cycling, air purification and carbon sequestration. However, their subsistence and profitability are seriously threatened by the advent of global change (Albrich *et al.* 2020).

Tree height is a good indicator of biological productivity and site quality (Grace *et al.* 2002). It has recently been demonstrated to be relevant for estimates of above ground biomass and carbon storage (Silva *et al.* 2018, Qi, Saarela, *et al.* 2019). Furthermore, it is also a proxy for ecosystem structure, its heterogeneity is an essential variable for predicting species richness at different scales (Lopatin *et al.* 2016, Cazzolla Gatti *et al.* 2017). Hence the establishment of global canopy height as a high priority variable to be monitored from space (Skidmore *et al.* 2021). Alternatively, tree height can help to monitor and anticipate the possible effects of global change on forest ecosystems (Grace *et al.* 2002). Many studies point at climate as the main driver of the maximum height development of trees (Grace *et al.* 2002, Körner and Paulsen 2004, Paulsen and Körner 2014). Overall, temperature seems to limit maximum tree height at high latitudes and high elevation ranges (Körner and Paulsen 2004, Paulsen and Körner 2014, Reich *et al.* 2015), whereas precipitation and water availability mostly

influence tree development in the lowlands (Liénard *et al.* 2016, Fricker *et al.* 2019). The tree height is often analyzed at the local scale via forest inventory or field campaigns (Larjavaara and Muller-Landau 2013), which are expensive and time-consuming, and do not provide a global picture of the phenomenon. LiDAR sensors are able collect highly accurate and dense forest structure samplings (Valbuena *et al.* 2020), notwithstanding only some countries have a periodic and wall-to-wall coverage due its expensive cost. In this sense, recent space-borne laser sensors, such as Global Ecosystem Dynamics Investigation (GEDI) - an active remote sensing sensor onboard the International Space Station that provides detailed 3D information about forest structure and responses at the regional/global level-, are a trade-off solution for tree height sampling at global scale (Dubayah, Blair, *et al.* 2020).

Recent experiences leveraging airborne LiDAR to derive canopy height (Wulder *et al.* 2012, Chen 2013, Gelabert *et al.* 2020) report non-linear relations between elevation and tree height (Ameztegui *et al.* 2021). They identify a piecewise response with a sharp downward profile above a certain elevation threshold or *breakpoint*, beyond which conditions are increasingly adverse for tree development (Coops *et al.* 2013, Ameztegui *et al.* 2021). These studies suggest the existence of region-wide patterns in canopy height decline with elevation and hypothesize the universality of the piecewise pattern, but this extreme have yet to be confirmed via regional or global studies.

In this work we use the GEDI full-waveform space-borne laser instrument to investigate tree height in the main European mountainous areas relating it with elevation, temperature and rainfall. We hypothesize that the point observed in the Pyrenees holds over the main European mountain ranges. Our main goals were to (i) ascertain whether the 'breakpoint' hypothesis for the relationship between tree height and elevation holds over the main European mountain ranges; (ii) identity the climatic drivers of variations in tree height; and (iii) foresee the displacement of the breakpoint under different climate change scenarios.

6.2. Methods

6.2.1. Study area

We have analyzed the four main European mountain ranges: Pyrenees, Alps, Carpathians and Caucasus. The analyses were restricted by the latitudinal scanning range of GEDI (51.6ºN to 51.6ºS) and the defined mountain forests area according the FAO global ecological zoning (mountain forests at > 800 m (FAO 2012)).

The Pyrenees are located along the border between Spain and France reaching 3,400 m at the highest summits. Their east-west disposition creates a marked contrast between the northern and southern slopes of the mountain range, and even between the two sides of the same valley. The lower elevations of the southern side are dominated by a Mediterranean climate, with an average annual temperature around 8ºC and an average rainfall circa 800 mm $year^{-1}$, but often with some degree of summer drought. The climate of the northern valleys is clearly oceanic, with mean annual mean temperature around 4 ºC and precipitations ranging between 1000 and 2700 mm $year^{-1}$. At higher altitude, in the alpine belt, the conditions transition into "high mountain" climate with mild temperatures and annual rainfall over 2500 mm $year^{-1}$. The forests are dominated by *Pinus sylvestris*, *Fagus sylvatica L.*, *Albies alba Mill.* and *Pinus uncinata*.

The Alps are the natural border between Italy, Switzerland and France, Slovenia and Austria, reaching nearly 4800 m at its highest summit. The mountain forests of the Alps are characterized by a complex mosaic of mixed coniferous forests. The main species are spruce, fir, beech and a variety of pines. Climatically, the Alps are highly variable, with an uneven precipitation ranging from 2,300 mm $year^{-1}$ near the Adriatic Sea to 800 mm $year^{-1}$ in the central Alps.

The Carpathians are a latitudinally oriented mountain range in central Europe, being the most continental among those analyzed. This range crosses part of northern Serbia, central Romania, eastern Ukraine, southern

Poland, western Czech Republic, northern Hungary and an important part of Slovakia. The highest peaks reach 2650 m. Average yearly temperatures range from 7ºC at the lowest altitudes to 0ºC at the highest peaks. Rainfall is more abundant in the northern end (1400 mm $year^{-1}$) and rather scarce in the center of Romania (500 mm $year^{-1}$). The dominant tree species are *Acer pseudoplatanus, Fagus sylvatica, Abies alba, Picea abies, and Picea sylvatica*.

The Caucasus Mountains are the natural border separating Georgia and Azerbaijan from Russia. The Caucasus Mountains is the largest mountain range analyzed in terms of area and elevation, exceeding 5500 m.a.s.l. at the highest summits. At lower elevations, *Fagus orientalis* and a variety of *Quercus spp.* predominate. At elevations located in the subalpine belt, forests are dominated by *Picea orientalis*), *Abies nordmanniana* and a variety of *Pinus spp.*. It is the most arid mountain system analyzed, with temperatures above 10°C and precipitation around 600 mm $year^{-1}$ in lower elevations, while in the higher elevations low temperatures predominate, with an annual average of about 0°C, and precipitation around 1000 mm $year^{-1}$.

6.2.2. GEDI dataset

We used the Global Ecosystem Dynamics Investigation (GEDI) dataset, collected between May 2019 and September 2020 (Dubayah, Hofton, *et al.* 2020). GEDI is a space-borne high-resolution laser ranging scanner aboard the International Space Station. GEDI was specifically designed to capture the vertical structure of the canopy layer across the temperate and tropical forests (between 51.6° latitude, northern and southern hemisphere) (Dubayah, Blair, *et al.* 2020). The GEDI instrument consists of 3 laser sensors, scanning 8 transects spaced 600 m along sensor acquisition range. Each transect collects waveforms at 25 m radial footprints every 60 m along-track direction, with a geolocation error lower than 8 m in X/Y coordinates and 10 cm in Z. The GEDI science team derived the tree height subtracting the highest return (first received return) and the elevation, interpreted as the mode of the lowest value in the received waveform

(Fig.3.2). We used the Level 2A product, which consists of footprint-level elevation and relative canopy heights (RH) referred to as the height above the ground of each energy percentile along the waveform profile. To avoid noise in canopy height detection, we selected only high quality footprints (quality flag =1) collected during nighttime, with a sensitivity greater than 0.97, as recommended by the GEDI science team (Beck *et al.* 2020).

To reduce signal noise, we applied a sequence of filters. First, we restricted the analysis domain to mountain forests, i.e., locations higher than 800 m.a.s.l. according to the FAO criteria (FAO 2012). Since the noise is mainly located in the upper lands (due to the effect of steep slopes and snow cover (Hancock *et al.* 2019, Qi, Lee, *et al.* 2019, Potapov *et al.* 2021)), we defined the maximum elevation where the tree stratum can be found, excluding the top 0.1% footprints to cleanse the upper tail of the distribution where the signal consists mostly of outliers and detection errors (Fig S2 exemplifies the procedure). Then, we applied an outlier filter along the entire elevation gradient. We grouped GEDI's footprints into 50 m interval classes of elevation. Inside each 50 m interval, we retained only those footprints comprised within the interval's mean of the tree height (RH95) ±3 standard deviations (Zhao *et al.* 2013).

To retrieve the maximum tree height, we processed the remaining retaining those with tree heights between the 90th and 95th percentiles of RH95 in each 25 m elevation interval. Temperature and precipitation data were submitted to the same procedure. In this case we defined the interval classes to cleanse noise and calculate maximum height using in their respective units. We adapted the interval size to retrieve approximately the same number of classes obtained in the case of elevation.

6.2.3. Ancillary data

Since GEDI does not provide the actual elevation of the ground but only a baseline to calculate the relative heights, elevation data was retrieved from the NASADEM_HGT digital elevation model (DEM), an enhancement of the former STRM DEM with improved accuracy by incorporating

data from SAR, LiDAR and optical sensors (NASA JPL 2020). Climate data was retrieved from the WorldClim 2.1 (Fick and Hijmans 2017)https://www.zotero.org/google-docs/?rad2OO climate dataset. We extracted historical (1970-2000) information about minimum temperature (Tmin), maximum temperature (Tmax), and Precipitation (Prec), at a spatial resolution of 30 arc seconds (0.65 Km at latitude 45º). In addition, we also incorporate spatial predictions of Tmin and Tmax in the period 2080-2100. We retrieved and merged the predictions from eight global climate models (GCM): BCC-CSM2-MR (Wu *et al.* 2021), CNRM-CM6-1 (Voldoire *et al.* 2019), CNRM-ESM2-1 (Séférian *et al.* 2019), CanESM5 (Swart *et al.* 2019), IPSL-CM6A-LR (Boucher *et al.* 2020), MIROC-ES2L (Hajima *et al.* 2020), MIROC6 (Tatebe *et al.* 2019, p. 6), MRI-ESM2-0 (Yukimoto *et al.* 2019) for the 245 and 585 shared socioeconomic pathways (SSPs). Since data were not available at 30 arc seconds, data were acquired at 2.5 minutes and resampled using bicubic interpolation.

6.2.4. Modeling

After filtering the data, we ran a set of regression models to assess the strength and shape of the relationship between maximum tree height, elevation and climatic variable. To this purpose, we tested log-linear, segmented (Eq.1), and Gaussian models (Eq.2). Segmented models were parameterized searching for the optimal number of breakpoints through 50 iterations with 5 folds. To avoid the potential misspecification of the model due to spatial autocorrelation, we fitted 1000 models, in each of which we randomly retained half of the dataset as training dataset and the other half as test subsamples. We retrieved the median and the standard deviation of all parameter estimates across the 1000 models. In the case of segmented models, we retrieved the median and the standard deviation of the breakpoint position and the slope below and above the breakpoint. We computed the R-squared (R^2) and root mean standard error (RMSE) – calculated using the validation sample – as indicators of model performance.

$$\log(y) = \begin{cases} \alpha_1 + \beta_1 \cdot x \; \forall x \; \leq \Psi \\ \alpha_2 + \beta_2 \cdot x \; \forall x \; > \Psi \end{cases} \# \quad (1)$$

Where α1 and α2 are the intercepts, β1 and β2 are the slopes of the ratios above and below the cut-off point, while ψis the cut-off point.

$$\mathrm{y} = exp\left[-\frac{1}{2}\left(\frac{x-a}{b}\right)\right]^2 \quad (3.2)$$

Where a and b are parameters estimated by the model.

Finally, we analyzed the effect of climate, we extracted the elevation values located in the area contained between the isohyet and isotherms of Tmin, Tmax, Prec as defined by their respective median breakpoints ±1 standard deviations (from the 1000 model runs). The elevation distribution within these regions was compared with the position of the elevation breakpoint to determine the degree of association. The effect exerted by climate change in the position of the elevation breakpoint was assessed by forecasting the position of the climatic breakpoints under the scenarios SSP245 and SSP585 projected using the ensemble of the general circulation models. We then retrieved the elevation distribution of the projected isotherms and isohyets. We explored the differences between the current, SSP245 and SSP585 scenarios using the non-parametric Kruskal-Wallis test for rank sum group comparison with Holm's post-hoc correction (Holm 1979).

6.3. Results

6.3.1. Tree-height decrease in elevation follows a non-linear profile

We observed a non-linear response in the elevation-maximum tree height relationship along all European mountain systems. Non-linear modeling alternatives outperformed the linear regression baseline (Table1 and Table S1) with both the *Gaussian* and the *Segmented* models providing a good fit (R^2 >0.74). Given the slim differences between them, we kept the *Segmented* approach due to its ability to simplify the link into piecewise relationships and breakpoint thresholds (Fig. 6.1). Besides, it facilitates further investigation regarding the strength of tree-height decrease along the elevation gradient.

The data supported the existence of a unique breakpoint in all mountain ranges but the elevation where it appears varied. The Caucasus (1740±3.95 m.a.s.l.) and Alps (1474±10.82 m.a.s.l.) displayed the tipping point at higher elevations than Pyrenees (1490±5.74 m.a.s.l.) and Carpathians (1416±7.05 m.a.s.l.). In turn, we found faster declines in Eastern Mountain ranges – Carpathians, -3.31 m /100 m; Caucasus -2.28 m/100 m – as opposed to mountain ranges under greater oceanic influence – Alps, -1.4 m/100 m; Pyrenees, -1.24 m/100 m.

6.3.2. The drivers of tree height decrease

Models predicting maximum tree height from elevation were generally as good - if not better - than the best model using climatic covariates (Table 1 and Table S1). For the Alps, Caucasus and Carpathians, maximum temperature was the best climatic predictor of tree height. In the Pyrenees, precipitation emerged as the most influential factor (Table 1). Non-linear relationships were observed for all climate factors, with strong evidence for piecewise trends and the existence of a breakpoint, except for precipitation in the Caucasus and Carpathian Mountains (Fig. 6.1). Notwithstanding, the position of the elevation breakpoint is closely related to either maximum or minimum temperature, precipitation, or both. For instance, the elevation breakpoint falls within the 1st and 3rd quartile of the Tmax's isotherm altitude in all mountain ranges. However, in the Alps and the Pyrenees, the position of the breakpoint seems to be more closely related to Tmin and precipitation, respectively (Fig 6.2). This indicates the elevation is able to

integrate the effects of the most influential climate driver(s), which makes it a powerful indirect indicator.

6.3.3. Climate effects on the breakpoint position

All the considered climate change models and scenarios foresee an increase in temperature. As mentioned above, vegetation development is closely tied to temperature, so climate warming is expected to alter the position of the thermal optimum of growth and, thus, the observed breakpoints. We expect a generalized upward shift in the altitude of the Tmax breakpoints by the end of the century. In average, the breakpoint would ascend 698 m.a.s.l. under the Shared Socioeconomic Pathway 245 (SSP245; CO_2 emissions around current levels until 2050, then falling but not reaching net zero by 2100), and 1109 m.a.s.l. in SSP585 (CO_2 emissions triple by 2075), with the upward shift being most pronounced in the Caucasus Mountains (increment of 822 m.a.s.l. in SSP245 scenario) and least in the Pyrenees (increment of 531 m.a.s.l. in ssp245 scenario) (Fig. 6.3). In any case, all differences between historical conditions and SSP245, and between SSP245 and SSP585 are statistically significant ($p<0.05$). Should be noted that in Carpathian Mountains the estimated elevation breakpoint position overpasses the highest summits levels, effect that drop off any thermal constraint to vegetation development.

Table 6.1: *Summary of model performance and breakpoint location. Bold font indicates the highest correlation per variable; highlighted in gray indicates the highest correlation per mountain system.*

		R^2				Breakpoint (segmented only)			
	Model	**P**	**T_{max}**	**T_{min}**	**Elev**	**P**	**T_{max}**	**T_{min}**	**Elev**
Alps	*Linear*	0.09±0.01	0.01±0.00	0.00±0.00	0.53±0.02				
	Segmented	0.24±0.01	**0.84**±0.01	**0.77**±0.00	0.78±0.00	1535.97 ±3.62	11.08 ±0.01	1.79 ±0.01	1474 ±10.82
	Gaussian	0.14±0.01	0.82±0.01	0.74±0.00	**0.80**±0.00				
Pyrenees	*Linear*	0.28±0.01	0.00±0.00	0.10±0.01	0.40±0.01				
	Segmented	**0.85**±0.02	0.67±0.01	0.50±0.01	**0.71**±0.01	1143.8 ±3.06	13.34 ±0.05	4.08 ±0.08	1490 ±5.74
	Gaussian	0.81±0.01	**0.74**±0.01	**0.55**±0.01	0.68±0.01				
Carpathian	*Linear*	0.36±0.04	0.53±0.01	0.61±0.00	0.58±0.00				
	Segmented	**0.61**±0.04	0.86±0.01	0.84±0.00	0.85±0.00	NA	7.4± 0.02	-0.21 ±0.01	1416 ±7.05
	Gaussian	0.36±0.01	**0.87**±0.00	**0.85**±0.00	**0.88**±0.00				
Caucasus	*Linear*	0.23±0.02	0.36±0.00	0.27±0.00	0.46±0.00				
	Segmented	**0.86**±0.02	**0.91**±0.00	**0.89**±0.00	**0.92**±0.00	NA	9.84 ±0.02	0.4 3±0.01	1740 ±3.95
	Gaussian	0.22±0.01	0.89±0.00	0.84±0.00	0.90±0.00				

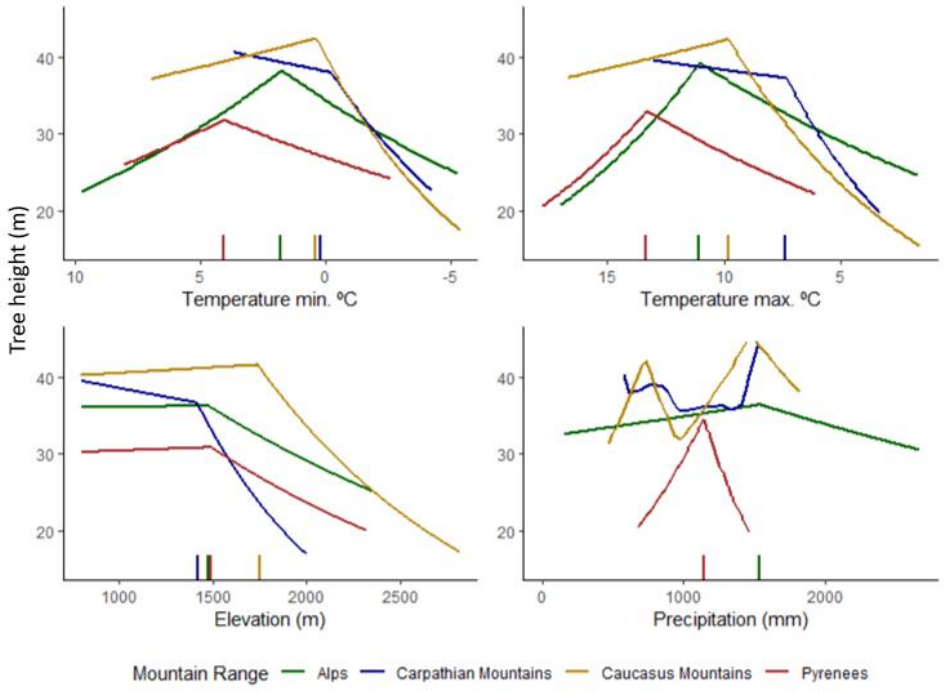

Figure 6.1: *Maximum tree height prediction by elevation and climatic variables in all analyzed mountain ranges. Lines represent the median of bootstrapped predictions.*

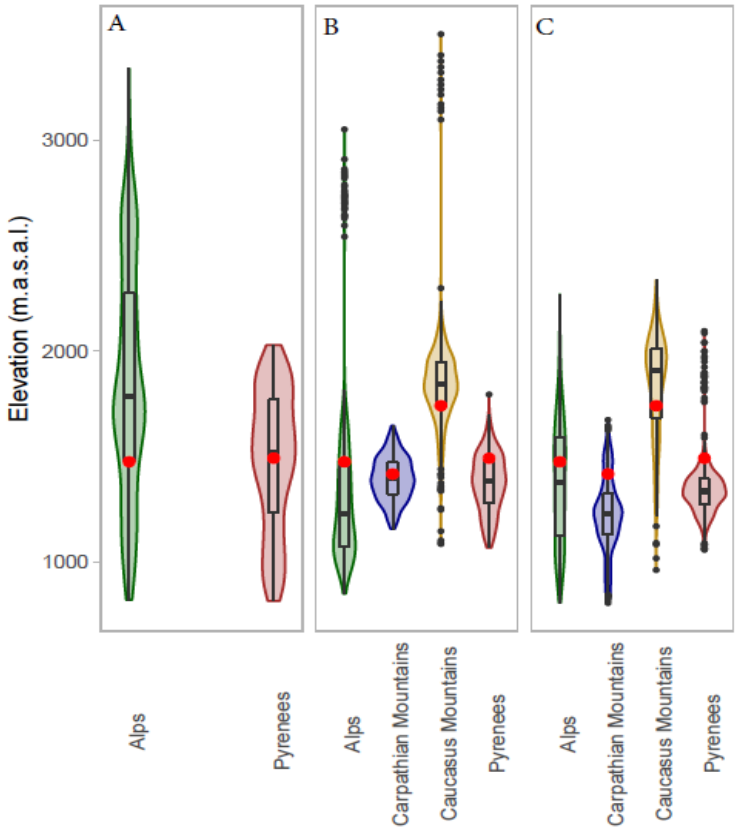

Figure 6.2: *Box and violins plots represent the distribution of the elevation values corresponding to the area comprised within the isoline of the Precipitation (A), Tmax (B) or Tmin (C) by their corresponding the breakpoint±1 sd (Table 1) in each mountain range. Red points represent the elevation of the breakpoint at each mountain range.*

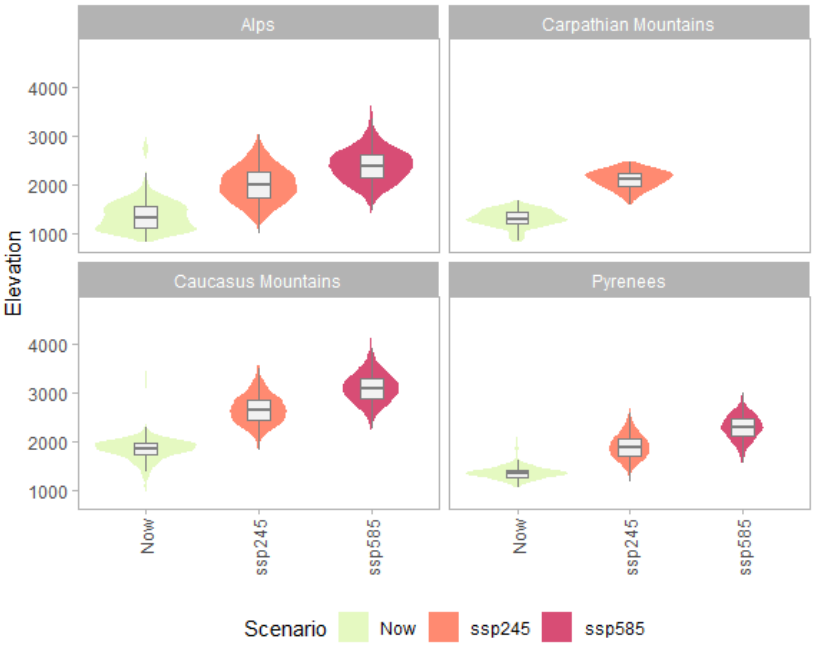

Figure 6.3: *Box and violins plots represents the distribution of elevation values in the different isohyets isotherms described at Prec., Tmax. or Tmin breakpoint in each mountain range and scenario. Colored boxes represent the range between minimum maximum values.*

6.4. Discussion

Maximum tree height showed a clear non-linear decrease along the altitudinal gradient in all mountain ranges analyzed, supporting the existence of a regional pattern in the control of the height development of tree vegetation. The non-linear, segmented trend allows the detection of an explicit breakpoint above which tree height starts to drop. This breakpoint may reflect the climatic limit beyond which the suitability for vegetation growth decreases gradually (Ameztegui et al. 2021). In three out of the four mountain ranges we analyzed (Alps, Carpathian and Caucasus Mountains), the decrease in vegetation height with elevation was due to thermal limitation as shown in figure 6.2 and table 6.1. Numerous studies have pointed out the limitation to vegetation development caused by temperature (Körner and Paulsen 2004, Paulsen and Körner 2014, Tao *et al.* 2016), particularly in mountain ecosystems and high latitudes (Paulsen and Körner 2014). The

strongest evidence of this phenomenon is the existence of the treeline, defined as the elevation limit of arboreal growth form (Körner 2012). However, such thermal limitation begins at much lower elevations (Zhang *et al.* 2016, Ameztegui *et al.* 2021) and the results of our study contribute to identify the elevation threshold where these processes start in different mountain ranges (Zhang *et al.* 2016, Ameztegui *et al.* 2021). We recognize that elevation acts here as a proxy for climate variability. The uneven and sparse distribution of stations feeding climate interpolation models such as WorldClim (Fick and Hijmans 2017) and their low spatial accuracy, hinders their reliability in mountain areas (Paulsen and Körner 2014, Gonzalez-Hidalgo *et al.* 2020). Although not without drawbacks, the high correlation of climate variables with elevation and the global availability of topographic data makes the latter a suitable variable for monitoring the effects of climate change in mountain areas. In contrast to the others mountain ranges, maximum tree height development in the Pyrenees seems to be particularly conditioned by precipitation than by thermal limitations. Due to its proximity to the Mediterranean Sea and its west-east disposition, a large part of the Pyrenees features a Mediterranean climate, characterized by a very marked summer drought period, especially on the southern slopes. However, even when precipitation was the main driver of tree height development, elevation was also a good estimator of the breakpoint, which suggests it could be used globally as an indicator of the relationship between climate and tree height development (Klein *et al.* 2015, Fricker *et al.* 2019, Ameztegui *et al.* 2021).

A shift of the optimal growing conditions towards higher elevations is to be expected in response to global warming (Elsen *et al.* 2020) (Fig. 6.3). Our results suggest an upward shift of the breakpoint, even potentially beyond the summit in the case of the Carpathian Mountains. Upward shifts in species distribution and the position of the treeline have already been observed as a response to global warming (Hansson *et al.* 2021), but the displacement is far from being universal due to the complexity of factors and nuances influencing natural afforestation of treeless areas at the limit of their physiological tolerance (Körner and Paulsen 2004, Coops *et al.* 2013). The height-elevation breakpoint, however, is more likely to relocate,

since it is indicative of a physiological relationship between tree development and climate, not an actual physical limit. As observed in boreal forests (Wilmking and Juday 2005, Henttonen *et al.* 2017, Lloyd *et al.* 2017), the upward displacement of such elevation point may imply a substantial increase in the productivity of these cold-limited forests (Hilmers *et al.* 2019). Furthermore, negative effects and reductions in the provision of ecosystem services are not expected under the effects of global warming. (Mina *et al.* 2017).

6.5. References

Albrich, K., Rammer, W., and Seidl, R., 2020. Climate change causes critical transitions and irreversible alterations of mountain forests. *Global Change Biology*, 26 (7), 4013–4027.

Ameztegui, A., Rodrigues, M., Gelabert, P., Lavaquiol, B., and Coll, L., 2021. Maximum height of mountain forests abruptly decreases above an elevation breakpoint. *GIScience & Remote Sensing*, 58 (3), 442–454.

Beck, J., Armston, J., Hofton, M., and Luthcke, S., 2020. *Global Ecosystem Dynamics Investigation (GEDI) Level 02 User Guide*. Sioux Falls, South Dakota, USA: EROS Center, U.S. Geological Survey.

Boucher, O., Servonnat, J., Albright, A.L., Aumont, O., Balkanski, Y., Bastrikov, V., Bekki, S., Bonnet, R., Bony, S., Bopp, L., Braconnot, P., Brockmann, P., Cadule, P., Caubel, A., Cheruy, F., Codron, F., Cozic, A., Cugnet, D., D'Andrea, F., Davini, P., de Lavergne, C., Denvil, S., Deshayes, J., Devilliers, M., Ducharne, A., Dufresne, J.-L., Dupont, E., Éthé, C., Fairhead, L., Falletti, L., Flavoni, S., Foujols, M.-A., Gardoll, S., Gastineau, G., Ghattas, J., Grandpeix, J.-Y., Guenet, B., Guez, E., Lionel, Guilyardi, E., Guimberteau, M., Hauglustaine, D., Hourdin, F., Idelkadi, A., Joussaume, S., Kageyama, M., Khodri, M., Krinner, G., Lebas, N., Levavasseur, G., Lévy, C., Li, L., Lott, F., Lurton, T., Luyssaert, S., Madec, G., Madeleine, J.-B., Maignan, F., Marchand, M., Marti, O., Mellul, L., Meurdesoif, Y., Mignot,

J., Musat, I., Ottlé, C., Peylin, P., Planton, Y., Polcher, J., Rio, C., Rochetin, N., Rousset, C., Sepulchre, P., Sima, A., Swingedouw, D., Thiéblemont, R., Traore, A.K., Vancoppenolle, M., Vial, J., Vialard, J., Viovy, N., and Vuichard, N., 2020. Presentation and Evaluation of the IPSL-CM6A-LR Climate Model. *Journal of Advances in Modeling Earth Systems*, 12 (7), e2019MS002010.

Cazzolla Gatti, R., Di Paola, A., Bombelli, A., Noce, S., and Valentini, R., 2017. Exploring the relationship between canopy height and terrestrial plant diversity. *Plant Ecology*, 218 (7), 899–908.

Chen, Q., 2013. LiDAR remote sensing of vegetation biomass. *Remote Sensing of Natural Resources*, (Asner 2009), 399–420.

Coops, N.C., Morsdorf, F., Schaepman, M.E., and Zimmermann, N.E., 2013. Characterization of an alpine tree line using airborne LiDAR data and physiological modeling. *Global Change Biology*, 19 (12), 3808–3821.

Dubayah, R., Blair, J.B., Goetz, S., Fatoyinbo, L., Hansen, M., Healey, S., Hofton, M., Hurtt, G., Kellner, J., Luthcke, S., Armston, J., Tang, H., Duncanson, L., Hancock, S., Jantz, P., Marselis, S., Patterson, P., Qi, W., and Silva, C., 2020. The Global Ecosystem Dynamics Investigation: High-resolution laser ranging of the Earth's forests and topography. *Science of Remote Sensing*.

Dubayah, R., Hofton, M., Blair, J.B., Armston, J., Tang, H., and Luthcke, S., 2020. GEDI L2A Elevation and Height Metrics Data Global Footprint Level V001 [Data set]. *NASA EOSDIS Land Processes DAAC*.

Elsen, P.R., Monahan, W.B., and Merenlender, A.M., 2020. Topography and human pressure in mountain ranges alter expected species responses to climate change. *Nature Communications*, 11 (1), 1974.

FAO, 2012. *Global ecological Zones for FAO forest reporting: 2010 update*. Rome.

Fick, S.E. and Hijmans, R.J., 2017. WorldClim 2: new 1-km spatial resolution climate surfaces for global land areas. *International Journal of Climatology*, 37 (12), 4302–4315.

Fricker, G.A., Synes, N.W., Serra-Diaz, J.M., North, M.P., Davis, F.W., and Franklin, J., 2019. More than climate? Predictors of tree canopy height vary with scale in complex terrain, Sierra Nevada, CA (USA). *Forest Ecology and Management*, 434, 142–153.

Gelabert, P., Montealegre, A.L., Lamelas, M.T., and Domingo, D., 2020. Forest structural diversity characterization in Mediterranean landscapes affected by fires using Airborne Laser Scanning data. *GIScience & Remote Sensing*, 57 (4).

Gonzalez-Hidalgo, J.C., Peña-Angulo, D., Beguería, S., and Brunetti, M., 2020. MOTEDAS century: A new high-resolution secular monthly maximum and minimum temperature grid for the Spanish mainland (1916–2015). *International Journal of Climatology*, 40 (12), 5308–5328.

Grace, J., Berninger, F., and Nagy, L., 2002. Impacts of Climate Change on the Tree Line. *Annals of Botany*, 90 (4), 537–544.

Hajima, T., Watanabe, M., Yamamoto, A., Tatebe, H., Noguchi, M.A., Abe, M., Ohgaito, R., Ito, A., Yamazaki, D., Okajima, H., Ito, A., Takata, K., Ogochi, K., Watanabe, S., and Kawamiya, M., 2020. Development of the MIROC-ES2L Earth system model and the evaluation of biogeochemical processes and feedbacks. *Geoscientific Model Development*, 13 (5), 2197–2244.

Hancock, S., Armston, J., Hofton, M., Sun, X., Tang, H., Duncanson, L.I., Kellner, J.R., and Dubayah, R., 2019. The GEDI Simulator: A Large-Footprint Waveform Lidar Simulator for Calibration and Validation of Spaceborne Missions. *Earth and Space Science*, 6 (2), 294–310.

Hansson, A., Dargusch, P., and Shulmeister, J., 2021. A review of modern treeline migration, the factors controlling it and the implications for carbon storage. *Journal of Mountain Science*, 18 (2), 291–306.

Henttonen, H.M., Nöjd, P., and Mäkinen, H., 2017. Environment-induced growth changes in the Finnish forests during 1971–2010 – An analysis based on National Forest Inventory. *Forest Ecology and Management*, 386, 22–36.

Hilmers, T., Avdagić, A., Bartkowicz, L., Bielak, K., Binder, F., Bončina, A., Dobor, L., Forrester, D.I., Hobi, M.L., Ibrahimspahić, A., Jaworski, A., Klopčič, M., Matović, B., Nagel, T.A., Petráš, R., del Rio, M., Stajić, B., Uhl, E., Zlatanov, T., Tognetti, R., and Pretzsch, H., 2019. The productivity of mixed mountain forests comprised of Fagus sylvatica, Picea abies, and Abies alba across Europe. *Forestry: An International Journal of Forest Research*, 92 (5), 512–522.

Holm, S., 1979. A Simple Sequentially Rejective Multiple Test Procedure. *Scandinavian Journal of Statistics*, 6 (2), 65–70.

Klein, T., Randin, C., and Körner, C., 2015. Water availability predicts forest canopy height at the global scale. *Ecology Letters*, 18 (12), 1311–1320.

Körner, C., 2012. *Alpine Treelines: Functional Ecology of the Global High Elevation Tree Limits*. Springer Science & Business Media.

Körner, C. and Paulsen, J., 2004. A world-wide study of high altitude treeline temperatures. *Journal of Biogeography*, 31 (5), 713–732.

Larjavaara, M. and Muller-Landau, H.C., 2013. Measuring tree height: a quantitative comparison of two common field methods in a moist tropical forest. *Methods in Ecology and Evolution*, 4 (9), 793–801.

Liénard, J., Harrison, J., and Strigul, N., 2016. US forest response to projected climate-related stress: a tolerance perspective. *Global Change Biology*, 22 (8), 2875–2886.

Lloyd, A.H., Sullivan, P.F., and Bunn, A.G., 2017. Integrating dendroecology with other disciplines improves understanding of upper and latitudinal treelines. *In*: M.M. Amoroso, L.D. Daniels, P.J. Baker, and J.J. Camarero, eds. *Dendroecology: Tree-Ring Analyses Applied to Ecological Studies*.

Cham: Springer International Publishing, 135–157.

Lopatin, J., Dolos, K., Hernández, H.J., Galleguillos, M., and Fassnacht, F.E., 2016. Comparing Generalized Linear Models and random forest to model vascular plant species richness using LiDAR data in a natural forest in central Chile. *Remote Sensing of Environment*, 173, 200–210.

Mina, M., Bugmann, H., Cordonnier, T., Irauschek, F., Klopcic, M., Pardos, M., and Cailleret, M., 2017. Future ecosystem services from European mountain forests under climate change. *Journal of Applied Ecology*, 54 (2), 389–401.

NASA JPL, 2020. NASADEM Merged DEM Global 1 arc second V001 [Data set]. *NASA EOSDIS Land Processes DAAC*.

Paulsen, J. and Körner, C., 2014. A climate-based model to predict potential treeline position around the globe. *Alpine Botany*, 124 (1), 1–12.

Potapov, P., Li, X., Hernandez-Serna, A., Tyukavina, A., Hansen, M.C., Kommareddy, A., Pickens, A., Turubanova, S., Tang, H., Silva, C.E., Armston, J., Dubayah, R., Blair, J.B., and Hofton, M., 2021. Mapping global forest canopy height through integration of GEDI and Landsat data. *Remote Sensing of Environment*, 253, 112165.

Price, M., Gratzer, G., Alemayehu Duguma, L., Kohler, T., and Maselli, D., 2011. *Mountain Forests in a Changing World: Realizing Values, Adressing Challenges*. Rome: FAO/MPS and SDC.

Qi, W., Lee, S.-K., Hancock, S., Luthcke, S., Tang, H., Armston, J., and Dubayah, R., 2019. Improved forest height estimation by fusion of simulated GEDI Lidar data and TanDEM-X InSAR data. *Remote Sensing of Environment*, 221, 621–634.

Qi, W., Saarela, S., Armston, J., Ståhl, G., and Dubayah, R., 2019. Forest biomass estimation over three distinct forest types using TanDEM-X InSAR data and simulated GEDI lidar data. *Remote Sensing of Environment*, 232, 111283.

Reich, P.B., Sendall, K.M., Rice, K., Rich, R.L., Stefanski, A., Hobbie, S.E., and Montgomery, R.A., 2015. Geographic range predicts photosynthetic and growth response to warming in co-occurring tree species. *Nature Climate Change*, 5 (2), 148–152.

Séférian, R., Nabat, P., Michou, M., Saint-Martin, D., Voldoire, A., Colin, J., Decharme, B., Delire, C., Berthet, S., Chevallier, M., Sénési, S., Franchisteguy, L., Vial, J., Mallet, M., Joetzjer, E., Geoffroy, O., Guérémy, J.-F., Moine, M.-P., Msadek, R., Ribes, A., Rocher, M., Roehrig, R., Salas-y-Mélia, D., Sanchez, E., Terray, L., Valcke, S., Waldman, R., Aumont, O., Bopp, L., Deshayes, J., Éthé, C., and Madec, G., 2019. Evaluation of CNRM Earth System Model, CNRM-ESM2-1: Role of Earth System Processes in Present-Day and Future Climate. *Journal of Advances in Modeling Earth Systems*, 11 (12), 4182–4227.

Silva, C.A., Saatchi, S., Garcia, M., Labrière, N., Klauberg, C., Ferraz, A., Meyer, V., Jeffery, K.J., Abernethy, K., White, L., Zhao, K., Lewis, S.L., and Hudak, A.T., 2018. Comparison of Small- and Large-Footprint Lidar Characterization of Tropical Forest Aboveground Structure and Biomass: A Case Study From Central Gabon. *IEEE Journal of Selected Topics in Applied Earth Observations and Remote Sensing*, 11 (10), 3512–3526.

Skidmore, A.K., Coops, N.C., Neinavaz, E., Ali, A., Schaepman, M.E., Paganini, M., Kissling, W.D., Vihervaara, P., Darvishzadeh, R., Feilhauer, H., Fernandez, M., Fernández, N., Gorelick, N., Geijzendorffer, I., Heiden, U., Heurich, M., Hobern, D., Holzwarth, S., Muller-Karger, F.E., Van De Kerchove, R., Lausch, A., Leitão, P.J., Lock, M.C., Mücher, C.A., O'Connor, B., Rocchini, D., Roeoesli, C., Turner, W., Vis, J.K., Wang, T., Wegmann, M., and Wingate, V., 2021. Priority list of biodiversity metrics to observe from space. *Nature Ecology & Evolution*, 5 (7), 896–906.

Swart, N.C., Cole, J.N.S., Kharin, V.V., Lazare, M., Scinocca, J.F., Gillett, N.P., Anstey, J., Arora, V., Christian, J.R., Hanna, S., Jiao, Y., Lee, W.G.,

Majaess, F., Saenko, O.A., Seiler, C., Seinen, C., Shao, A., Sigmond, M., Solheim, L., von Salzen, K., Yang, D., and Winter, B., 2019. The Canadian Earth System Model version 5 (CanESM5.0.3). *Geoscientific Model Development*, 12 (11), 4823–4873.

Tao, S., Guo, Q., Li, C., Wang, Z., and Fang, J., 2016. Global patterns and determinants of forest canopy height. *Ecology*, 97 (12), 3265–3270.

Tatebe, H., Ogura, T., Nitta, T., Komuro, Y., Ogochi, K., Takemura, T., Sudo, K., Sekiguchi, M., Abe, M., Saito, F., Chikira, M., Watanabe, S., Mori, M., Hirota, N., Kawatani, Y., Mochizuki, T., Yoshimura, K., Takata, K., O'ishi, R., Yamazaki, D., Suzuki, T., Kurogi, M., Kataoka, T., Watanabe, M., and Kimoto, M., 2019. Description and basic evaluation of simulated mean state, internal variability, and climate sensitivity in MIROC6. *Geoscientific Model Development*, 12 (7), 2727–2765.

Valbuena, R., O'Connor, B., Zellweger, F., Simonson, W., Vihervaara, P., Maltamo, M., Silva, C.A., Almeida, D.R.A., Danks, F., Morsdorf, F., Chirici, G., Lucas, R., Coomes, D.A., and Coops, N.C., 2020. Standardizing Ecosystem Morphological Traits from 3D Information Sources. *Trends in Ecology & Evolution*, 35 (8), 656–667.

Voldoire, A., Saint-Martin, D., Sénési, S., Decharme, B., Alias, A., Chevallier, M., Colin, J., Guérémy, J.-F., Michou, M., Moine, M.-P., Nabat, P., Roehrig, R., Salas y Mélia, D., Séférian, R., Valcke, S., Beau, I., Belamari, S., Berthet, S., Cassou, C., Cattiaux, J., Deshayes, J., Douville, H., Ethé, C., Franchistéguy, L., Geoffroy, O., Lévy, C., Madec, G., Meurdesoif, Y., Msadek, R., Ribes, A., Sanchez-Gomez, E., Terray, L., and Waldman, R., 2019. Evaluation of CMIP6 DECK Experiments With CNRM-CM6-1. *Journal of Advances in Modeling Earth Systems*, 11 (7), 2177–2213.

Wilmking, M. and Juday, G.P., 2005. Longitudinal variation of radial growth at Alaska's northern treeline—recent changes and possible scenarios for the 21st century. *Global and Planetary Change*, 47 (2), 282–300.

Wu, T., Yu, R., Lu, Y., Jie, W., Fang, Y., Zhang, J., Zhang, L., Xin, X., Li, L., Wang, Z., Liu, Y., Zhang, F., Wu, F., Chu, M., Li, J., Li, W., Zhang, Y., Shi, X., Zhou, W., Yao, J., Liu, X., Zhao, H., Yan, J., Wei, M., Xue, W., Huang, A., Zhang, Y., Zhang, Y., Shu, Q., and Hu, A., 2021. BCC-CSM2-HR: a high-resolution version of the Beijing Climate Center Climate System Model. *Geoscientific Model Development*, 14 (5), 2977–3006.

Wulder, M.A., White, J.C., Nelson, R.F., Næsset, E., Ole, H., Coops, N.C., Hilker, T., Bater, C.W., and Gobakken, T., 2012. Lidar sampling for large-area forest characterization : A review. *Remote Sensing of Environment*, 121, 196–209.

Yukimoto, S., Kawai, H., Koshiro, T., Oshima, N., Yoshida, K., Urakawa, S., Tsujino, H., Deushi, M., Tanaka, T., Hosaka, M., Yabu, S., Yoshimura, H., Shindo, E., Mizuta, R., Obata, A., Adachi, Y., and Ishii, M., 2019. The Meteorological Research Institute Earth System Model Version 2.0, MRI-ESM2.0: Description and Basic Evaluation of the Physical Component. *Journal of the Meteorological Society of Japan. Ser. II*, advpub.

Zhang, J., Nielsen, S.E., Mao, L., Chen, S., and Svenning, J.-C., 2016. Regional and historical factors supplement current climate in shaping global forest canopy height. *Journal of Ecology*, 104 (2), 469–478.

Zhao, Y., Lehman, B., Ball, R., Mosesian, J., and de Palma, J.-F., 2013. Outlier detection rules for fault detection in solar photovoltaic arrays. *In: 2013 Twenty-Eighth Annual IEEE Applied Power Electronics Conference and Exposition (APEC)*. Presented at the 2013 Twenty-Eighth Annual IEEE Applied Power Electronics Conference and Exposition (APEC), 2913–2920

.

Capítulo 7

Forest structural diversity characterization in Mediterranean landscapes affected by fires using Airborne Laser Scanning data

7. Forest structural diversity characterization in Mediterranean landscapes affected by fires using Airborne Laser Scanning data

Cita: Gelabert, P., Montealegre, A. L., Lamelas, M. T., & Domingo, D. (2020). Forest structural diversity characterization in Mediterranean landscapes affected by fires using Airborne Laser Scanning data. *GIScience & Remote Sensing*. https://doi.org/10.1080/15481603.2020.1738060

Abstract

Forest fires can change forest structure and composition, and low-density Airborne Laser Scanning (ALS) can be a valuable tool for evaluating post-fire vegetation response. The aim of this study is to analyze the structural diversity differences in Mediterranean *Pinus halepensis* Mill. forests affected by wildfires on different dates from 1986 to 2009. Several types of ALS metrics, such as the Light Detection and Ranging (LiDAR) Height Diversity Index (LHDI), the LiDAR Height Evenness Index (LHEI), and vertical and horizontal continuity of vegetation, as well as topographic metrics were obtained in raster format from low point density data. In order to map burned and unburned areas, differentiate fire occurrence dates, and distinguish between old and more recent fires, a sample of pixels was previously selected to assess the existence of differences in forest structure using the Kruskal-Wallis test. Then, *k*-nearest neighbors algorithm (*k*-NN), support vector machine (SVM) and random forest (RF) classifiers were compared to select the most accurate technique. The results showed that, in more recent fires, around 70% of the laser returns came from grass and shrub layers, yielding low LHDI and LHEI values (0.37-0.65 and 0.28-0.46, respectively). In contrast, the areas burned more than 20 years ago had higher LHDI and LHEI values due to the growth of the shrub and tree

strata. The classification of burned and unburned areas yielded an overall accuracy of 89.64% using the RF method. SVM was the best classifier for identifying the structural differences between fires occurring on different dates, with an overall accuracy of 68.79%. Furthermore, SVM yielded an overall accuracy of 75.49% for the classification between old and more recent fires.

Keywords: *Forest structure; LiDAR; machine learning, landscape*

7.1. Introduction

The Mediterranean Basin is very biodiverse (Medail and Quezel 1999), but it is an environment that is frequently affected by wildfires (Gonçalves and Sousa 2017) mainly induced by climate and human activity (Jiménez-Ruano *et al.* 2017). However, a downward trend in burned area size has been observed in the Mediterranean region over the past 30 years due to fire suppression policies (Rodrigues *et al.* 2013).

Pinus halepensis Mill. (Aleppo pine) is the most common pine species dominating forest ecosystems in low altitude areas of the Mediterranean Basin. This is a pyrophyte species with a post-fire seeder strategy (Goubitz *et al.* 2004), which is influenced by fire severity. There is a greater probability of growth and floristic richness under low and moderate burn severity (González-De Vega *et al.* 2018). According to Rodrigues et al. (2014), such Aleppo pine forests affected by fire need an average of 20 years to reach the mature stage prior to burning. Changes in fire frequency can limit post-fire regeneration as a mature reproductive stage cannot be reached (Fernández-García *et al.* 2019). Furthermore, an increase in the frequency of extreme fires (San-Miguel-Ayanz *et al.* 2013, p.) can also alter the recovery capacity because post-fire seedling density is reduced (González-De Vega *et al.* 2016, Fernández-García *et al.* 2019).

In this regard, forest fires play an important ecological role in Mediterranean ecosystems (Pausas 2004), shaping forest structure and composition and reducing forest canopy and species richness (Cochrane and Schulze

1999). Forest structure, defined as the variability in vegetation height within a forest stand, is a relevant indicator for biodiversity evaluation in forest ecosystems (Kimmins 1997). This assertion is based on the assumption that greater structural diversity will produce more ecological niches and more animal habitats (Kimmins 1997, McElhinny *et al.* 2005). Compositional indices are powerful indicators of biodiversity, although their estimation is costly and time consuming, so structural indices are commonly used instead (Listopad *et al.* 2015).

The Shannon index (H', also termed the Shannon-Wiener index), is a quantitative measure that reflects the number of different species coexisting in a community (Shannon and Wiener 1949). This index is highly positively correlated with canopy height (Hansen et al. 2014). The Pielous index was developed to depict the relative abundance of coexisting species (Pielou 1975), because plant species are not evenly distributed across the landscape. (Staudhammer and LeMay 2001) extended these indices to analyze forest vertical structure using three-dimensional information.

Within this context, Airborne Laser Scanning (ALS) is currently the most accurate technique for acquiring three-dimensional georeferenced information of the Earth's surface from local to regional scales (Su and Bork 2006, Liu 2008, Aguilar *et al.* 2010). This is accomplished by national or regional surveys, and by the high vertical and horizontal accuracy of this technology. In fact, several studies such as the ones by Dubayah and Drake (2000), Lefsky *et al.* (2002), Lim *et al.* (2003), Zimble *et al.* (2003), Kelly and Di Tommaso (2015) have demonstrated its usefulness for characterizing forest stands.

Several European countries, such as the United Kingdom, Denmark, Finland, the Czech Republic, the Flanders region of Belgium, and Spain, have collected ALS data at regional level with low-moderate point density and high vertical and horizontal accuracies. These datasets do not allow for studies based on the individual tree-based approach (ITB) (Hamraz *et al.* 2017), especially in dense forests due to their low point density (below 4 points per square meter). Furthermore, low-density data do not provide a

sufficient number of laser returns to characterize forest understory (Lim *et al.* 2003, Wulder *et al.* 2012) because the majority of returns do not penetrate the canopy. Despite these limitations, ALS metrics computed from the vertical distribution of laser returns have been useful for describing the vegetation structure (Lim *et al.* 2003, Montealegre *et al.* 2016, Domingo *et al.* 2017).

Other studies such as the ones by García *et al.* (2011), Manzanera *et al.* (2016) and Teobaldelli *et al.* (2017) have combined ALS data with in situ data and optical imagery, thus improving the accuracies of fuel type classification estimations and stand parameter estimation by regression, respectively. Additionally, Lamelas *et al.* (2019) demonstrated the usefulness of 3D radiative transfer models to simulate and classify fuel models.

ALS data from the Spanish National Plan for Aerial Orthophotography (PNOA) have yielded good results for monitoring post-fire recovery and forest structural diversity, either using regressions (Kane *et al.* 2013), or classifications using ALS data alone (Debouk *et al.* 2013) or in combination with optical data (Martín-Alcón *et al.* 2015). New approaches, such as the one developed by Listopad *et al.* (2015), have emerged to provide estimations of vegetation structural diversity based on the proportion of returns in different canopy height ranges. However, these studies were conducted with high density ALS data. Accordingly, this study aims to assess the usefulness of low point density ALS data to characterize forest structural diversity in a Mediterranean area frequently affected by wildfires. We hypothesize that ALS-derived metrics provide information of the structural diversity of Aleppo pine forests that allows to identify the date of fire occurrence.

The specific objectives are (1) to derive four types of ALS metrics (diversity indices, vertical structure, horizontal continuity and topographic metrics); (2) to select the metrics that provide relevant information on the structural differences between burned areas; (3) and to map burned and unburned areas, differentiate fire occurrence dates, and distinguish between

old and more recent fires by comparing the k-nearest neighbors algorithm (k-NN), support vector machine (SVM) and random forest (RF) methods.

7.2. Methods

7.2.1. Study area

The area of interest is located in the central sector of the Ebro basin in north eastern Spain (41° 57' N, 0° 57' W). This area is dominated by Aleppo pine forests, and the evergreen understory is mainly composed of *Quercus ilex*, *Quercus coccifera*, *Juniperus oxycedrus*, *Thymus vulgaris* and *Rosmarinus officinalis*. Part of the study area (see Fig 7.1) is covered by crops and occupied by a military training area, the latter of which has been excluded from the analysis. This sector of the Iberian Peninsula constitutes the northernmost semiarid region in Europe. The climate is Mediterranean with continental features (Cuadrat *et al.* 2007). The geomorphology of the area consists of structural platforms of Miocene carbonate and marl sediments (IGME 1995). It has a rough topography with a mean slope steepness ranging from 12 to 18º.

Fig 7.1 shows the extension of the forests altered by five wildfires occurring between 1986 and 2009. The burned forest, excluding the military training area, totals 8,075 ha and the unburned area 12,047 ha. More recent fires (2006-2009) underwent a post-fire intervention based on crushing burned wood and creating log erosion barriers to control erosion and seed loss (Miranda and Echevarría 2015).

7.2.2. ALS data source and pre-processing

ALS data were provided by the Geographical Institute of Aragón (IGEAR) and collected by the Spanish National Plan for Aerial Orthophotography (PNOA) between September and November 2016. The dataset was captured using a small-footprint discrete-return airborne sensor (Leica ALS80), operating at 1.064 µm wavelength and ±28 scan angle degrees from nadir. The resulting point density of the study area ranged from 1.1 to 2.0

point/m^2, with a vertical accuracy of ±0.1 m and a horizontal accuracy of ≤0.3 m. Data were delivered in 2×2 km tiles of raw data points, in LAS binary file format (v. 1.2), with up to four returns recorded per pulse.

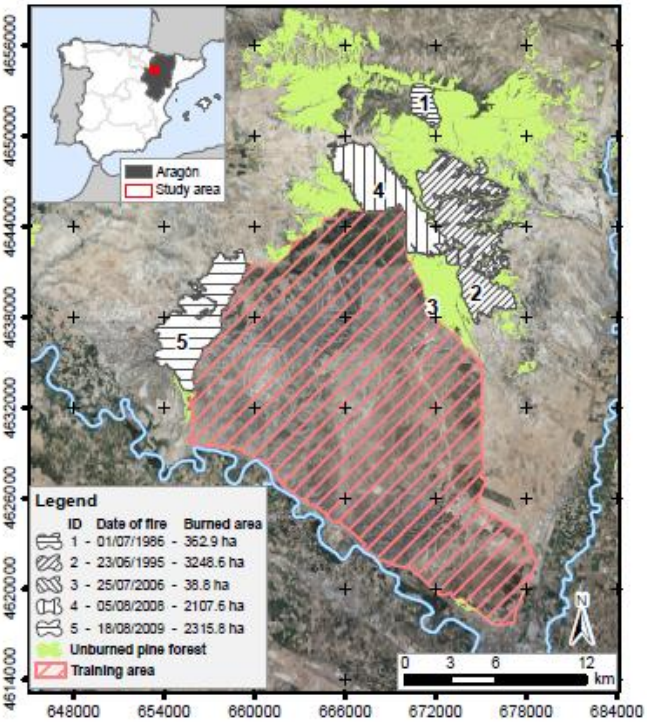

Figure 7.1: *Location of the fires and the unburned area. High spatial resolution orthophotography from PNOA Spatial Data Infrastructure (SDI) is included as backdrop.*

ALS tiles were classified using the multiscale curvature classification algorithm (MCC) (Evans and Hudak 2007), implemented in the MCC 2.1 command-line tool, which was specifically developed to process discrete-return ALS data in forested environments, and is considered suitable for the study area in accordance with Montealegre *et al.* (2015a). The Point-TIN-Raster interpolation method (ArcGIS v. 10.5) was applied to the classified ground points to generate a Digital Elevation Model (DEM) with a 1 m spatial resolution in accordance with Montealegre *et al.* (2015b). The

structural diversity of vegetation was analyzed using three types of ALS metrics: i) structural diversity indices; ii) vertical structure-related metrics; and iii) horizontal continuity metrics. These metrics were derived directly from the laser returns in accordance with (Bottalico *et al.* (2017). Topographic metrics were also obtained from ALS data to characterize the topography of the study area.

7.2.3. Structural diversity indices

The LiDAR Height Diversity Index (LHDI) and the LiDAR Height Evenness Index (LHEI) were calculated in accordance with Listopad et al. (2015) (Equations 1 and 2).

$$LHDI = -\sum[(p_h) \times ln(p_h)] \quad (1)$$

$$LHEI = \frac{LHDI}{ln(p_h)} \quad (2)$$

Where p is the proportion of returns at a defined height interval (h). In order to calculate the proportion of returns required by these indices, the command "DensityMetrics" (FUSION v. 3.60, (McGaughey 2014)) was applied. This command provides a series of raster layers where each cell contains the total number of returns for a specific range of height above ground. The metrics were computed with 10, 15 and 20 m pixel sizes to assess which spatial resolution had the best accuracies. A minimum pixel size value of 10 m was established in order to gather a sufficient number of laser returns to derive the ALS metrics. The indices were also computed at 0.5, 0.3 and 0.15 m height intervals to ascertain which vertical resolution best reflected the diversity. 3.3.4 Vertical structure related metrics

A suite of statistical metrics related to the vertical height distribution of returns, commonly used as independent metrics in forestry applications, was generated using the "GridMetrics" command in FUSION 3.60 (McGaughey 2014). These metrics were also computed at 10, 15 and 20 m

spatial resolutions. The height 99th percentile (H_{P99}) (Equation 3) (Magnussen and Boudewyn 1998), mean height (H_{mean}) (Equation 4), standard deviation (H_{sd}) (Equation 5), kurtosis ($H_{kurtosis}$) (Equation 6), skewness ($H_{skewness}$) (Equation 7) and the canopy relief ratio (CRR) (Equation 8) (Parker and Russ 2004) were calculated.

$$(N-1)P = I + d \begin{Bmatrix} I \text{ is the entire part of } (N-1)P \\ d \text{ is the entire part of } (N-1)P \end{Bmatrix}$$

Where N is the number of observations and P is the percentile divided by 100.

(3)

$$if\ d = 0\ then\ P = x_{i+1}$$

$$if\ d > 0\ then\ P = x_{i+1} + d(x_{i+2} - x_{x+1})$$

$$H_{\text{mean}} = \frac{\sum_{i=1}^{N} x_i}{N} \quad (4)$$

$$\mathrm{H}_{sd} = \sqrt{\frac{\sum_{i=1}^{N}(x_i - \bar{x})^2}{N}} \quad (5)$$

$$H_{kurtosis} = \frac{\sum_{i=1}^{N}(x_i - \bar{x})^4}{(N-1)\sigma^4} \quad (6)$$

$$H_{skewness} = \frac{\sum_{i=1}^{N}(x_i - \bar{x})^3}{(N-1)\sigma^3} \quad (7)$$

$$Canopy\ relief\ ratio\ (CCR) = \frac{\bar{x} - x_{i\,min}}{x_{i\,max} - x_{i\,min}} \quad (8)$$

Where i is the laser return, N is the total number of returns, x is the height value, $\bar{x}$ is the mean height value, and σ is the standard deviation.

7.2.4. Horizontal continuity metrics

The canopy cover (CC) (Equation 9) was calculated using a 0.2 m height threshold to avoid ground returns, as the percentage of ground covered by the vertical projection of vegetation (Jennings *et al.* 1999).

$$Canopy\ Cover\ (CC) = \frac{\sum_{i=1}^{N} r_{i\ first} > 0.2\ m}{\sum_{i=1}^{N} r_{i\ first}} \times 100 \qquad (9)$$

In addition, a standard deviation filter with a 3×3 kernel size was applied to the vertical structure metrics described previously, generating nine new horizontal continuity metrics (HCM): LHDI, LHEI, H_{mean}, H_{sd}, $H_{skewness}$, $H_{kurtosis}$, CC, CRR, H_{p99}).

7.2.5. Topographic metrics

A set of topographic metrics, such as Topographic position index (TPI), Aspect, Slope and Roughness (Wilson *et al.* 2007), were also calculated to analyze the influence of terrain on vegetation structure.

7.2.6. Structural diversity analysis of wildfires on different dates

The percentage of returns from 0.5 to 2 m, from 2 to 4 m, and above 4 m was calculated for each wildfire, according to height ranges defined by the PROMETHEUS fuel model classification (Prometheus 2000). These ranges are suitable for the study area because the PROMETHEUS project was carried out in Mediterranean environments. The average values of LHDI and LHEI, and the forest structural metrics were calculated to describe the differences between fires.

The burned areas under analysis were grouped to test whether the ALS metrics were able to distinguish between burned and unburned areas, areas burned in different years, and between old and more recent fires using a two phase approach: i) a sample of a variable number of pixels was considered inside and outside of the fire perimeter, taking into account a minimum separation between samples to avoid spatial autocorrelation, which was analyzed using Moran's I index; ii) the normality of the metric value distribution was tested using the Anderson-Darling test (Anderson and Darling 1954). The Kruskal-Wallis test (Kruskal and Wallis 1952) was applied when normality was not fulfilled.

7.2.7. Digital classification of burned areas

In order to map the burned areas, three digital classifications were performed to distinguish between burned and unburned areas (Classification 1); to differentiate the fire occurrence dates (Classification 2), and to distinguish between old and more recent fires (Classification 3). Furthermore, k-nearest neighbors algorithm (k-NN), support vector machine (SVM) and random forest (RF) methods were compared in each classification to select the most accurate technique.

k-NN is a non-parametric Machine Learning (ML) approach for classifying populations whose distributions are unknown (Fix and Hodges 1989). k-NN optimization and computation were carried out with the R package "caret" (Kuhn 2008). SVM is a ML algorithm created to analyze and recognize patterns. SVM constructs a set of hyperplanes in a high-dimensional space and tries to find the hyperplane that maximizes the separation between classes (Rodrigues and de la Riva 2014, Domingo *et al.* 2018). SVM parameters require optimization. In this sense, the kernel type was calibrated using the R package "kernlab", and cost and gamma parameters were tuned, within the intervals 1–1000 and 0.01–1, respectively. SVM was computed with the R package "e1071" (Meyer *et al.* 2017). RF is a ML ensemble classifier that uses decision trees. The nodes of each decision tree are divided using the best variables selected from a random sample (Rodrigues and de la Riva 2014, Domingo *et al.* 2018). The *ntree* parameter

was tuned within the interval 1–3000, and the *number of selected variables*, between 1 and the maximum number of variables -1, using the R packages "*randomForest*" (Liaw and Wiener 2002) and "caret" (Kuhn 2008).

Training and testing datasets to perform the digital classification were obtained from a random sample of pixels from raster metrics (Tab. 7.1). Prior to classification, variable selection was performed using the exhaustive subset selection method in accordance with (Domingo *et al.* 2018), taking into consideration the most important metric of each type of variables analyzed (i.e., diversity indices, vertical structure, horizontal continuity and topographic metrics). This selection was computed using the R package "leaps" (Lumley and Miller 2017).

Digital classifications were validated using the test sample. Contingency tables and the percentage of overall success, which refers to the ratio between pixels correctly classified and the total number of pixels in the sample, were calculated. Moreover, Cohen's Kappa coefficient (K) was computed to measure inter-rater agreement (Chuvieco 2010).

Table 7.1: *Training and test data set for digital classifications. Classification 1 stands for burned and unburned areas. Classification 2 stands for fire occurrence dates. Classification 3 stands for old and more recent fires.*

Classification 1			Classification 2			Classification 3		
Class	Training set	Test set	Class	Training set	Test set	Class	Training set	Test set
Unburned	1000 pixels	500 pixels	Unburned	1000 pixels	500 pixels	Unburned	1000 pixels	500 pixels
Burned	5000 pixels	2500 pixels	Burned in 1986	1000 pixels	500 pixels	Old fires	2000 pixels	1000 pixels
			Burned in 1995	1000 pixels	500 pixels			
			Burned in 2006	1000 pixels	500 pixels	More recent fires	3000 pixels	1500 pixels
			Burned in 2008	1000 pixels	500 pixels			
			Burned in 2009	1000 pixels	500 pixels			

7.3. Results

Fig 7.2 shows the percentage of returns grouped by the PROMETHEUS strata for each wildfire and unburned area. In general, all areas have a similar percentage of returns in the shrub stratum (around 20%). In contrast, considerable differences are found between the tree and grass strata. For example, more than 40% of returns in unburned areas are located above 4 m, thus showing the predominance of the tree layer and a lower presence of grasslands (34.5%). In contrast, burned areas have higher variability. Those burned in relatively recent fires (2006-2009) are mainly covered by a grass layer (around 70%), while those burned in older fires have a moderate presence of grasslands (around 30%). In the case of tree strata, the presence of returns is low in more recent fires (approx. 10%) and higher in older ones (approx. 30%).

Tab 7.2 shows the average values of the computed metrics for each wildfire and unburned area. The vegetation structure of unburned areas has high LHDI and LHEI values (1.83 and 0.71, respectively). Wildfires can be grouped into the oldest ones occurring in 1986 and 1995, and more recent ones occurring in 2006, 2008 and 2009. The areas where the oldest fires occurred have return distributions similar to the unburned areas, thus indicating an advanced stage of vegetation recovery. In particular, the area where the fire occurred in 1986 has a higher percentage of returns in the herbaceous layer than the area burned in 1995 does. This is also accompanied by higher LHDI and LHEI values (Tab 7.2). There is a predominance of returns in the herbaceous and shrub layers, with low LHDI and LHEI values, in areas burned in relatively recent fires (2006, 2008 and 2009). In general, the areas burned in those fires have lower mean values of height (1.1-0.68 m), CC (22-37%) and CRR (0.34-0.39 m) compared to those burned in older fires and to unburned areas (Tab 7.2).

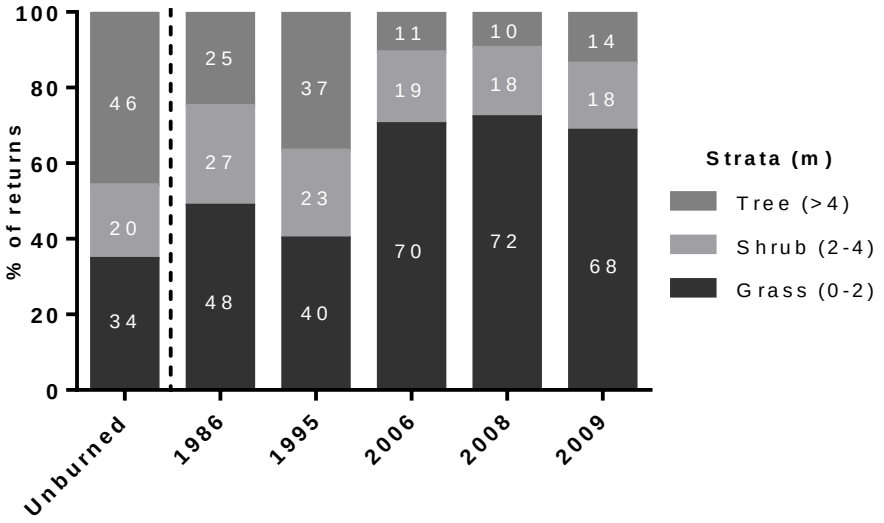

Figure 7.2: *Percentage of returns grouped by PROMETHEUS strata and date of fire occurrence.*

Table 7.2: *Mean values of ALS vertical metrics and diversity indices for the different occurrence dates and the unburned area.*

ALS metric	Unburned	Year of the fire				
		1986	1995	2006	2008	2009
LHDI	1.83	1.92	1.37	0.44	0.65	0.38
LHEI	0.71	0.81	0.72	0.32	0.47	0.28
$\mathbf{H_{mean}}$**(m)**	3.34	2.57	1.67	1.10	0.87	0.68
$\mathbf{H_{sd}}$ **(m)**	1.94	1.45	0.82	0.58	0.49	0.40
$\mathbf{H_{skewness}}$ **(m)**	0.16	0.00	0.26	0.49	0.77	0.86
$\mathbf{H_{kurtosis}}$ **(m)**	2.75	2.40	2.09	2.86	3.45	3.44
CC (%)	71.24	81.34	64.60	22.16	37.33	24.87
CRR	0.44	0.45	0.43	0.39	35	0.34
$\mathbf{H_{P99}}$ **(m)**	6.68	5.24	3.29	2.07	1.99	1.56

As shown in Tab 7.3, the results of the Kruskal-Wallis test indicate that nearly all computed metrics have statistically significant differences when considering the three different classifications, i.e., burned and unburned areas (Classification 1), fire occurrence dates (Classification 2), and old and more recent fires (Classification 3). The general tendency is similar, regardless of the pixel size and height interval for computing the diversity indices. Furthermore, there are no significant differences in the topographic metrics apart from roughness and slope in classifications 2 (fire occurrence dates) and 3 (old and more recent fires) (Tab 7.3).

Table 7.3: *Chi-square values for each classification (Class.), spatial resolution (10, 15, 20 m) and ALS metric. Values with non-asymptotic significance, p-value > 0.05 (^{ns}). Class. 1 stands for burned and unburned areas. Class. 2 stands for fire occurrence dates. Class. 3 stands for old and more recent fires. (HCM) stands for horizontal continuity metrics.*

Metric	10 m			15 m			20 m		
	Cl. 1	Cl. 2	Cl. 3	Cl. 1	Cl. 2	Cl. 3	Cl. 1	Cl. 2	Cl. 3
Aspect	1,24^{ns}	3.53^{ns}	2.83^{ns}	0.80^{ns}	2.56^{ns}	1.42^{ns}	0.57^{ns}	2.43^{ns}	1.95^{ns}
CRR	14,60	72.5	71.06	24.87	98.74	94.86	41.26	122.96	120.25
CRR (HCM)	35.22	59.23	55.9	15.76	32.90	30.65	7.02	37.41	33.75
FCC	69.25	146.16	138.56	69.68	150.28	141.96	82.15	162.05	153.90
FCC (HCM)	21.67	47.34	37.96	27.36	46.43	40.16	31.28	44.02	39.44
$H_{kurtosis}$	59.08	98.95	95.83	67.56	127.68	118.17	90.49	154.47	147.88
$H_{kurtosis}$ (HCM)	9.04	56.79	53.54	24.88	81.18	77.26	37.29	96.23	90.20
H_{mean}	178.91	234.08	223.58	200.58	253.70	244.71	210.46	263.47	255.11
H_{mean} (HCM)	219.22	25.39	246.05	184.22	212.74	209.96	169.75	201.96	198.10
H_{p99}	238.65	271.66	261.73	263.07	291.77	284.56	266.74	292.16	285.00
H_{p99} (HCM)	109.68	115.82	113.32	71.28	77.99	72.29	68.84	77.98	69.11
H_{sd}	232.65	269.92	259.18	259.26	292.94	284.92	267.62	299.77	291.78
H_{sd} (HCM)	172.01	182.48	179	147.58	158.14	153.91	141.60	155.11	148.40
$H_{skewness}$	12.96	82.30	80.24	19.10	101.02	97.07	32.37	125.92	123.54
$H_{skewness}$ (HCM)	2.79^{ns}	11.55	8.74	0.27^{ns}	14.34^{ns}	12.89	5.91	20.71	16.88

Continue

Table 1: Continuation

Metric	10 m			15 m			30 m		
	Cl. 1	**Cl. 2**	**Cl. 3**	**Cl. 1**	**Cl. 2**	**Cl. 3**	**Cl. 1**	**Cl. 2**	**Cl. 3**
LHDI and $LHEI_{0.15}$	217.31	263.08	255.15	242.02	287.23	279.00	256.66	301.91	294.28
LHDI and $LHEI_{0.15}$ (HCM)	15.77	52.28	45.89	26.86	54.93	50.27	24.17	51.88	45.43
LHDI and $LHEI_{0.3}$	229.53	268.43	260.73	248.55	288.44	280.03	268.08	309.09	300.62
LHDI and $LHEI_{0.3}$ (HCM)	16.90	269.17	30.64	16.87	30.31	24.96	11.80	23.22	17.87
LHDI and $LHEI_{0.5}$	231.66	39.12	261.37	247.18	287.66	279.13	268.59	308.90	300.79
LHDI and $LHEI_{0.5}$ (HCM)	16.16	263.08	34.19	13.16	28.57	23.21	9.64	22.20	15.47
Roughness	0.08^{ns}	42.21	29.9	0.07^{ns}	45.09	30.29	0.15^{ns}	37.67	26.59

The exhaustive subset selection method selected $LHDI_{0.15}$ and H_{mean} (HCM) as the best metrics (Tab 7.4) for all the classifications, regardless of the spatial resolution. H_{sd} was also selected for classifications 1 (burned

and unburned) and 3 (old and more recent fires). H_{mean} was selected to differentiate the fire occurrence dates (Classification 2). None of the topographic metrics were selected by the exhaustive subset method.

Table 7.4: *Summary of the best-selected ALS metrics in Subset Selection (exhaustive method) in all classifications.*

Classification	ALS metrics
Classification 1	$LHDI_{0.15}$ + Hsd + Hmean (HCM)
Classification 2	$LHDI_{0.15}$ + Hmean + Hmean (HCM)
Classification 3	$LHDI_{0.15}$ + Hsd + Hmean (HCM)

Tab 7.5 shows a summary of the overall classification accuracies and K indices of each classification performed with different methods and at different spatial resolutions. In the case of Classification 1 (burned and unburned areas), the best accuracy and K index was obtained using the SVM method tuned with a gamma value of 0.1 and a cost value of 500, at 15 m spatial resolution. The map obtained for Classification 1 with this method is shown in Fig 7.3. The overall classification accuracy was 89.44%, obtaining a K value of 0.56. Burned areas achieved the highest classification accuracy from the two defined classes (Tab 7.6), with an omission error of 8.12%. Other classification methods and resolutions had slightly lower overall accuracy, ranging from 89.44% to 88.01%, and lower values of agreement (K= 0.56-0.48) (Tab 7.5).

Table 7.5: *Summary of overall classification accuracy (Acc.) and K index of each Classification performed at different spatial resolutions.*

Spatial resolution	Method	Class. 1		Class. 2		Class. 3	
		Acc.	K	Acc.	K	Acc.	K
10	SVM	88.72	0.54	65.60	0.59	74.73	0.57
	RF	88.79	0.55	64.20	0.57	73.45	0.54
	KNN	88.01	0.50	62.03	0.54	60.17	0.27
15	SVM	89.44	0.56	66.67	0.60	72.99	0.54
	RF	89.20	0.55	66.41	0.60	74.12	0.55
	KNN	88.44	0.50	63.50	0.56	59.83	0.26
20	SVM	89.44	0.54	65.94	0.59	75.49	0.57
	RF	88.40	0.49	67.79	0.61	75.42	0.57
	KNN	88.17	0.48	62.07	0.54	61.29	0.29

Table 7.6: *Accuracy assessment (confusion matrix, omission and commission errors, and K index) for Classification 1 using the SVM method at 15 m resolution.*

Reference data				
Classification data (number of pixels)	Unburned	Burned	Total	Omission error (%)
Unburned	226	87	313	27,80%
Burned	198	2240	2438	8.12%
Total	424	2327		
Commission error (%)	53.30%	3.74%		
Overall classification accuracy = 89.44%; K: 0.56.				

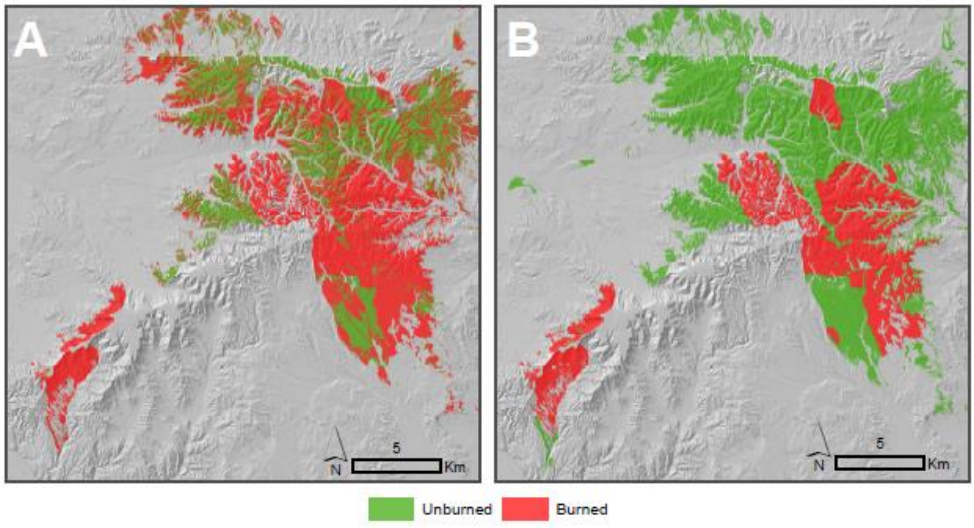

Figure 7.3: *Classification 1 map using SVM (A) and, reference burned surface (B). A shaded relief surface is used as backdrop.*

The RF method with a gamma value of 500 *ntree* and *mtry* value of 2, and at 20 m spatial resolution, was the best method for performing Classification 2 (fire occurrence dates), which considers the year of each wildfire since 1986 and the unburned area (Tab 7.5). This classification had a moderate-high accuracy with a value of 67.79% and an overall K value of 0.61. The area burned in 2008 had the lowest classification accuracy from the six

classes (Tab 7.7), with an omission error of 46.81%. Slightly lower accuracy values were obtained for areas burned in 1986, 2009 and the unburned area (33.83%, 35.60% and 38.82%, respectively). In contrast, a lower omission error prevailed for the area burned in 2006. Consequently, all fires can generally be distinguished with the same accuracy. According to the results shown in Tab 7.7, there is confusion between the oldest fires and the unburned area. There is also confusion between the more recent fires, with the fire occurring in 2008 being the most misclassified one. The low variability of ALS metric values among near fire episodes may cause this confusion. In addition, small height variations between more recent fires were found when analyzing the standard deviation, thus leading to a strong confusion between them. The RF method allowed an old fire to be detected (red box in Fig 7.4), one that had not been recorded in the database. According to Tanase et al., this fire occurred in 1970, and its pixels were classified mostly as the 1986 fire. The other analyzed classification methods and resolutions had slightly lower overall accuracy variation, ranging from 62.07% to 67.79%, and moderate-high agreements (K= 0.54-0.61) (Tab 7.5).

Table 7.7: *Accuracy assessment (confusion matrix, omission and commission errors presented as percentage, and K index) for Classification 2 using the RF method at 20 m resolution.*

Reference data								
Classification data (number of pixels)	*Unburned*	*1986*	*1995*	*2006*	*2008*	*2009*	*Total*	*Omission error (%)*
Unburned	249	85	50	3	15	5	407	38.82%
1986	88	352	76	0	6	10	532	33.83%
1995	39	55	237	5	50	21	407	41.77%
2006	10	0	21	485	35	6	557	12.93%
2008	11	2	21	2	225	97	358	46.81%
2009	7	1	51	1	92	275	427	35.60%
Total	404	495	456	496	423	414		
Commission error (%)	38.37%	28.89%	48.03%	2.22%	46.81%	33.57%		
Overall classification accuracy = 67.79%; K: 0.61								

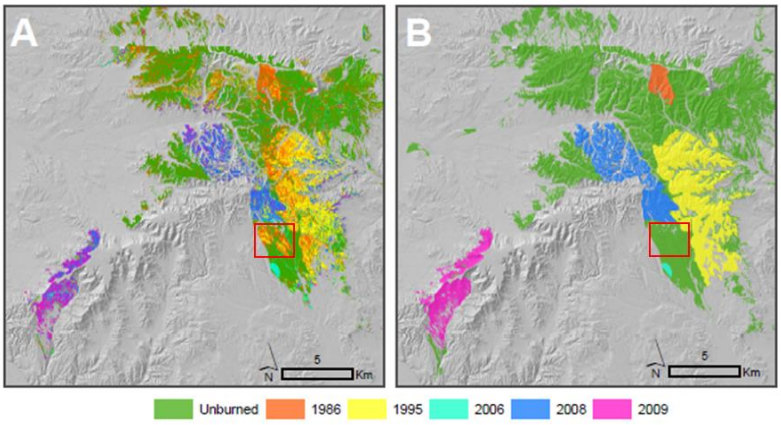

Figure 7.4: *Classification 2 map using RF (A) and reference burned surface (B). A shaded relief surface is used as backdrop. Red box is the fire occurred in 1970.*

The radial-basis kernel SVM with a gamma value of 0.1 and a cost value of 50, at 20 m spatial resolution, was the best method for performing Classification 3 (Tab 7.8, Fig 7.5). This classification had a moderate-high accuracy with a value of 75.49% and an overall K value of 0.57. Tab 7.8 shows the difficulty in accurately differentiating the older fires from the unburned area. This classification has slight differences in terms of overall accuracy compared with RF and SVM with radial kernel (75.42 and 75.42%, respectively), and a greater difference compared with k-NN (61.29%). The K index values range from 0.26 to 0.57 (Tab 7.5).

Table 7.8: *Accuracy assessment (confusion matrix, omission and commission errors presented as percentage, and K index) for Classification 3 using the SVM method at 20 m resolution.*

Reference data					
Classification data (number of pixels)	*Unburned*	*Old fires*	*Recent fires*	*Total*	*Omission error (%)*
Unburned	22	11	11	44	50.00%
Old fires	338	799	113	1250	36.08%
Recent fires	44	142	1209	1395	13.33%
Total	404	952	1333		
Commission error (%)	5.45%	83.93%	90.70%		
Overall classification accuracy = 75.49%; K: 0.57					

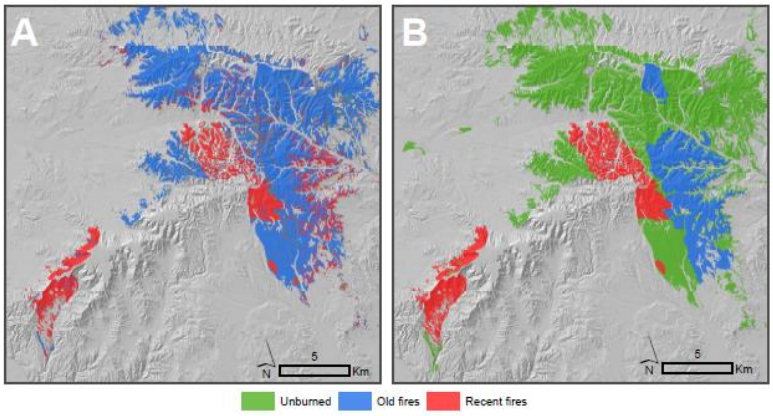

Figure 7.5: *Classification 3 using SVM (A), and reference burned surface (B). A shaded relief surface is used as backdrop.*

7.4. Discussion

Forest fires are significant events in the Mediterranean basin, causing partial or total destruction of the forest structure (Alexandrian *et al.* 1999). Post-fire Aleppo pine forest regeneration has high variability due to weather conditions, land uses and post-dispersal seed predation (Pausas *et al.* 2009). Our results show that relatively recent fires (occurring in 2006, 2008 and 2009) have similar return distributions in all strata, consistent with the temporal proximity of the fire episodes. These wildfires have the lowest LHDI and LHEI values, and most of the laser returns are located in the shrub layer (70%), thus implying structural homogeneity of the vegetation. As defined in Parker and Russ (2004), lower CRR values also indicate that tree branches are located in the lower part of the trunk. As mentioned further above, it should be noted that these fires underwent a post-fire intervention (Miranda and Echevarría 2015).

The oldest fires, occurring in 1986 and 1995, have return distributions closer to the unburned area. This could be a consequence of the time that has passed since the fire. According to Rodrigues *et al.* (2014), that may have led to an advanced stage of recovery. Consistent with the equitable distribution of laser returns in height ranges, the LHDI and LHEI indices have high values, thus implying greater forest structural diversity compared to areas burned in relatively recent fires (Listopad *et al.* 2015). The increase in structural diversity is especially high, even surpassing the values of the unburned area, in the case of the area burned in the fire occurring in 1986. This area was affected by an extensive extraction of burned wood, a common practice in post-fire treatment in Spain (Castro *et al.* 2009). In comparison to 0.3 or 0.5 m height intervals, the generation of diversity indices (LHDI-LHEI) at a 0.15 m height interval better reflects the distribution of the forest structure due to the dense understory in Pinus halepensis forests. This distribution variability is also well reflected by the H_{sd} metric, in agreement with Zimble et al. (2003) and (Brandtberg *et al.* 2003).

In terms of distinguishing between similar classes, SVM and RF had better accuracies than k-NN. Similar results were obtained by Abu Alfeilat

et al. (2019). Given the proximity of dates between some fires, it was difficult to accurately classify them individually. However, the moderate accuracy results obtained and the fact that an unrecorded fire occurring in 1970 was found together reinforce the validity of the method in Classification 2. Despite the difficulty in distinguishing between the unburned area and the old fires (83.93% commission error in the old fire class), there were significant differences in the Kruskal-Wallis test, given the mature stage of these burned forests. Previous studies have analyzed post-fire regeneration using Tasseled Cap transformation or vegetation index time series (Vicente-Serrano *et al.* 2011, Fernandez-Manso *et al.* 2016, Martínez *et al.* 2017), and they too had problems differentiating older disturbances from mature forests.

Gómez *et al.* (2019) reviewed the recent publications devoted to forest studies employing remote sensing in Spain, and they concluded that, based on recovery values calculated using optical data, the pre-fire state was reached somewhere between 7 and 20 years after the time of the disturbance because regrowth processes were affected by a complex mosaic of bare soil, shrubs and herbaceous species (Vicente-Serrano *et al.* 2011). The main advantage of active sensors over multispectral instruments is their ability to capture three-dimensional information of the vegetation structure (Chen 2013, Montealegre *et al.* 2016, Fernandez-Carrillo *et al.* 2018). Montealegre *et al.* (2016, 2017) and Domingo *et al.* (2017, 2019) used a PNOA ALS dataset to calculate forest-stand metrics, achieving good models for relating mean height, squared mean diameter, basal area, timber volume, and even carbon dioxide emissions of the aboveground tree biomass in case of a fire event. Synthetic Aperture Radar (SAR) data have been used for detecting wildfires by Tanase *et al.* (2011), who detected disturbances some 40 to 60 years after their occurrence. In this regard, our study offers results with accuracies comparable to SAR, with the ability to classify fires ~35 years after their occurrence. Although SAR sensors may be suitable for the three-dimensional characterization of forest ecosystems, and despite the fact that there have been recent advances in data processing, difficulties still arise when estimating forest structure in heterogeneous and dense forests (Hyde *et al.* 2006, Tanase *et al.* 2011). Our approach provides valuable information

and reduces the time and costs involved in analyzing forest structural diversity at the landscape level. Furthermore, it is spatially transferable to other forest environments when 3D LiDAR data captured at regional scales are made available (Listopad *et al.* 2015).

The main limitation of the data source used in this study is that of capturing post-fire forest structure regeneration in a highly recurrent fire regime scenario. Within the context of climate change, San-Miguel-Ayanz *et al.* (2013) have suggested that more arid conditions could increase the frequency of extreme fires, which would alter recovery capacity (González-De Vega *et al.* 2018) and produce a loss of species diversity (Fernández-García *et al.* 2019). Fire recurrence might reduce forest vertical complexity, thus generating forested environments dominated by grasslands and shrublands, where trees do not reach their mature stage.

7.5. Conclusions

ALS datasets are becoming available to users, but applications focusing on the analysis of forest structural diversity are still limited. Our results demonstrate the feasibility of low point density ALS data to obtain structural diversity indices and a suite of metrics that enable the characterization of the *Pinus halepensis* forest structure, one that is recurrently affected by fires in the Mediterranean basin. The most suitable ALS-derived metrics were $LHDI_{0.15}$, H_{sd}, H_{mean} (HCM), which were used to perform digital classifications for mapping burned and unburned areas (Classification 1); to differentiate fire occurrence dates (Classification 2); and to distinguish between old and more recent fires (Classification 3). In general, the SVM classification method offered higher accuracies. RF also showed a similar performance, although it was slightly better at differentiating between occurrence dates. In contrast, *k*-NN provided the least accurate results. The proposed methodology has enabled burned areas to be detected at least 35 years after their occurrence, and is therefore useful for assisting forest management at the landscape scale.

7.6. Funding

This work was supported by the Instituto de Investigación en Ciencias Ambientales de Aragón (IUCA) under scholarship [University of Zaragoza PEX-16-076], and by the research grant program Ajuts UdL, Jade Plus i Fundació Bancària La Caixa [Agreement 79/2018 of the Governing Council of the University of Lleida]. This research article has received a grant for its linguistic revision from the Language Institute of the University of Lleida (2020 call).

7.7. References

Abu Alfeilat, H.A., Hassanat, A.B.A., Lasassmeh, O., Tarawneh, A.S., Alhasanat, M.B., Eyal Salman, H.S., and Prasath, V.B.S., 2019. Effects of Distance Measure Choice on K-Nearest Neighbor Classifier Performance: A Review. *Big Data*.

Aguilar, F.J., Mills, J.P., Delgado, J., Aguilar, M.A., Negreiros, J.G., and Pérez, J.L., 2010. Modelling vertical error in LiDAR-derived digital elevation models. *ISPRS Journal of Photogrammetry and Remote Sensing*.

Alexandrian, D., Esnault, F., and Calabri, G., 1999. Forest fires in the Mediterranean area. *Unasylva (FAO)*.

Anderson, T.W. and Darling, D.A., 1954. A Test of Goodness of Fit. *Journal of the American Statistical Association*, 49, 765–769.

Bottalico, F., Chirici, G., Giannini, R., Mele, S., Mura, M., Puxeddu, M., McRoberts, R.E., Valbuena, R., and Travaglini, D., 2017. Modeling Mediterranean forest structure using airborne laser scanning data. *International journal of applied earth observation and geoinformation*, 57, 145–153.

Brandtberg, T., Warne, T.A., Landenberger, R.E., and

McGraw, J.B., 2003. Detection and analysis of individual leaf-off tree crowns in small footprint, high sampling density lidar data from the eastern deciduous forest in North America. *Remote Sensing of Environment*.

Castro, J., Navarro, R., Guzmán, J.R., Zamora, R., and Bautista, S., 2009. ¿Es conveniente retirar la madera quemada tras un incendio forestal? *Quercus*, 281, 34–41.

Chen, Q., 2013. LiDAR remote sensing of vegetation biomass. *Remote Sensing of Natural Resources*, (Asner 2009), 399–420.

Chuvieco, E., 2010. *Teledetección ambiental. La observación de la Tierra desde el espacio*. Barcelona: Ariel Ciencia.

Cochrane, M.A. and Schulze, M.D., 1999. Fire as a Recurrent Event in Tropical Forests of the Eastern Amazon: Effects on Forest Structure, Biomass, and Species Composition. *Biotropica*, 31 (1), 2–16.

Cuadrat, J.M., Saz, M.A., and Vicente-Serrano, S.M., 2007. Atlas climático de Aragón. *Gobierno de Aragón*.

Debouk, H., Riera-Tatché, R., and Vega-Garcia, C., 2013. Assessing post-fire regeneration in a Mediterranean mixed forest using LiDAR data and artificial neural networks. *Photogrammetric Engineering & Remote Sensing*, 79 (12), 1121–1130.

Domingo, D., Lamelas, M.T., Montealegre, A.L., García-Martín, A., and de la Riva, J., 2018. Estimation of Total Biomass in Aleppo Pine Forest Stands Applying Parametric and Nonparametric Methods to Low-Density Airborne Laser Scanning Data. *Forests*, 9 (4), 158.

Domingo, D., Lamelas, M.T., Montealegre, A.L., and de la Riva, J., 2017. Comparison of regression models to estimate biomass losses and CO2 emissions using

low-density airborne laser scanning data in a burnt Aleppo pine forest. *European Journal of Remote Sensing*, 50 (1), 384–396.

Domingo, D., Montealegre, A.L., Lamelas, M.T., García-Martín, A., de la Riva, J., Rodríguez, F., and Alonso, R., 2019. Quantifying forest residual biomass in Pinus halepensis Miller stands using Airborne Laser Scanning data. *GIScience and Remote Sensing*, 56 (8), 1210–1232.

Dubayah, R.O. and Drake, J.B., 2000. Lidar remote sensing for forestry. *Journal of Forestry*, 98 (6), 44–46.

Evans, J.S. and Hudak, A.T., 2007. A multiscale curvature algorithm for classifying discrete return LiDAR in forested environments. *IEEE Transactions on Geoscience and Remote Sensing*, 45 (4), 1029–1038.

Fernandez-Carrillo, A., McCaw, L., Belenguer-Plomer, M.A., and Tanase, M.A., 2018. L-band SAR sensitivity to prescribed burning effects in eucalypt forests of Western Australia. *In: Active and Passive Microwave Remote Sensing for Environmental Monitoring II.* International Society for Optics and Photonics, 107880U.

Fernández-García, V., Fulé, P.Z., Marcos, E., and Calvo, L., 2019. The role of fire frequency and severity on the regeneration of Mediterranean serotinous pines under different environmental conditions. *Forest Ecology and Management.*

Fernandez-Manso, A., Quintano, C., and Roberts, D.A., 2016. Burn severity influence on post-fire vegetation cover resilience from Landsat MESMA fraction images time series in Mediterranean forest ecosystems. *Remote Sensing of Environment*, 184, 112–123.

Fix, E. and Hodges, J.L., 1989. Discriminatory Analysis.

Nonparametric Discrimination: Consistency Properties. *International Statistical Review*, 57, 238–247.

García, M., Riaño, D., Chuvieco, E., Salas, J., and Danson, F., 2011. Multispectral and LiDAR data fusion for fuel type mapping using Support Vector Machine and decision rules. *Remote Sensing of Environment*, 115 (6), 1369–1379.

Gómez, C., Alejandro, P., Hermosilla, T., Montes, F., Pascual, C., Ruiz, L.A., Álvarez-Taboada, F., Tanase, M.A., and Valbuena, R., 2019. Remote sensing for the Spanish forests in the 21st century: a review of advances, needs, and opportunities. *Forest Systems*.

Gonçalves, A.C. and Sousa, A., 2017. The fire in the Mediterranean region: a case study of forest fires in Portugal. *In*: *Mediterranean identities: environment, society, culture*.

González-De Vega, S., De las Heras, J., and Moya, D., 2016. Resilience of Mediterranean terrestrial ecosystems and fire severity in semiarid areas: Responses of Aleppo pine forests in the short, mid and long term. *Science of the Total Environment*.

González-De Vega, S., de las Heras, J., and Moya, D., 2018. Post-Fire Regeneration and Diversity Response to Burn Severity in Pinus halepensis Mill. Forests. *Forests*, 9 (6), 299.

Goubitz, S., Nathan, R., Roitemberg, R., Shmida, A., and Ne'eman, G., 2004. Canopy seed bank structure in relation to: fire, tree size and density. *Plant Ecology*, 173 (2), 191–201.

Hamraz, H., Contreras, M.A., and Zhang, J., 2017. Forest understory trees can be segmented accurately within sufficiently dense airborne laser scanning point clouds. *Scientific Reports*.

Hyde, P., Dubayah, R., Walker, W., Blair, J.B., Hofton, M., and Hunsaker, C., 2006. Mapping forest structure for wildlife habitat analysis using multi-sensor (LiDAR, SAR/InSAR, ETM+, Quickbird) synergy. *Remote Sensing of Environment*, 102 (1–2), 63–73.

Jennings, S.B., Brown, N.D., and Sheil, D., 1999. Assessing forest canopies and understorey illumination: canopy closure, canopy cover and other measures. *Forestry: An International Journal of Forest Research*, 72 (1), 59–74.

Jiménez-Ruano, A., Rodrigues, M., and de la Riva, J., 2017. Exploring spatial–temporal dynamics of fire regime features in mainland Spain. *Natural Hazards and Earth System Sciences*.

Kane, V.R., Lutz, J.A., Roberts, S.L., Smith, D.F., McGaughey, R.J., Povak, N.A., and Brooks, M.L., 2013. Landscape-scale effects of fire severity on mixed-conifer and red fir forest structure in Yosemite National Park. *Forest Ecology and Management*, 287, 17–31.

Kelly, M. and Di Tommaso, S., 2015. Mapping forests with Lidar provides flexible, accurate data with many uses. *California Agriculture*, 69 (1), 14–20.

Kimmins, J.P., 1997. Biodiversity and its relationship to ecosystem health and integrity. *The forestry chronicle*, 73 (2), 229–232.

Kruskal, W.H. and Wallis, W.A., 1952. Use of ranks in one-criterion variance analysis. *Journal of the American Statistical Association*, 47 (260), 583–621.

Kuhn, M., 2008. Building predictive models in R using the caret package. *Journal of statistical software*, 28 (5), 1–26.

Lamelas, M.T., Riaño, D., and Ustin, S., 2019. A LiDAR

signature library simulated from 3-dimensional Discrete Anisotropic Radiative Transfer (DART) model to classify fuel types using spectral matching algorithms. *GIScience and Remote Sensing*, 56 (7), 988–1023.

Lefsky, M.A., Cohen, W.B., Parker, G.G., and Harding, D.J., 2002. Lidar remote sensing for ecosystem studies. *BioScience*, 52 (1), 19–30.

Liaw, A. and Wiener, M., 2002. Classification and regression by randomForest. *R news*, 2 (3), 18–22.

Lim, K., Treitz, P., Wulder, M.A., St-Onge, B., and Flood, M., 2003. LiDAR remote sensing of forest structure. *Progress in Physical Geography*, 27 (1), 88–106.

Listopad, C.M.C.S., Masters, R.E., Drake, J., Weishampel, J., and Branquinho, C., 2015. Structural diversity indices based on airborne LiDAR as ecological indicators for managing highly dynamic landscapes. *Ecological Indicators*, 57, 268–279.

Liu, X., 2008. Airborne LiDAR for DEM generation: some critical issues. *Progress in Physical Geography*, 32 (1), 31–49.

Lumley, T. and Miller, A., 2017. *Leaps: Regression Subset Selection.*

Magnussen, S. and Boudewyn, P., 1998. Derivations of stand heights from airborne laser scanner data with canopy-based quantile estimators. *Canadian journal of forest research*, 28 (7), 1016–1031.

Manzanera, J.A., García-Abril, A., Pascual, C., Tejera, R., Martín-Fernández, S., Tokola, T., and Valbuena, R., 2016. Fusion of airborne LiDAR and multispectral sensors reveals synergic capabilities in forest structure characterization. *GIScience and Remote Sensing*, 53 (6), 723–738.

Martín-Alcón, S., Coll, Ll., De Cáceres, M., Guitart, L., Cabré, M., Just, A., and González-Olabarría, J.R., 2015. Combining aerial LiDAR and multispectral imagery to assess postfire regeneration types in a Mediterranean forest. *Canadian Journal of Forest Research*.

Martínez, S., Chuvieco, E., Aguado, I., and Salas, J., 2017. Severidad y regeneración en grandes incendios forestales: Análisis a partir de series temporales de imágenes landsat. *Revista de Teledeteccion*, 2017 (49 Special Issue), 17–32.

McElhinny, C., Gibbons, P., Brack, C., and Bauhus, J., 2005. Forest and woodland stand structural complexity: its definition and measurement. *Forest Ecology and Management*, 218 (1–3), 1–24.

McGaughey, R.J., 2014. FUSION/LDV: Software for LIDAR data analysis and visualization. March 2014–FUSION, version 3.42. *United States Department of Agriculture Forest Service Pacific Northwest Research Station*.

Medail, F. and Quezel, P., 1999. *Biodiversity hotspots in the Mediterranean Basin: Setting global conservation priorities*. Conservation Biology.

Meyer, D., Dimitriadou, E., Hornik, K., Weingessel, A., and Leisch, F., 2017. *e1071: misc functions of the department of statistics, probability theory group (Formerly: E1071), TU Wien. R package version 1.6-8*.

Miranda, J. and Echevarría, M.T., 2015. Aproximación, a partir de un modelo de vulnerabilidad, a técnicas de rehabilitación en zonas afectadas por incendios forestales. *Análisis espacial y representación geográfica: innovación y aplicación*, 691–697.

Montealegre, A.L., Lamelas, M.T., García-Martín, A., de la Riva, J., and Francisco, E., 2017. Using low-density discrete Airborne Laser Scanning data to assess the potential carbon dioxide emission in case of a fire event in a Mediterranean pine forest. *GIScience and Remote Sensing*, 54 (5), 721–740.

Montealegre, A.L., Lamelas, M.T., and de la Riva, J., 2015a. A Comparison of Open-Source LiDAR Filtering Algorithms in a Mediterranean Forest Environment. *IEEE Journal of Selected Topics in Applied Earth Observations and Remote Sensing*, 8 (8), 4072–4085.

Montealegre, A.L., Lamelas, M.T., and de la Riva, J., 2015b. Interpolation routines assessment in ALS-derived digital elevation models for forestry applications. *Remote sensing*, 7 (7), 8631–8654.

Montealegre, A.L., Lamelas, M.T., de la Riva, J., García-Martín, A., and Escribano, F., 2016. Use of low point density ALS data to estimate stand-level structural variables in Mediterranean Aleppo pine forest. *Forestry*, 89 (4), 373–382.

Parker, G.G. and Russ, M.E., 2004. The canopy surface and stand development: assessing forest canopy structure and complexity with near-surface altimetry. *Forest Ecology and Management*, 189 (1–3), 307–315.

Pausas, J., 2004. Changes in fire and climate in the eastern Iberian Peninsula (Mediterranean basin). *Climatic change*, 63 (3), 337–350.

Pausas, J., Llovet, J., Rodrigo, A., and Vallejo, R., 2009. Are wildfires a disaster in the Mediterranean basin?–A review. *International Journal of wildland fire*, 17 (6), 713–723.

Pielou, E.C., 1975. *Ecological diversity*. Wiley.

Prometheus, S.V., 2000. Management techniques for optimization of suppression and minimization of wildfire effects. *System validation. European Commission–contract number ENV4-CT98-0716*.

Rodrigues, M., Paloma, I., Echeverría, M.T., Pérez-Cabello, F., and de la Riva, J., 2014. A method for regional-scale assessment of vegetation recovery time after high-severity wildfires: Case study of Spain. *Progress in Physical Geography*, 38 (5), 556–575.

Rodrigues, M. and de la Riva, J., 2014. An insight into machine-learning algorithms to model human-caused wildfire occurrence. *Environmental Modelling & Software*, 57, 192–201.

Rodrigues, M., San-Miguel-Ayanz, J., Oliveira, S., Moreira, F., and Camia, A., 2013. An insight into spatial-temporal trends of fire ignitions and burned areas in the European Mediterranean countries. *Journal of Earth Science and Engineering*, 3 (7), 497.

San-Miguel-Ayanz, J., Moreno, J.M., and Camia, A., 2013. Analysis of large fires in European Mediterranean landscapes: Lessons learned and perspectives. *Forest Ecology and Management*.

Shannon, C.E. and Wiener, W., 1949. *The mathematical theory of communication (Urbana, IL.* University of illinois Press IL.

Staudhammer, C.L. and LeMay, V.M., 2001. Introduction and evaluation of possible indices of stand structural diversity. *Canadian journal of forest research*, 31 (7), 1105–1115.

Su, J. and Bork, E., 2006. Influence of vegetation, slope, and lidar sampling angle on DEM accuracy. *Photogrammetric Engineering & Remote Sensing*, 72 (11), 1265–1274.

Tanase, M., de la Riva, J., Santoro, M., Pérez-Cabello,

F., and Kasischke, E., 2011. Sensitivity of SAR data to post-fire forest regrowth in Mediterranean and boreal forests. *Remote Sensing of Environment*, 115 (8), 2075–2085.

Teobaldelli, M., Cona, F., Saulino, L., Migliozzi, A., D'Urso, G., Langella, G., Manna, P., and Saracino, A., 2017. Detection of diversity and stand parameters in Mediterranean forests using leaf-off discrete return LiDAR data. *Remote sensing of environment*, 192, 126–138.

Vicente-Serrano, S.M., Pérez-Cabello, F., and Lasanta, T., 2011. Pinus halepensis regeneration after a wildfire in a semiarid environment: Assessment using multitemporal Landsat images. *International Journal of Wildland Fire*.

Wilson, M.F.J., O'Connell, B., Brown, C., Guinan, J.C., and Grehan, A.J., 2007. Multiscale terrain analysis of multibeam bathymetry data for habitat mapping on the continental slope. *Marine Geodesy*.

Wulder, M.A., White, J.C., Nelson, R.F., Næsset, E., Ole, H., Coops, N.C., Hilker, T., Bater, C.W., and Gobakken, T., 2012. Lidar sampling for large-area forest characterization : A review. *Remote Sensing of Environment*, 121, 196–209.

Zimble, D.A., Evans, D.L., Carlson, G.C., Parker, R.C., Grado, S.C., and Gerard, P.D., 2003. Characterizing vertical forest structure using small-footprint airborne LiDAR. *Remote sensing of Environment*, 87 (2–3), 171–182.

Capítulo 8

Discusión

8. Discusión

Los resultados obtenidos en esta Tesis doctoral suponen una contribución original al conocimiento actual relativo a los efectos del cambio global en el medio natural. Se ha profundizado principalmente (aunque no exclusivamente) en aspectos técnicos y metodológicos relacionados con la obtención, procesado y análisis de datos provenientes de teledetección combinando fuentes, herramientas y tecnologías novedosas (GEE, GEDI, LandTrendr) y tradicionales (RF, SVM, Landsat y LiDAR PNOA). Primeramente, se plantea una metodología para monitorizar la dinámica espacio-temporal de la sucesión secundaria con imágenes Landsat. Una vez conocida la dinámica de la sucesión secundaria, la comprensión del proceso se completa con un conocimiento detallado de los factores que desencadenan el abandono y los patrones espaciales subyacentes. Por otro lado, frente al actual aumento en biomasa por la sucesión secundaria derivada del creciente abandono agrícola en zonas de montaña, resulta de sumo interés conocer cómo se desarrollan los bosques en los diferentes ambientes de montaña y como los limitantes actuales se verán modificados por el cambio global. Finalmente, el cambio global modifica nuestros ambientes con mayores cargas de biomasa y contribuye a la alteración del régimen de incendios. Es por dicho motivo que es de suma importancia conocer la recuperación de la estructura forestal después de un incendio. En el último capítulo se adapta una metodología para poder caracterizar la diversidad de estructuras generada después de incendios forestales y su semejanza con el estado previo décadas después. A continuación, se pretende dar respuesta a las preguntas de investigación formuladas en la sección 2.

OG1 – Conocer la dinámica espacio-temporal de la sucesión secundaria a causa del abandono agrícola en áreas montañosas mediterráneas

Los incendios forestales son la mayor perturbación en los bosques de la cuenca mediterránea (Pausas *et al.* 2009), no obstante, en las zonas de montaña la dinámica forestal se asocia principalmente al abandono de tierras agrícolas favorecido por la incorporación de actividades económicas relacionadas con el sector terciario (Ameztegui et al., 2016; Cap. 4 Gelabert et al., 2021; Lasanta et al., 2017). El fenómeno del abandono se traduce en sucesión secundaria (SS), es decir, la colonización del bosque sobre espacios antes ocupados por pastos y cultivos. La SS es un proceso ambiental con un impacto potencial positivo en la provisión de algunos servicios ecosistémicos en cuanto a su consideración como espacios con presencia de vegetación leñosa (e.g. captura de carbono, refugio para fauna, madera, etc.) y un detrimento en comparación con aquellos provistos por espacios abiertos, con vegetación dispersa o de porte herbáceo (e.g.: infiltración de aguas subterráneas, conservación de la biodiversidad de espacios abiertos, alimento para ganado, etc.). Por otra parte, el incremento en el combustible y homogeneización del paisaje asociado a la SS puede suponer un incremento en el peligro de incendio (Pausas and Bond 2020). Dado el gran potencial de los sensores multiespectrales para la monitorización de los cambios en las cubiertas y usos del suelo (Wulder *et al.* 2018), en la presente tesis se ha desarrollado un procedimiento (ver Cap. 4 – sec. 4.3.3) para monitorizar la progresión espacio-temporal de la SS en los Pirineo, revelando que en los últimos 36 años el bosque ha recubierto el 64% de los espacios previamente ocupados por pastos y cultivos.

Los modelos de clasificación que intervienen en el proceso de seguimiento de la SS permitieron identificar los ejes *tasseled Cap* del brillo (TCB) y la humedad (TCW) como los neocanales espectrales más apropiados para

capturar los cambios en la estructura forestal (Healey et al., 2005). Esto se debe a que las comunidades forestales densas, con portes desarrollados, y, en menor medida, los matorrales, se caracterizan por una mayor capacidad de retención de la humedad, lo que se recoge con valores más elevados de humedad (TCW). En cambio, el brillo (TCB) registra valores más bajos en las zonas boscosas debido al comportamiento lambertiano por la rugosidad de su superficie, y en contraposición, las zonas abiertas presentan un comportamiento más especular registrándose valores más elevados de brillo (Healey *et al.* 2005). Por otro lado, el TCG y el TCA se consideran variables con poco poder predictivo de las diferencias estructurales entre las diferentes comunidades forestales, ya que son índices relacionados con el verdor y no captan óptimamente las diferencias entre tipos de vegetación (Tanase *et al.* 2011, Frazier *et al.* 2015, Pickell *et al.* 2016).

La utilización del algoritmo de Landtrendr (LT) supone una ventaja frente al análisis tradicional de series temporales dado que en su proceso reduce ruidos e homogeniza la serie temporal (Kennedy *et al.* 2010). El procedimiento se basa en la segmentación de la serie en base a cambios abruptos y, como resultado, ofrece tres productos: la serie temporal sin ajustar (TC Raw), la serie temporal con los valores ajustados (LTTC), y una serie de métricas que resumen cada segmento (LT Output). Dado que la progresión de la SS es prologada en el tiempo y no se produce de forma abrupta, se ha seleccionado la métrica de la magnitud -definida como la diferencia entre el valor final e inicial- del segmento más duradero en el tiempo.

El uso de la información espectral ajustada con LT redujo significativamente el ruido derivado de las diferencias producidas por las condiciones de iluminación, los cambios fenológicos, las condiciones atmosféricas o el registro geométrico (Kennedy *et al.* 2010). A pesar de que tanto los modelos

de salida LTTC como LT mostraron una muy buena precisión en la detección de patrones espaciales de SS (Fig. 4.3, Fig. 4.5), la mayor precisión espacial se obtuvo utilizando LTTC (Tab. 4.2). Los métodos basados en la LT (LTTC y LT output) predijeron que 464.626 ha (64% de los antiguos pastizales y cultivos) y 533.043 ha (77%) experimentaron SS en el periodo 1984-2019, respectivamente. En cambio, los modelos TC Raw sobreestiman la superficie afectada por el SS (error de comisión = 0,34). En el aspecto temporal, por los efectos de ruido en la señal, el modelo calibrado utilizando TC Raw la detección del año de inicio de la SS se concentran siempre al principio de la serie temporal por efecto del ruido. En cambio, en el modelo en el que se usan los TC armonizados con LT (LTTC) la señal es más homogénea y presenta tasas de SS elevadas durante los primeros años, disminuyendo drásticamente hasta principios de los 90, seguidos de una estabilización en la perdida de espacios abiertas posterior (Fig. 4.6). El fenómeno que observamos coincide con la literatura referente al abandono agrícola en los espacios de montaña de España y Europa (Lasanta and Vicente-Serrano 2007, Ameztegui *et al.* 2010, García-Ruiz *et al.* 2015, van Leeuwen *et al.* 2019). En este sentido, los resultados obtenidos justifican el uso de algoritmos de segmentación temporal (LT) para analizar el fenómeno de la SS.

Se puede concluir que en los Pirineos españoles se ha reducido un 64% la extensión de los pastizales y cultivos gestionados durante los últimos 36 años, lo que supone un drástico descenso de la biodiversidad – referida a las especies herbáceas y fauna de estos espacios- y de otros servicios ecosistémicos vinculados a estos ecosistemas abiertos.

OG2 – Analizar qué factores son los principales responsables del reciente aban-dono agrícola.

El avance de la SS es un análisis que, si bien de interés por sí mismo, se beneficiaría de una mejor y más detallada comprensión de los factores

que desencadenan el abandono y los patrones espaciales subyacentes. A pesar de ser un fenómeno ampliamente analizado, el abandono agrícola generalmente ha sido estudiado de forma local, generalizando estudios realizados a escala de valle (Poyatos *et al.* 2003, Vicente-Serrano *et al.* 2003, Serra *et al.* 2014). El reto metodológico es la translación de ese conocimiento local a una escala regional. Para ello se han usado, en base a literatura existente, una serie de variables socioeconómicas, ambientales, climáticas y topográficas que pueden tener relación directa con el abandono agrícola. Una vez conocidas las relaciones e intensidad de las mismas, la espacializacion del fenómeno genera un valor añadido al análisis generando una cartografía que puede ser usada como soporte para la toma de decisiones.

De esta Tesis Doctoral se deriva que el proceso de abandono en las regiones de montaña está vinculado al desarrollo de las actividades terciarias, principalmente al turismo y las segundas residencias, y sus servicios asociados (Prados 2008, Serra *et al.* 2014). Las actividades primarias, como la agricultura y la ganadería, han sido abandonadas en favor de actividades turísticas, o complementarias con la dedicación a tiempo parcial a actividades terciarias destinadas a proporcionar una salida de productos agrícolas con mayor valor añadido (e.g.: Embutidos, lácteos y derivados, aceites, apicultura, etc.) (Petrou *et al.* 2007, Vidal-Macua *et al.* 2018). Además, esto se ve agravado por las políticas desarrolladas durante la década de 1960, cuando el Gobierno financió numerosas infraestructuras hidráulicas para fomentar la agricultura en las regiones más áridas, pero con mayor potencial de mecanización y de monocultivo extensivo (Alonso-Sarría *et al.* 2016). Todo ello sumado a las prioridades establecidas actualmente en la Política Agraria Común europea, que también prioriza la agricultura extensiva e irrigada (Cazcarro *et al.* 2015). Todo ello provocó la pérdida de competitividad de las tierras agrícolas en las regiones de montaña y su paulatino abandono. Otros programas europeos de subvención -como los LEADER e INTERREG- destinados a estabilizar población y financiar iniciativas

transnacionales han acabado en inversiones que favorecen el desarrollo de actividades terciarias vinculadas con el turismo rural, fomentando el uso recreativo de estos espacios en detrimento de las actividades tradicionales (Lasanta and Marín-Yaseli 2007).

Nuestro análisis revela que el abandono no es espacialmente homogéneo a lo largo del territorio pirenaico, sino que responde a combinaciones específicas de factores que operan a diferentes escalas. La zona con mayor potencial de abandono se ubica en el extremo oriental del macizo (Badía *et al.* 2004, Vilà-Cabrera *et al.* 2017), donde existe una expansión de la segunda residencia y la actividad turística, en parte fomentado por su buena accesibilidad a través de vías de alta capacidad (C-17 y C-16) que la conectan con el área metropolitana de Barcelona. La existencia de esa conexión rápida ha favorecido también la expansión de otras formas de alojamiento como los campings y los hoteles (Fig. 5.6D). En Aragón se observa un patrón similar en los corredores cercanos a las autovías A-23, A-21 y carreteras N-330 y N-240 que conectan con ciudad de Zaragoza. En la línea de lo previamente comentado, la accesibilidad juega un papel muy importante en el desarrollo turístico y se observan mayores tasas de abandono en las localidades conectadas por carreteras de la red principal (Vidal-Macua *et al.* 2018). No obstante, en las localidades conectadas por la red secundaria no existe un proceso de abandono agrícola tan evidente, dado que no conectan con las zonas más pobladas y demandantes de espacios de recreo y ocio.

Otro motor económico vinculado a la actividad turística, característico de la alta montaña, son las estaciones de esquí y otros deportes de invierno. La localización de las estaciones de esquí en Aragón y Cataluña es diferente. En Aragón se ubican habitualmente cerca de poblaciones o alojamientos turísticos, mientras que en Cataluña tienden a estar más alejados de estos (Lasanta *et al.* 2013). En el mapa de probabilidad de abandono (Fig. 5.2),

se observan altas tasas de abandono cerca de las estaciones de esquí aragonesas mientras que en las catalanas se observan valores mucho menores. Esto se debe a que las estaciones no ejercen una influencia en dicha probabilidad por sí mismas, sino que su efecto es indirectamente producido por la oferta complementaria asociada que se alberga en los núcleos urbanos más cercanos. Cabe mencionar que la dinámica demográfica también parece estar vinculada al abandono rural. Debido a la oferta laboral asociada al sector terciario, aquellos municipios que registran un aumento de la densidad de población son aquellos que tienen mayor probabilidad de abandono (Fig. C5-6 G) (MacDonald *et al.* 2000, Gellrich and Zimmermann 2007, Lasanta and Vicente-Serrano 2007, Ameztegui *et al.* 2010, Lasanta *et al.* 2013, 2017).

En otro orden de magnitud, la configuración topográfica presenta una menor importancia en la distribución del abandono agrícola, operando a escala local. Los relieves complejos de las zonas montañosas dificultan la mecanización lo que, unido a una población envejecida, restan competitividad económica a la zona (MacDonald *et al.* 2000, Corbelle-Rico *et al.* 2012, Terres *et al.* 2015). La probabilidad de abandono aumenta a medida que ganamos elevación, siendo más probable en las laderas con mayor pendiente y orientadas al sur y al este (Fig. 5.6F y J).

En los Pirineos las parcelas agrícolas son relativamente grandes, a excepción de las localizadas en los fondos de valle. De acuerdo con (Renwick *et al.* 2013), encontramos que las parcelas más pequeñas son más propensas al abandono debido a que no se mecanizan por su baja rentabilidad. Sin embargo, las parcelas más grandes, aunque no son abundantes, también están relacionadas con una mayor probabilidad de abandono (Fig. 5.6H). El tamaño de la parcela no parece tener un efecto claro en la probabilidad de abandono, las parcelas más abandonadas son las pequeñas, ubicadas de

los fondos de valle (Fig. 5.6 K), que, por ende, están cercanas a núcleos urbanos y servicios turísticos.

Por último, los resultados del análisis de la variación del Standardised Precipitation-Evapotranspiration Index (SPEI) (Vicente-Serrano *et al.* 2010) evidencia que el abandono no responde a limitantes bioclimáticos; ya que en las zonas donde se espera una mayor productividad– zonas con balance hídrico positivo, SPEI>0 - es donde se dan mayores probabilidades de abandono. Por otro lado, en las zonas abandonadas existen valores más elevados de la densidad aparente (menor porosidad) del suelo, efecto de la compactación y menor estructura del suelo que caracteriza a los suelos abandonados (Koulouri and Giourga 2007).

Como conclusión general, se extrae que el sector terciario es el principal motor de cambio económico en los Pirineos. Particularmente, las infraestructuras viarias de acceso rápido, en vez de fijar población y fomentar el desarrollo rural, están contribuyendo a la expansión turística. Esta dependencia turística está bien referenciada en la literatura (MacDonald *et al.* 2000, Lasanta *et al.* 2017, Vidal-Macua *et al.* 2018). El principal aporte de este capítulo (Cap. 5 - (Gelabert *et al.* 2022) es la caracterización espacial de las relaciones entre variables que promueven el abandono rural.

OG3 – Caracterizar mediante el uso de sensores activos los factores limitantes que condicionan el desarrollo del arbolado en zonas de montaña

En un escenario de aumento en biomasa por la sucesión secundaria derivada del creciente abandono agrícola resulta de sumo interés conocer cómo se desarrollan los bosques en los diferentes ambientes de montaña.

En ecología es ampliamente conocido el concepto de *treeline* (o límite superior del estrato arbóreo) definido como la elevación máxima donde se desarrolla el arbolado (Körner 2012). El treeline a escala global corresponde a una limitación térmica que imposibilita el desarrollo de la vegetación arbórea (Körner and Paulsen 2004, Paulsen and Körner 2014). No obstante, la aparición de los limitantes es progresiva y es esperable que el desarrollo de la vegetación empiece a reducirse en cotas más bajas (Ameztegui *et al.* 2021).

La altura del arbolado es una variable ampliamente utilizada para estimar diversos parámetros estructurales y la productividad de los bosques (Grace *et al.* 2002, Silva *et al.* 2018, Qi *et al.* 2019). Dada su alta utilidad se ha convertido en una de las variables con mayor prioridad para ser monitorizada desde el espacio (Skidmore *et al.* 2021). En la presente Tesis se han aprovechado los novedosos datos del sensor GEDI (LiDAR espacial), los cuales nos permiten estimar la altura del arbolado con elevada precisión (Beck *et al.* 2020, Dubayah *et al.* 2020) con el objetivo de caracterizar el desarrollo del arbolado en los gradientes de elevación en las principales cadenas montañosas europeas.

La altura máxima de los árboles mostró un claro descenso no lineal a lo largo del gradiente altitudinal en todas las cordilleras analizadas (Pirineos, Alpes, Cárpatos, Cáucaso), apoyando la existencia de un patrón regional en el control del desarrollo de la altura de la vegetación arbórea. La tendencia no lineal y segmentada permite detectar un punto de ruptura (*breakpoint)* explícito por encima del cual la altura de los árboles desciende abruptamente. Este punto de ruptura puede reflejar el límite del óptimo climático a partir del cual la idoneidad climática para el crecimiento de la vegetación disminuye (Ameztegui *et al.* 2021). En tres de las cuatro cordilleras analizadas (Alpes, Cárpatos y Cáucaso), la disminución de la altura de la vegetación con la elevación se debió a la limitación térmica (Fig. 6.2)

(Zhang *et al.* 2016, Ameztegui *et al.* 2021). Por otro lado, a diferencia de las otras cordilleras, el desarrollo de la altura máxima de los árboles en los Pirineos parece estar más condicionado por las precipitaciones que por las limitaciones térmicas. Esto es debido a su proximidad a los mares Mediterráneo y Cantábrico, además de una marcada sequía estival típica del clima mediterráneo.

Los resultados este capítulo (Cap. 6) contribuyen a identificar el valor de elevación donde se inician estos procesos en diferentes cordilleras (Zhang *et al.* 2016, Ameztegui *et al.* 2021) y la existencia de un patrón segmentado de la relación cota-altura del arbolado a escala europea. Reconocemos que la elevación actúa aquí como un indicador de la variabilidad climática (Hijmans et al., 2005). La desigual y escasa distribución de las estaciones que alimentan los modelos de interpolación climática como WorldClim (Fick and Hijmans 2017) y su baja precisión espacial, dificultan su fiabilidad en las zonas de montaña (Paulsen and Körner 2014, Gonzalez-Hidalgo *et al.* 2020). Aunque no está exenta de inconvenientes, la alta correlación de las variables climáticas con la altitud y la disponibilidad global de datos topográficos hacen de esta última una variable adecuada para el seguimiento de los efectos del clima en las zonas de montaña. Incluso cuando la precipitación fue el principal impulsor del desarrollo de la altura de los árboles, la elevación también fue un buen estimador del punto de ruptura, lo que sugiere que podría utilizarse globalmente como indicador de la relación entre el clima y el desarrollo de la altura de los árboles (Klein *et al.* 2015, Fricker *et al.* 2019, Ameztegui *et al.* 2021).

OG4 – Predecir la expansión de los bosques de montaña bajo los efectos del calentamiento global.

Las diferentes proyecciones climáticas estiman un incremento de la temperatura global durante el presente siglo (IPCC 2022). Conociendo que

el principal limitante al crecimiento del arbolado en zonas de montaña corresponde a la temperatura, es importante plantear como afectara el calentamiento global al desarrollo de los árboles en las zonas de alta montaña. Nuestros resultados sugieren un desplazamiento en elevación del punto de ruptura, es decir de las condiciones óptimas de crecimiento del arbolado. En los Cárpatos, bajo el escenario de mayor concentración de emisiones, desaparecería el limitante térmico, ya que el punto de ruptura se ubicaría fuera del rango de cota de la cadena montañosa.

Este desplazamiento potencial no se traducirá en un desplazamiento universal debido a la complejidad de factores que influyen en la aforestación natural en el límite de su tolerancia fisiológica (e.g. disponibilidad de suelo) (Körner and Paulsen 2004, Coops *et al.* 2013). Sin embargo, es más probable que el punto de ruptura altura-elevación se desplace, ya que es indicativo de una relación fisiológica entre el desarrollo de los árboles y el clima, y no un límite físico propiamente dicho. Como se ha observado en los bosques boreales (Wilmking and Juday 2005, Henttonen *et al.* 2017, Lloyd *et al.* 2017), el desplazamiento hacia arriba de dicho punto de elevación puede implicar un aumento sustancial de la productividad de estos bosques limitados por el frío que también puede aumentar su productividad (Hilmers *et al.* 2019)(Hilmers et al., 2019). Además, las comunidades forestales existentes entre el acutal *breakpoint* y el futuro *breakpoint* tendrán una mayor productividad, pudiendo prestar más servicios ecosistémicos (Mina et al., 2017), como un incremento en el valor de la madera o el secuestro de carbono.

OG5 – Identificación de la ocurrencia y efectos de perturbaciones pasadas so-bre masas forestales utilizando sensores activos

En un escenario de mayor acumulación de biomasa y de mayor peligro de incendio forestal derivado de los efectos del cambio global, es imprescindible conocer y comprender en mayor profundidad la recuperación de ecosistemas forestales después de sufrir incendios. Para ello, en esta Tesis se ha aplicado una metodología basada en la tecnología LiDAR aereotransportada, que permite detectar diferencias estructurales hasta ca. 35 años después de la perturbación (Gelabert *et al.* 2020).

Estudios anteriores han analizado la regeneración post-incendio utilizando la información derivada de sensores ópticos, principalmente mediante transformaciones Tasseled Cap o series temporales de índices de vegetación (Vicente-Serrano *et al.* 2011, Fernandez-Manso *et al.* 2016), los cuales reportaron problemas para diferenciar las perturbaciones más antiguas de los bosques maduros. Esto es debido a que existe una saturación de los índices utilizados entre los 7 y 20 años después de la perturbación (Díaz-Delgado and Pons 2001, Tanase *et al.* 2011). El LiDAR-ALS del PNOA es una fuente de datos ampliamente utilizada en la derivación de métricas relacionadas con estructura forestal (Montealegre *et al.* 2016, 2017, Domingo *et al.* 2018, 2019), debido a que registran información relativa a la estructura vertical del bosque y el sotobosque (Lim *et al.* 2003). La aplicación de índices de uso extendido en la ecología, concretamente los diseñados para medir la biodiversidad específica (Shannon and Wiener 1949, Pielou 1975), al análisis de la diversidad de los diferentes estratos del bosque ha permitido sintetizar y comparar las diferentes estructuras verticales resultantes de la alteración por incendios forestales (Listopad *et al.* 2015). La caracterización de diversidad de estratos se ha realizado adaptando los índices de diversidad mencionados a los datos LiDAR-ALS del PNOA de baja densidad.

Los resultados obtenidos muestran que los incendios relativamente recientes (ocurridos en 2006, 2008 y 2009) presentan los valores más bajos de diversidad estructural, donde la mayoría de los retornos láser se localizan en el estrato de arbustivo, lo que implica una concentración estructural y poco desarrollo de la vegetación. En contraposición, los incendios más antiguos, ocurridos en 1986 y 1995, tienen distribuciones de los retornos LiDAR más parecidas a la zona no quemada, evidenciando la regeneración o revegetación de estas masas. En consonancia con la distribución equitativa de los retornos láser en los diferentes rangos de altura, los índices de diversidad estructural presentan valores elevados, lo que implica una mayor diversidad estructural del bosque en comparación con las áreas quemadas en incendios relativamente recientes (Listopad *et al.* 2015). La principal limitación de esta metodología es la caracterización de las diferencias entre episodios concretos, que resulta imposible si estos están próximos en el tiempo ($<$ 5 años). Esta limitación es parcialmente superable mediante el uso de sensores activos que recojan mayor densidad de puntos y definan con mayor precisión la estructura vertical, lo que mejoría la sensibilidad al capturar los diferentes estadios de recuperación post-incendio (Tanase *et al.* 2011). Las diferencias existentes entre masas perturbadas y no perturbadas, ha permitido encontrar diferencias estructurales significativas hasta 35 años después de la perturbación. Es esperable que, con sensores que ofrezcan la captura de una mayor densidad de puntos, se puedan estimar diferencias en masas afectadas más allá de los 35 años pudiendo detectar áreas perturbadas no recogidas en los registros estadísticos actuales.

La mayor ventaja que presenta la metodología propuesta es su escalabilidad a otras regiones donde exista una cobertura LiDAR. Se deberá tener en cuenta el tamaño intervalo en el cual se computan los índices de diversidad estructural. En nuestro caso, la utilización del tamaño de intervalo de altura de 0,15 m refleja mejor la distribución de la estructura forestal

debido al poblado sotobosque en los bosques de *Pinus halepensis*. En contraposición, la principal limitación que puede darse es la dificultad de captar la regeneración de la estructura forestal tras el incendio en un escenario donde el régimen de incendios sea más recurrente. En el contexto del cambio climático, se prevé un aumento en la frecuencia de incendios extremos y la recurrencia de los mismos (San-Miguel-Ayanz *et al.* 2013), lo que alteraría la capacidad de recuperación de la masa forestal (González-De Vega *et al.* 2016) reduciendo la diversidad estructural, cosa que reduciría la utilidad de la metodología planteada.

Capítulo 9

Conclusiones finales y futuras líneas de investigación

9. Conclusiones y futuras líneas de investigación

9.1. Conclusiones

1. Las tecnologías de la información geográfica permiten analizar las masas forestales y los fenómenos derivados del cambio global como son el abandono agrícola, el análisis del incremento en biomasa, o las diferencias en la recuperación de la masa forestal después de un incendio, y por tanto planificar acciones para paliar sus efectos negativos.

2. La sucesión secundaria es un fenómeno natural que se origina tras el abandono agrícola. En la vertiente sur de los Pirineos, en los últimos 36 años, el bosque ha colonizado dos terceras partes de los espacios abiertos. Esta pérdida de pastos y campos se produce principalmente entre la década de 1980 y principios de la década de 1990, seguida de una estabilización en la tendencia. En los últimos 10 años la tasa promedio de abandono agrícola ha sido de 6000 ha/año.

3. El uso de algoritmos de segmentación temporal, como el de Landtrendr, ha permitido caracterizar la dinámica espacio-temporal de la sucesión secundaria dado que elimina ruidos derivados de la iluminación, cambios fenológicos, condiciones atmosféricas o co-registro de las imágenes. Evitándose así errores en la detección temprana del fenómeno, ubicando la mayoría de detecciones en los primeros años. Además, su utilización también reduce los errores de comisión y omisión.

4. Se observa una detección cosistente en las zonas donde se producen mayores tasas de abandono, hecho que refuerza la solidez de las relaciones encotradas entre las diferentes variables.

5. Las variables socioeconómicas y ambientales espacialmente explícitas permiten elaborar mapas de alta resolución de la probabilidad de abandono agrícola y definir que variables contribuyen con una mayor importancia en el proceso de abandono. Se puede concluir que la actividad turística, el incremento poblacional y la accesibilidad impulsan en mayor medida que las variables ambientales y topográficas el abandono agrícola en la vertiente sur del Pirineo durante las últimas décadas.

6. La tecnología LiDAR-ALS, al estar basada en un sensor activo que emite y recibe su propio haz energético, presenta la habilidad de penetrar el dosel de la vegetación y capturar la estructura forestal, habilitando así el análisis de diferencias estructurales en ecosistemas afectados por perturbaciones. Además, los sensores activos ubicados en plataformas espaciales han supuesto una revolución en el análisis de las masas forestales a escala global. Se ha constatado la existencia de un patrón segmentado en la relación cota-altura del arbolado, en el que la vegetación decrece de forma abrupta a partir de cierta cota, en las principales cadenas montañosas europeas.

7. La aptación de los índices de biodiversidad a los datos LiDAR-ALS de baja densidad han permitido sintetizar la información estructural y siendo de alta utilidad para los análisis de difenecias estructurales entre masas forestales perturbadas en diferentes momentos y la masa control.

8. El uso de datos LiDAR-ALS de baja densidad y la derivación de métricas de síntesis de la estructura forestal, permite encontrar diferencias estadísticamente significativas en la estructura forestal hasta c.a. 36 años después de la perturbación. Recuperación de la estructura forestal post incendio.

9. La cota a la que empieza a decrecer abruptamente la altura de la vegetación se corresponde con limitantes climáticos, principalmente térmicos. Bajo las proyecciones de calentamiento global se estima un desplazamiento cota arriba de este punto y se prevén incrementos en la

productividad y en la prestación de servicios ecosistémicos en el rango del desplazamiento.

9.2. Líneas de investigación futura

En la presente tesis se han analizado los patrones de regeneración post incendio en un entorno local y en masas de la misma especie (*Pinus halepensis* Mill.). Dada la habilidad de los datos LiDAR ALS para caracterizar diferencias en la regeneración post-incendio, y con la expectativa de adquisición de nuevas coberturas más detalladas - las cuales ofrecerán una densidad de 10pt/m^2 -, se pretende analizar el comportamiento de la regeneración en diferentes ambientes y múltiples especies. Además, se plantea buscar la existencia de relaciones entre la diversidad estructural y la severidad del incendio, el tipo de suelo y los periodos de sequía posteriores.

Por otro lado, se pretende seguir investigando y ampliando conocimientos sobre distintas aplicaciones que permiten los algoritmos de segmentación temporal en la detección y análisis de perturbaciones. Además, tomar ventaja de las nuevas plataformas de procesado en la nube para ampliar la escala de análisis a regional o global.

Finalmente, conociendo el desplazamiento de los limitantes climáticos del desarrollo del arbolado a causa del calentamiento global, se plantea la estimación del incremento de productividad de los bosques de montaña en el rango definido por la ubicación actual de los limitantes climáticos y la proyección futura, durante el presente siglo.

Material suplementario

Material suplementario capítulo 4

Table S-4.1: *TM Tasseled Cap equivalent transformation matrix for band reflectance factor data. Source: (Crist 1985).*

	B1	B2	B3	B4	B5	B7
Brightness	0.2043	0.4158	0.5524	0.5741	0.3124	0.2303
Greenness	-0.1603	-0.2819	-0.4934	0.794	-0.0002	-0.1446
Wetness	0.0315	0.2021	0.3102	0.1594	-0.6806	-0.6109

Table S-4.2: *Accuracy assessment for each variable combination.*

Model	Season	Type	F1-Score	MCC	Commission	Omission
TCB	**spr**	**FIT**	**0,8566**	**0,6756**	**0,0490**	**0,3041**
TCB+TCW	**spr**	**FIT**	**0,8534**	**0,6680**	**0,0612**	**0,2949**
TCB+TCG+TCW	sum	FIT	0,8430	0,6425	0,0285	0,3779
TCB+TCG	sum	FIT	0,8383	0,6318	0,0203	0,4055
TCB+TCW	sum	FIT	0,8362	0,6259	0,0244	0,4055
TCB+TCG+TCW	spr	FIT	0,8315	0,6125	0,0531	0,3733
TCB	sum	FIT	0,8308	0,6146	0,0122	0,4424
TCB+TCG	spr	FIT	0,8287	0,6064	0,0327	0,4147
TCB+TCG	aut	FIT	0,8255	0,5968	0,0772	0,3548
TCA+TCW	aut	FIT	0,8144	0,5679	0,0813	0,3825
TCW	sum	FIT	0,8090	0,5516	0,0528	0,4470
TCB+TCG+TCW	aut	FIT	0,8080	0,5524	0,0935	0,3825
TCB+TCW	aut	FIT	0,8062	0,5441	0,0447	0,4700
TCB	aut	FIT	0,8007	0,5288	0,0447	0,4885

TCW	aut	FIT	0,7972	0,5190	0,0650	0,4654
TCG+TCW	aut	FIT	0,7938	0,5091	0,0610	0,4839
TCB+TCW	**sum**	**SR**	**0,7905**	**0,5396**	**0,1870**	**0,2765**
TCB	sum	SR	0,7821	0,5137	0,1829	0,3088
TCG+TCW	sum	FIT	0,7798	0,4698	0,0285	0,5899
TCB+TCG	sum	SR	0,7751	0,5137	0,2154	0,2719
TCG+TCW	spr	FIT	0,7654	0,4251	0,0612	0,5806
TCA+TCW	sum	FIT	0,7636	0,4175	0,0610	0,5899
TCW	spr	FIT	0,7595	0,4128	0,0980	0,5346
TCA+TCW	spr	FIT	0,7586	0,4114	0,1020	0,5300
TCA	spr	FIT	0,7562	0,4123	0,1265	0,4931
TCW	sum	SR	0,7495	0,4769	0,2642	0,2581
TCB+TCG+TCW	sum	SR	0,7490	0,4719	0,2602	0,2673
TCA	sum	FIT	0,7174	0,2723	0,1179	0,6544
TCG+TCW	sum	SR	0,7034	0,3207	0,2480	0,4378
TCG	aut	FIT	0,6944	0,0647	0,0163	0,9631
TCG	spr	FIT	0,6923	0,0943	0,0449	0,9078
TCA+TCW	sum	SR	0,6883	0,2898	0,2683	0,4470
TCG	sum	FIT	0,6697	0,0223	0,1057	0,8802
TCA	aut	FIT	0,6485	0,2747	0,3699	0,3548
TCA	sum	SR	0,6349	0,1279	0,2967	0,5806
TCB+TCG	aut	SR	0,6262	0,3682	0,4756	0,1705
TCG+TCW	aut	SR	0,6080	0,3709	0,5081	0,1429
TCG	sum	SR	0,5986	-0,0326	0,2967	0,7327
TCB	aut	SR	0,5902	0,3065	0,5081	0,1982
TCW	aut	SR	0,5586	0,2719	0,5447	0,1982
TCA+TCW	aut	SR	0,5580	0,3932	0,5894	0,0691
TCB+TCW	aut	SR	0,5506	0,3036	0,5691	0,1521
TCB+TCG+TCW	aut	SR	0,5178	0,2169	0,5854	0,2120

TCG	aut	SR	0,4619	0,0769	0,6179	0,3088
TCA	aut	SR	0,4486	0,1673	0,6626	0,1889
TCB	spr	SR	0,4024	0,2543	0,7317	0,0737
TCB+TCW	spr	SR	0,3797	0,2756	0,7561	0,0461
TCB+TCG+TCW	spr	SR	0,3497	0,1659	0,7683	0,1060
TCB+TCG	spr	SR	0,3141	0,1725	0,8008	0,0783
TCA+TCW	spr	SR	0,2690	-0,0534	0,8130	0,2304
TCG+TCW	spr	SR	0,2566	-0,0802	0,8211	0,2442
TCW	spr	SR	0,2463	-0,0908	0,8293	0,2442
TCA	spr	SR	0,2442	-0,1067	0,8293	0,2581
TCG	spr	SR	0,2165	-0,1839	0,8455	0,3088

Table S-4.3: *Accuracy assessment for each variable combination using LT outputs in spring season.*

Model	**F1-Score**	**MCC**
TCA	0.72	0.30
TCB	0.79	0.55
TCG	0.69	0.29
TCW	0.74	0.43
TCA+TCW	0.74	0.43
TCB+TCG	0.74	0.46
TCB+TCW	**0.82**	**0.61**
TCG+TCW	0.74	0.44
TCB+TCG+TCW	0.80	0.59

Material suplementario capítulo 5

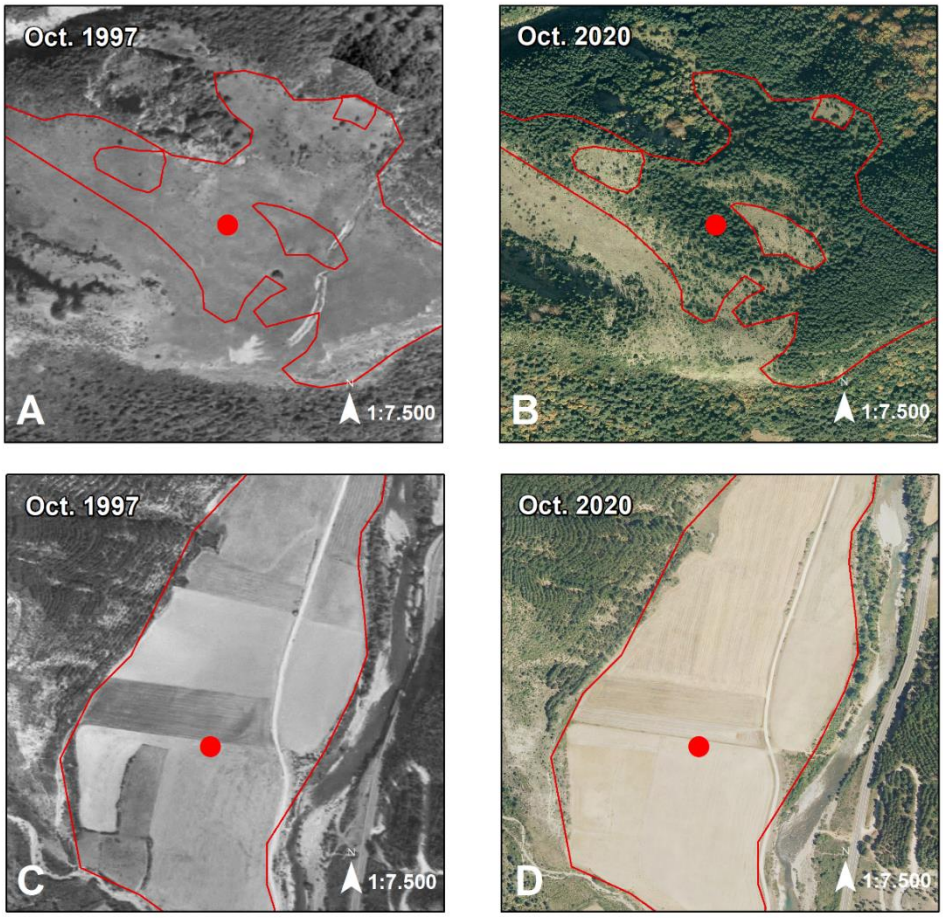

Figure S-5.1: *Example of sampling procedure. A & B abandonment example; C & D non-abandonment example. Ortophoto source (IGN-PNOA, 2022).*

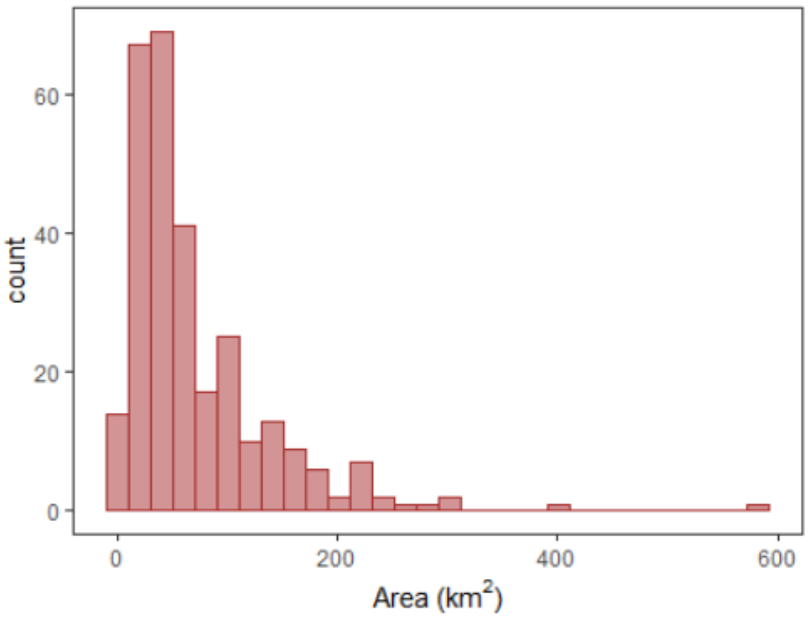

Figure S-5.2: *Analized municipalities area distribution. (Idescat,2022; IAEST, 2022).*

Table S-5.1: *Pyrenees Subregions (comarcas) área. (Idescat,2022; IAEST, 2022).*

CCAA	ID	Sub-region	Area km²
Aragon	1	La Jacetania	1858
	2	Alto Gállego	1360
	3	Sobrarbe	2204
	4	La Ribargorza	2464
Catalonia	5	Val d'Aran	634
	6	Alta Ribagorça	427
	7	Pallars Jussà	1343
	8	Pallars Sobirà	1377
	9	Alt Urgell	1448
	10	Solsonès	1000
	11	Cerdanya	547
	12	Berguedà	1186
	13	Ripollès	957
	14	Osona	1247
	15	Garrotxa	733
	16	Selva	994

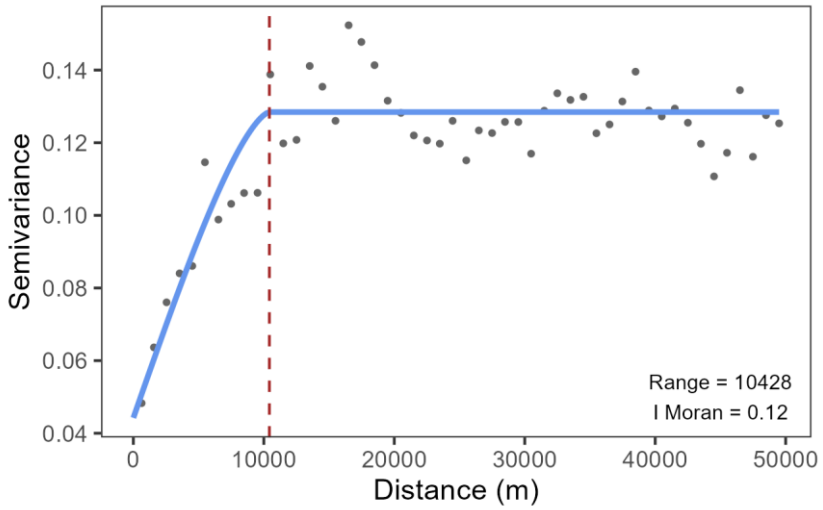

Figure S-5.3: *Residual semivariogram of all points.*

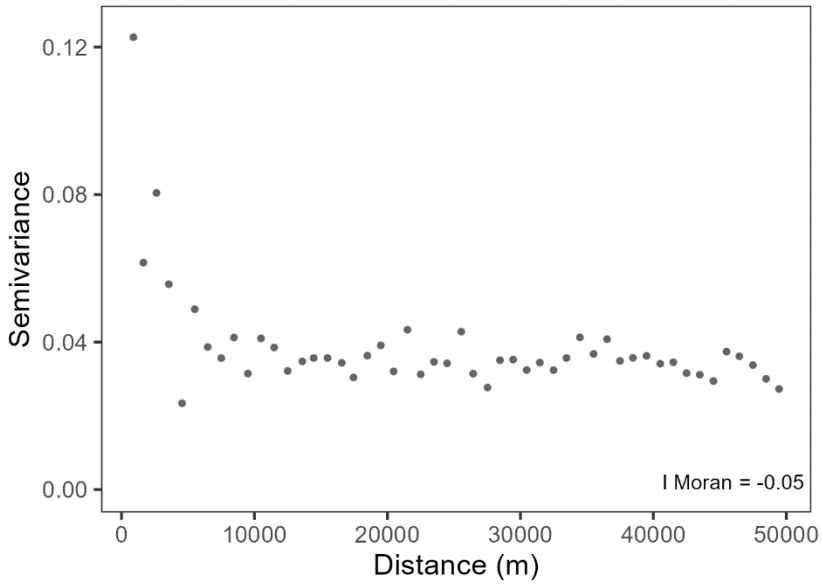

Figure S-5.4: *Residuals semivariogram of train subsample after applying a spatial distance subset.*

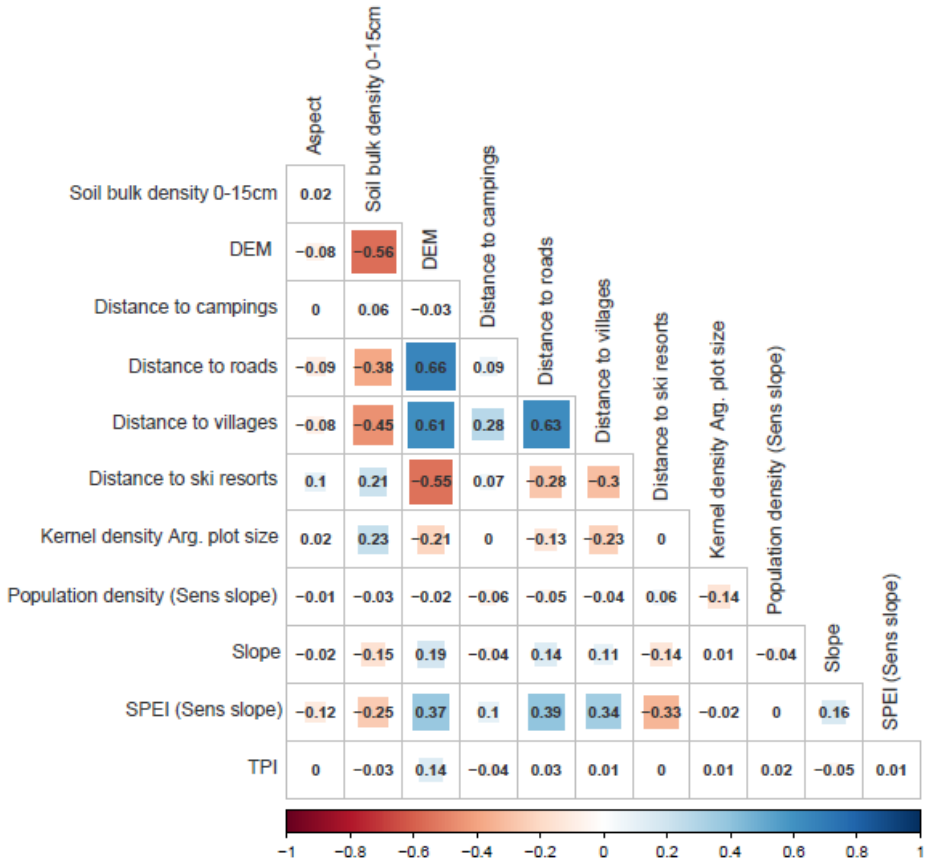

Figure S-5.5: *pairwise variables correlations.*

Material suplementario capítulo 6

Figure S-7.1: *Outline of the procedure of height estimation with GEDI data*

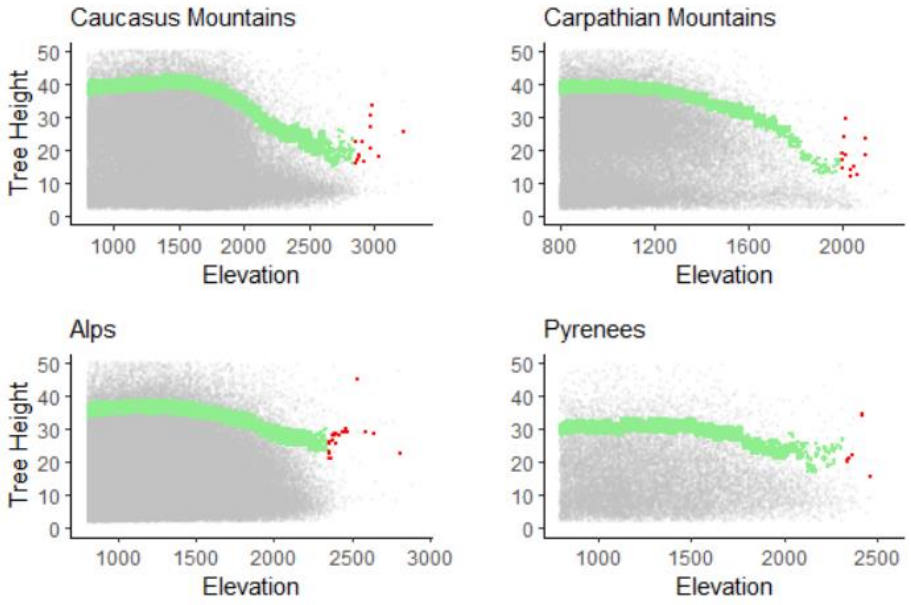

Figure S-7.2: *Example of the histogram tile noise removal procedure. Herein we remove 0.1% of points located at higher altitudes (red color). The noise in this regions may be induced by snow cover or topographical complexity.*

Referencias bibliográficas

Albrich, K., Rammer, W., and Seidl, R., 2020. Climate change causes critical transitions and irreversible alterations of mountain forests. *Global Change Biology*, 26 (7), 4013–4027.

Alcantara, C., Kuemmerle, T., Prishchepov, A.V., and Radeloff, V.C., 2012. Mapping abandoned agriculture with multi-temporal MODIS satellite data. *Remote Sensing of Environment*, 124, 334–347.

Alonso-Sarría, F., Martínez-Hernández, C., Romero-Díaz, A., Cánovas-García, F., and Gomariz-Castillo, F., 2016. Main Environmental Features Leading to Recent Land Abandonment in Murcia Region (Southeast Spain). *Land Degradation and Development*, 27 (3), 654–670.

Ameztegui, A., Brotons, L., and Coll, L., 2010. Land-use changes as major drivers of mountain pine (Pinus uncinata Ram.) expansion in the Pyrenees. *Global Ecology and Biogeography*, 19 (5), 632–641.

Ameztegui, A., Coll, L., Brotons, L., and Ninot, J.M., 2016. Land-use legacies rather than climate change are driving the recent upward shift of the mountain tree line in the Pyrenees. *Global Ecology and Biogeography*, 25 (3), 263–273.

Ameztegui, A., Rodrigues, M., Gelabert, P., Lavaquiol, B., and Coll, L., 2021. Maximum height of mountain forests abruptly decreases above an elevation breakpoint. *GIScience & Remote Sensing*, 58 (3), 442–454.

Aquilué, N., Fortin, M.-J., Messier, C., and Brotons, L., 2020. The Potential of Agricultural Conversion to Shape Forest Fire Regimes in Mediterranean Landscapes. *Ecosystems*, 23 (1), 34–51.

Arab, S.T., Islam, Md.M., Shamsuzzoha, Md., Alam, K.F., Muhsin, N., Noguchi, R., and Ahamed, T., 2022. A Review of Remote Sensing Applications in Agriculture and Forestry to Establish Big Data Analytics. *In*: T. Ahamed, ed. *Remote Sensing Application: Regional Perspectives in Agriculture and Forestry*.

Singapore: Springer Nature, 1–24.

Aurelle, D., Thomas, S., Albert, C., Bally, M., Bondeau, A., Boudouresque, C.-F., Cahill, A.E., Carlotti, F., Chenuil, A., Cramer, W., Davi, H., De Jode, A., Ereskovsky, A., Farnet, A.-M., Fernandez, C., Gauquelin, T., Mirleau, P., Monnet, A.-C., Prévosto, B., Rossi, V., Sartoretto, S., Van Wambeke, F., and Fady, B., 2022. Biodiversity, climate change, and adaptation in the Mediterranean. *Ecosphere*, 13 (4), e3915.

Badía, A., Pèlachs, A., Vera, A., Tulla, A.F., and Soriano, J.M., 2004. Cambios en los usos y cubiertas del suelo y los efectos en la vulnerabilidad en las comarcas de montaña de Cataluña. Del rol del fuego como herramienta de gestión a los incendios como amenaza. *Pirineos*, 169.

Balde, B. and Vega-García, C., 2019. Estimación de emisiones de GEI y sus trayectorias en grandes incendios forestales en Cataluña, España. *Madera y bosques*, 25 (2 (Verano 2019)), 12.

Beck, J., Armston, J., Hofton, M., and Luthcke, S., 2020. *Global Ecosystem Dynamics Investigation (GEDI) Level 02 User Guide*. Sioux Falls, South Dakota, USA: EROS Center, U.S. Geological Survey.

Bedia, J., Herrera, S., Camia, A., Moreno, J.M., and Gutiérrez, J.M., 2014. Forest fire danger projections in the Mediterranean using ENSEMBLES regional climate change scenarios. *Climatic Change*, 122 (1), 185–199.

Blanco, J.A., Ameztegui, A., and Rodríguez, F., 2020. Modelling Forest Ecosystems: a crossroad between scales, techniques and applications. *Ecological Modelling*, 425, 109030.

Bravo, F., LeMay, V., and Jandl, R., 2017. *Managing Forest Ecosystems: The Challenge of Climate Change*.

Breiman, L., 2001. Random forests. *Machine Learning*, 45, 5–32.

Camarero, J.J., Gazol, A., Sangüesa-Barreda, G., Oliva, J., and Vicente-Serrano, S.M., 2015. To die or not to die: early warnings of tree dieback in response to a severe drought. *Journal of Ecology*, 103 (1), 44–57.

Castaldi, F., Palombo, A., Pascucci, S., Pignatti, S., Santini, F., and Casa, R., 2015. Reducing the Influence of Soil Moisture on the Estimation of Clay from Hyperspectral Data: A Case Study Using Simulated PRISMA Data. *Remote Sensing*, 7 (11), 15561–15582.

Cavender-Bares, J., Schneider, F.D., Santos, M.J., Armstrong, A., Carnaval, A., Dahlin, K.M., Fatoyinbo, L., Hurtt, G.C., Schimel, D., Townsend, P.A., Ustin, S.L., Wang, Z., and Wilson, A.M., 2022. Integrating remote sensing with ecology and evolution to advance biodiversity conservation. *Nature Ecology & Evolution*, 6 (5), 506–519.

Cazcarro, I., Duarte, R., Martín-Retortillo, M., Pinilla, V., and Serrano, A., 2015. Water scarcity and agricultural growth in Spain: from curse to blessing? *In*: *Natural Resources and Economic Growth*.

Chazdon, R.L., Brancalion, P.H.S., Laestadius, L., Bennett-Curry, A., Buckingham, K., Kumar, C., Moll-Rocek, J., Vieira, I.C.G., and Wilson, S.J., 2016. When is a forest a forest? Forest concepts and definitions in the era of forest and landscape restoration. *Ambio*, 45 (5), 538–550.

Cochrane, M.A. and Bowman, D.M.J.S., 2021. Manage fire regimes, not fires. *Nature Geoscience*, 14 (7), 455–457.

Cook, B.I., Mankin, J.S., and Anchukaitis, K.J., 2018. Climate Change and Drought: From Past to Future. *Current Climate Change Reports*, 4 (2), 164–179.

Coops, N.C., Morsdorf, F., Schaepman, M.E., and Zimmermann, N.E., 2013. Characterization of an alpine tree line using airborne LiDAR data and physiological modeling. *Global Change Biology*, 19 (12), 3808–3821.

Coops, N.C., Tompalski, P., Goodbody, T.R.H., Achim, A., and Mulverhill, C., 2022. Framework for near real-time forest inventory using multi source remote sensing data. *Forestry: An International Journal of Forest Research*, cpac015.

Copernicus Climate Change Service, 2022. *ERA5: Fifth generation of ECMWF atmospheric reanalyses of the global climate.*

Corbelle-Rico, E., Crecente-Maseda, R., and Santé-Riveira, I.,

2012. Multi-scale assessment and spatial modelling of agricultural land abandonment in a European peripheral region: Galicia (Spain), 1956–2004. *Land Use Policy*, 29 (3), 493–501.

Cortes, C. and Vapnik, V., 1995. Support-Vector Networks. *Machine Learning*.

Costa, R.L., Prevedello, J.A., de Souza, B.G., and Cabral, D.C., 2017. Forest transitions in tropical landscapes: A test in the Atlantic Forest biodiversity hotspot. *Applied Geography*.

Costafreda-Aumedes, S., Comas, C., Vega-Garcia, C., Costafreda-Aumedes, S., Comas, C., and Vega-Garcia, C., 2017. Human-caused fire occurrence modelling in perspective: a review. *International Journal of Wildland Fire*, 26 (12), 983–998.

Crist, E.P., 1985. A TM Tasseled Cap equivalent transformation for reflectance factor data. *Remote Sensing of Environment*.

Crist, E.P. and Cicone, R.C., 1984. A Physically-Based Transformation of Thematic Mapper Data—The TM Tasseled Cap. *IEEE Transactions on Geoscience and Remote Sensing*.

Daily, G.C., 1997. *Nature's Services: Societal Dependence On Natural Ecosystems*. Island Press.

Dale, V.H., Joyce, L.A., McNulty, S., Neilson, R.P., Ayres, M.P., Flannigan, M.D., Hanson, P.J., Irland, L.C., Lugo, A.E., Peterson, C.J., Simberloff, D., Swanson, F.J., Stocks, B.J., and Wotton, B.M., 2001. Climate Change and Forest Disturbances: Climate change can affect forests by altering the frequency, intensity, duration, and timing of fire, drought, introduced species, insect and pathogen outbreaks, hurricanes, windstorms, ice storms, or landslides. *BioScience*, 51 (9), 723–734.

Davidson, H., Jabbari, Y., Patton, H., O'Hagan, F., Peters, K., and Cribbie, R., 2019. Statistical Software Use in Canadian University Courses: Current Trends and Future Directions. *Teaching of Psychology*, 46 (3), 246–250.

Díaz-Delgado, R. and Pons, X., 2001. Spatial patterns of forest fires in Catalonia (NE of Spain) along the period

1975–1995: Analysis of vegetation recovery after fire. *Forest Ecology and Management*, 147 (1), 67–74.

Domingo, D., Lamelas, M.T., Montealegre, A.L., García-Martín, A., and de la Riva, J., 2018. Estimation of Total Biomass in Aleppo Pine Forest Stands Applying Parametric and Nonparametric Methods to Low-Density Airborne Laser Scanning Data. *Forests*, 9 (4), 158.

Domingo, D., Montealegre, A.L., Lamelas, M.T., García-Martín, A., de la Riva, J., Rodríguez, F., and Alonso, R., 2019. Quantifying forest residual biomass in Pinus halepensis Miller stands using Airborne Laser Scanning data. *GIScience and Remote Sensing*, 56 (8), 1210–1232.

Domingo, D., de la Riva, J., Lamelas, M.T., García-Martín, A., Ibarra, P., Echeverría, M., and Hoffrén, R., 2020. Fuel Type Classification Using Airborne Laser Scanning and Sentinel 2 Data in Mediterranean Forest Affected by Wildfires. *Remote Sensing*, 12 (21), 3660.

Dubayah, R., Blair, J.B., Goetz, S., Fatoyinbo, L., Hansen, M., Healey, S., Hofton, M., Hurtt, G., Kellner, J., Luthcke, S., Armston, J., Tang, H., Duncanson, L., Hancock, S., Jantz, P., Marselis, S., Patterson, P., Qi, W., and Silva, C., 2020. The Global Ecosystem Dynamics Investigation: High-resolution laser ranging of the Earth's forests and topography. *Science of Remote Sensing*.

Dubayah, R., Hofton, M., Blair, J.B., Armston, J., Tang, H., and Luthcke, S., 2020. GEDI L2A Elevation and Height Metrics Data Global Footprint Level V001 [Data set]. *NASA EOSDIS Land Processes DAAC*.

Duncanson, L., Neuenschwander, A., Hancock, S., Thomas, N., Fatoyinbo, T., Simard, M., Silva, C.A., Armston, J., Luthcke, S.B., Hofton, M., Kellner, J.R., and Dubayah, R., 2020. Biomass estimation from simulated GEDI, ICESat-2 and NISAR across environmental gradients in Sonoma County, California. *Remote Sensing of Environment*, 242, 111779.

Dupuy, J., Fargeon, H., Martin-StPaul, N., Pimont, F., Ruffault, J., Guijarro, M., Hernando, C., Madrigal, J., and Fernandes, P., 2020. Climate change impact on future

wildfire danger and activity in southern Europe: a review. *Annals of Forest Science*, 77 (2), 35.

Elsen, P.R., Monahan, W.B., and Merenlender, A.M., 2020. Topography and human pressure in mountain ranges alter expected species responses to climate change. *Nature Communications*, 11 (1), 1974.

FAO, 2020a. Evaluación de los recursos forestales mundiales.

FAO, 2020b. Statistical yearbook. World food and agriculture.

Fernandes, P.M., 2013. Fire-smart management of forest landscapes in the Mediterranean basin under global change. *Landscape and Urban Planning*, 110, 175–182.

Fernández-García, V., Fulé, P.Z., Marcos, E., and Calvo, L., 2019. The role of fire frequency and severity on the regeneration of Mediterranean serotinous pines under different environmental conditions. *Forest Ecology and Management*.

Fernández-García, V., Santamarta, M., Fernández-Manso, A., Quintano, C., Marcos, E., and Calvo, L., 2018. Burn severity metrics in fire-prone pine ecosystems along a climatic gradient using Landsat imagery. *Remote Sensing of Environment*, 206, 205–217.

Fernandez-Manso, A., Quintano, C., and Roberts, D.A., 2016. Burn severity influence on post-fire vegetation cover resilience from Landsat MESMA fraction images time series in Mediterranean forest ecosystems. *Remote Sensing of Environment*, 184, 112–123.

Fick, S.E. and Hijmans, R.J., 2017. WorldClim 2: new 1-km spatial resolution climate surfaces for global land areas. *International Journal of Climatology*, 37 (12), 4302–4315.

Fix, E. and Hodges, J.L., 1951. Discriminatory Analysis - Nonparametric Discrimination: Consistency Properties. *CALIFORNIA UNIV BERKELEY*.

Frazier, R.J., Coops, N.C., and Wulder, M.A., 2015. Boreal Shield forest disturbance and recovery trends using Landsat time series. *Remote Sensing of Environment*, 170, 317–327.

Fricker, G.A., Synes, N.W., Serra-Diaz, J.M., North, M.P., Davis, F.W., and Franklin, J.,

2019. More than climate? Predictors of tree canopy height vary with scale in complex terrain, Sierra Nevada, CA (USA). *Forest Ecology and Management*, 434, 142–153.

García-Ruiz, J.M., López-Moreno, J.I., Lasanta, T., Vicente-Serrano, S.M., González-Sampériz, P., Valero-Garcés, B.L., Sanjuán, Y., Beguería, S., Nadal-Romero, E., Lana-Renault, N., and Gómez-Villar, A., 2015. Los efectos geoecológicos del cambio global en el pirineo central español: Una revisión a distintas escalas espaciales y temporales. *Pirineos*, 170.

Gelabert, P., Montealegre, A.L., Lamelas, M.T., and Domingo, D., 2020. Forest structural diversity characterization in Mediterranean landscapes affected by fires using Airborne Laser Scanning data. *GIScience & Remote Sensing*, 57 (4).

Gelabert, P., Rodrigues, M., de la Riva, J., Ameztegui, A., Sebastià, M.T., and Vega-Garcia, C., 2021. LandTrendr smoothed spectral profiles enhance woody encroachment monitoring. *Remote Sensing of Environment*, 262, 112521.

Gelabert, P., Rodrigues, M., Vidal-Macua, J.J., Ameztegui, A., and Vega-Garcia, C., 2022. Spatially explicit modeling of the probability of land abandonment in the Spanish Pyrenees. *Landscape and Urban Planning*, 226, 104487.

Gellrich, M. and Zimmermann, N.E., 2007. Investigating the regional-scale pattern of agricultural land abandonment in the Swiss mountains: A spatial statistical modelling approach. *Landscape and Urban Planning*, 79 (1), 65–76.

Gely, C., Laurance, S.G.W., and Stork, N.E., 2020. How do herbivorous insects respond to drought stress in trees? *Biological Reviews*, 95 (2), 434–448.

Gómez, C., Alejandro, P., Hermosilla, T., Montes, F., Pascual, C., Ruiz, L.A., Álvarez-Taboada, F., Tanase, M.A., and Valbuena, R., 2019. Remote sensing for the Spanish forests in the 21st century: a review of advances, needs, and opportunities. *Forest Systems*.

González-Alemán, J.J., Pascale, S., Gutierrez-Fernandez, J., Murakami, H., Gaertner, M.A., and Vecchi, G.A.,

2019. Potential Increase in Hazard From Mediterranean Hurricane Activity With Global Warming. *Geophysical Research Letters*, 46 (3), 1754–1764.

González-De Vega, S., De las Heras, J., and Moya, D., 2016. Resilience of Mediterranean terrestrial ecosystems and fire severity in semiarid areas: Responses of Aleppo pine forests in the short, mid and long term. *Science of the Total Environment*.

Gonzalez-Hidalgo, J.C., Peña-Angulo, D., Beguería, S., and Brunetti, M., 2020. MOTEDAS century: A new high-resolution secular monthly maximum and minimum temperature grid for the Spanish mainland (1916–2015). *International Journal of Climatology*, 40 (12), 5308–5328.

Goodchild, M.F., 2010. Twenty years of progress: GIScience in 2010. *Journal of Spatial Information Science*, 1 (2010), 3–20.

Gorelick, N., Hancher, M., Dixon, M., Ilyushchenko, S., Thau, D., and Moore, R., 2017. Google Earth Engine: Planetary-scale geospatial analysis for everyone. *Remote Sensing of Environment*.

Grace, J., Berninger, F., and Nagy, L., 2002. Impacts of Climate Change on the Tree Line. *Annals of Botany*, 90 (4), 537–544.

Greenwood, S. and Jump, A.S., 2014. Consequences of Treeline Shifts for the Diversity and Function of High Altitude Ecosystems. *Arctic, Antarctic, and Alpine Research*, 46 (4), 829–840.

Healey, S.P., Cohen, W.B., Zhiqiang, Y., and Krankina, O.N., 2005. Comparison of Tasseled Cap-based Landsat data structures for use in forest disturbance detection. *Remote Sensing of Environment*, 97 (3), 301–310.

Henttonen, H.M., Nöjd, P., and Mäkinen, H., 2017. Environment-induced growth changes in the Finnish forests during 1971–2010 – An analysis based on National Forest Inventory. *Forest Ecology and Management*, 386, 22–36.

Hermosilla, T., Wulder, M.A., White, J.C., Coops, N.C., and Hobart, G.W., 2018. Disturbance-Informed Annual Land Cover Classification Maps of Canada's Forested

Ecosystems for a 29-Year Landsat Time Series. *Canadian Journal of Remote Sensing*, 44 (1), 67–87.

Hilmers, T., Avdagić, A., Bartkowicz, L., Bielak, K., Binder, F., Bončina, A., Dobor, L., Forrester, D.I., Hobi, M.L., Ibrahimspahić, A., Jaworski, A., Klopčič, M., Matović, B., Nagel, T.A., Petráš, R., del Rio, M., Stajić, B., Uhl, E., Zlatanov, T., Tognetti, R., and Pretzsch, H., 2019. The productivity of mixed mountain forests comprised of Fagus sylvatica, Picea abies, and Abies alba across Europe. *Forestry: An International Journal of Forest Research*, 92 (5), 512–522.

IPCC, 2019. Climate Change and Land: an IPCC special report on climate change, desertification, land degradation, sustainable land management, food security, and greenhouse gas fluxes in terrestrial ecosystems [P.R. Shukla, J. Skea, E. Calvo Buendia, V. Masson-Delmotte, H.-O. Pörtner, D. C. Roberts, P. Zhai, R. Slade, S. Connors, R. van Diemen, M. Ferrat, E. Haughey, S. Luz, S. Neogi, M. Pathak, J. Petzold, J. Portugal Pereira, P. Vyas, E. Huntley, K. Kissick, M, Belkacemi, J. Malley, (eds.)].

IPCC, 2022. *Climate Change 2022: Impacts, Adaptation, and Vulnerability. Contribution of Working Group II to the Sixth Assessment Report of the Intergovernmental Panel on Climate Change [H.-O. Pörtner, D.C. Roberts, M. Tignor, E.S. Poloczanska, K. Mintenbeck, A. Alegría, M. Craig, S. Langsdorf, S. Löschke, V. Möller, A. Okem, B. Rama (eds.)].* Cambridge University Press. Cambridge.

Jenkins, M. and Schaap, B., 2018. Forest Ecosystem Services. *United Nations Forum on forests*, 41.

Kennedy, R., Yang, Z., and Cohen, W.B., 2010. Detecting trends in forest disturbance and recovery using yearly Landsat time series: 1. LandTrendr - Temporal segmentation algorithms. *Remote Sensing of Environment*.

Kim, Y.-S., Rodrigues, M., and Robinne, F.-N., 2021. Economic drivers of global fire activity: A critical review using the DPSIR framework. *Forest Policy and Economics*, 131, 102563.

Klein, T., Randin, C., and Körner, C., 2015. Water availability predicts forest canopy height at the global scale. *Ecology Letters*, 18 (12), 1311–1320.

Körner, C., 2012. *Alpine Treelines: Functional Ecology of the Global High Elevation Tree Limits*. Springer Science & Business Media.

Körner, C. and Paulsen, J., 2004. A world-wide study of high altitude treeline temperatures. *Journal of Biogeography*, 31 (5), 713–732.

Kotsiantis, S.B., Zaharakis, I.D., and Pintelas, P.E., 2006. Machine learning: a review of classification and combining techniques. *Artificial Intelligence Review*, 26 (3), 159–190.

Koulouri, M. and Giourga, Chr., 2007. Land abandonment and slope gradient as key factors of soil erosion in Mediterranean terraced lands. *CATENA*, 69 (3), 274–281.

Kowalski, K., Senf, C., Hostert, P., and Pflugmacher, D., 2020. Characterizing spring phenology of temperate broadleaf forests using Landsat and Sentinel-2 time series. *International Journal of Applied Earth Observation and Geoinformation*, 92, 102172.

Kumar, B., Dikshit, O., Gupta, A., and Singh, M.K., 2020. Feature extraction for hyperspectral image classification: a review. *International Journal of Remote Sensing*, 41 (16), 6248–6287.

Kwenda, C., Gwetu, M., and Dombeu, J.V.F., 2022. Machine Learning Methods for Forest Image Analysis and Classification: A Survey of the State of the Art. *IEEE Access*, 10, 45290–45316.

Lasanta, T., Arnáez, J., Pascual, N., Ruiz-Flaño, P., Errea, M.P., and Lana-Renault, N., 2017. Space–time process and drivers of land abandonment in Europe. *Catena*, 149, 810–823.

Lasanta, T., Beltrán, O., and Vaccaro, I., 2013. Impactos socioeconómicos y territoriales de la industria del esquí en los Pirineos españoles: desarrollo de la montaña y urbanización inducida por el ocio. *Pirineos*, 168, 103–128.

Lasanta, T. and Marín-Yaseli, M.L., 2007. Effects of European Common Agricultural Policy and Regional Policy on the Socioeconomic Development of the Central Pyrenees, Spain. *Mountain Research*

and Development, 27 (2), 130–137.

Lasanta, T. and Vicente-Serrano, S.M., 2007. Cambios en la cubierta vegetal en el pirineo aragonés en los últimos 50 años. *Pirineos*, (162), 125–154.

Le Houerou, H.N., 1974. Fire and vegetation in the Mediterranean basin. *Proceedings*.

Lechner, A.M., Foody, G.M., and Boyd, D.S., 2020. Applications in Remote Sensing to Forest Ecology and Management. *One Earth*, 2 (5), 405–412.

van Leeuwen, C.C.E., Cammeraat, E.L.H., de Vente, J., and Boix-Fayos, C., 2019. The evolution of soil conservation policies targeting land abandonment and soil erosion in Spain: A review. *Land Use Policy*, 83 (February), 174–186.

Lehmann, E.A., Wallace, J.F., Caccetta, P.A., Furby, S.L., and Zdunic, K., 2013. Forest cover trends from time series Landsat data for the Australian continent. *International Journal of Applied Earth Observation and Geoinformation*, 21, 453–462.

Liaw, A. and Wiener, M., 2002. Classification and regression by randomForest. *R news*, 2 (3), 18–22.

Libonati, R., DaCamara, C.C., Setzer, A.W., Morelli, F., and Melchiori, A.E., 2015. An Algorithm for Burned Area Detection in the Brazilian Cerrado Using 4 µm MODIS Imagery. *Remote Sensing*, 7 (11), 15782–15803.

Lim, K., Treitz, P., Wulder, M.A., St-Onge, B., and Flood, M., 2003. LiDAR remote sensing of forest structure. *Progress in Physical Geography*, 27 (1), 88–106.

Lionello, P. and Scarascia, L., 2018. The relation between climate change in the Mediterranean region and global warming. *Regional Environmental Change*, 18 (5), 1481–1493.

Listopad, C.M.C.S., Masters, R.E., Drake, J., Weishampel, J., and Branquinho, C., 2015. Structural diversity indices based on airborne LiDAR as ecological indicators for managing highly dynamic landscapes. *Ecological Indicators*, 57, 268–279.

Lizundia-Loiola, J., Otón, G., Ramo, R., and Chuvieco, E., 2020. A spatio-temporal active-fire

clustering approach for global burned area mapping at 250 m from MODIS data. *Remote Sensing of Environment*, 236, 111493.

Lloyd, A.H., Sullivan, P.F., and Bunn, A.G., 2017. Integrating dendroecology with other disciplines improves understanding of upper and latitudinal treelines. *In*: M.M. Amoroso, L.D. Daniels, P.J. Baker, and J.J. Camarero, eds. *Dendroecology: Tree-Ring Analyses Applied to Ecological Studies*. Cham: Springer International Publishing, 135–157.

MacDonald, D., Crabtree, J.R., Wiesinger, G., Dax, T., Stamou, N., Fleury, P., Gutierrez Lazpita, J., and Gibon, A., 2000. Agricultural abandonment in mountain areas of Europe: Environmental consequences and policy response. *Journal of Environmental Management*, 59 (1), 47–69.

Marengo, J.A., Galdos, M.V., Challinor, A., Cunha, A.P., Marin, F.R., Vianna, M. dos S., Alvala, R.C.S., Alves, L.M., Moraes, O.L., and Bender, F., 2022. Drought in Northeast Brazil: A review of agricultural and policy adaptation options for food security. *Climate Resilience and Sustainability*, 1 (1), e17.

Martínez de Pisón, E., 2000. Imagen de la naturaleza de las montañas. *In*: *Estudios sobre el paisaje, 2000, ISBN 84-7477-801-8, págs. 15-54*. Presented at the Estudios sobre el paisaje, Fundación Duques de Soria, 15–54.

Masek, J.G., Wulder, M.A., Markham, B., McCorkel, J., Crawford, C.J., Storey, J., and Jenstrom, D.T., 2020. Landsat 9: Empowering open science and applications through continuity. *Remote Sensing of Environment*, 248, 111968.

McDowell, N.G., Allen, C.D., Anderson-Teixeira, K., Aukema, B.H., Bond-Lamberty, B., Chini, L., Clark, J.S., Dietze, M., Grossiord, C., Hanbury-Brown, A., Hurtt, G.C., Jackson, R.B., Johnson, D.J., Kueppers, L., Lichstein, J.W., Ogle, K., Poulter, B., Pugh, T.A.M., Seidl, R., Turner, M.G., Uriarte, M., Walker, A.P., and Xu, C., 2020. Pervasive shifts in forest dynamics in a changing world. *Science*, 368 (6494), eaaz9463.

Montealegre, A.L., Lamelas, M.T., García-Martín, A., de la Riva, J., and Francisco, E., 2017. Using low-density discrete Airborne Laser Scanning data to assess the potential carbon dioxide emission in case of a fire event in a Mediterranean pine forest. *GIScience and Remote Sensing*, 54 (5), 721–740.

Montealegre, A.L., Lamelas, M.T., de la Riva, J., García-Martín, A., and Escribano, F., 2016. Use of low point density ALS data to estimate stand-level structural variables in Mediterranean Aleppo pine forest. *Forestry*, 89 (4), 373–382.

Moreira, F., Ascoli, D., Safford, H., Adams, M.A., Moreno, J.M., Pereira, J.M.C., Catry, F.X., Armesto, J., Bond, W., González, M.E., Curt, T., Koutsias, N., McCaw, L., Price, O., Pausas, J.G., Rigolot, E., Stephens, S., Tavsanoglu, C., Vallejo, V.R., Wilgen, B.W.V., Xanthopoulos, G., and Fernandes, P.M., 2020. Wildfire management in Mediterranean-type regions: paradigm change needed. *Environmental Research Letters*, 15 (1), 011001.

Mzid, N., Castaldi, F., Tolomio, M., Pascucci, S., Casa, R., and Pignatti, S., 2022. Evaluation of Agricultural Bare Soil Properties Retrieval from Landsat 8, Sentinel-2 and PRISMA Satellite Data. *Remote Sensing*, 14 (3), 714.

Nolan, R.H., Boer, M.M., Collins, L., Resco de Dios, V., Clarke, H., Jenkins, M., Kenny, B., and Bradstock, R.A., 2020. Causes and consequences of eastern Australia's 2019–20 season of mega-fires. *Global Change Biology*, 26 (3), 1039–1041.

Nolan, R.H., Collins, L., Leigh, A., Ooi, M.K.J., Curran, T.J., Fairman, T.A., Resco de Dios, V., and Bradstock, R., 2021. Limits to post-fire vegetation recovery under climate change. *Plant, Cell & Environment*, 44 (11), 3471–3489.

Ojeda-Rivera, J.F., 1999. Naturaleza y desarrollo. Cambios en la consideración política de lo ambiental durante la segunda mitad del siglo XX. *Papeles de Geografía*, 30, 103–117.

Ojeda-Sánchez, C., 2022. Asociación entre factores ambientales urbanos y leucemia infantil.

Olaya, V., 2020. *Sistemas de información Geografica*.

Pascual, S., 2022. Landscape composition and configuration affect bees in the olive agroecosystem. *Journal of Applied Entomology*, 146 (1–2), 1–18.

Pasquarella, V.J., Arévalo, P., Bratley, K.H., Bullock, E.L., Gorelick, N., Yang, Z., and Kennedy, R.E., 2022. Demystifying LandTrendr and CCDC temporal segmentation. *International Journal of Applied Earth Observation and Geoinformation*, 110, 102806.

Paulsen, J. and Körner, C., 2014. A climate-based model to predict potential treeline position around the globe. *Alpine Botany*, 124 (1), 1–12.

Pausas, J., Llovet, J., Rodrigo, A., and Vallejo, R., 2009. Are wildfires a disaster in the Mediterranean basin?–A review. *International Journal of wildland fire*, 17 (6), 713–723.

Pausas, J.G. and Bond, W.J., 2020. Alternative Biome States in Terrestrial Ecosystems. *Trends in Plant Science*, 1–14.

Pausas, J.G. and Keeley, J.E., 2014. Abrupt Climate-Independent Fire Regime Changes. *Ecosystems*, 17 (6), 1109–1120.

Peñuelas, J. and Sardans, J., 2021. Global Change and Forest Disturbances in the Mediterranean Basin: Breakthroughs, Knowledge Gaps, and Recommendations. *Forests*, 12 (5), 603.

Petrou, A., Pantziou, E.F., Dimara, E., and Skuras, D., 2007. Resources and Activities Complementarities: the Role of Business Networks in the Provision of Integrated Rural Tourism. *Tourism Geographies*, 9 (4), 421–440.

Pickell, P.D., Hermosilla, T., Frazier, R.J., Coops, N.C., and Wulder, M.A., 2016. Forest recovery trends derived from Landsat time series for North American boreal forests. *International Journal of Remote Sensing*, 37 (1), 138–149.

Pielou, E.C., 1975. *Ecological diversity*. Wiley.

Poggio, L., de Sousa, L.M., Batjes, N.H., Heuvelink, G.B.M., Kempen, B., Ribeiro, E., and Rossiter, D., 2021. SoilGrids 2.0: producing soil information for the globe with quantified spatial uncertainty. *SOIL*, 7 (1), 217–240.

Potapov, P., Li, X., Hernandez-Serna, A., Tyukavina, A., Hansen, M.C., Kommareddy, A., Pickens, A., Turubanova, S., Tang, H., Silva, C.E., Armston, J., Dubayah, R., Blair, J.B., and Hofton, M., 2021. Mapping global forest canopy height through integration of GEDI and Landsat data. *Remote Sensing of Environment*, 253, 112165.

Poyatos, R., Latron, J., and Llorens, P., 2003. Land use and land cover change after agricultural abandonment: The case of a Mediterranean Mountain area (Catalan Pre-Pyrenees). *Mountain Research and Development*.

Prados, M.J., 2008. Naturbanization: New identities and processes for rural-natural areas [online]. *Naturbanization*. Available from: https://www.taylorfrancis.com/ [Accessed 10 Jun 2020].

Price, M., Gratzer, G., Alemayehu Duguma, L., Kohler, T., and Maselli, D., 2011. *Mountain Forests in a Changing World: Realizing Values, Adressing Challenges*. Rome: FAO/MPS and SDC.

Pueyo, Y. and Beguería, S., 2007. Modelling the rate of secondary succession after farmland abandonment in a Mediterranean mountain area. *Landscape and Urban Planning*, 83 (4), 245–254.

Qi, W., Lee, S.-K., Hancock, S., Luthcke, S., Tang, H., Armston, J., and Dubayah, R., 2019. Improved forest height estimation by fusion of simulated GEDI Lidar data and TanDEM-X InSAR data. *Remote Sensing of Environment*, 221, 621–634.

R Core Team, 2022. *R: A Language and Environment for Statistical Computing*. Vienna, Austria: R Foundation for Statistical Computing.

Ramos-Gorostiza, J.L., 2007. Jovellanos y la naturaleza: economía, ciencia y sentimiento. *Sripta Nova*, XI (241).

Renwick, A., Jansson, T., Verburg, P.H., Revoredo-Giha, C., Britz, W., Gocht, A., and McCracken, D., 2013. Policy reform and agricultural land abandonment in the EU. *Land Use Policy*, 30 (1), 446–457.

Rey Benayas, J.M., Martins, A., Nicolau, J.M., and Schulz, J.J., 2007. Abandonment of agricultural land: an overview of

drivers and consequences. *CAB Reviews: Perspectives in Agriculture, Veterinary Science, Nutrition and Natural Resources*, 2 (057).

Rodrigues, M., Alcasena, F., Gelabert, P., and Vega-García, C., 2020. Geospatial Modeling of Containment Probability for Escaped Wildfires in a Mediterranean Region. *Risk Analysis*, 40 (9), 1762–1779.

Rodrigues, M., Jiménez, A., and de la Riva, J., 2016. Analysis of recent spatial–temporal evolution of human driving factors of wildfires in Spain. *Natural Hazards*, 84 (3), 2049–2070.

Rodrigues, M., Jiménez-Ruano, A., and de la Riva, J., 2020. Fire regime dynamics in mainland Spain. Part 1: Drivers of change. *Science of The Total Environment*, 721, 135841.

Rodrigues, M. and de la Riva, J., 2014. An insight into machine-learning algorithms to model human-caused wildfire occurrence. *Environmental Modelling & Software*, 57, 192–201.

Rodrigues, M., Trigo, R.M., Vega-García, C., and Cardil, A., 2020. Identifying large fire weather typologies in the Iberian Peninsula. *Agricultural and Forest Meteorology*, 280, 107789.

Roy, D.P., Kovalskyy, V., Zhang, H.K., Vermote, E.F., Yan, L., Kumar, S.S., and Egorov, A., 2016. Characterization of Landsat-7 to Landsat-8 reflective wavelength and normalized difference vegetation index continuity. *Remote Sensing of Environment*, 185, 57–70.

Roy, D.P., Wulder, M.A., Loveland, T.R., C.E., W., Allen, R.G., Anderson, M.C., Helder, D., Irons, J.R., Johnson, D.M., Kennedy, R., Scambos, T.A., Schaaf, C.B., Schott, J.R., Sheng, Y., Vermote, E.F., Belward, A.S., Bindschadler, R., Cohen, W.B., Gao, F., Hipple, J.D., Hostert, P., Huntington, J., Justice, C.O., Kilic, A., Kovalskyy, V., Lee, Z.P., Lymburner, L., Masek, J.G., McCorkel, J., Shuai, Y., Trezza, R., Vogelmann, J., Wynne, R.H., and Zhu, Z., 2014. Landsat-8: Science and product vision for terrestrial global change research. *Remote Sensing of Environment*, 145, 154–172.

Saatchi, S.S., Harris, N.L., Brown, S., Lefsky, M., Mitchard, E.T.A., Salas, W., Zutta, B.R., Buermann, W., Lewis,

S.L., Hagen, S., Petrova, S., White, L., Silman, M., and Morel, A., 2011. Benchmark map of forest carbon stocks in tropical regions across three continents. *Proceedings of the National Academy of Sciences*, 108 (24), 9899–9904.

Sangüesa-Barreda, G., Camarero, J.J., Oliva, J., Montes, F., and Gazol, A., 2015. Past logging, drought and pathogens interact and contribute to forest dieback. *Agricultural and Forest Meteorology*, 208, 85–94.

San-Miguel-Ayanz, J., Moreno, J.M., and Camia, A., 2013. Analysis of large fires in European Mediterranean landscapes: Lessons learned and perspectives. *Forest Ecology and Management*.

Santamarina-Campos, B., 2019. El inicio de la protección de la naturaleza en España. Orígenes y balance de la conservación. *Revista Española de Investigaciones Sociológicas*, 168.

Schirpke, U., Altzinger, A., Leitinger, G., and Tasser, E., 2019. Change from agricultural to touristic use: Effects on the aesthetic value of landscapes over the last 150 years. *Landscape and Urban Planning*, 187, 23–35.

Schlund, M. and Davidson, M.W.J., 2018. Aboveground Forest Biomass Estimation Combining L- and P-Band SAR Acquisitions. *Remote Sensing*, 10 (7), 1151.

Seidl, R., Schelhaas, M.-J., and Lexer, M.J., 2011. Unraveling the drivers of intensifying forest disturbance regimes in Europe. *Global Change Biology*, 17 (9), 2842–2852.

Serra, P., Vera, A., Tulla, A.F., and Salvati, L., 2014. Beyond urban–rural dichotomy: Exploring socioeconomic and land-use processes of change in Spain (1991–2011). *Applied Geography*, 55, 71–81.

Shafique, A., Cao, G., Khan, Z., Asad, M., and Aslam, M., 2022. Deep Learning-Based Change Detection in Remote Sensing Images: A Review. *Remote Sensing*, 14 (4), 871.

Shakesby, R.A., 2011. Post-wildfire soil erosion in the Mediterranean: Review and future research directions. *Earth-Science Reviews*, 105 (3), 71–100.

Shannon, C.E. and Wiener, W., 1949. *The mathematical theory of communication (Urbana, IL.*

University of illinois Press IL.

Silva, C.A., Saatchi, S., Garcia, M., Labrière, N., Klauberg, C., Ferraz, A., Meyer, V., Jeffery, K.J., Abernethy, K., White, L., Zhao, K., Lewis, S.L., and Hudak, A.T., 2018. Comparison of Small- and Large-Footprint Lidar Characterization of Tropical Forest Aboveground Structure and Biomass: A Case Study From Central Gabon. *IEEE Journal of Selected Topics in Applied Earth Observations and Remote Sensing*, 11 (10), 3512–3526.

Sinha, S., Jeganathan, C., Sharma, L.K., and Nathawat, M.S., 2015. A review of radar remote sensing for biomass estimation. *International Journal of Environmental Science and Technology*, 12 (5), 1779–1792.

Skidmore, A.K., Coops, N.C., Neinavaz, E., Ali, A., Schaepman, M.E., Paganini, M., Kissling, W.D., Vihervaara, P., Darvishzadeh, R., Feilhauer, H., Fernandez, M., Fernández, N., Gorelick, N., Geijzendorffer, I., Heiden, U., Heurich, M., Hobern, D., Holzwarth, S., Muller-Karger, F.E., Van De Kerchove, R., Lausch, A., Leitão, P.J., Lock, M.C., Mücher, C.A., O'Connor, B., Rocchini, D., Roeoesli, C., Turner, W., Vis, J.K., Wang, T., Wegmann, M., and Wingate, V., 2021. Priority list of biodiversity metrics to observe from space. *Nature Ecology & Evolution*, 5 (7), 896–906.

Smith, V., Portillo-Quintero, C., Sanchez-Azofeifa, A., and Hernandez-Stefanoni, J.L., 2019. Assessing the accuracy of detected breaks in Landsat time series as predictors of small scale deforestation in tropical dry forests of Mexico and Costa Rica. *Remote Sensing of Environment*, 221, 707–721.

Steffen, W., Broadgate, W., Deutsch, L., Gaffney, O., and Ludwig, C., 2015. The trajectory of the Anthropocene: The Great Acceleration. *The Anthropocene Review*, 2 (1), 81–98.

Tanase, M., de la Riva, J., Santoro, M., Pérez-Cabello, F., and Kasischke, E., 2011. Sensitivity of SAR data to post-fire forest regrowth in Mediterranean and boreal forests. *Remote Sensing of Environment*, 115 (8), 2075–2085.

Terres, J.-M., Scacchiafichi, L.N., Wania, A., Ambar, M., Anguiano, E., Buckwell, A., Coppola, A., Gocht, A., Källström, H.N., Pointereau, P., Strijker, D., Visek, L., Vranken, L., and Zobena, A., 2015. Farmland abandonment in Europe: Identification of drivers and indicators, and development of a composite indicator of risk. *Land Use Policy*, 49, 20–34.

Tippmann, S., 2015. Programming tools: Adventures with R. *Nature*, 517 (7532), 109–110.

Torres, P., Rodes-Blanco, M., Viana-Soto, A., Nieto, H., and García, M., 2021. The Role of Remote Sensing for the Assessment and Monitoring of Forest Health: A Systematic Evidence Synthesis. *Forests*, 12 (8), 1134.

Trumbore, S., Brando, P., and Hartmann, H., 2015. Forest health and global change. *Science*, 349 (6250), 814–818.

Turco, M., Rosa-Cánovas, J.J., Bedia, J., Jerez, S., Montávez, J.P., Llasat, M.C., and Provenzale, A., 2018. Exacerbated fires in Mediterranean Europe due to anthropogenic warming projected with non-stationary climate-fire models. *Nature Communications*, 9 (1), 3821.

Turner, M.G., 2010. Disturbance and landscape dynamics in a changing world. *Ecology*, 91 (10), 2833–2849.

UNFCCC, 1997. Kyoto Protocol to the United Nations Framework Convention on Climate Change adopted at COP3 in Kyoto.

Vangi, E., D'Amico, G., Francini, S., Giannetti, F., Lasserre, B., Marchetti, M., and Chirici, G., 2021. The New Hyperspectral Satellite PRISMA: Imagery for Forest Types Discrimination. *Sensors*, 21 (4), 1182.

Vapnik, V., 1998. *Statistical Learning Theory*. New York: Wiley.

Viana-Soto, A., Aguado, I., and Martínez, S., 2017. Assessment of Post-Fire Vegetation Recovery Using Fire Severity and Geographical Data in the Mediterranean Region (Spain). *Environments*, 4 (4), 90.

Vicente-Serrano, S.M., Beguería, S., and López-Moreno, J.I., 2010. A Multiscalar Drought Index Sensitive to Global Warming: The Standardized

Precipitation Evapotranspiration Index. *Journal of Climate*, 23 (7), 1696–1718.

Vicente-Serrano, S.M., Lasanta, T., and Romo, A., 2003. Diferencias espaciales en la evolución del NDVI en la cuenca alta del Aragón : efectos de los caminos en el uso del suelo. *Cuadernos de Investigación Geográfica*, 29 (0), 51.

Vicente-Serrano, S.M., Pérez-Cabello, F., and Lasanta, T., 2011. Pinus halepensis regeneration after a wildfire in a semiarid environment: Assessment using multitemporal Landsat images. *International Journal of Wildland Fire*.

Vidal-Macua, J.J., Ninyerola, M., Zabala, A., Domingo-Marimon, C., Gonzalez-Guerrero, O., and Pons, X., 2018. Environmental and socioeconomic factors of abandonment of rainfed and irrigated crops in northeast Spain. *Applied Geography*, 90 (September 2017), 155–174.

Vilà-Cabrera, A., Coll, L., Martínez-Vilalta, J., and Retana, J., 2018. Forest management for adaptation to climate change in the Mediterranean basin: A synthesis of evidence. *Forest Ecology and Management*, 407, 16–22.

Vilà-Cabrera, A., Espelta, J.M., Vayreda, J., and Pino, J., 2017. "New Forests" from the Twentieth Century are a Relevant Contribution for C Storage in the Iberian Peninsula. *Ecosystems*, 20 (1), 130–143.

Vosselman, G. and Maas, H.-G., 2010. *Airborne and terrestrial laser scanning*. Dunbeath: Whittles Publishing.

Wang, T., Wang, Y., Zhao, F., Feng, H., Liu, J., Zhang, L., Zhang, N., Yuan, G., and Wang, D., 2022. A spatio-temporal temperature-based thresholding algorithm for underground coal fire detection with satellite thermal infrared and radar remote sensing. *International Journal of Applied Earth Observation and Geoinformation*, 110, 102805.

Wegmuller, U. and Werner, C.L., 1995. SAR interferometric signatures of forest. *IEEE Transactions on Geoscience and Remote Sensing*, 33 (5), 1153–1161.

Wilmking, M. and Juday, G.P., 2005. Longitudinal variation of ra-

dial growth at Alaska's northern treeline—recent changes and possible scenarios for the 21st century. *Global and Planetary Change*, 47 (2), 282–300.

WMO, 2021a. Greenhouse gas bulletin [online]. Available from: https://library.wmo.int/doc_num.php?explnum_id=10904.

WMO, 2021b. State of Climate in 2021: Extreme events and major impacts.

Wooster, M.J., Xu, W., and Nightingale, T., 2012. Sentinel-3 SLSTR active fire detection and FRP product: Pre-launch algorithm development and performance evaluation using MODIS and ASTER datasets. *Remote Sensing of Environment*, 120, 236–254.

World Bank, 2022. International Debt Statistics 2022.

Wulder, M.A., Coops, N.C., Roy, D.P., White, J.C., and Hermosilla, T., 2018. Land cover 2.0. *International Journal of Remote Sensing*, 39 (12), 4254–4284.

Wulder, M.A., White, J.C., Nelson, R.F., Næsset, E., Ole, H., Coops, N.C., Hilker, T., Bater, C.W., and Gobakken, T., 2012. Lidar sampling for large-area forest characterization : A review. *Remote Sensing of Environment*, 121, 196–209.

Xu, H., Zhang, G., Zhou, Z., Zhou, X., and Zhou, C., 2022. Forest Fire Monitoring and Positioning Improvement at Subpixel Level: Application to Himawari-8 Fire Products. *Remote Sensing*, 14 (10), 2460.

Yang, G., Huang, K., Sun, W., Meng, X., Mao, D., and Ge, Y., 2022. Enhanced mangrove vegetation index based on hyperspectral images for mapping mangrove. *ISPRS Journal of Photogrammetry and Remote Sensing*, 189, 236–254.

Zhang, J., Nielsen, S.E., Mao, L., Chen, S., and Svenning, J.-C., 2016. Regional and historical factors supplement current climate in shaping global forest canopy height. *Journal of Ecology*, 104 (2), 469–478.

Zhu, Z., Wulder, M.A., Roy, D.P., Woodcock, C.E., Hansen, M.C., Radeloff, V.C., Healey, S.P., Schaaf, C., Hostert, P., Strobl, P., Pekel, J.F., Lymburner, L., Pahlevan, N., and Scambos, T.A., 2019.

Benefits of the free and open Landsat data policy. *Remote Sensing of Environment*.